FINAL REPORT

Facilitated Transport Enabled In-Situ Chemical Oxidation of 1,4-Dioxane-Contaminated Groundwater

SERDP Project ER-2302

AUGUST 2018

Kenneth C. Carroll
New Mexico State University

Mark L. Brusseau
University of Arizona

Thomas B. Boving
University of Rhode Island

Raymond Ball
EnChem Engineering, Inc.

SERDP
DOD ▪ EPA ▪ DOE

Page Intentionally Left Blank

Page Intentionally Left Blank

REPORT DOCUMENTATION PAGE

Form Approved
OMB No. 0704-0188

1. REPORT DATE *(DD-MM-YYYY)*	2. REPORT TYPE	3. DATES COVERED *(From - To)*
08/16/2018	SERDP Final Report	

4. TITLE AND SUBTITLE
Facilitated Transport Enabled In-Situ Chemical Oxidation of 1,4-Dioxane-Contaminated Groundwater

5a. CONTRACT NUMBER
W912HQ-13-C-0033

5b. GRANT NUMBER

5c. PROGRAM ELEMENT NUMBER

6. AUTHOR(S)
Kenneth Carroll, Mark Brusseau, Thomas Boving, Raymond Ball

5d. PROJECT NUMBER
ER-2302

5e. TASK NUMBER

5f. WORK UNIT NUMBER

7. PERFORMING ORGANIZATION NAME(S) AND ADDRESS(ES)
New Mexico State University
PO Box 30003, MSC 3Q, Skeen Hall, Room N127
Las Cruces, NM 88003-8003

8. PERFORMING ORGANIZATION REPORT NUMBER
ER-2302

9. SPONSORING/MONITORING AGENCY NAME(S) AND ADDRESS(ES)
Strategic Environmental Research and Development Program
4800 Mark Center Drive, Suite 16F16
Alexandria, VA 22350-3605

10. SPONSOR/MONITOR'S ACRONYM(S)
SERDP

11. SPONSOR/MONITOR'S REPORT NUMBER(S)
ER-2302

12. DISTRIBUTION/AVAILABILITY STATEMENT
Distribution A; unlimited public release

13. SUPPLEMENTARY NOTES

14. ABSTRACT

In situ chemical oxidation (ISCO) is a remediation alternative for organic contaminants in groundwater. This project has enhanced our ability to deliver strong oxidants by complexing them with other compounds (i.e., delivery agents) that facilitate the transport and improve the stability of oxidants within the subsurface. We have also successfully demonstrated methods for stabilizing and prolonging the reactivity of oxidants, including oxidant catalysis methods using oxidant mixtures and aquifer materials. Finally, we examined the potential for oxidants to oxidize and transform the delivery agents, and we have been testing methods to prolong oxidant reactivity lifetime.

15. SUBJECT TERMS

in-situ, chemical oxidation, ISCO, remediation, groundwater contamination, oxidant transport, oxidant delivery, oxidant reactivity, oxidant catalysis, delivery agents, 1,4-dioxane

16. SECURITY CLASSIFICATION OF:			17. LIMITATION OF ABSTRACT	18. NUMBER OF PAGES	19a. NAME OF RESPONSIBLE PERSON
a. REPORT	b. ABSTRACT	c. THIS PAGE			Kenneth Carroll
					19b. TELEPHONE NUMBER *(Include area code)*
UNCLASS	UNCLASS	UNCLASS	UNCLASS	218	575-646-3406

TABLE OF CONTENTS

LIST OF TABLES

LIST OF FIGURES

LIST OF ACRONYMS

1,4-D	1,4-Dioxane
A	Absorbance
AFP	Air Force Plant
AFP44	Air Force Plant 44, Tucson, AZ
AOP	Advanced oxidation process
ASTM	American Society for Testing and Materials
ATSDR	Agency for Toxic Substances and Disease Registry
CD	Cyclodextrin (here: Hydroxypropyl-β-cyclodextrin; HPBCD)
CEC	Cation exchange capacity
CMCD	Carboxymethyl-beta-cyclodextrin
D	Dispersion coefficient
DA	Delivery agent
DCA	1,1,-Dichloroethane
DI	Deionized
DoD	Department of Defense
EC	Electrical conductivity
EDTA	Ethylenediaminetetraacetic acid
EPA	Environmental Protection Agency
EPR	Electron paramagnetic resonance
ESTCP	Environmental Security Technology Certification Program
FID	Flame ionization detection
FT-ICR-MS	Fourier Transform Ion Cyclotron Resonance Mass Spectrometer
G-CD	Gamma cyclodextrin
GC-MS	Gas chromatography-mass spectrometry
H_2O_2	Hydrogen peroxide
HPβCD	Hydroxypropyl-β-cyclodextrin
HPLC	High performance liquid chromatography
I	Intensity
ICP-MS	Inductively coupled plasma-mass spectrometry
ISCO	In situ chemical oxidation
K	Binding constant
k	Rate constant
K_d	Sorption partitioning constant
$KMnO_4$	Potassium permanganate
MCL	Maximum contaminant limit
MnO_4	Permanganate
$Na_2S_2O_8$	Sodium persulfate
NMR	Nuclear Magnetic Resonance
NOD	Natual oxidant demand
O&M	Operations & monitoring
O_3	Ozone
ORP	Oxidation reduction potential
P	Peclet number
PAMAM	Polyamidoamine

PAP	Perozone activated persulfate
PCE	Tetrachloroethene
PRB	Permeable reactive barrier
PV	Pore volume
PVC	Polyvinyl chloride
Q	Refers to (I0-I)/I where I is the observed fluorescence intensity after addition of the guest molecule
RPM	Revolutions per minute
S_2O_8	Persulfate
SEM-EDS	Scanning electron microscopy-energy dispersive X-ray spectroscopy
SERDP	Strategic Environmental Research and Development Program
SIM	Selected ion monitoring
SO	Siderite activated-hydrogen peroxide
SOM	Soil organic matter
SPME	Solid phase micro extraction
STO	Siderite activated-hydrogen peroxide combined with persulfate
TCA	1,1,1-Trichloroethane
TCE	Trichloroethene
TNS	6-p toluidine-2-naphthalenesulfonic acid
TOD	Total oxidant demand
UCMR3	Unregulated Contaminant Monitoring Rule 3rd Round
URI	University of Rhode Island
US	United States
UV	Ultraviolet light
V	Volts
VOA	Volatile organic analysis
VOC	Volatile organic compound
XRD	X-ray diffraction
ZVI	Zero valent iron

KEYWORDS

1,4-dioxane, trichloroethane, trichloroethene, ozone, cyclodextrin, persulfate, peroxone, iron filings, binding constant, clathrate, advanced oxidation, contaminant, pollutant, contamination, remediation, groundwater, wastewater, ISCO, *in situ* chemical oxidation, radical, permeable reactive barrier

ACKNOWLEDGEMENTS

This research was supported by the US Department of Defense Strategic Environmental Research and Development Program (ER-2302), with additional support provided by the USDA National Institute of Food and Agriculture (Hatch project 1006845), the U.S. Air Force Civil Engineer Center (AFCEC) Project FA8903-11-C-8004, and the Plant & Environmental Science Department at NMSU is appreciated. EnChem Engineering, Inc.'s patents were utilized herein (US Patent 7,667,087, US Patent 8,049,056, and US Patent 9,409,216). This work would not have been possible without the hard work of several students including Naima Khan, Adam

Dettmer, Logan Bridges, Justin Milavec, Dylan Eberle, Hao Chen, Ni Yan, Fie Liu, Yifei Chen, Hua Zhong, Yake Wang, Lauren Quig, Mengjiao Li, Yali Liu, Nilusha Sudasinghe, and Michaela Cashman. We also appreciate the support of Michael Johnson, Omar Holguin, Barry Dungan, Tanner Schaub, Alan Moore, Barbara Hunter, Sativa Cruz, April Ulery, Gwynn Johnson, Carlos Fernandez, and other members of the graduate student research labs of Kenneth C. Carroll (NMSU), Mark Brusseau (University of Arizona), and Thomas Boving (University of Rhode Island). We thank Bill DiGuiseppi and Jim Hatton (CH2MHill) for their discussions and support of this project. Finally, we thank Andrea Leeson, Hans Stroo, and other members of the SERDP staff for their support and assistance with this project.

EXECUTIVE SUMMARY

ABSTRACT

In situ chemical oxidation (ISCO) is a remediation alternative for organic contaminants in groundwater. It involves the injection of oxidants, which transform contaminants into benign products within the groundwater. For ISCO to be effective, oxidants must come in contact with contaminants within the subsurface. Thus, delivery of oxidants is critical, and heterogeneity of the subsurface constrains the delivery of oxidants. This is especially the case for short-lived strong oxidants, which are required for some contaminants, such as 1,4-dioxane. This project has enhanced our ability to deliver strong oxidants by complexing them with other compounds (i.e., delivery agents) that facilitate the transport and improve the stability of oxidants within the subsurface. We have also successfully demonstrated methods for stabilizing and prolonging the reactivity of oxidants, including oxidant catalysis methods using oxidant mixtures and aquifer materials. Finally, we examined the potential for oxidants to oxidize and transform the delivery agents, and we have been testing methods to prolong oxidant reactivity lifetime.

Objectives

Presently, chlorinated solvents and 1,4-dioxane mixtures are primary contaminants of concern at Department of Defense (DoD) sites. 1,4-Dioxane occurrence in large groundwater contamination plumes represents a liability due to potential adverse health risks and remediation costs. Properties of 1,4-dioxane, including its high water solubility, resistance to adsorption, and low volatilization, have resulted in extensive groundwater contaminant plumes that are often as large as, or larger, than those associated with chlorinated solvents.

Our objective was to develop advanced ISCO as a viable technology for 1,4-dioxane by enhancing the solubility, stability, activation, and transportability of strong oxidants (e.g., O_3 and activated persulfate), which enables *in situ* treatment of groundwater plumes. This goal has been achieved through the 1) co-injection of oxidants with chemical delivery agents that facilitate the transport and stability of the oxidant, 2) co-injection of oxidant mixtures that stabilize and activate oxidation, and 3) *in situ* activation of oxidants. The specific objectives of this project included: 1) Develop the ability to remediate 1,4-dioxane using *in situ* oxidation combined with facilitated transport, or delivery, of the oxidants within the subsurface; 2) Investigate oxidant activation methods and use of delivery agents to stabilize commonly used advanced oxidation process (AOP) reagents, such as O_3, persulfate, and oxidant mixtures, through complexation and activation; 3) Investigate the ability of delivery agents to increase the specificity of oxidant reactivity for 1,4-dioxane, and to enhance the stability and longevity of the oxidant; 4) Investigate the effectiveness of facilitated transport of oxidants complexed with delivery agents within sediments; 5) Investigate delayed activation or timed-release of oxidants from complexation.

Technical Approach

This project has developed ISCO as a viable technology for 1,4-dioxane groundwater plume remediation by enhancing the solubility, stability, activation, and transportability of strong oxidants (e.g., ozone or O_3), which facilitates the *in situ* treatment of groundwater plumes. This goal was achieved through the co-injection of oxidants with chemical agents that facilitate the transport of the oxidant. In case of ozone-based AOP, O_3 forms an inclusion complex or

partitions into the delivery agent cyclodextrin, which increases the amount of oxidant delivered. Also, facilitated transport increased specificity of oxidation for 1,4-dioxane and co-contaminant chlorinated solvents as they also partition into the cyclodextrin. Additional methods for stabilizing and activating oxidants were developed by injecting mixtures of oxidants, such as persulfate, and using *in situ* aquifer materials and solid forms of iron (siderite, iron filings) to support delayed activation of injected oxidants to allow ISCO reagents to transport into contaminated groundwater systems.

Results

During initial screening tests, we examined polyamidoamine (PAMAM) dendrimers, Tween 80, and EDTA, which were all not effective for oxidant complexation. However, we found a potential for dendrimer application for extracting various ionic contaminants, such as nitrate and copper, from soil and groundwater. Importantly, cyclodextrin complexation with O_3 was proven to increase O_3 stability by more than a factor of 30. Multiple spectroscopic methods including UV and fluorescence for direct and competitive complexation, of O_3, 1,4-dioxane, and chlorinated co-contaminants (TCE and TCA) with HPβCD and γ-CD, produced comparable binding constant results although method applicability and accuracy can vary with guest compound analysis properties. Aqueous O_3, delivered with and without HPβCD, was capable of degrading 1,4-dioxane, TCE, and TCA to nondetectable concentrations, and the rate constants increased with addition of co-contaminants and salts whereas bicarbonate (i.e., radical scavenger) did not inhibit kinetics for 1,4-dioxane removal in HPβCD solutions. 1,4-Dioxane was successfully degraded by the siderite-activated binary H_2O_2-persulfate system, and the impact of radical scavengers was evaluated. A perozone activated persulfate (PAP) mixture was highly effective at transforming 1,4-dioxane, TCE, and TCA individually and in mixtures, and the degradation process was continuous for at least 13 days. The PAP application, such as the OxyZone® formulation, was demonstrated in both pulse and continuous injections into 1,4-dioxane contaminated plume experimental systems, which indicated oxidation potential extended long after the end of injection, thereby extending the oxidant solution's range of influence. Also, iron filing were demonstrated for activating persulfate and 1,4-dioxane treatment within a permeable reactive barrier, and the results show that >99% removal would typically occur for bed lengths of ~3-4 meters.

Benefits

This research developed multiple, novel, cost effective, *in situ* treatment alternatives for 1,4-dioxane-contaminated source zones and groundwater plumes. It also advanced our understanding of processes controlling the complexation of oxidants and the impact of complexation, or other transport-related processes, on oxidation reactions. Three oxidant delivery methods were shown effective for 1,4-dioxane treatment, namely (1) co-injecting oxidants, (2) using complexing agents to facilitate reagent transport, and (3) exploiting aquifer materials to delay activation of oxidants. All three enhance longevity and transportability of oxidants result enhanced AOP treatment by reaching farther into the 1,4-dioxane contaminated aquifer. These findings suggest the potential for each of the 3 oxidant delivery methods to support sustained oxidation of recalcitrant organic contaminants that are difficult to treat using standard methods. These novel approaches enhance contaminated site remediation, and they could also reduce cleanup cost while increasing cleanup efficiency, which supports the effective management of DoD sites contaminated with 1,4-dioxane.

1. OBJECTIVE:

In situ chemical oxidation (ISCO) is an effective method for remediation of source zones contaminated by several classes of organic compounds. In theory, high-oxidation potential reagents can be used to remediate contaminated groundwater. However, such reagents are too short-lived, and become costly for groundwater remediation applications. If the oxidant longevity could be enhanced, this technology could also feasibly be used for ISCO of complex source zones and also for groundwater plumes. These limitations may be reduced by co-injecting oxidants with a complexing agent (i.e., delivery agent), which facilitates the transport of oxidants into groundwater plumes to increase the longevity and transportability of oxidants and thereby enhances the effective subsurface treatment volume. A similar approach to facilitating the longevity of an oxidant in the subsurface is to chemically stabilize or activate it.

The purpose of this project was to develop advanced ISCO as a viable technology for recalcitrant organic contaminants, such as 1,4-dioxane, by enhancing the solubility, stability, and transportability of strong oxidants (e.g., O_3 and persulfate), which enables effective *in situ* treatment of recalcitrant contaminants. Several delivery enhancement alternatives were initially considered, and based on elimination of the least efficient, three have been developed. The first is the co-injection of oxidants with a delivery agent, i.e. O_3 complexed with cyclodextrin. If oxidants complex or partition into a delivery-agent molecule, the amount of oxidant that can be delivered to the plume can increase. Also, decreases in reactivity during facilitated transport may increase specificity of oxidation for compounds of concern and reduce oxidant consumption due to natural oxidant demand of subsurface sediments. The second is the co-injection of mixtures of oxidants such as perozone activated persulfate, which is a mixture of O_3, hydrogen peroxide, persulfate, and phosphate buffers. One particular co-injection mixture commercially available through EnChem Engineering under the trade name OxyZone®. Common to these two methods is that they involve the use of aqueous solutions that can be injected into groundwater plumes and used to develop an aqueous flow-through treatment system. Our third approach, an additional application uses solid materials to stabilize and catalyze oxidants. The system developed herein used iron (either iron filings or iron-bearing minerals naturally present in sediments) to catalyze persulfate. A potential application of this approach is using iron filings in conjunction with persulfate injections within a permeable reactive barrier for *in situ* treatment of contaminated groundwater plumes. Another example is the use of the natural activation capacity of aquifer sediment that contain iron and manganese oxides to activate persulfate *in situ*.

This report summarizes research conducted to support SERDP project ER-2302, which addressed the SERDP SON ERSON-13-01 need to develop cost-effective *in situ* remedial alternatives for 1,4-dioxane-contaminated groundwater at DoD sites. We developed advanced-oxidation ISCO as a viable technology for 1,4-dioxane by enhancing the solubility, stability, activation, and transportability of strong oxidants (e.g., O_3 and persulfate), which enable the *in situ* treatment of groundwater plumes. The specific objectives of the proposed research include:

1) Develop the ability to remediate 1,4-dioxane using *in situ* oxidation combined with facilitated transport, or delivery, of the oxidants within the subsurface. *Hypothesis*: Facilitated transport of strong oxidants promotes delivery of oxidants for enhanced *in situ* destruction of 1,4-dioxane to below proposed regulatory levels.

2) Investigate oxidant activation methods and use of delivery agents to stabilize commonly used AOP reagents, such as O_3, persulfate, and oxidant mixtures, through complexation and activation. *Hypothesis*: Delivery agents (e.g., cyclodextrin) increases the oxidant solubility and

facilitate oxidant transport without significant decreases in 1,4-dioxane oxidation kinetics or effectiveness.

3) Investigate the ability of delivery agents to increase the specificity of oxidant reactivity for 1,4-dioxane, and to enhance the stability and longevity of the oxidant. *Hypothesis*: Delivery agents (e.g., cyclodextrin) increase the solubility and facilitate oxidant transport extending the life of short-lived oxidants (e.g., O_3), increase oxidation specificity, and also increase the radius of influence of AOPs injection.

4) Investigate the effectiveness of facilitated transport of oxidants complexed with delivery agents within sediments. *Hypothesis*: Delivery agents (e.g., cyclodextrin) enable facilitated transport of oxidants such as O_3 which decreases natural oxidant demand limitations.

5) Investigate delayed activation or timed-release of oxidants from complexation. *Hypothesis*: A time-release oxidant complex can be implemented within a groundwater plume through the coupling of facilitated transport/delivery of oxidant reagents with delivery agent decay.

2. BACKGROUND:

2.1 Groundwater Contamination with 1,4-Dioxane and Chlorinated Solvents

1,4-Dioxane is a heterocyclic organic contaminant found in wastewater and groundwater contamination plumes at industrial sites worldwide. This cyclic ether (Figure 2.1) was historically used in many industrial products and processes, including usage as a stabilizer or a wetting and dispersing agent for textile processing and printing (Anderson et al., 2012; Klecka, 1986; Mohr et al., 2010). 1,4-Dioxane is released as a byproduct of polyester production and disposal of various consumer products (DiGuiseppi et al., 2016; DiGuiseppi and Whitesides, 2007; Mohr et al., 2010; Zenker et al., 2003). 1,4-Dioxane was previously used as a solvent stabilizer mixed with chlorinated solvents (Mohr et al., 2010), including 1,1,1-trichloroethane (TCA) and trichloroethene (TCE) (Adamson et al., 2015; Anderson et al., 2012; Zenker et al., 2003). Stabilizers such as 1,4-dioxane were commonly added to solvents to serve as antioxidants, acid inhibitors, and metal stabilizers, which inhibit breakdown of the solvent (Mohr et al., 2010). Historically, 1,4-dioxane has been included with common chlorinated solvents in mixtures at 2 to 8 percent by volume (Mohr et al., 2010). In 1985, for instance, approximately 90% of 1,4-dioxane produced was used as a stabilizer for chlorinated solvents, particularly TCA and to some extent TCE (Mohr et al., 2010). Chlorinated solvents, such as TCA and TCE, are found at approximately 80% of all EPA Superfund sites with groundwater contamination (SERDP, 2006). Historic records of poor handling, storage, and disposal practices of chlorinated solvents highlights the significant potential for 1,4-dioxane contamination in groundwater.

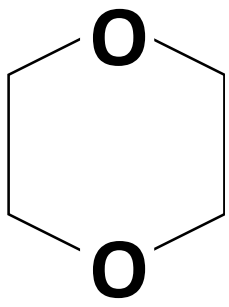

Figure 2.1. 1,4-Dioxane, a heterocyclic ether.

1,4-Dioxane frequently occurs with 1,1,-dichloroethane (DCA), a byproduct of TCA degradation (Adamson et al., 2015; Adamson et al., 2017; Anderson et al., 2012; EPA, 2013a). The association of 1,4-dioxane with TCA is well documented. However, its association with TCE has previously been a topic of debate (Mohr et al., 2010; Zenker et al., 2003). A survey of 20 wells in Kanagaw, Japan showed that detection of 1,4-dioxane was highly correlated with detection of TCA, while correlation with TCE was much weaker (Abe, 1999). However, a recent survey of groundwater data from 49 U.S. Air Force installations found 64.4% of all 1,4-dioxane detections were observed in wells with records of TCE contamination, but without detection of TCA (Anderson et al., 2012). In addition, 93.7% of all 1,4-dioxane detections were in wells with records of TCA and/or TCE contamination (Anderson et al., 2012). These studies suggest that 1,4-dioxane can co-exist with TCA, TCE, or more likely both. Hence, from the perspective of a site manager the presence of chlorinated volatile organic compounds (VOCs), particular TCA or TCE, is a likely indicator of 1,4-dioxane contamination (Anderson et al., 2012). With the number of known 1,4-dioxane sites increasing, there is a need for cost-effective remediation technologies, particularly for simultaneously treating 1,4-dioxane and its co-contaminants TCE and TCA.

Chlorinated solvents are regulated as hazardous materials and have been the focus of contaminant investigation programs, however, 1,4-dioxane is not currently classified as a U.S. EPA priority pollutant, and does not have a maximum contaminant level (MCL) for drinking water (Mohr et al., 2010). Consequently, it has not been routinely analyzed in groundwater at solvent release sites or included in the cleanup objectives of regulatory orders (Mohr, 2001). Even sites where full Appendix IX (40 Code of Federal Regulations Part 261) analyses were conducted in the 1980s or 1990s may not have identified lower levels of 1,4-dioxane, because detection limits at the time were higher (e.g., 100's of µg/L) than they are now. More recent advances now permit detection at concentrations less than 100 µg/L (Draper et al., 2000; EPA, 2008). Because many 1,4-dioxane plumes are below 100 µg/L, this chemical would have been missed during characterization and remediation. Decreases in the analytical detection limits for groundwater sample analyses have revealed the presence of this contaminant at sites where no 1,4-dioxane was identified during earlier, higher-detection limit sampling events. Due to this lack of regulation, 1,4-dioxane was not routinely monitored at solvent release sites. Furthermore, prior to 1997, reliable low-level (<100 µg/L) 1,4-dioxane analysis was not routinely available (Draper et al., 2000; Mohr et al., 2010).

1,4-Dioxane is an emerging groundwater contaminant and a likely human carcinogen (EPA, 2013b; IARC, 1999; Mohr et al., 2010; Stickney et al., 2003). EPA risk assessments indicate that a drinking water concentration of 0.35 µg/L represents a 10^{-6} cancer risk and the current screening level for 1,4-dioxane in tap water is 0.67 µg/L (EPA, 2013b). However, while 1,4-dioxane is regulated as a hazardous waste, there are currently no federal drinking water standards for this compound. Toxicological studies suggest that 1,4-dioxane may be harmful, and it is a regulated hazardous material and 2B Probable Carcinogen. Even though it is not currently classified as a US EPA priority pollutant (as noted above) without a MCL for drinking water (EPA, 2013b; IARC, 1999; Mohr et al., 2010; Mohr et al., 2016), many states have developed screening levels for 1,4-dioxane, but state regulated thresholds vary over an order of magnitude (Suthersan et al., 2016). While there are no federal standards for 1,4-dioxane in groundwater, the EPA has established drinking water advisories. The EPA 1-day health advisory is 4 mg/L of 1,4-dioxane in drinking water, whereas the 10-day health advisory is 0.4 mg/L. The lifetime health

advisory for 1,4-dioxane in drinking water is 0.2 mg/L. The EPA Integrated Risk Information System states that cancer development could occur in 1 out of 1,000,000 people exposed to a concentration of 0.35 ppb 1,4-dioxane over a lifetime. Therefore, the Unregulated Contaminant Monitoring Rule (UCMR3) is set to 0.07 μg/L for the United States.

The solvent stabilizer, 1,4-dioxane, has emerged in the environmental remediation arena as an unexpected and recalcitrant groundwater contaminant at many sites across the U.S., including Air Force Plant (AFP) 44, AFP 3, Edwards AFB, Tinker AFB, Hill AFB, Fort Carson, Naval Air Station Whidbey Island, and others. 1,4-Dioxane concentrations in the environment vary greatly across the United States. Historical data (prior to 1990) suggests that ambient levels of 1,4-dioxane in groundwater are about 1 μg/L (Kraybill, 1978). Because of its widespread occurrence, 1,4-dioxane was included in the third round of the UCMR to evaluate its persistence in the environment and potential exposure to drinking water reservoirs. 1,4-Dioxane was detected in 21% of the 4864 public water systems monitored, and it exceeded the health-based reference concentration (0.35 μg/L) at 6.9% of these sites (Adamson et al., 2017). The mean concentration is 1.1 μg/L for public water supplies (Adamson et al., 2017), but significantly higher levels have been found in various aquifers across the country. 1,4-Dioxane concentrations have been reported at 2,100 μg/L in Massachusetts (Burmaster, 1982), 31,000 μg/L in Westville, Indiana (Duwelius et al., 2002) and as high as 250,000 μg/L at a San Jose, California solvent recycling facility in 1998 (Gandesbery et al., 1998). Studies have shown that conventional wastewater treatment plants are often incapable of treating for 1,4-dioxane, leading to discharge into surface waters (Simonich et al., 2013; Stepien et al., 2014). Large groundwater contaminant plumes of 1,4-dioxane often form, usually co-occurring with chlorinated-constituent plumes (Adamson et al., 2015; Adamson et al., 2014; Anderson et al., 2012).

2.2 1,4-Dioxane Properties, Transport, and Treatment

Chlorinated solvents are found at approximately 80% of all EPA Superfund sites with groundwater contamination and more than 3,000 DoD sites (SERDP, 2006), 1,4-dioxane is a co-contaminant at many of these sites, and it is generally found to be the most highly mobile contaminant (Zenker et al., 2003). The chemical structure of 1,4-dioxane (Figure 2.1) includes two oxygen atoms that make it hydrophilic and highly soluble (miscible) in water. Additionally, properties of 1,4-dioxane (Table 2.1), including low or negligible adsorption, and low volatilization, have resulted in extensive groundwater contaminant plumes that are often as large as, or larger than, those associated with the chlorinated solvents (Adamson et al., 2015; Mohr et al., 2010). The properties of 1,4-dioxane that make it useful for solvent stabilization, such as the high polarity, which results in its high aqueous solubility and low adsorption and volatilization (DiGuiseppi et al., 2016; DiGuiseppi and Whitesides, 2007; Mohr et al., 2010; Zenker et al., 2003), have resulted in extensive wastewater and groundwater contaminant plumes that are often as large as those associated with the chlorinated solvents and make it a challenge for water treatment. The chemical characteristics, associated fate and transport mechanisms, recently toxicity concerns, and potentially more stringent standards combine to make 1,4-dioxane a difficult and costly contaminant to address, which has impacted ongoing groundwater cleanup programs at a number of sites.

Despite the co-disposal and coincidence of plumes, 1,4-dioxane is not effectively removed from groundwater through sorption or volatilization technologies typically used for chlorinated co-

contaminant treatment (DiGuiseppi et al., 2016; DiGuiseppi and Whitesides, 2007; Mohr et al., 2010; Zenker et al., 2003), and the cleanup targets being proposed for 1,4-dioxane are potentially as low as, or lower than, those for most chlorinated solvents. Due to its low volatility and K_{oc} (Table 2.1), air stripping and adsorption are generally considered poor treatment options for 1,4-dioxane contaminated groundwater (DiGuiseppi et al., 2016; DiGuiseppi and Whitesides, 2007; Mohr et al., 2010; Otto and Nagaraja, 2007; Zenker et al., 2003). Groundwater extraction (pump-and-treat) followed by standard treatment methods such as air stripping or carbon adsorption yield ~10-50% removal rates (respectively), which is far below requirements to reach the 3 μg/L regulatory level currently proposed by California and Colorado, or lower standards on the order of 0.35 μg/L, which may be impending.

Table 2.1. Physiochemical properties of 1,4-dioxane (DiGuiseppi and Whitesides, 2007; Mohr et al., 2016).

Molecular Mass (g/mol)	88.12
Log K_{ow}	0.43
Log K_{oc}	0.54
Vapor Pressure (mm Hg @ 25°C)	38.09
Henry's Constant (atm-m^3/mol)	$4.80*10^6$
Boiling Point (°C @ 760 mm Hg)	101.32

Natural attenuation potential of 1,4-dioxane would be limited to physical processes (e.g., dilution and dispersion), as natural adsorption and biodegradation has been observed to be negligible at many sites (DiGuiseppi and Whitesides, 2007; Mohr et al., 2010; Zenker et al., 2003). 1,4-Dioxane biodegradation has not been determined to be a dominant attenuation process as aerobic microbes generally do not receive enough energy from 1,4-dioxane to increase activity or growth significantly (Adamson et al., 2015; Mahendra et al., 2013; Zhang et al., 2017), and costly bioamendments are needed. It is generally resistant to biological treatment under both aerobic and anaerobic conditions (Adams et al., 1994; Raj et al., 1997; Zhang et al., 2017). Furthermore, the presence of chlorinated co-contaminants have been shown to inhibit the biodegradation of 1,4-dioxane by both metabolizing and co-metabolizing bacteria strains (Hand et al., 2015; Mahendra et al., 2013; Zhang et al., 2016; Zhang et al., 2017). Phytoremediation using hybrid poplars has been demonstrated for shallow contamination treatment, but its application may be limited by climactic and hydrogeological (i.e., depth to groundwater) conditions (Mohr et al., 2010; Zenker et al., 2003).

2.3 In Situ and Ex Situ Chemical Oxidation

Chemical oxidation processes can be used to treat 1,4-dioxane either *in situ* or *ex situ* (Huling and Pivetz, 2006; Zenker et al., 2003). *In situ* applications typically involve oxidant injection in the subsurface to for oxidative transformation at the location of the contaminant, and *ex situ* treatment typically involves pumping contaminated groundwater for above ground treatment. Pump and treat systems are considered *ex situ* treatment, because groundwater is used to extract contaminants to the land surface where the treatment process occurs. For *ex situ* systems,

contaminated groundwater must be extracted, treated, and then reinjected or redistributed. Both capital costs (including drilling, construction, storage, and pumps/pipes) and O&M costs (including electricity, reagents, waste disposal, and operations/monitoring) are expensive. These groundwater extraction costs amount to a significant portion of the total site remediation costs, especially for sites like AFP44 where the water table is relatively deep. Overall, *ex situ* treatment is costly, and development of a more cost effective *in situ* technology is needed to remediate 1,4-dioxane plumes (Zenker et al., 2003). Compared to *ex situ* treatment, *in situ* chemical oxidation methods are desirable for their ability to treat groundwater without extraction. Both *in situ* and *ex situ* systems have been used at AFP44, and if oxidant delivery is feasible *in situ* systems may be developed to replace *ex situ* systems.

In situ chemical oxidation (ISCO) relies on the delivery of chemical oxidizing agents directly into the subsurface for the purpose of breaking down contaminants into less harmful chemical species such as carbon dioxide (Huling and Pivetz, 2006). In general, chemical oxidation is the process of reducing an oxidant through accepting electrons released from the transformation of reactive species. Oxidation of targeted organic compounds is accomplished through hydrogen abstraction, oxygen addition, or electron removal. Commonly used ISCO oxidants include permanganate (MnO_4^-), hydrogen peroxide (H_2O_2), ozone (O_3), and activated persulfate ($S_2O_8^-$) (Ferrarese et al., 2008; Rivas, 2006). Potassium permanganate ($KMnO_4$), a mid-range oxidant that is sufficiently stable to be injected extensively into a groundwater plume, is typically used for ISCO of chlorinated solvent contaminants such as TCE (Brusseau et al., 2011; Krembs et al., 2010; Marble et al., 2010; Seol et al., 2003). However, 1,4-dioxane oxidation via permanganate (1.7 V) is possible, but the reactions rates are very slow (half-life (t½) > days) (Huling and Pivetz, 2006; Waldemer and Tratnyek, 2006).

Application of ISCO can be coupled with pump and treat infrastructure by using groundwater wells for dissolved oxidant injection for plume or source zone treatment. One alternative for management of source zones and groundwater plumes is the use of permeable reactive barriers (PRBs). PRBs can be developed for groundwater plumes by injecting oxidants along a transect perpendicular to the plume transport direction such that contaminated groundwater transports through the oxidant zone in the subsurface. PRBs employing iron filings or related materials have been used successfully for many chlorinated-solvent contaminated sites, and have proven to be a cost-effective method for long-term management. We hypothesize that supplementing a standard iron-filings-based PRB with persulfate could significantly enhance the range of contaminants treated, as well as increase rates of treatment.

In terms of treatment using chemical oxidation, mineralization of 1,4-dioxane typically requires strong oxidants (i.e., AOP) that have a standard redox potential greater than two electron volts (DiGuiseppi et al., 2016; DiGuiseppi and Whitesides, 2007; Zenker et al., 2003). Conventional chemical oxidation technologies with oxidants having a standard oxidation potential of less than 2.0 V are generally considered ineffective for the treatment of 1,4-dioxane (Table 2.2). Currently, the most common method used to remediate 1,4-dioxane involves *ex situ* treatment using advanced oxidation (e.g., O_3 and H_2O_2 or UV and H_2O_2), which is effective for complete transformation to below proposed regulatory levels (DiGuiseppi et al., 2016; DiGuiseppi and Whitesides, 2007; Mohr et al., 2010; Zenker et al., 2003).

2.4 Advanced Oxidation

The strength of an oxidant can be described in terms of oxidation and reduction potential (ORP). The ORP is a measure of a substance's ability to scavenge or donate electrons. The electrons that pass through these exchanges emit energy, which can be quantified as volts. The higher an oxidation potential, the stronger electron acceptor it is within an oxidizing system (Table 2.2).

Table 2.2. Oxidants and radical species with standard oxidation potential (Huling and Pivetz, 2006; Siegrist, 2001).

Oxidant	**Standard Oxidation Potential (Volts)**
Hydroxyl Radical (•OH)	2.8
Sulfate Radical (•$S0_4$)	2.5
Ozone (O_3)	2.1
Persulfate (S_2O^{8-})	2.0
Hydrogen Peroxide (H_2O_2)	1.8
Perhydroxyl Radical (•HO_2)	1.7
Permanganate (MnO_4^-)	1.7
Chlorine (Cl^-)	1.4
Oxygen (O_2)	1.2
Hydroperoxide Anion (HO_2^-)	-0.9
Superoxide Radical (•O_2^-)	-2.4

As noted above, the use of $KMnO_4$ for 1,4-dioxane is generally not typically considered viable, because it requires stronger oxidants (>2 electron volts) such as O_3-peroxide, UV-peroxide, $Na_2S_2O_8$, and Fenton's Reagent (H_2O_2 and ferrous iron) (DiGuiseppi and Whitesides, 2007). AOPs include treatment using strong oxidants, and they rely on the synergistic effects of combining strong oxidants for enhanced pollutant degradation in aqueous phase oxidation processes (Glaze and Kang, 1988). Some of the strongest oxidants available are radicals. A radical, in chemistry, is a molecule that contains at least one unpaired electron. While many radical species can be used for contaminant remediation, commonly used radicals for *in situ* and *ex situ* chemical oxidation processes include hydroxyl (•OH) and or sulfate (•SO_4) radicals. Depending on the system, radical formation may lead to further oxidation via secondary reactions, such as sulfate radical propagation.

In radical oxidation, oxidation rates depend largely on the quantity and type of radicals produced. Hydroxyl radicals can non-selectively oxidize most organic pollutants at rapid rates due to their high reactivity and oxidation potential (Buxton et al., 1988). Common •OH based AOPs include O_3, O_3/H_2O_2, UV/O_3, UV/H_2O_2, UV/O_3/H_2O_2, Fe^{2+}/H_2O_2, and electrolysis (Shen et al., 2017). However, hydroxyl radicals have a short lifetime (Table 2.3) which hinders the delivery of this oxidant to pockets of contaminant that are distant from the oxidant injection well(s).

AOPs capable of producing hydroxyl and/or sulfate radicals, have been investigated for treating 1,4-dioxane. In fact, hydroxyl radical production is a well-established mechanism for

oxidizing 1,4-dioxane (Adams et al., 1994; Barndok et al., 2014a; Ikehata et al., 2016; Kishimoto, 2007; Kishimoto et al., 2008; Kishimoto et al., 2007; Kwon et al., 2012; Tian et al., 2014; Wang et al., 2015; Zeng et al., 2017). Interest in AOP use for treatment of various refractory organic pollutants in water has been growing (Chaplin, 2014; Coleman et al., 2007; Gassie and Englehardt, 2017; Ghosh et al., 2010; Loeb, 2018; Lofrano et al., 2017; Mirzaei et al., 2017; Moreira et al., 2017; Nidheesh, 2017; Pera-Titus et al., 2004; Salimi et al., 2017; Sillanpaa et al., 2018; Wei et al., 2017; Zhao et al., 2017) especially for ozone (i.e., O_3), which has been widely used for AOP of various recalcitrant water contaminants (Bertanza et al., 2013; Bhuyan and Latin, 2012; Clayton et al., 2011; Deegan et al., 2011; Gassie and Englehardt, 2017; Gomes et al., 2017; Huling and Pivetz, 2006; Ikehata et al., 2016; Larsen et al., 2004; Loeb, 2018; Salimi et al., 2017; Suh and Mohseni, 2004; von Sonntag and von Gunten, 2012; Wei et al., 2017). Currently, the most effective chemical oxidation treatments for 1,4-dioxane are hydroxyl radical based AOPs. These technologies include photocatalytic degradation (Coleman et al., 2007; Hill et al., 1997; Lam et al., 2007; Mehrvar et al., 2000; Mehrvar et al., 2001; Mehrvar et al., 2002; Vescovi et al., 2010), sonochemical oxidation (Beckett and Hua, 2000; Son et al., 2006), peroxone (Adams et al., 1994; Suh and Mohseni, 2004), combined ultraviolet light and hydrogen peroxide (Coleman et al., 2007; Maurino et al., 1997), and combined photocatalytic and sonochemical oxidation (Nakajima et al., 2007; Nakajima et al., 2004).

Table 2.3. Persistence of AOP reactive species (Block et al., 2004; Huling and Pivetz, 2006).

Oxidant	**Reactive Species**	**Reaction**	**Literature Referenced Persistence**
Hydrogen Peroxide	Hydrogen Peroxide (H_2O_2)	$H_2O_2 + 2H^+ + 2e^- \rightarrow 2\ H_2O$	Minutes-hours
Ozone	Ozone (O_3) Hydroxyl radical (•OH)	$O_3 + 2H^+ + 2e^- \rightarrow O_2 + 2H_2O$ $2O_3 + 3H_2O \rightarrow 4O_2 + 2\ •OH + 2H_2O$	Minutes-hours
Activated Persulfate ($S_2O_8^{2-}$)	Sulfate radical ($•SO_4^-$) Hydroxyl radical (•OH)	$S_2O_8^{2-}$ + Peroxone $\rightarrow 2\ •SO_4^{—}$ (initiation) $2•SO_4^- + 2H_2O \rightarrow 2HSO_4^- + 2\ •OH$ $2\ •OH + 2H^+ + 2e^- \rightarrow 2\ H_2O$	Minutes-weeks

Hydrogen peroxide use, without activation (<2 electron volts), is not strong enough of an oxidant for 1,4-dioxane treatment. Hydrogen peroxide has a direct oxidation potential of 1.8 V, but when catalyzed, peroxide forms •OH radicals with an oxidation potential of 2.8 V (Table 2.2). The persulfate anion has a redox potential of 2.01 V (Latimer, 1938). When activated, persulfate is capable of producing both hydroxyl and sulfate radicals (Block et al., 2004; Huling and Pivetz, 2006). The •SO4 radical has redox potential of 2.5 V (Table 2.2). O_3 dissolved in water reacts to yield hydroxyl radicals, which have the ability to self-propagate. O_3 oxidation yields the hydroxyl radical, a stronger but short-lived oxidant compared to nonradical oxidants such as permanganate.

Several researchers have demonstrated the successful degradation of 1,4-dioxane with O_3 (Adams et al., 1994; Barndok et al., 2014a; Ikehata et al., 2016; Kosaka et al., 2000; Kwon et al., 2012; Suh and Mohseni, 2004; Tian et al., 2014). Organic contaminant oxidative transformation may occur directly by O_3 or indirectly by OH•, which is produced through reaction with hydroxide (Hoigne and Bader, 1976; Kwon et al., 2012; Masten and Hoigne, 1992). OH• is a stronger and less selective oxidant compared to O_3 (Hoigne and Bader, 1983a; Ross, 1975), and reactivity may be altered with pH as OH• radical formation depends on hydroxide concentrations (Bijan and Mohseni, 2005; Glaze et al., 1987; Hoigne and Bader, 1976). O_3 use in wastewater treatment has efficient pollutant-removal for several toxic non-biodegradable compounds (Acero et al., 2001; Beltran et al., 1999; Ikehata and El-Din, 2005a; Ikehata and El-Din, 2005b). The use of O_3 in water treatment processes has shown to be effective for various natural waters (Hoigne and Bader, 1976; Ikehata and El-Din, 2005a; Ikehata and El-Din, 2005b; Ikehata et al., 2016) and in secondary effluents (Hoigne and Bader, 1976; Kwon et al., 2012). O_3 has also been shown to increase the biodegradability of recalcitrant organics (Medley and Stover, 1983; Suzuki et al., 1978; Zhang et al., 2017). Few studies have investigated the degradation of 1,4-dioxane using O_3, but most previous research has focused on the H_2O_2 assisted ozonation (Adams et al., 1994; Ikehata et al., 2016; Kosaka et al., 2000; Kwon et al., 2012; Suh and Mohseni, 2004).

Solubility limitations, oxidant consumption, and short half-life due to instability all act to limit O_3 efficiency for ISCO of groundwater contaminants (Huling and Pivetz, 2006). O_3 is only sparingly soluble (~208 μM or 10 mg L^{-1}) in typical aqueous systems, and has mainly been applied in the subsurface as a gas (Masten and Davies, 1997). The half-life for aqueous O_3 is typically up to one hour due to the reactivity of the OH•, which could make subsurface injection challenging (Dettmer et al., 2017). Radical scavengers, such as salts, transition metals, and organic matter, either dissolved or associated with the subsurface solid materials, can consume oxidant or inhibit radical formation, which ultimately reduces the amount of oxidant available for reaction with contaminants (Brusseau et al., 2011; Crimi and Siegrist, 2003; Marble et al., 2010; Masten and Davies, 1997; Wang et al., 2012; Xu and Thomson, 2009). Recently, interest has increased in developing methods for O_3 stabilization and delivery enhancement to enable the feasibility of ISCO using O_3 (Huling and Pivetz, 2006). These include sparging with mixed surfactant and dissolved O_3 (Kim et al., 2013), the injection of micro and nano-sized bubbles containing O_3 (Scheffer and van de Ven, 2010; Sung et al., 2017), and coupled injection of acetic acid solutions containing dissolved O_3 (Alcantara-Garduno et al., 2008a; Alcantara-Garduno et al., 2008b).

Due to the various reaction mechanisms and relatively high standard oxidation potential of O_3, it has proven to be an effective reagent for ISCO of contaminated soil and groundwater (Bhuyan and Latin, 2012; Clayton et al., 2011; Huling and Pivetz, 2006). However, O_3 is sparingly soluble in typical groundwater systems, and has mainly been introduced as a gas (Masten and Davies, 1997). The above noted rapid half-life for aqueous O_3 severely limits O_3 delivery and treatment potential for groundwater contaminants. O_3 transforms contaminants through either direct oxidation or through decomposition and production of hydroxyl radicals, which then react with contaminants (Clayton et al., 2011). Clayton et al. review the relatively selective direct O_3:contaminant reaction mechanisms and indirect contaminant oxidation by radicals generated by O_3 (Table 2.4). The reactions that produce radicals from O_3 are generally thought to follow either the Hoigne, Staehelin, and Bader model (Hoigne and Bader, 1983a; Hoigne and Bader, 1983b; Hoigne et al., 1985) or the Tomiyasu, Fukutomi, and Gordan model (Tomiyasu et al., 1985) mechanisms. In aqueous solutions, radicals react with a variety of organic and inorganic species,

termed radical scavengers (Clayton et al., 2011). Readers are referred to recent reviews on O_3 chemistry (von Sonntag and von Gunten, 2012).

In general, persulfate activation refers to the use of energy or specific reagents to cause generation of the sulfate radical ($SO_4\bullet^-$) and/or hydroxyl radical ($HO\bullet^-$) in sufficient quantities for contaminant degradation. Activated sodium persulfate can yield both hydroxyl and sulfate radicals. The sulfate radical is slightly lower in electrode potential, but has the ability to persist for weeks. Activated sodium persulfate is capable of producing both hydroxyl and sulfate radicals (Table 2.4) (Block et al., 2004; Tsitonaki et al., 2010). Persulfate can be activated by UV light (He et al., 2014; Tsitonaki et al., 2010), heat (Liang and Bruell, 2008; Liang et al., 2003), alkaline base (Furman et al., 2010),or iron (Ahn et al., 2013; Block et al., 2004; Cai et al., 2014; Chaplin, 2014; Drzewicz et al., 2012; Zhong et al., 2015). Recent focus has been on efficient and low-cost transition metal catalysis including Cu, Co, and others (Anipsitakis and Dionysiou, 2003; Anipsitakis and Dionysiou, 2004; Chaplin, 2014). The release of toxic metal catalysts during treatment is a significant concern and carbon-based graphene alternatives have also recently been proposed (Chen and Carroll, 2016).

Activated hydrogen peroxide and activated persulfate have received increased attention for treatment of recalcitrant contaminants (Ahuja et al., 2007; Ciotti et al., 2009; Fang et al., 2013a; Miller et al., 2012), including use in combined-oxidant approaches. Prior research has shown for example that oxidant decomposition rates and radical generation rates are moderated in binary oxidant systems, thus overcoming the drawbacks of using hydrogen peroxide or persulfate alone (Block et al., 2004; Yan et al., 2016; Yan et al., 2013). One particular peroxone oxidant formulation developed by EnChem Engineering (Newton, MA), OxyZone® is a peroxone activated persulfate based AOP technology. OxyZone® uses a blend of O_3, sodium persulfate, phosphate buffers, and hydrogen peroxide. It is assumed that the presence of O_3 and hydrogen peroxide in the persulfanated oxidant mix results in the production of hydroxyl (•OH) and sulfate ($\bullet SO_4^-$) radicals (Table 2.3 and 2.4). Further, a decrease in pH during oxidation is well documented in this and other activated persulfate-oxidant systems (Block et al., 2004).

A key limitation for implementation of AOP for ISCO of recalcitrant contaminant remediation in groundwater is the short half-lives of strong oxidants (e.g. up to one hour for aqueous O_3 depending on aqueous chemistry) in the subsurface environment (Huling and Pivetz, 2006). These high oxidation-potential or AOP methods are proven *ex situ* applications, but they are considered ineffective for *in situ* application due mainly to short half-lives of the oxidants (e.g., hydroxyl radical) or consumption of oxidant through reaction with oxidizable material other than 1,4-dioxane. Injection of O_3 as a gas into aquifers has been proposed, but the low solubility and instability of O_3 would not allow the transport of the oxidant across the distances needed to treat contaminant plumes. ISCO with $Na_2S_2O_8$ has also been proposed, but it requires mixing the activating agent either above ground (resulting in a highly reactive oxidant with similar transport limitation issues mentioned for O_3) or below ground where mixing effectiveness is questionable. Regardless of the oxidant used, enhanced distribution across larger radii of influence and greater longevity would decrease cost and increase effectiveness.

1,4-Dioxane plumes often consist of low-level contamination dispersed over a large area (Adamson et al., 2014; Anderson et al., 2012). Activated persulfate AOPs are promising because persulfate is more stable in the subsurface than hydrogen peroxide and O_3 permitting oxidative

solutions to travel further when injected in the subsurface (Huling and Pivetz, 2006; Tsitonaki et al., 2010). The potentially larger radius influenced by injected activated persulfate solutions makes these treatments attractive for *in situ* remediation of 1,4-dioxane. Field practitioners have reported success treating 1,4-dioxane *in situ* with activated persulfate (Cronk, 2008). However, there are currently only a few studies in the literature detailing activated persulfate based 1,4-dioxane treatments amenable to *in situ* application (Zhong et al., 2015).

Table 2.4. AOP reaction pathways (Block et al., 2004; Huling and Pivetz, 2006).

Primary Oxidation via Ozone	$O_3 + 2H^+ + 2e^- \rightarrow O_2 + H_2O$
Hydroxyl Radical Formation	$O_3 + H_2O \rightarrow O_2 + 2\bullet OH$ $2O_3 + 3H_2O_2 \rightarrow 4O_2 + 2\bullet OH + 2\ H_2O$
Oxidation by Hydroxyl Radical	$2\bullet OH + 2H^+ + 2e^- \rightarrow 2H_2O$
Primary Oxidation via Persulfate	$S_2O_8^{-2} + 2H^+ + 2e^- \rightarrow 2HSO_4^{-1}$
Hydroxyl and Sulfate Radical Formation	$S_2O_8^{2-} + H_2O_2 \rightarrow 2\bullet SO_4^- + 2\bullet OH$
Oxidation by Hydroxyl Radical	$2\bullet OH + 2H^+ + 2e^- \rightarrow 2H_2O$
Oxidation by Sulfate Radical	$\bullet SO_4^- + e^- \rightarrow SO_4^{2-}$

2.5 Subsurface Oxidant Demand

Strong oxidants may react with water and a variety of dissolved and solid species, and may undergo a series of reactions that cause rapid oxidant decay. Several chemicals (e.g., including transition metals, organics, and radical scavengers) associated with the subsurface materials, both aqueous and solid, can impose a significant oxidant demand, which is the bulk consumption of oxidants by the soil solution, minerals, and soil organic matter (SOM) that ultimately reduces the amount of oxidant available for reaction with contaminants (Brusseau et al., 2011; Crimi and Siegrist, 2003; Marble et al., 2010; Mumford et al., 2004; Urynowicz, 2008; Xu and Thomson, 2009). Xu and Thomson (Xu and Thomson, 2010) investigated the effect of various experimental conditions on the permanganate oxidant demand. They discovered that the initial permanganate concentration, the nature and quantity of oxidizable sediment, and the oxidant solution to sediment mass ratio were the primary determining factors for permanganate consumption rates. The permanganate oxidant demand also showed a strong correlation to sediment total organic carbon while sediment pH, surface area, cation exchange capacity (CEC), and total iron and manganese correlated to a lesser extent. Other studies have focused on the relative reduction capacities of aquifer solids and microbial activity (Hartog et al., 2002; Korom et al., 1996; Mumford et al., 2004). The oxidant demand, as well as the reactivity of the oxidants, provides a serious challenge for the development of ISCO using AOP. Non-specific oxidation of various dissolved and solid species can limit treatment for contaminants of concern. Application of AOP oxidants, such as O_3, for ISCO in groundwater would also be limited by oxidant demand due to the reactivity and non-specificity of radical oxidants. However, little effort has been devoted to investigating the variability and potential controls of O_3 oxidant demand (Clayton et al., 2011; Huling and Pivetz, 2006; Lim et al., 2002; Masten, 1991; Masten and Davies, 1997; Wang et al., 2012).

Groundwater temperature and pH can also influence ISCO reactions. In addition, for field applications, the overall remediation efficiency of ISCO may be significantly influenced by the presence of inorganic salts in groundwater (De Laat and Le, 2005; De Laat and Le, 2006; Riga et al., 2007). Therefore, the influence of inorganic ions on ISCO processes should be examined for each approach. It has also been shown that various inorganic constituents (e.g., salts) present in groundwater may influence ISCO through scavenger effects. Salts can interact with and quench radicals or complex with a metal activator and thus reduce radical production, both of which would reduce contaminant degradation (Beltrán et al., 1998; Bennedsen et al., 2012; Liang et al., 2006; Lipczynska-Kochany et al., 1995; Valentine and Wang, 1998). Furthermore, the presence of some anions (such as ClO_4^-) leads to acidification, which has been observed to inhibit some oxidation reactions (Barbeni et al., 1987; Bennedsen et al., 2012; Lipczynska-Kochany et al., 1995). While the influence of anions (e.g., Cl^-, CO_3^{2-}, HCO_3^{2-}) on the degradation of selected contaminants (e.g., trichloroethene) during ISCO have been reported, minimal research has focused on the inhibition effect of cations.

2.6 Facilitated Transport Using Cyclodextrin

Facilitated transport involves encapsulation and transport of one compound within another compound including host-guest clathrate forming compounds such as surfactants, chelating agents, or cyclodextrins. The host-guest clathrate formation allows additional guest compound dissolution compared to solubility without the complexing agent. Facilitated transport involves the injection of these clathrate-forming compounds to increase the apparent aqueous solubility of low-solubility compounds, which increases the concentrations and enhances transportability of low-solubility compounds in groundwater. At elevated concentrations, surfactants form micelle structures that enhance solubility of organics (e.g., (Adeel and Luthy, 1995; Boving and Brusseau, 2000; Brusseau et al., 1995; Clifford et al., 2007; Edwards et al., 1991; Fountain et al., 1991; Ghoshal and Hill, 2002; McCray et al., 2001; Pennell et al., 1996; Pennell et al., 1997; Rouse et al., 1995; Saba et al., 2001; Schaerlaekens and Feyen, 2004; Shiau et al., 1994; Taylor et al., 2001; West and Harwell, 1992; Yeom et al., 1995; Zhao et al., 2007).

Here we focus on cyclodextrins, which are cyclic D-glucopyranoses bonded through α-1,4-glucosidic linkages, the exterior is hydrophilic (Figure 2.2). They also have a hydrophobic interior into which compounds can partition (Bender and Komiyama, 1978; Boving and McCray, 2000; Connors, 1997; French, 1957; Landy et al., 2012b; Szejtli, 1998). Reviews have discussed inclusion complexation formation within cyclodextrins (Boving and McCray, 2000; Connors, 1997; Landy et al., 2012b). The mechanism that is generally accepted for inclusion-complex formation within the HPβCD cavities is hydrophobic partitioning and displacement of water molecules from the cavity (Connors, 1997), and this partitioning is generally considered to be a weak attraction force that is generally reversible.

Once cyclodextrin (also referred to as CD) complexes the low-solubility compound, transport is dependent on the transportability of CD within the groundwater. The hydrophilic exterior structure allows CD to have relatively high aqueous solubilities for the large size of the organic molecule (Bender and Komiyama, 1978; Blanford et al., 2001). The hydrophilic nature of CD's exterior (especially HPβCD; Figure 2.2) allows the molecules to be transported in groundwater systems with little or no adsorption to the soil, or aquifer, solid surfaces (Brusseau et

al., 1994). Brusseau (Brusseau et al., 1994) found that CD has a negligible effect on the bulk aqueous chemical properties such as pH and ionic strength, and pH or ionic strength variability do not impact the facilitated transport capability of CD (Wang and Brusseau, 1995). Wang and others found that they are generally resistant to biological decay for a period of at least a few months (Wang et al., 1998), and Bender and Komiyama (1978) have suggested that cyclodextrins have a half-life of 48 days while undergoing hydrolysis in extremely reactive conditions. However, CDs may be expected to degrade over the long-term. The simple sugar molecular structure should allow it to be degraded by most indigenous microbial populations. Additionally, CDs have negligible toxicity, because they are sugar-based (Wang et al., 1998).

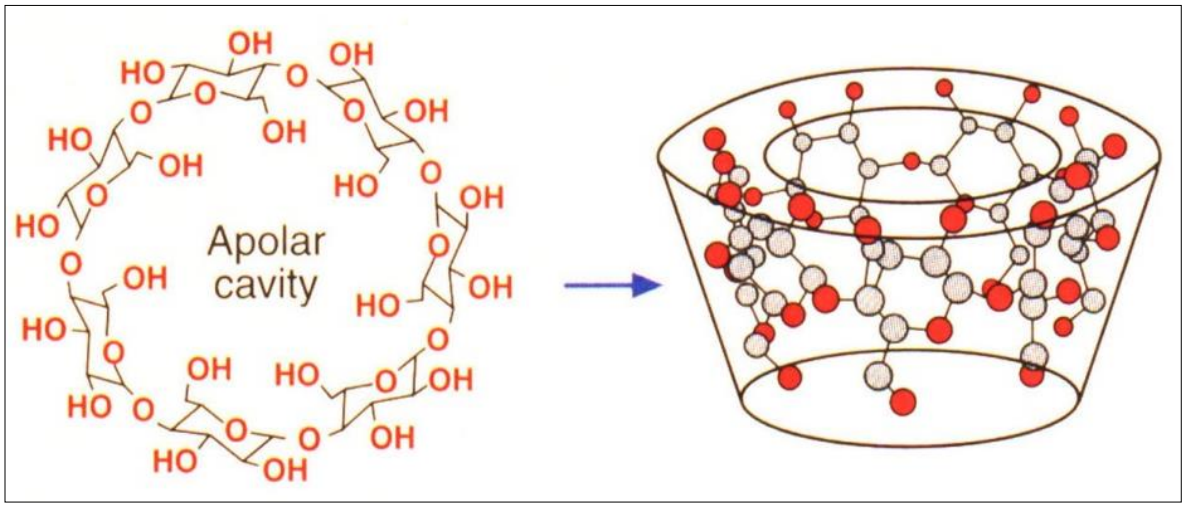

Figure 2.2. Hydroxypropyl-beta-cyclodextrin (HPβCD) chemical structure (Wang and Brusseau, 1993).

Inclusion complex formation has long been an important area in cyclodextrin research (Bender and Komiyama, 1978; Connors, 1997; Saenger, 1980; Szejtli, 1998), which has had increased interest recently for contaminant remediation (Boving and McCray, 2000; Landy et al., 2012b). Although originally developed for drug delivery, cyclodextrins have been used to enhance contaminant solubility, facilitate the transport of both organics and metals, and enhance contaminant extraction for groundwater remediation (Allan et al., 2007; Bizzigotti et al., 1997; Blanford et al., 2001; Boving and McCray, 2000; Boving et al., 2004; Boving et al., 1999; Brusseau et al., 1996; Brusseau et al., 1997; Carroll and Brusseau, 2009; Landy et al., 2012a; McCray et al., 2000; McCray and Brusseau, 1998; McCray and Brusseau, 1999; Skold et al., 2008; Tick et al., 2003; Wang and Matsui, 1994; Wang and Brusseau, 1993; Wang and Brusseau, 1995). CD enhanced contaminant extraction has been successfully used to enhance remediation of sites contaminated with chlorinated solvents and other compounds including pilot tests at Hill AFB (McCray and Brusseau, 1998; McCray and Brusseau, 1999), AFP44 (Blanford et al., 2001), Dover AFB (Tick et al., 2003), and the Naval Amphibious Base Little Creek (Boving et al., 2004). However, until recently, little work has been completed to evaluate CD for delivery of remediation reagents.

2.7 Binding Constant Determination of Complexation Equilibration

A critical area of supramolecular chemistry includes the investigation of host-guest

complex formation processes and the determination of complexation binding constants (K) values for aqueous systems (Connors, 1987), which is the equilibrium constant for the aqueous complex formation reaction as follows (Connors, 1987):

$$Guest + CD \overset{K}{\leftrightarrow} Guest - CD \quad (1)$$

here Guest (or G) is the activity of target compound in the aqueous phase, CD refers to the activity of cyclodextrin molecules, Guest-CD (or G-CD) is the activity of the inclusion complex when the guest compound has partitioned into the CD cavity, and the K is the equilibrium binding (i.e., or formation stability) constant, which can also be defined as:

$$K = \frac{[G-CD]}{[G][CD]} \quad (2)$$

NMR instruments are capable of obtaining high-quality spectra with sub-millimolar concentrations (routinely as low as 10^{-4} M^{-1}) for measuring and determining complexation binding constants up to 106 M^{-1} (Connors, 1987). Shirin et al. (Shirin et al., 2003) evaluated several β-cyclodextrins derivatives as agents for enhancement of the aqueous solubility of two major organic pollutants (e.g., TCE) using ^{1}H-NMR. Yang et al. (Yang et al., 2006) also reported inclusion constants for three different contaminants, including TCE, with two types of cyclodextrins using gas chromatography and partitioning relationships.

Perhaps the most common method for supra-molecular titration experiments is UV-visible spectroscopy. With the right chromospheres, host concentrations in the sub micro molar (10^{-7} M^{-1}) can be used, making the determination of binding constants as high as 109 M^{-1} in simple 1:1 systems (Connors, 1987). For example, Garcia-Rio et al. (Garcia-Rio et al., 2006) used UV-visible spectroscopy to examine competitive binding equilibrium and kinetics for 1,4-dioxane in presence of α-cyclodextrin and β-cyclodextrin.

Another analytical method that is often used is fluorescence spectroscopy that can determine binding constants with analytes at the micromolar or nanomolar (nM) ranges (Connors, 1987). However, few comparisons of these spectroscopic methods for determining binding constants and inclusion complex stoichiometries have been reported. In addition, use of these spectroscopic methods can be applied for direct measurement of the binding equilibria as well as indirectly by competition for complexation when more than one guest compound is present (Connors, 1987; Johnson and Reinsborough, 1992). Development and application of these competitive methods for K determination has been lacking compared to direct spectroscopic methods, and comparisons of these direct and competitive methods are needed for further understanding of method applicability.

2.8 Oxidant Complexation Background

Although AOP would be the preferred ISCO remediation method for 1,4-dioxane, as noted above, there is a significant reagent stability and delivery limitation in our ability to apply AOP as an ISCO remedy. Use of oxidant stabilizers has been considered for increased oxidant stability and transportability within the subsurface (Huling and Pivetz, 2006). Oxidant stabilization generally involves addition of a chemical that forms a complex with an oxidant, which limits oxidant reactivity. Stabilizers have been developed mainly for iron (i.e., chelators) and hydrogen peroxide (H_2O_2) (i.e., phosphates) (Watts et al., 2007). These modified-Fenton reaction methods utilize a

facilitated-transport approach to apply the Fenton reaction for ISCO of organic contaminants (Lee and Lee, 2010; Lewis et al., 2009; Lindsey et al., 2003a; Wang and Brusseau, 1998). Various organic acids have proven effective in enhancing the lifespan of H_2O_2 in soil (Chang et al., 2013; Jung et al., 2013; Watts et al., 2007).

Several researchers have evaluated inclusion complexation formation for various types of chemicals within cyclodextrins (Boving and McCray, 2000; Connors, 1997; Landy et al., 2012b). Although oxidant complexation has not been thoroughly examined for contaminant remediation, it can be considered as similar to the recent development of modified-Fenton reaction methods that utilize a facilitated-transport approach to apply the Fenton reaction for chemical oxidation of organic contaminants including chlorinated solvents (e.g., PCE and TCE), phenol, polycyclic aromatic hydrocarbons, and polychlorinated biphenyls (Lee and Lee, 2010; Lindsey et al., 2003b; Wang and Brusseau, 1998). Cyclodextrins have also been used to complex iron, preventing the consumption of H_2O_2 and precipitation (enhanced solubility) of iron through facilitated transport, using a modified-Fenton reaction (Lindsey et al., 2003a). The effectiveness of the process was found to be dependent both on the chemical nature of CD and pollutant. For instance, a 13-fold increase in the decontamination rate over the control experiment was obtained when degrading PCB-80 in a carboxymethyl-beta-cyclodextrin (CMCD) solution (Lindsay et al., 2003). The oxidation rate was impacted and efficiency was enhanced for polychlorinated biphenyl decay in a CMCD solution, which was linked to formation of a ternary supramolecular complex (i.e., pollutant-cyclodextrin-iron) (Lindsey et al., 2003a). As identified by electrospray-MS and by absorbance spectra (Landy et al., 2012a), this version of CD forms a ternary supramolecular complex (pollutant-cyclodextrin-iron). It is assumed that the degradation of the pollutant in the complex is enhanced by the proximity of the pollutant to the Fenton reaction hydroxyl radical formation site. A ternary complex between hydroxypropyl-beta-cyclodextrin (HPβCD), Fe^{2+}, and pollutants has also been observed (Liang et al., 2007a). Veignie et al. also demonstrated that various types of cyclodextrin increase contaminant apparent solubility and degradation by Fenton's reaction, and they also note formation of a formation of a ternary complex (i.e., pollutant-cyclodextrin-iron) could increase the proximity of the contaminant and oxidant (Liang et al., 2007a; Lindsey et al., 2003a; Veignie et al., 2009). The formation of a ternary complex (i.e., pollutant-cyclodextrin-iron) enhances contaminant degradation by increasing the proximity of the contaminant to the Fenton reaction radical formation location (Lindsey et al., 2003a; Veignie et al., 2009).

The modified-Fenton reactions utilize a complexation agent to facilitate the transport of oxidants (and the oxidation-target contaminants), which improves the reaction effectiveness. Similarly, EnChem Engineering, Inc. has proposed CD co-injection with O_3 to desorb and oxidize contaminants (Ball, 2011). Although O_3 is ionic, it is relatively hydrophobic, and could potentially be attracted to the hydrophobic cavity of HPβCD. Oxidant complexation was investigated through this project to support oxidant facilitated transport and delivery into the subsurface. We have developed facilitated transport of injected oxidants within a CD complex to increase the oxidant transport distance away from an injection well, which can increase the amount of subsurface 1,4-dioxane oxidation. O_3 forms a complex or partitions into the CD cavity, which in turn, increases the oxidant solubility in water and enhances its stability. This leads to an increase in the amount of oxidant (relative to the aqueous solubility) that can be delivered to the target contaminant zone. CD also increases the apparent solubility of co-contaminants (e.g., TCA, TCE) making them more available for degradation by the injected oxidants.

3.0 MATERIALS AND METHODS

3.1 Project Design

Three ISCO approaches for 1,4-dioxane contaminated groundwater treatment were developed through this project. The first is the co-injection of oxidants with delivery agents, and O_3 complexed with cyclodextrin is an example of this system. If oxidants complex or partition into a delivery-agent molecule, the amount of oxidant that can be delivered to the plume can increase. Also, decreases in reactivity during facilitated transport could increase specificity of oxidation for compounds of concern and reduce oxidant consumption due to natural oxidant demand or radical scavengers. The second is the co-injection of mixtures of oxidants including perozone activated persulfate (i.e., OxyZone®; a mix of O_3, hydrogen peroxide, persulfate, and phosphate buffers). These two methods involve the use of aqueous solutions that can be injected into groundwater plumes and used to develop an aqueous flow-through treatment system. An additional application uses solid materials to stabilize and catalyze oxidants. The system developed herein uses iron (either filings or minerals in sediments) to catalyze persulfate. Persulfate may be transported significant distances in contaminated groundwater systems, and *in situ* persulfate activation could be used to target treatment of 1,4-dioxane contaminated groundwater. These approaches have been examined through nine studies that are listed below with the objective of each study. The publication citation information is also listed below and along with additional project publications in the Appendices, and the remainder of this report documents the approaches and results of these studies.

3.1.2 Ozone Oxidant Demand Impact Stabilized by Cyclodextrin (Ozone Stabilized by Cyclodextrin)

The purpose of this study was to examine the ability of HPβCD to complex O_3, determine the potential for O_3 to transform HPβCD, and observe the effect of the complexation on the lifespan of O_3 in aqueous solution. Secondly, variance in the O_3 oxidant demand of aquifer solids due to varying amounts of SOM and the presence of HPβCD was examined.

Dettmer, A., Ball, R., Boving, T.B., Khan N.A., Schaub, T., Sudasinghe, N., Fernandez, C.A., Carroll, K.C. (2017) Stabilization and Prolonged Reactivity of Aqueous-Phase Ozone with Cyclodextrin. Journal of Contaminant Hydrology, 196:1–9.

3.1.3 Oxidant Demand and Scavenging of 1,4-Dioxane Decay (Oxidant Mixture with Iron Activation)

The purpose of this study was to investigate the influence of groundwater ionic composition (i.e., radical scavengers) on the degradation of 1,4-dioxane. A promising binary oxidant system, siderite-activated hydrogen peroxide (H_2O_2) coupled with persulfate, was used as a representative ISCO reagent within batch experiments due to its high oxidation potential and moderate oxidant decomposition rate.

Yan, N., Liu, F., Chen, Y., Brusseau, M.L. (2016) Influence of groundwater constituents on 1,4-dioxane degradation by a binary oxidant system. Water Air Soil Pollution, 227: article 436.

3.1.4 Cyclodextrin Inclusion Complex Measurement (Ozone Stabilized by Cyclodextrin)

The purpose of this investigation was to measure and compare the inclusion binding constant values (i.e., formation constant for complex equilibration) and complexation stoichiometry for 1,4-dioxane, TCE, TCA, and O_3 with HPβCD using both direct and competitive spectroscopic methods. In addition, the impacts of aqueous chemistry variability (e.g., pH and ionic strength) on binding constant values were examined to evaluate variability within natural water systems.

Khan, N.A., Johnson, M.D., Carroll, K.C. (2018) Spectroscopic Methods for Aqueous Cyclodextrin Inclusion Complex Binding Measurement for 1,4-Dioxane, Chlorinated Co-Contaminants, and Ozone. Journal of Contaminant Hydrology, 210(March): 31-41.

3.1.5 Cyclodextrin Enhanced Ozonation of 1,4-Dioxane (Ozone Stabilized by Cyclodextrin)

The purpose of this study was to quantify and compare removal kinetics for 1,4-dioxane and its co-contaminants, TCE and TCA, both in single and multiple contaminant systems with aqueous O_3 alone and O_3 with HPβCD. Batch experiments were used to quantify pseudo first order reaction rate constants.

Khan, N.A., Johnson, M.D., Kubicki, J.D., Holguin, F.O., Dungan, B., Carroll, K.C. (In Review) Cyclodextrin-Enhanced 1,4-Dioxane Treatment Kinetics with TCE and 1,1,1-TCA Using Aqueous Ozone. In review.

3.1.6 Peroxone Activated Persulfate Treatment of 1,4-Dioxane (Peroxone Activated Persulfate)

This purpose of this study was to quantify and compare removal kinetics of 1,4-dioxane and its common co-contaminants TCE and TCA during treatment with a peroxone activated persulfate (PAP) based AOP (OxyZone®). Batch experiments were used to quantify pseudo first order reaction rate constants.

Eberle, D., Ball, R., Boving, T.B. (2016) Peroxone activated persulfate treatment of 1,4-dioxane in the presence of chlorinated solvent co-contaminants. Chemosphere 144:728-735.

3.1.7 Siderite Activated Peroxide & Persulfate Contaminant Treatment (Oxidant Mixture with Iron Activation)

This purpose of this study was to explore reaction thermodynamics for the activated hydrogen peroxide and the activated binary hydrogen peroxide-persulfate oxidant systems. In this study, oxidation of TCE and DCA was examined at several temperatures. Iron, through the use of siderite, a common sedimentary mineral, was employed as the persulfate activation reagent. Batch experiments were used to quantify reaction rate constants.

Yan, N., Li, M., Liu, Y., Liu, F., Brusseau, M.L. (2017) Kinetic and Thermodynamic Studies of Chlorinated Organic Compound Degradation by Siderite-Activated Peroxide and Persulfate. Water Air Soil Pollution, 228, article 453.

3.1.8 Aqueous Ozone Transport and Oxidant Demand Reactivity (Ozone Stabilized by Cyclodextrin)

The purpose of this study was to quantify aqueous O_3 solute transport in sedimentary aquifer materials. Batch experiments, dynamic soil column tracer experiments, and reactive solute transport modeling was used to observe the mass recovery of aqueous-phase O_3 at different flow rate and different column distances, to compare the reaction kinetics of O_3 from column experiment and predictive modeling; and to compare the reaction kinetics of aqueous-phase O_3 in batch and column experiments, which examined system performance of O_3 injection for ISCO treatment of groundwater contaminants.

Khan, N.A., Carroll, K.C. (In Review) Transport of Aqueous Ozone in Saturated Porous Media with Oxidant Attenuation and Demand Assessment for In Situ Contaminant Oxidation. In Review.

3.1.9 Transport and Peroxone Activated Persulfate Treatment of 1,4-Dioxane (Peroxone Activated Persulfate)

The principal objective of this study was to investigate the degradation of 1,4-dioxane through oxidation with OxyZone® (i.e., PAP) under dynamic, flow through (i.e., dynamic soil column tracer experiments) conditions that mimic the *in situ* treatment of groundwater plumes.

Cashman, M.A., Boving, T.B. (In Preparation 2018) 1,4-Dioxane treatment with peroxone activated persulfate: Large scale column experiments. Manuscript prepared for submission.

3.1.10 1,4-Dioxane Treatment Using Persulfate Activated By Iron Filings (Oxidant Mixture with Iron Activation)

The objective of this study was to investigate the activation of persulfate by iron filings, and the resultant degradation of 1,4-dioxane. Batch and dynamic soil column tracer experiments were conducted to determine magnitudes and rates of degradation. Furthermore, the mechanisms for persulfate activation and1,4-dioxane degradation were explored by using electron scanning microscopy-energy dispersive X-ray spectroscopy (SEM-EDS), X-ray diffraction (XRD), and inductively coupled plasma mass spectrometry (ICP-MS) to characterize solid and aqueous phase geochemistry, while free-radical formation was measured using electron paramagnetic resonance (EPR) spectroscopy.

Zhong, H., Brusseau, M.L., Wang, Y., Yan, N., Quig, L., Johnson, G.R. (2015) In situ activation of persulfate by iron filings and degradation of 1,4-dioxane. Water Research, 83, 104-111.

3.2 Ozone Oxidant Demand Impact Stabilized by Cyclodextrin Materials and Methods

3.2.1. Materials

Hydroxypropyl-β-cyclodextrin (90% purity technical grade with an average molecular weight of 1375 g mol^{-1}, Lot #BCBK6962V) was purchased from Sigma-Aldrich (Milwaukee, WI). A synthetic groundwater solution containing 9 mg/L $Ca(NO_3)_2$, 85 mg/L $CaCl_2$, 124 mg/L $MgSO_4$, 171 mg/L $NaHCO_3$, and 20 mg/L NaCl was used for all experiments. The synthetic groundwater was used to represent the chemistry of the groundwater at Tucson, Arizona, USA (Matthieu et al.,

2013), which is the location of the AFP44, 1,4-dioxane-contaminated site. Characteristics of the synthetic groundwater are presented in Table 3.1. A Barnstead NANOpure II (Series 550, Dubuque, Iowa) system was used to purify water used for all solutions to >18 MΩ-cm, and all experiments were conducted at 20(±1)°C.

Table 3.1**.** Characteristics of synthetic groundwater used for all experiments.

Description	pH	TDS (mg/L)	Conductivity (µS/cm)	Eh (mV)
Synthetic Groundwater	7.9	379	565	212

Table 3.2 Average groundwater composition used to develop synthetic groundwater composition (after Mattieu et al., 2013).

Tucson Groundwater	**Composition (mg/L)**
Sodium	54.7
Calcium	32.9
Magnesium	25.0
Nitrate	6.8
Chloride	66.5
Bicarbonate	99.0
Sulfate	124.0

3.2.2. Soil characterization and biosolid amendment

Subsurface solids for the oxidant demand experiments were collected during drilling at AFP44 in Tucson, Arizona. 10 mL subsamples were collected and placed in 40 mL borosilicate glass volatile organic analysis (VOA) vials containing 20 mL of methanol (99.9% pure). The subsamples were placed on a Lab-Line Orbit shaker table to equilibrate for 24 hours at 250 RPM after which they were centrifuged at 5,000 RPM for 10 minutes 2 mL subsamples of the supernatant were removed from the vials with a gastight syringe (Hamilton Company, Reno, Nevada), and injected into 2 mL auto sampler vials with no headspace. Gas chromatography-mass spectrometry (GC-MS; LECO) analyses did not detect any contaminants, which confirmed that the sediment was uncontaminated or contaminants had volatilized. Additionally, wastewater biosolids (dry powder) were obtained from the waste-water treatment plant in Las Cruces, New Mexico, and variable amounts were added to two subsamples of AFP44 sediment to generate a total of three soils with increasing amounts of SOM (Table 3.3), as determined by the Walkley and Black titration method (Nelson and Sommers, 1996). The three soils all had a clay loam texture. Bulk density and porosity were determined by gravimetric and volumetric methods. Sediment pH, CEC, textural analysis, and total extracted metals by inductively coupled plasma – optical emission spectroscopy (ICP-OES; Perkin Elmer) measurements were completed.

Table 3.3 Characteristics of AFP44 soil and two biosolid-amended AFP44 soils.

Property	AFP44	Amended-1	Amended -2
Soil Organic Matter or SOM (%)	0.22	0.62	1.17
Cation Exchange Capacity or CEC (meq/100g)	20.6	23.4	26.6
Paste pH	8.27	7.54	7.46
Porosity	0.65	0.56	0.55
Bulk Density (g/cm^3)	0.88	0.96	1.0

3.2.3. Chemical analysis

Aqueous O_3 concentrations were determined according to the indigo method (Bader and Hoigné, 1981) using a Milton Roy Spectronic 401 spectrophotometer, which has a reported precision to be 2% or 3 μg/L for O_3 analysis. Aqueous HPβCD samples were analyzed by fluorescence methods (Kondo et al., 1976) using a LS-55 Perkin Elmer spectrofluorometer. UV-vis spectroscopy wavelength scans were also used to confirm HPβCD:O_3 complexation (SpectraMax M2, Molecular Devices). Additionally, HPβCD samples were analyzed by positive-ion electrospray ionization (ESI) Fourier transform ion cyclotron resonance (FT-ICR) mass spectrometry (MS), performed with a hybrid linear ion trap 7 T FT-ICR mass spectrometer (LTQ FT, Thermo, San Jose, CA). The mass spectrometer was equipped with a chip-based nano-electrospray ionization and sample-handling robot (Advion Triversa NanoMate) to produce positively- and negatively-charged ions. Prior to mass spectral analysis, samples were diluted 2-fold in methanol that contains 0.1% formic acid and 0.3 μM reserpine as an internal standard for signal normalization. Mass spectra were collected at a mass range of 300-2000 m/z and at mass resolving power of $m/\Delta m_{50\%}$ = 400,000 (m/z 400). Internal mass calibration of FT-ICR mass spectra produces sub-part-per-million mass measurement accuracy, and enables the direct determination of elemental composition from measured mass to charge ratios. Thus, compounds were identified at the level of elemental composition based on accurate mass measurement by FT-ICR MS and linear ion trap mass spectra were used for relative quantitation. Peak lists generated from linear ion trap mass spectra were normalized to the internal standard signal by summation of all signals for doubly-charged HPβCD ions (singly-charged ions were not observed for all samples) and division by the internal standard signal intensity.

3.2.4. Ozone and HPβCD decay experiments

Batch, time-series experiments were conducted to measure the decay kinetics of O_3 in HPβCD solutions of various concentrations including 728 μM, 364 μM, 72.8 μM and 2.2 μM (1.0 g/L, 0.5 g/L, 0.10 g/L and 3.0 mg/L, respectively). The above HPβCD concentrations were prepared as 500 mL in synthetic groundwater, and then transferred to 1 L volumetric flasks. Gas-phase O_3 was generated using a G-series Pacific O_3 Generator (model #G1110101, Benicia, California), and sparged into another 500 mL of synthetic groundwater until the desired aqueous-phase O_3 concentration was reached (1.0 mg/L O_3 for experiments with 728 μM, 364 μM, 72.8 μM, and 0 μM HPβCD and 1.5 mg/L O_3 for the experiment with 2.2 μM HPβCD). The O_3 solutions were then mixed with the HPβCD solutions, diluting both solutions 50% by volume. The O_3 and HPβCD solutions were then transferred to 125 mL amber VOA vials in triplicate without

headspace. Two control experiments were conducted with O_3 in synthetic groundwater without HPβCD. The vials were inverted every 24 hours to ensure thorough mixing. Samples were prepared in triplicate, the vials were sampled sacrificially at predetermined time intervals, through 70 hours of reaction time, with a gastight syringe (Hamilton Company, Reno, Nevada) for indigo method analysis of O_3, and 95% confidence intervals were calculated. Samples collected at each time point were also monitored for pH, temperature, and oxidation-reduction potential. Samples collected at the end of these experiments and additional mixtures prepared at various HPβCD (5-500 mg/L; 7-688 M) and O_3 (0.5-2 mg/L; 0.024-0.096 M) concentrations, which were analyzed for HPβCD and transformation potential.

3.2.5. Ozone delayed release experiments

Additionally, the delayed release of O_3 from the HPβCD cavity was measured in a separate set of batch, time-series experiments. The primary difference between the delayed release and O_3 decay experiments was that the former contained indigo in the reactor vial which was monitored over time during the experiment, and the later experiments did not contain indigo. The O_3 and HPβCD solutions were prepared as above (with various O_3 and HPβCD mixture concentrations). 90 mL subsamples of the mixture were immediately transferred to 125 mL amber VOA vials containing 10 mL of a potassium indigo trisulfonate solution according to the method of O_3 analysis. Control experiments, used to monitor natural indigo decay, were also conducted as above except they did not contain O_3. Samples were collected at various time points to measure the decrease in absorbance, indigo transformation, and apparent cumulative release of O_3 into solution. Samples were prepared in triplicate, 95% confidence intervals were calculated, and subsamples were also monitored for pH, temperature, and oxidation-reduction potential.

3.2.6. Oxidant demand

The ASTM method D7262-10 (permanganate) (ASTM, 2010) is a 48 hour measure of oxidant loss upon equilibration with excess oxidant (100 ml of 20,000 mg/l $KMnO_4$ mixed with 50 ml soil), and this method was modified to examine the effect of HPβCD on the O_3 oxidant demand of the AFP44 sediment. The oxidant demand method was modified by reducing the amount of time and soil to allow excess O_3 to be present and measureable at the end of the experiment. The oxidant demand procedure used 0.1 grams of the sediment weighed out into triplicate amber 125 mL VOA vials. A fourth vial was used as the control, and contained no aquifer sediment. This oxidant demand method was repeated for all three soil samples to evaluate the impact of biosolid amendment. Another experiment was used to compare the demand with and without HPβCD for the non-bioamended, AFP44 soil. The O_3-HPβCD solution was prepared as above using 1.5-mg/L O_3 and 1.5-g/L HPβCD (after mixing) then 124 mL of the solution was added to each of the vials, and was then inverted to ensure the solution was thoroughly introduced to the aquifer solids. After one minute for each experiment, the supernatant was filtered using oxidant-resistant glass fiber filter paper (from Advantec; Japan, Lot #31115709), and was immediately analyzed for O_3 concentration using the indigo method.

3.3 Oxidant Demand and Scavenging of 1,4-Dioxane Decay Materials and Methods

3.3.1. Chemicals

All solutions used in this study were prepared using ultrapure (filtered, distilled, deionized) water (Millipore Model Milli-Q Academic A10), except where noted. All of the reagents were reagent grade or higher. Siderite was purchased from the Wuhan Iron and Steel (Group)

Corporation, China; hydrogen peroxide (H_2O_2, ~30 wt. % in water), 1,4-dioxane ($C_4H_8O_2$, ≥99%), ascorbic acid, sodium chloride (NaCl, ≥99.8%), sodium sulfate (Na_2SO_4, ≥95%), sodium bicarbonate ($NaHCO_3$, ≥99.8%), potassium chloride (KCl, ≥99.8%), calcium chloride ($CaCl_2$, ≥96%), magnesium chloride ($MgCl_2$, ≥97%) were obtained from Beijing Chemical Works, China; sodium persulfate ($Na_2S_2O_8$, >98%) was purchased from the Xilong Chemical Co., Ltd, China.

The following reagent concentrations were used for all of the experiments. For 1,4-dioxane, 10 μL of 1,4-dioxane was added to each vial for the relevant experiments. This quantity is equivalent to 11.69 mM (1,030 mg/L) in solution. Concentrations of persulfate, H_2O_2, and siderite in the final solutions were 6.3 mM (1,500 mg/L), 0.15 M (5100 mg/L), and 11,450 mg/L respectively for all experiments. The oxidant concentrations are much lower than the concentrations typically used for standard field ISCO applications. Thus, use of these concentrations will produce conservative results.

3.3.2. Experiment setup

Batch experiments (in triplicate) were conducted at 20±1 ^oC with 20 mL borosilicate vials fitted with PTFE septum caps. Two sets of control experiments were set up. One set comprised only ultrapure water and 1,4-dioxane, and was used to evaluate the loss of 1,4-dioxane through any potential mass-loss processes during the study. Another control group contained oxidant and contaminant to determine whether 1,4-dioxane could be degraded in the absence of activator.

Three sets of treatment reactors were used. One set of reactors was designed to compare 1,4-dioxane degradation efficiency in ultrapure water and groundwater. The groundwater was collected from a monitoring well located in the China University of Geosciences (Beijing), China. The chemical composition of the groundwater is shown in Table 3.4. The estimated mineralization of the studied groundwater is 412.45 mg/L by solving Eq. (3), which indicates the groundwater used herein was a relatively low mineral content.

$$M = \sum M_{cation} + \sum M_{anion} \quad (3)$$

Ultrapure water or groundwater was used to create the solutions of $Na_2S_2O_8$, and H_2O_2. Then 1,4-dioxane was added to the vial. The total solution volume was 10 mL. Each vial contained 0.1145 g siderite.

The second reaction group was designed to evaluate the influence of anions on 1,4-dioxane degradation by the binary oxidant system. Three common anions (Cl^-, SO_4^{2-}, HCO_3^-) were tested. Solutions of 0.6 mM NaCl or $NaSO_4$ or $NaHCO_3$, 6.3 mM $Na_2S_2O_8$, and 150 mM H_2O_2 were added to the vial. Then 1,4-dioxane was added to the vial. The total solution volume was 10 mL. Each vial contained 0.1145 g siderite.

The third reaction group was designed to evaluate the influence of cations on 1,4-dioxane degradation by the binary oxidant system. Three common cations (K^+, Ca^{2+}, Mg^{2+}) were tested. Solutions of 0.6 mM KCl or $CaCl_2$ or $MgCl_2$, 6.3 mM $Na_2S_2O_8$, and 150 mM H_2O_2 were added to the vial. Then 1,4-dioxane was added into the vial. The total solution volume was 10 mL. Each vial contained 0.1145 g siderite.

Table 3.4 The chemistry compositions of the groundwater.

Major ions detected in the groundwater (mg/L)									
K^+	Na^+	Ca^{2+}	Mg^{2+}	Fe^{3+}	Fe^{2+}	Cl^-	NO_3^-	SO_4^{2-}	HCO_3^-
2.22	18.38	80.75	38.18	ND[a]	ND	52.94	17.19	74.89	255.8
Trace elements detected in the groundwater (μg/L)									
Co	Cr	Cu	Mn	Mo	Ni	Ti	Sr	V	Zn
0.24	6.44	2.75	0.52	4.38	0.65	0.82	2733	1.19	3.31
As	Ba	Be	Cd	Ga	Li	Pb	Rb	Sc	U
0.65	81.9	0.12	0.13	0.02	3.21	0.14	0.94	0.76	2.58

[a] Not detected

Another reaction group was designed to evaluate the influence of ion concentrations on 1,4-dioxane degradation by the binary oxidant system. Two ions (HCO_3^- and Ca^{2+}) were tested. Solutions of 0.2/0.6/1/2 mM $NaHCO_3$ or $CaCl_2$, 6.3 mM $Na_2S_2O_8$, and 150 mM H_2O_2 were added to the vial. Then 1,4-dioxane was added to the vial. The total reaction volume was 10 mL. Each vial contained 0.1145 g siderite.

After preparation, the vials were maintained at 20 ± 1 ºC in an air bath for the experiments. At selected time-points, samples were collected and ascorbic acid was added to quench further oxidation. The pH of the siderite-activated binary H_2O_2-persulfate system is ~3. HCO_3^-/H_2CO_3 is expected to be the dominant carbonate species at equilibrium in the system.

3.3.3. Analytical methods

Dioxane was analyzed using gas chromatography (Agilent GC6820) equipped with a headspace autosampler, a flame ionization detector (FID), and a 30 m × 0.53 mm DB-5 capillary column. External standards were used for quantification. The temperatures of the injection port and detector were 200 and 250 ºC, respectively. The initial oven temperature was 50 ºC, maintained 2 minutes, and then heated at a rate of 10 ºC/min to a final temperature of 110 ºC.

3.4 Cyclodextrin Inclusion Complex Measurement Materials and Methods

3.4.1. Materials

Cyclodextrins (or CDs) used herein included HPβCD (1460 g mol^{-1} from Sigma Aldrich with ≤7.0% loss on drying and ≤5.0% polypropylene glycol) and gamma cyclodextrin or γ-CD (1297 g mol^{-1} from Wacke Chemie AG.Company). These were selected as they are two of the most commonly used CDs, and γ-CD has a larger cavity and aqueous solubility. Reagent grade 1,4-dioxane, TCA, and TCE were purchased from Sigma Aldrich with 99% purity. Reagent grade sodium hydroxide (NaOH) and hydrochloric acid (HCl) were purchased from Sigma Aldrich with 99% purity. Reagent grade sodium chloride (EM Science; 99% purity) and 6-p toluidine-2-naphthalenesulfonic acid or TNS (Eastman Kodak Company with 99% purity) were used as described below. O_3 was generated by in-lab O_3 generator (Pacific Ozone; Model no. G1110101; Serial no. 8496). For all experiment, a Barnstead NANOpure II (Series 550, Dubuque, Iowa) dionization system was used after reverse osmosis to purify water to >18 MΩ-cm, which was then used (hereafter termed DI water) for all solutions. All experiments were conducted at 22(±1)°C (controlled by thermostat).

3.4.2. Chemical Analysis

All measurements – UV and fluorescence - were performed with a Molecular Devices SpetraMax M2 spectrophotometer. Aqueous O_3 concentrations were determined spectrophotometrically using the indigo method (Bader and Hoigné, 1981) and also with an O_3 probe (Model Q46H/64; ATi). Aqueous HPβCD and TNS sample concentrations were analyzed by fluorescence methods (Kondo et al., 1976), and the lower detection limit of HPβCD for both fluorescence and UV was $6.8x10^{-3}$ mM and upper detection limit was 13.7 mM. Fluorescence intensities of HPβCD:TNS, γ-CD:TNS, and CD:TNS:guest complexes were measured with excitation at 387 nm and emission at 478 nm. UV spectroscopy was conducted from 180 – 700 nm. The lower detection limit of TCE and TCA by UV was 0.075 mM and upper detection limit was 3.0 mM, and the lower to upper detection limit of O_3 for UV was 0.0208-0.2083 mM. All measurements were triplicated, and mean and standard deviation intervals are reported.

3.4.3. Direct Measurement of Binding Constants

UV measurements of solutions with and without the combination of a host and guest indicates inclusion complex through the formation of absorbance shifts (magnitude changes) and an isosbestic point (or the cross over intersection of absorbance versus wavelength spectra) (Connors, 1987). Stoichiometry and the binding constants of the complexes can be evaluated upon examination of differences in relative level absorbance at the wavelengths between single (i.e., uncomplexed) and multiple compound (i.e., complexed) solutions. Our analysis was based on the assumption that the inclusion-complex stoichiometry of each guest within HPβCD was 1:1 (Boving and McCray, 2000; Connors, 1997; Landy et al., 2012b).

Separate host and guest stock solutions were mixed to create various compositions, and spectroscopic measurements were conducted upon equilibration. The inclusion complex formation kinetics and time to equilibrium for guest compounds within CD are known to proceed rapidly within seconds (Nakatani and Hiromi, 1984). UV spectra of solutions containing HPβCD with and without guest molecules (i.e., 1,4-dioxane, TCA, TCE, or O_3) were measured over a range of HPβCD concentrations (0.08 mM - 2.7 mM) and at two different concentrations of TCE (0.76 and 1.52 mM), TCA (0.75 mM and 1.5 mM), O_3 (0.03 mM and 0.015 mM), and 1,4-dioxane (0.014 M and 0.03 M). For TCA, 1,4-dioxane, and TCE experiments, samples were collected with an air-tight syringe (Hamilton) and stored in amber vials without headspace. Absorption maxima were used to determine absorbance changes, and two direct spectroscopic approaches were used to calculate the binding constants. One method is the Benesi-Hildebrand approach. The relevant equation is shown as follows:

$$\frac{b}{\Delta A} = \frac{1}{[G]_i K \Delta \varepsilon [L]} + \frac{1}{[G]_i \Delta \varepsilon} \qquad (4)$$

where b is the length of cuvette (i.e., 1 cm), ΔA is the change in absorbance due to adding HPβCD, $[G]_i$ is the concentration (mM) of the guest substrate (i.e., TCE, TCA, 1,4-dioxane, or O_3), K (mM^{-1}) is the complex formation constant or binding constant, Δε is the extinction coefficient, and [L] is the concentration (mM) of ligand HPβCD. If the plots of 1/ΔA as a function of 1/HPβCD concentration are linear, then based on the Benesi-Hildebrand equation, binding constants were calculated as the linear regression y-intercept divided by the slope (Connors, 1987). The second method is the Scott's equation:

$$\frac{b[L]}{\Delta A} = \frac{[L]}{[G]_i \Delta \varepsilon} + \frac{1}{[G]_i K \Delta \varepsilon} \quad (5)$$

where b, ΔA, $[G]_i$, K, Δε, and [L] are as defined previously. A plot of HPβCD concentration divided by the change in absorbance as a function of 1/HPβCD concentration was used with the Scott's equation to determine binding constants as the slope divided by the y-intercept (Connors, 1987). All experiments were conducted at least three times, measurements for HPβCD:TCE were also conducted three additional times (Supplementary Data), and mean and standard deviations for binding constants are reported.

3.4.4. Indirect Measurement of Binding Constants

Two experiments were generally required for measuring the K values for two guest compounds (present in the same solution) through competitive complexation, which included a first experiment with one guest only to determine K for that guest followed by a second experiment with two guests in solution to determine the K for the second guest. Here, we used TNS as a competitive guest compound (i.e., the first guest) in combination with each of the other individual guest compounds. In the first series of experiments (i.e., TNS and HPβCD or γ-CD), a consistent amount of TNS was added to a series of HPβCD (0.01 to 10 mM) or γ-CD (0.048 to 12.34 mM) solutions, and increases in fluorescence intensity were used to determine the K of the HPβCD and γ-CD with TNS using Equation 4. The second series of experiments were used to determine K values for a second guest in solutions with the first guest (i.e., TNS) also present, and both sets of experiments were conducted with identical concentrations of HPβCD or γ-CD and with the identical concentration of TNS. The solutions for the second series of experiments also contained the additional guest compound (O_3, TCE, TCA, or 1,4-dioxane) without dilution of TNS and HPβCD or γ-CD.

Aqueous stock solutions of TCE and TCA were prepared with a concentration of 3 mM in 250 ml volatile organic analysis vials, and were equilibrated on a shaker table at 400 rpm for 1 week, and aqueous stock solution of 1,4-dioxane was prepared at a concentration of 0.11 M in 500 mL volumetric flask. A series of HPβCD solutions were prepared from a 11 mM HPβCD aqueous stock. The fluorescence titration experimental solutions contained 10 µM or 1 µM of TNS, and the concentration of HPβCD was from 0.08 to 2.7 mM to avoid dilution. Experiments were repeated at differing initial pH values (i.e., DI was pH 6 and pH was adjusted to 9 by titration using 0.1 M NaOH) and ionic strengths (i.e., addition of appropriate amounts of NaCl to prepare 100 mM and 50 mM solutions) to investigate the impact of natural water chemistry variability on these inclusion complexation reactions.

Inclusion binding constant values for HPβCD or γ-CD with TNS (i.e., K_1) and HPβCD or γ-CD with the other guest (K_2) complexes were determined from the following equations. Here, guest (G) was an additional compound including TCE, TCA, 1,4-dioxane, or O_3. For a CD solution containing both TNS and G, where both TNS and G are competing for complexation with CD, the total CD concentration can be observed by the following equation (Johnson and Reinsborough, 1992):

$$[CD]_i = \frac{1}{QK_1} + \frac{[G]_i K_2}{QK_1 + K_2} + \frac{[TNS]_i}{Q+1} \quad (6)$$

where K_1 is the inclusion binding constant for the 1:1 CD:TNS complex; K_2, the inclusion binding constant for the 1:1 HPβCD or γ-CD and G complex; [G]i, the initial concentration of guest; and [TNS]i, the initial concentration of TNS. Q is defined as the ratio of free TNS to CD-bound TNS. In terms of fluorescence intensities, Q equates to $(I_0\text{-}I)/I$ where I is the observed fluorescence intensity after addition of the guest molecule, and I_0 is fluorescence due to the 1:1 HPβCD:TNS or γ-CD:TNS complex when all TNS is complexed into the CD cavity. From a Benesi-Hildebrand-type plot (Equation 4) of the data from the first experiment (with TNS but no additional guest present), the K_1 for the 1:1 HPβCD:TNS or γ-CD:TNS complex was determined from the ratio of the y-intercept to the slope. The linearity of these plots gives assurance of 1:1 complexes stoichiometry. The dilute solution concentration ranges were used here for binding equilibrium measurements, whereas higher concentration solutions may develop for applications of CD with O_3 for contaminant remediation.

The relevant equation, for solutions containing TNS and another guest compound, quantifying the competing complexation equilibriums is the following (Johnson and Reinsborough, 1992):

$$\frac{Q_1 Q_2}{Q2-Q1} = \left(\frac{1}{[G]_i K_2}\right) Q_2 + \frac{1}{[G]_i K_1} \qquad (7)$$

where Q_1 and Q_2 denote the Q values for the first experiment (TNS only without competitive guest) and second experiment (with TNS and the competitive guest), respectively. A linear plot of $Q_1Q_2/(Q_2\text{-}Q_1)$ against Q_2 has a slope of $1/[G]_iK_2$. The ratio of the y-intercept to the slope should be K_2/K_1, and these plots were used to evaluate the stoichiometry of the complexes and for determination of K_2 values. All experiments were conducted at least three times, competitive measurements for HPβCD:TCA were also conducted six additional times (Supplementary Data), and mean and standard deviations for binding constants are reported.

3.5 Cyclodextrin Enhanced Ozonation of 1,4-Dioxane Materials and Methods

3.5.1. Materials

1,4-Dioxane was the recalcitrant water contaminant under investigation, and experiments were conducted with and without this solvent stabilizer's chlorinated co-contaminants (Mohr et al., 2010), TCA and TCE (Adamson et al., 2015; Anderson et al., 2012; Zenker et al., 2003). Reagent grade 1,4-dioxane (99% purity, Sigma Aldrich), TCE (99.5% purity, Sigma Aldrich), and TCA (99% purity, Division of Green Technology Inc.) organic contaminants were obtained and used as purchased. Reagent grade sodium thiosulfate pentahydrate, sodium bicarbonate, sodium hydroxide, and hydrochloric acid were purchased from Sigma Aldrich, and reagent grade sodium chloride was purchased from EM Science. O_3 was generated by in-lab O_3 generator (Pacific Ozone; Model no. G1110101; Serial no. 8496), which was sparged through aqueous solutions to dissolve O_3 before each experiment. HPβCD was purchased from Sigma Aldrich with ≤7.0% loss on drying, ≤5.0% polypropylene glycol, and average molecular weight 1460 g $mole^{-1}$. For all experiments, a Barnstead NANOpure II (Series 550, Dubuque, Iowa) system was used to purify reverse osmosis water to >18 MΩ-cm, which was then used (DI water) to prepare all solutions.

3.5.2. Contaminant removal kinetic experiments

1,4-Dioxane, TCE, and TCA contaminant and O_3 solutions prepared in DI water with and without HPβCD were mixed to create desired concentrations in 1 L amber glass bottles without

headspace, and samples were collected. This mixed solution was immediately transferred to a number of 40 mL amber volatile organic analysis vials (reaction vial with Teflon seal without headspace), and these vials were sampled sacrificially at predetermined time intervals with a gastight syringe (Hamilton Company, Reno, Nevada). For each sampling event, 8.5 mL of sample (with additional duplicate samples) were collected from the 40 mL volatile organic analysis vial and placed into 20 mL glass vials containing 1.5 mL of 2 M sodium thiosulfate solution to quench remaining oxidant upon sample collection.

This series of well-mixed 40 mL reaction vial time course experiments were conducted to evaluate reaction trends and kinetics over a range of experimental parameters. To determine the relationship between the rate constant of oxidative removal of contaminants and the amount of oxidant required, various initial solution concentrations of 1,4-dioxane, TCE, and TCA solutions (e.g., for 3:1 oxidant:contaminant ratio: 0.056 mM 1,4-dioxane, 0.076 mM TCE, and 0.037 mM TCA) were treated with the highest concentration of initial dissolved O_3 (0.125 mM to 0.2 mM) in DI water. This resulted in a series of experiments that spanned a wide range of oxidant to contaminant molar ratios. In fact, the range of oxidant:contaminant molar ratios in the single contaminant systems was 0:1 (control) to 1830:1, and the range of oxidant:contaminant molar ratios in the multiple contaminant systems were 0:1 (control), 4.7:1, and 18:1. Use of this wide range of oxidant to contaminant ratios was conducted to quantify the impact of reactant concentration variability, which can be significant for applications in groundwater systems or in wastewater treatment applications. The multi-contaminant system experimental procedures were identical to the single-contaminant systems except that the solution contained a mixture (e.g., for 18:1 oxidant:contaminant ratio: 0.00034 mM 1,4-dioxane, 0.006 mM TCE, and 0.006 mM TCA). The multi-contaminant experiments were then treated with 0.2 mM of O_3. Both the single component and multiple component experiments were replicated with and without HPβCD. The experiments without HPβCD were conducted as above, and the experiments with HPβCD were identical except for the addition of HPβCD as a constant concentration of 303 mg L^{-1} (0.208 mM).

Additionally, a series of reaction kinetic experiments were conducted as described above with various initial pH values (i.e., 4, 6, and 10), and for these the initial pH was adjusted by addition of appropriate amounts of 0.1 M HCl or NaOH. Similarly, a series of experiments were conducted to evaluate the variability in aqueous salinity, and for these either the appropriate amounts (i.e., 50 or 100 mM) of NaCl or $NaHCO_3$ were added to the reactor vials. Control experiments were also conducted for both the single and multiple contaminant experiments. Controls were conducted in the same manner (i.e., identical sampling times, methods, quenching, and analysis) as the reaction kinetic experiments, except that the solutions were prepared with DI water only instead of ozonated water. All experiments were conducted at 22(±1)°C, and several experiments were replicated (i.e., 1,4-dioxane mixture with HPβCD, TCE mixture with HPβCD, 1,4-dioxane at pH 10 with and without HPβCD, TCE at pH 6 with and without HPβCD, TCE at pH 10 with and without HPβCD).

Contaminant removal (i.e., oxidative transformation) was quantified by loss from the aqueous solution. The final measurable decay time concentrations (C_∞) were subtracted from the concentrations at each time (C), and the results were normalized by the initial concentration (C_o) minus the final concentration. C_∞ was either the lower detection limit or the remaining contaminant concentration upon consumption of O_3 in the reactor system. Then the natural log of the relative concentration was plotted versus time, the slope was determined as the pseudo 1st order

rate constant (i.e., k) by linear regression, and the mean values and 95% confidence intervals for reaction over time data were quantified using the regression analysis. Reaction results were interpreted based on rate constant comparisons.

3.5.3. Chemical analysis

Aqueous O_3 concentrations were determined spectrophotometrically using a Molecular Devices SpetraMax M2 spectrophotometer, the indigo method (Bader and Hoigné, 1981), and also with an O_3 probe (Model Q46H/64). The lower to upper quantification range of O_3 analysis was 0.0208-0.2083 mM. 1,4-Dioxane, TCE, and TCA were analyzed using gas chromatography (7890A Agilent) LECO time of flight mass spectrometry (GC-ToF-MS) equipped with ZB-5ms column (30m length, 0.25mm I.D., 0.25µm film thickness). All water samples were placed in headspace vials, and analytes were volatilized into headspace and concentrated using solid phase micro extraction (SPME) fiber (85 µm Carboxen-Polydimethylesiloxane metal fiber) using a CombiPal CTC Analytics auto sampler. Analytes were then injected into a 7890A Gas Chromatograph with a desorption time of 4 min and injector temperature 310 ^oC. Oven temperature was 50 ^oC (1.5 min), and ramped 16 $^oC\ min^{-1}$ to 230 ^oC (3 min).

All samples were incubated at 55 °C before starting sample extraction from SPME fiber. Whereas, two methods were used to increase the concentration quantification range. The full range of quantification (upper to lower limits including both methods) for 1,4-dioxane was 0.11mM to 0.0001mM, and the range for both TCE and TCA was 0.075 mM to $7.5x10^{-6}$ mM. For the higher concentration range (i.e., 0.11 to 0.011 mM for 1,4-dioxane; and 0.075 to 0.0075 mM for TCE and TCA), samples were incubated for 5 min and extracted for 5 min. For the lower concentration range (i.e., 0.011 to 0.00011 mM for 1,4-dioxane; and 0.0075 to $7.6x10^{-6}$ mM for TCE and TCA), samples were incubated for 20 min and extracted for 20 min. Analytes were quantified using standard curves based on the experimental matrix (i.e., standard curves developed for single contaminant experiments were separate from multiple contaminant experiment curves). The combined experimental and analytical precision for duplicate sample analyses results were within ~6% error for approximately ~300 experiment samples.

3.6 Peroxone Activated Persulfate Treatment of 1,4-Dioxane Materials and Methods

3.6.1 Materials

The target contaminants were 1,4-dioxane (99.5% purity, ACROS), TCE, (99.5+% purity, Fisher Scientific), and TCA (99.0+% purity, Fluka). Chemicals used for preparing, measuring, and quenching the PAP oxidant solution were purchased from Fisher Scientific and included sodium persulfate, sodium phosphate dibasic anhydrous, 30% hydrogen peroxide, potassium iodide, 1% starch indicator and 1N sodium thiosulfate pentahydrate. Calcium chloride dihydrate was used to alter ionic strength and was also purchased from Fisher Scientific. TCA, TCE, and pentafluorobenzene standards were obtained from Ultra Scientific. 1,4-Dioxane and 1,4-dioxane-D8 standards were obtained from SPEX CertiPrep. Working standards were diluted in purge-and-trap grade methanol (99.9+% purity, Fisher Scientific). ACS grade methanol (99.8% purity, Fisher Scientific) was used for rinsing and cleaning of equipment. An incubator (Fisher Scientific) was used for regulating the sample temperature. Deionized water was prepared using a MilliQ water filtration system (DI water). O_3 was generated using a Pacific Ozone L11 O_3 Generator and ultra-high purity oxygen (Airgas, OX300).

3.6.2 Analytical

1,4-Dioxane, TCE, and TCA were analyzed by gas chromatography-mass spectrometry (GCMS) using a Shimadzu GC-17A/GCMS-QP5000 equipped with a Restek Rxi®-624Sil MS Column (30 m, 0.25 mmID, 1.4 um). Aqueous samples were injected into the GCMS via an OI Analytical Eclipse 4660 purge-and-trap sample concentrator equipped with a #7 trap (Tenax) and a 25 mL sparge vessel.

Analysis of 1,4-dioxane was performed in selected ion monitoring (SIM) mode. A 1,4-dioxane-D8 internal standard was used to correct for variations in purge efficiency. The following equation was used for sample correction

$$\boldsymbol{C_a = C_i \times \left(\frac{M_a}{M_i}\right)}$$

where $\boldsymbol{C_a}$ is the estimated concentration of the target analyte, $\boldsymbol{C_i}$ is the known concentration of the added internal standard, $\boldsymbol{M_a}$ is the measured concentration of the target analyte and $\boldsymbol{M_i}$ is the measured concentration of the internal standard. 1,4-Dioxane samples with internal standard recovery less than 60% or greater than 140% were re-run until recovery was within the desired range. The purge- and-trap and GCMS conditions used for analysis of 1,4-dioxane are listed in the Supplementary Data.

Analysis of TCE and TCA was performed in Scan mode. A pentafluorobenzene internal standard tracked the purge efficiency of TCA and TCE samples, but was not used for concentration correction. TCA and TCE samples were accepted if pentafluorobenzene internal standard recovery was between 80-120%. The detailed VOC purge-and-trap and GCMS conditions are listed in the Supplementary Data.

3.6.3 Oxidant Generation

The formulation of PAP used herein is commercially available as OxyZone® from EnChem Engineering, Inc. (Newton, MA). Both dissolved O_3 and dilute hydrogen peroxide are used to activate buffered sodium persulfate at ambient temperatures. O_3 gas may also be used to supplement the dissolved O_3. This facilitates the production of hydroxyl (2.8 V) and sulfate (2.5 V) radicals, two of the strongest oxidants available. As a result, PAP destroys organic contaminants through primary oxidation reactions by O_3 (2.1 V) and persulfate (2.0 V), as well as through more vigorous secondary oxidation reactions involving hydroxyl radical and sulfate radicals (Huling and Pivetz, 2006).

The PAP solution was prepared in a bench-scale reactor (Figure 3.1). No more than 3 h prior to use, 3.5 L of a 60 g/L sodium persulfate and 7.29 g/L disodium phosphate buffer solutions were prepared in an amber glass vessel and mixed with deionized water using a Teflon-coated stir bar. A 3% hydrogen peroxide solution was prepared from a 30% stock solution. Once fully dissolved, the buffered persulfate solution was pumped into the reactor through the bottom. Oxygen flow was initiated and the reactor was pressurized to 15 psig. Gaseous O_3 was then supplied to the reactor at a rate of 0.38 g/h for 25 min. 220 µl of the 3% hydrogen peroxide

solution was injected at 6 min, 9 min, 12 min, 15 min, and 18 min. At 25 min, gas flow to the reactor was interrupted and the PAP solution was withdrawn from the bottom valve of the reactor for immediate use.

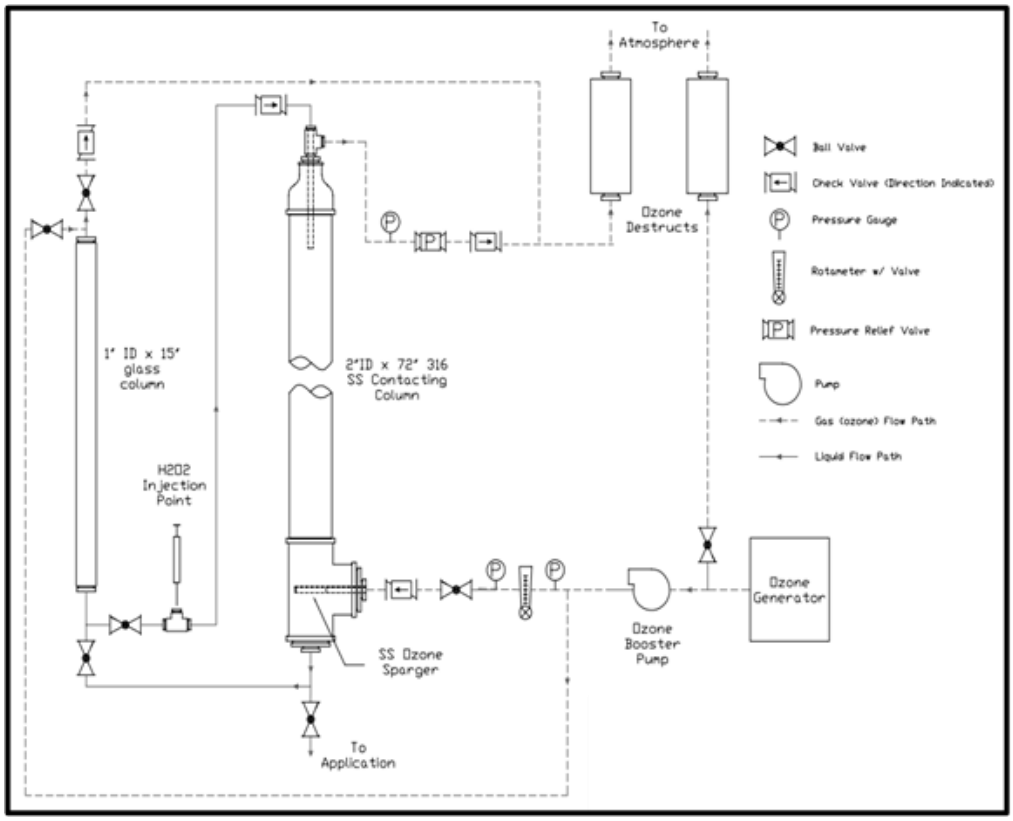

Figure 3.1. PAP Generator Design.

3.6.4 Experimental Procedure

Contaminant solutions were prepared from stock solutions containing 40 mg/L 1,4-dioxane, 60 mg/L TCA, 60 mg/L TCE, and 60 g/L PAP. Appropriate volumes of contaminant solution, ultrapure DI water, and PAP were combined in amber glass bottles with Teflon seals. For the ionic strength experiment the appropriate amount of calcium chloride dihydrate was dissolved in the combined ultrapure DI water and 1,4-dioxane stock prior to the addition of PAP. In the individual contaminant experiments, 1 L of the reactive solution was prepared, while for the multi-contaminant experiments the volume was 4 L.

The solutions were gently mixed by hand for 1 min and allowed to equilibrate for 15 min in an incubator at 25 ^{o}C. The solutions were then quickly transferred to labeled 125 ml amber glass jars using a glass separatory funnel. The glass jars were capped with Teflon lids, sealed with no headspace, and returned to the incubator for storage at 25 ^{o}C. At the time of sampling, the jars were opened and duplicate samples were quickly transferred (using disposable glass pipets) to 40 ml VOA amber glass vials containing 6 ml of a 1N sodium thiosulfate solution to quench any remaining oxidant. Each vial was stored at 4 ^{o}C until analysis. The mass of the VOA, added volume of thiosulfate and sample volume were recorded. The remaining solution was used to

measure ORP and pH were measured using Cole-Parmer probes (59001-77, 059001-12).

In the multi-contaminant experiment persulfate anion concentrations were measured by thiosulfate titration. A 16 ml subsample was transferred to a 20 ml VOA and mixed with 4 ml of 22 g/L potassium iodide solution. The solution was mixed on a vortex shaker for 15 seconds and then allowed to react for 1 h. The solution was then titrated with 2.1 g/L thiosulfate against 1 ml of starch solution, which was added near the end of the titration (Haselow et al., 2003).

To determine the relationship between the rate of oxidative destruction of the contaminants and the amount of oxidant required, approximately 0.04 mM 1,4-dioxane, TCA, and TCE solutions, either as single compounds or as mixtures, were treated with increasing amounts of PAP. Oxidant:contaminant molar ratios were calculated as moles persulfate prior to activation to moles VOC. The ratios in the single-contaminant systems ranged from 0:1 (control) to 1900:1. A 500:1 ratio was used in the ionic strength experiment.

The multi-contaminant system experimental procedures were identical to the single-contaminant systems except that the solution contained a mixture of 1,4-dioxane (10.3 µM), TCA (9.4 µM), and TCE (14.8 µM) and was treated with 4.2 mM of PAP. The molar oxidant:contaminant ratios for the three compounds were 280:1, 450:1, and 410:1 for 1,4-dioxane, TCA and TCE, respectively. The total VOC oxidant:contaminant ratio was approximately 120:1.

3.7 Siderite Activated Peroxide & Persulfate Contaminant Treatment Materials and Methods

Experiments were conducted using batch reactors. The degradation of TCE and DCA in the two activated systems, siderite activated-hydrogen peroxide (designated as SO) and siderite activated-hydrogen peroxide combined with persulfate (designated as STO), at different temperatures was tested. The existing form of phosphate in aqueous phase varies under different pH conditions, and the most abundant species under weak acid conditions (pH~3) is dihydrogen phosphate ion ($H_2PO_4^-$). Therefore, the impact of $H_2PO_4^-$ on TCE degradation in the SO and the STO systems was also evaluated in this study.

3.7.1 Chemicals

All chemical stock solutions used in this study were prepared using ultrapure (filtered, distilled, deionized) water from a Millipore system (Millipore Model Milli-Q Academic A10). Siderite was obtained from the Wuhan Iron and Steel (Group) Corporation, China. Hydrogen peroxide (H_2O_2, ~30 wt. % in water), sodium persulfate ($Na_2S_2O_8$, >98%), trichloroethene (TCE, >99% purity), sodium phosphate monobasic (NaH_2PO_4, ≥99% purity), 1,2-dichloroethane (DCA, ~99.8% purity) were purchased from Beijing Chemical Works.

The following reagent concentrations were used for all of the experiments. Oxidant concentrations were selected based on the results of previous studies employing persulfate and H_2O_2 (Yan et al. 2013, 2015). For TCE, 10 µL of pure TCE was added to each vial for the relevant experiments. This quantity is equivalent to 11.15 mM (1,500 mg/L) in solution. This equivalent concentration exceeds the aqueous solubility of TCE, reflecting the presence of TCE liquid. DCA: 5 mM (495 mg/L), $Na_2S_2O_8$: 6.3 mM (1,500 mg/L), H_2O_2: 150 mM (5,100 mg/L), siderite: 11,450 mg/L. These oxidant concentrations are relatively low compared to typical concentrations used for

field applications. Thus, these concentrations will produce conservative results.

3.7.2 Experiment Setup

Batch experiments (in triplicate) were conducted with 20 mL borosilicate vials fitted with PTFE septum caps. Experiments were conducted to examine TCE or DCA degradation alone, and multiple temperatures (10, 20, 30, 40, and 50 ^{o}C) were used for the thermodynamic study. The blank control group contained only contaminant and ultrapure water. This group was used to evaluate the influence of volatilization and other mass-loss processes during the experiment. The siderite control group contained contaminant, siderite, and water. This control was used to determine whether the siderite sorbed or otherwise influenced TCE or DCA. The reaction group was created by adding the reagents in the following order: siderite, ultrapure water, persulfate (if the group contained), contaminant, and hydrogen peroxide. The vials were immediately capped after the addition of all the reagents.

After preparation, the vials were stored in an air bath to maintain constant temperature. The experiments were conducted for 48 hours. At each time-point, 5 mL of isopropanol solution were added to the selected vials to quench the reaction. The samples were immediately analyzed as described below.

3.7.3 Analytical Methods

TCE and DCA were analyzed using gas chromatography (Agilent GC6820, USA) with a headspace autosampler, a FID detector and a 30 m×0.53 mm DB-5 capillary column (film thickness was 1.5 µm). The temperature of injector and detector was 187 and 250 °C respectively. For TCE detection, the initial oven temperature was 40 °C and heated at a rate of 10 °C /min to a final temperature of 140 °C. For DCA detection, the initial oven temperature was held at 40 °C for 1 minute, and then heated at a rate of 30 °C/min to a final temperature of 120 °C, which was held at that final temperature for 2 minutes.

3.8 Aqueous Ozone Transport and Oxidant Demand Reactivity Materials and Methods

3.8.1 Materials

The porous medium used in all experiments was Accusand (20/30 mesh) purchased from Unimin Corporation, Le Suer, MN. This is a medium grain size, clean quartz sand with low organic matter content. This sand was selected because of its inert composition to avoid significant oxidant demand associated with the sediment (i.e., to quantify oxidant demand in the aqueous phase). O_3 was generated by in-lab O_3 generator (Pacific Ozone; Model no. G1110101; Serial no. 8496), which was sparged in water continuously to dissolve O_3 into water before each experiment. A 250 mg/L solution of ACS grade pentafluorobenzoic acid (PFBA, Aldrich Chemical Co., Milwaukee, WI) was used as a nonreactive tracer to characterize the hydrodynamic properties of packed columns. For all experiments, a Barnstead NANO pure II (Series 550, Dubuque, Iowa) system was used to deionize reverse osmosis treated water to >18 MΩ-cm, which was then used (DI water) for all experiments unless salt was added to DI. Reagent grade NaCl was purchased (Sigma Aldrich) and added to DI for a suite of the batch O_3 decay experiments.

Three different columns (152 cm PVC column, 60 cm stainless steel, and 20 cm stainless steel column) were used. The column with 60 cm and 20 cm length, were constructed of 316-stainless steel with 2.5 cm inner diameter. Porous frits were placed on each end of the column to

promote uniform flow and retain the porous media for stainless steel column. All tubing, frits, and connectors were stainless steel. For the longest column, a 152 cm section of clear polyvinyl chloride pipe with a 7.73 cm diameter (Everclear PVC) was used with glass wool placed within end caps of the column to promote uniform flow and retain the porous media. For this 152 cm column, there were sample collection ports (installed with septum and valves) at 41 cm, 111 cm, and 141 cm distances from the base, or injection location, of the column. High Performance Liquid Chromatographic pumps (Shimadzu LC-10AD) were used for water and reagent injection.

3.8.2 Batch experiments

Batch experiments were conducted at 22(±1) ^{o}C within 500 mL amber vials (kinetic reactor vials) to evaluate the reaction kinetics of O_3 with water, and experiments were conducted at three different salt concentrations including DI water, 50 mM NaCl, and 100 mM NaCl. O_3 gas was sparged into DI water to dissolve O_3, and all experiments were initiated at aqueous solubility (i.e., ~10 mg/L). Subsamples were collected using a 1 mL pipette into a cuvette at various times for immediate chemical analysis. Experiments conducted with and without NaCl were essentially only modified by salt addition. The 500 mL amber vials were prepared with target salt mass, aqueous O_3 solution was prepared in a 2 L conical flux, 500 mL of O_3 solution was added to the 500 mL amber vials containing salt, reactor vials were inverted multiple times to ensure salt and O_3 solution mixing, and subsamples were collected for analysis throughout the time course of each experiment. Each experiment was repeated three times, and statistical analysis was conducted to determine mean and standard deviation values using triplicate results.

3.8.3 Miscible displacement experiments

Column tracer tests were conducted by switching injection reservoirs to inject a constant concentration of tracer for a finite pulse (> 1 pore volume) before switching back to tracer-free DI water injection (all with constant flow rate), and concentrations were monitored in the injection reservoir as well as the effluent of the column by sampling at multiple times throughout the experiment. Nonreactive tracer, PFBA, experiments were conducted before and after O_3 tracer experiments to check the pore volume, flow rates, and quantify physical transport properties. Aqueous O_3 was injected (for a finite injection pulse) as a reactive tracer into sand packed columns to quantify reactive transport properties of O_3 for contaminant remediation applications using ISCO. O_3 gas was continuously sparged into a reservoir filled with DI water and maintained at constant volume to dissolve O_3 to maintain a constant, aqueous-solubility concentration (10 mg/L). After aqueous O_3 pulse injection, the injection reservoir was switched to DI water (i.e., devoid of O_3), and effluent monitoring of O_3 was used to determine O_3 concentrations, mass recovery, and O_3 decay through reaction with hydroxide in water.

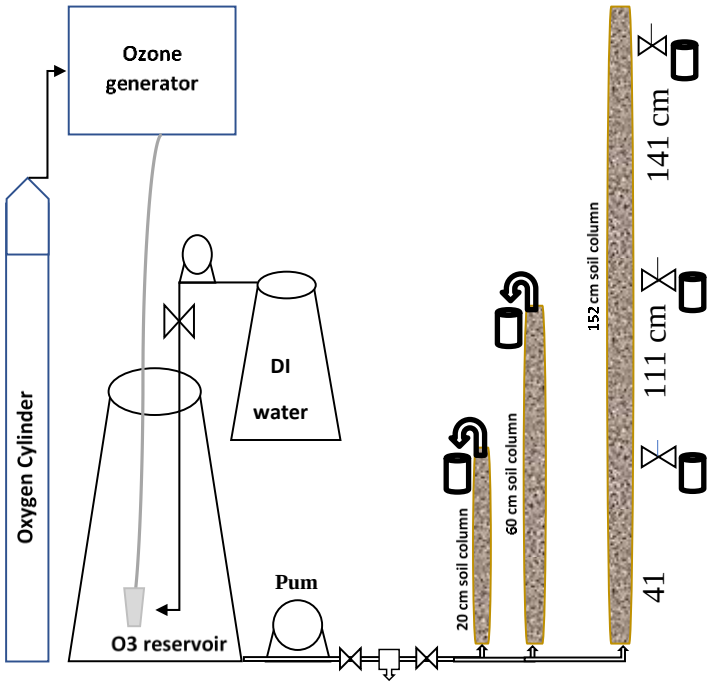

Figure 3.2. Schematic of O_3 generation and transport of O_3 through different soil columns.

The 20 cm, 60 cm, and 152 cm long column was packed to create uniform bulk density and porosity. The sand was packed into columns under ponded water to ensure water saturation. The water volumes (i.e., pore volume) in each column were approximately 14 cm^3 for 20 cm column, 75 cm^3 for 60 cm column, and 2302 cm^3 for the 152 cm column. Water, non-reactive tracer, or aqueous O_3 was introduced from the bottom of the column at three different pore water velocities: 0.872 cm/min, 1.745 cm/min, and 2.513 cm/min for 60 cm long column; 1.088 cm/min, 2.244 cm/min, and 3.549 cm/min for 20 cm long column; and 0.872 cm/min for 152 cm column. After 4-8 pore volumes of injection (depending on length of column or flow rates), the influents (both oxidant and contaminant) was switched to DI water. A pulse of non-reactive tracer or O_3 solution were injected separately for several pore volumes, after which the DI water solution was injected to elute the tracer or O_3 solution from the soil column. Samples were collected from column effluent throughout the experiment by using cuvette (2 ml) for immediate chemical analysis. The concentration of PFBA and O_3 in reservoir were measured before, during and after each experiment to monitor the transport and decay of O_3. The 152 cm long column was not replicated. Whereas, the 20 and 60 cm long column experiments conducted at three different velocities were each repeated three times. All miscible displacement experiments were conducted at 22(±1) ^oC.

3.8.4 Chemical analysis

Aqueous O_3 and PFBA concentrations were determined spectrophotometrically using a Molecular Devices SpetraMax M2 spectrophotometer with a wavelength set at 260 nm and 254 nm for O_3 and PFBA, respectively. The lower to upper detection limit of O_3 analysis was 0.0208-0.2083 mM and 7 - 250 mg/L for PFBA.

3.8.5 Data analysis

3.8.5.1 Moment analysis

Temporal moment analysis was used to calculate the mass balance and sorption retardation factors for all tracer experiments (Valocchi, 1985). The 0^{th} moment (integration of eluted tracer mass) was compared to the measured injected tracer mass to calculate mass recovery. The mean solute travel time was calculated using the normalized first moment. The ratio of the travel times was used to calculate the retardation factor for nonreactive tracer and aqueous O_3. The O_3 pseudo first order decay kinetic rate constant was calculated for each experiment by using moment analysis for three different flow rates for the 20 cm and 60 cm columns and three different distances for 152 cm column. Rate constants were estimated through exponential regression of % mass recovery (i.e., C/Co) versus mean arrival time (i.e., reactive solution transport time and/or contact time between O_3 and water without O_3).

3.8.5.2 Reactive transport modeling

STANMOD version 2, software was used with CXTFIT 2.1 (Inverse Modeling) program to solve analytical solutions of the convection-dispersion equation (Toride et al., 1999), which was used to simulate nonreactive and reactive tracer transport through each of the columns.

3.8.5.3 Convection-Dispersion Model (CXTFIT)

The results from each of the column tracer tests were used as input and compared to the results of the transport modeling. The transport velocity, length, and injection were used as input. Sorption retardation factors were determined from moment analysis of concentration changes in the effluent. The breakthrough curve for nonreactive tracer PFBA data were used with parameter estimation to determine the dispersion coefficients (D), which were used as input for the O_3 tracer test modeling. For the O_3 reactive tracer experiments, the effluent breakthrough data were used with parameter estimation to determine the first order reaction rate constant (μ).

The results of miscible-displacement experiments were simulated with the widely used equilibrium transport model for nonreactive and reactive tracer experiments to estimate the parameter dispersion coefficients or the reaction rate constants, respectively. The convection dispersion equation (assuming steady-state flow in a homogeneous soil) with equilibrium sorption and 1^{st} order decay kinetics can be written as:

$$R\frac{\partial c_r}{\partial t} = D\frac{\partial^2 c_r}{\partial x^2} - v\frac{\partial c_r}{\partial x} - \mu c_r \quad (8)$$

$$R = 1 + \frac{\rho_b K_b}{\theta} \quad (9)$$

$$\mu = \mu_l + \frac{\rho_b K_b \mu_s}{\theta} \quad (10)$$

where C_r is the solute concentration in solution (M/L^3), x is the column length (L), t is the elapsed time after injection (T), v is the average pore-water velocity (L/T), D is the dispersion coefficient (L^2/T), P is the Peclet number (-), K_b is the linear sorption partitioning coefficient, R is the retardation factor, ρ_b is the bulk density, theta is the water content or saturated porosity, and μ is the first order rate constants for reactive tracer decay. Here we assumed that degradation rate

constants were equal in liquid phase and in solid phase, such as $\mu = \mu_l R$. The results of miscible-displacement experiments were simulated with this transport model for reactive tracer O_3 to estimate the 1st order reaction rate constant (μ) using iterative inverse modeling parameter estimation by fitting model results to observed column tracer test results. The model-estimated O_3 decay rate constants were compared to rate constants determined using moment analysis of column effluent data and to rate constants derived from batch experimental results.

3.9 Transport and Peroxone Activated Persulfate Treatment of 1,4-Dioxane Materials and Methods

3.9.1 Materials and Analytical Methods

1,4-Dioxane was obtained from ACROS (99.5% purity). Unless stated otherwise, all other chemicals were purchased from Fisher Scientific, including sodium persulfate ($Na_2O_8S_2$, >98% purity), sodium phosphate dibasic anhydrous (HNa_2O_4P, >99% purity), hydrogen peroxide (H_2O_2, 30% solution) and sodium thiosulfate pentahydrate solution (1N, $Na_2S_2O_3 \cdot 5H_2O$). O_3 was generated with a Pacific Ozone L11 O_3 Generator with ultra-high purity oxygen (Airgas, OX300). 1,4-Dioxane and deuterated 1,4-dioxane-d8 standards were obtained from SPEX CertiPrep. Analytical samples were diluted in purge-and-trap grade methanol (99.9+% purity) whereas ACS grade methanol (99.8% purity) was used for cleaning equipment.

Homogenous silica quartz Accusand sand (2mm Mesh size #10) was purchased from Unimin Corporation, Le Suer, MN. Accusand is a well-characterized porous media used to standardize the efficiency of laboratory flow experiments (Schroth et al., 1996). ORP and pH were measured with a Hach HQd11d Portable Starter MTC101 ORP electrode from Cole-Parmer.

OxyZone® is a formulation of peroxone activated buffered persulfate solution that is commercialized by EnChem Engineering Inc., (Newton, MA). OxyZone® is generated by saturating a phosphate-buffered persulfate solution containing hydrogen peroxide with O_3 at ambient temperatures. Increased pressure to 1 or 2 atmospheres may also be used to increase dissolved O_3 and delivery pressure in the formation. The oxidant was produced in a semi-batch reactor provided by EnChem Engineering. The batch reactor is designed to ozonate 3.5 L of liquid. After 25 minutes of pumping O_3 gas through the reactor, gas flow was halted and the oxidant solution was drawn from the reactor for immediate use. The molar concentration of full-strength OxyZone® is 0.252 moles/L with respect to sodium persulfate. Table 3.5 shows the physical properties of OxyZone®.

Table 3.5 Table 3.5. Physical properties of OxyZone®.

Molar Concentration (moles/liter)	ORP (mV)	EC (µS/cm)	pH
0.252	612	4130	4.4

3.9.1.1 Analytical

1,4-Dioxane concentrations were analyzed with a gas chromatograph mass spectrometer from Shimadzu (GCMS-QP2010SE) equipped with a Restek Rxi®-624Sil MS column (30 m, 0.25

mm ID, 1.4 µm). Aqueous samples were introduced through an OI Analytical Eclipse 4660 Purge and Trap sample connector equipped with a #7 Tenax trap and a 25 mL sparging vessel. Samples were analyzed with ultra-pure helium gas (AirGas). Analysis of 1,4-dioxane was performed in SIM mode. 1,4-Dioxane and an internal standard of deuterated 1,4-dioxane-d8 was used to correct for purge accuracy variation. The following equation was used for sample correction:
$C_a = C_i \times (M_a/M_i)$

Where C_a is the estimated concentration of the target analyte, C_i is the known concentration of internal standard added, M_a is the target analyte's measured concentration, and M_i is the internal standard's measured concentration. Internal Standard 1,4-dioxane-d8 recovery must fall into 60-140% recovery to be accepted for statistical analysis. Samples with an internal standard recovery outside of these parameters were re-run until recovery fell into the accepted range.

3.9.1.2 Batch Scale Methods

Bench scale experiments were conducted to determine destruction rates of 1,4-dioxane exposed to OxyZone® in the presence of homogenous silica quartz sand (2mm Mesh size #10, Accusand®) through batch scale experiments. For the initial set of experiments, OxyZone® and 1,4-dioxane concentrations were adjusted to oxidant-to-contaminant molar ratio previously used (Eberle et al., 2016). Amber glass vials typically used for volatile organic analysis with Teflon seals (40 mL VOA, Fisher Scientific) were filled with 20 g (dry weight) of homogenized quartz sand (2mm, Mesh Size 10, Accusand).

Contaminant-solutions were prepared from stock solutions of 3533 µg/L +/- 249.84 µg/L 1,4-dioxane. Each vial was filled with 3.25 mL of 1,4-dioxane. OxyZone® was diluted with DI water to prepare solutions with molar oxidant: contaminant ratios ranging from 0:1, 100:1, 250:1, 500:1 to 1000:1. Each VOA vial was completely filled with their respective oxidant: contaminant solution to eliminate headspace and agitated at 25°C for 24 hours. After 24 hours of reaction time, all solutions were transferred to 20 mL VOA vials containing 1N sodium thiosulfate to quench the reactions. The vials were refrigerated at 4°C until analysis. For quality assurance, triplicate samples were taken for each oxidant: contaminant ratio. Control triplicates, containing 1,4-dioxane but no oxidant, were prepared and analyzed.

For elucidating the degradation kinetics of 1,4-dioxane oxidation in the presence of sand, a second bench scale test was conducted using a constant oxidant: contaminant molar ratio of 250:1. At this ratio, the reaction was sufficiently slow to ensure that 1,4-dioxane was measurable over the entire test duration (16 days). As before, 20 g of sand in amber 40 mL VOA vials was spiked with 3.25 mL of 1,4-dioxane solution (Co=3533 µg/L +/- 249.84 µg/L). The remaining space was filled with a solution containing a 250:1 molar ratio of oxidant: contaminant. Samples were agitated at 25° C at the rate of 4 rotations per minute. At different times, samples were transferred to 20 mL VOA vials and quenched 3mL 1N sodium thiosulfate. The time points were 0 hours, 2 hours, 8 hours, 24 hours, 2 days, 4 days, 8 days, and 16 days. Triplicate samples were taken at each time for quality assurance. After analysis, chemical kinetics were analyzed. Due to a great excess of sodium persulfate in the AOP system, relative to 1,4-dioxane, its concentration remains relatively constant throughout the duration of reactions. Therefore, the reactions taking place are considered to be pseudo-first order. By plotting the natural log of (C/Co) versus time, the slope of the line equals the rate constant of the overall reaction:

$$-d\left[\frac{\frac{C}{Co}}{dt}\right] = k\left[\frac{C}{Co}\right] \quad (11)$$

Once the rate constant, k, is determined, the half-life , $t_{½}$, can be calculated (Capellos and Bielski, 1972).

$$t\left(\frac{1}{2}\right) = \frac{1}{k\left[\frac{C}{Co}\right]} \quad (12)$$

3.9.1.3 Column Tests

A custom-made column was used to conduct column-scale tests of 1,4-dioxane degradation by OxyZone® under conditions mimicking *in situ* AOP treatment. The column was constructed from a 152.4 cm section of clear polyvinyl chloride pipe with 7.73 cm in diameter (Everclear PVC) (Figure 3.3). Teflon tape lined PVC caps were threaded on each end. The column was outfitted with five stainless steel septa ports (Swageloc) for sample collection or oxidant injection (Ports A through E). Three additional ports were installed for inserting GS3 Greenhouse Sensor Probes (Decagon) (Probes 1 through 3; Figure 3.3). Each probe was connected to an EM50 EC Data Logger (EM25312, Decagon) to store electrical conductivity (EC), soil moisture, and temperature readings at five minute intervals. The column was packed with homogenous quartz sand (2mm mesh size #10, Accusand). A layer of clean glass wool was inserted before capping the column to prevent headspace and the escape of sand particles. The caps on both ends of the column were fitted with stainless steel compressional tube adopters (Swageloc). The column was mounted vertically to the wall. The inlet at the bottom of the column was connected with 3/8 inch Teflon tubing leading to a peristaltic pump (Cole-Parmer Gear Pump System RN-74013-70). The column outlet on the top was also connected to 3/8 inch Teflon tubing, leading to the sample collection station. The dimensions of the column, including the amount of sand it contained, are summarized in Table 3.6.

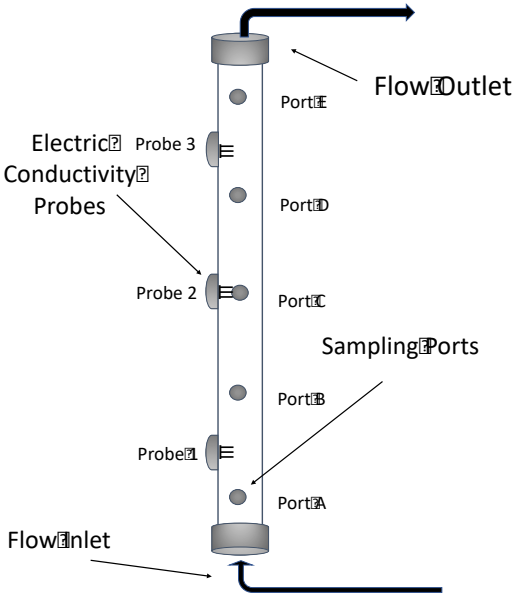

Figure 3.3. Schematic of column used for flow through experiments. The column is 152.4 cm in length and 7.73 cm in diameter.

Table 3.6 Properties of packed column.

Length (cm)	Diameter (cm)	Area (cm^2)	Volume (cm^3)	Weight Empty Column (g)	Weight Packed Column (g)	Weight Sand (g)	Weight Water Saturated Column (g)	Weight Water (g)	Porosity (%)
152.4	7.73	46.9	7,148.5	5,780	11,530	5,750	13,600	2,070	29

After packing the column with sand, deionized water was pumped at a rate of 4.1 mL/minute upwards through the column for several days, i.e. until effluent EC readings were similar to the influent (10 µS/cm) and until all entrapped air exited the column. This was determined by monitoring the moisture content at each probe. Once saturated, the weight of the column was determined and the porosity of the sand calculated from the difference of the weight of the dry and saturated sand (Table 3.6). The porosity was 29%, which is concurrent with the values reported for characterized Accusand (Schroth et al., 1996). In absolute terms, the volume of water inside the column represents 2070 cm^3 of the bulk volume of the column (7148.5 cm^3). For both tests, the column was saturated with 300 µg/L 1,4-dioxane (3 mM). This set the oxidant: contaminant ratio for all studies at 7,400:1. This ratio is an estimate due to the dynamic flow conditions of the column.

3.9.1.4 Conservative Tracer Test

A conservative tracer test was conducted to characterize the column hydraulics. A conservative tracer, e.g. sodium chloride (NaCl), is not expected to interact with the experimental matrix, such as the sand or the column material. 210 mL NaCl solution (2,000 mg/L, ACS reagent, ≥ 99%) was flushed through the column at the constant rate of 4.26 mL/min, followed by deionized water injection. EC readings were logged at Ports 1 through 3 every five minutes. EC measurement of column effluent samples were taken in 16-minute intervals. The EC readings were converted to NaCl concentration via a calibration line (R^2= 0.998). The NaCl concentrations were then transformed into dimensionless concentrations, C/C_o, where C_o is the initial NaCl concentration and C is the concentration measured at each time step. The data was plotted versus pore volume (PV) to determine the tracer transport through the column. Important characteristics of the breakthrough curve include the tracer arrival time, which is equivalent to the flow velocity of the water inside the column, the arrival of the tracer's center of mass, tracer mass recovery, and information about tracer pulse dispersion. The corresponding data can be quantified using the Method of Moments (described above).

The Agency for Toxic Substances and Disease Registry (ATSDR) screening level for 1,4-dioxane based on the EPA IRIS Reference Dose (US EPA, 2011) is set at 300 µg/L. This risk level was chosen as the starting concentration for all experiments. A solution of 300 µg/L 1,4-dioxane in water was pumped into the column until the effluent concentration was at equilibrium with the influent one. The pump rate was a constant 4.26 mL/min. Equilibrium was achieved after 36 hours.

3.9.1.4 AOP Treatment of 1,4-Dioxane with OxyZone

Two treatment scenarios were evaluated. First, two pulses of equal volume (100 mL each) of OxyZone® were injected at two ports into the 1,4-dioxane contaminated sand-packed column. Second, one pulse of 200 mL OxyZone® (equal in volume of the two pulses of the first test combined) was injected at the bottom of the column. During both tests, the rate of discharge flow was Q=4.1 mL/min and the specific discharge (v=Q/A) was 0.13 cm/min. The pulses were injected into 1,4-dioxane contaminated water moving at an average linear velocity of 0.45 cm/min. During all experiments, the following parameters were monitored: EC, ORP, pH, temperature, 1,4-dioxane concentration. The persulfate concentration was monitored indirectly by EC proxy for persulfate during the first test scenario. That is, the EC of OxyZone® is approximately 41 mS/cm, whereas that of 1,4-dioxane is $2*10^{-3}$ mS/cm. Assuming that the great excess of persulfate and the resulting high EC does not change measurably during the test, EC can be used as a proxy for oxidant transport throughout the column.

3.9.2 Treatment Scenario I - Slug injection in two ports:

Pulsed injections of 100 ml OxyZone® were simultaneously released into Ports A and C (Figure 3.3) at a rate of about 4 mL/minute, using gas-tight Duran syringes (total duration of injection: 25 min). Each syringe was equipped with a stainless steel 6 inch leur-lock needle (Thermo Scientific). The longer needles allowed for OxyZone® to be injected directly into the center of the packed column. Effluent samples were continuously collected in 15 minute intervals over the duration of the experiment (10 hrs). Each effluent sample, approximately 60 mL, was aliquoted into two samples (three when taking duplicates). The first aliquot was consumed for measuring pH, ORP, and electric conductivity. The second sample was quenched with 1N sodium thiosulfate and refrigerated at 4°C until 1,4-dioxane analysis. For quality control, a replicate sample was collected at every 9^{th} time point. A second test of treatment scenario I was conducted, following the same procedure except that OxyZone® was injected at half the rate (2 mL/minute) for 50 minutes to obtain a greater mixing and dispersion.

3.9.3 Treatment Scenario II – Single pulse injection:

One pulse of 200 mL OxyZone® was injected at the bottom of the column at a rate of 13 mL/min (total duration of injection: 15.5 minutes). The sampling and analysis procedures were identical to Treatment Scenario I procedures.

3.10 1,4-Dioxane Treatment Using Persulfate Activated By Iron Filings Materials and Methods

3.10.1 Materials and Chemicals

Iron filings (lab grade, Ward's Science, Rochester, NY), sieved (45-mesh) to exclude the ≤ 355 µm size fraction, were used in batch and column experiments. Compositional analysis of these iron filings was conducted using XRD (X'Pert Pro MPD, PANalytical, Almelo, Netherlands) and variable pressure SEM (S-3400N) equipped with an energy dispersive X-ray spectrometer (UltraDry EDS, Thermo Scientific, Madison, WI). Commercially available natural silica sand (40/50 mesh Accusand, Unimin Corporation) was used to represent a natural porous medium for the column experiments.

Sodium persulfate ($Na_2S_2O_8$, 98+%) was obtained from Acros Organics. Hydrogen peroxide (H_2O_2, 35%) was obtained from Sigma-Aldrich. 1,4-Dioxane ($C_4H_8O_2$) was from Fisher Scientific (Fair Lawn, NJ). 5,5-Dimethyl-1-pyrroline-N-oxide (DMPO, 98%) was from Matrix Scientific (Columbia, SC). All other chemicals used in this study were of reagent grade and used as received. The concentration of 1,4-dioxane was 0.5 mM (44 mg/L) for all the experiments, which is representative of the upper range of groundwater concentrations reported for contaminated sites (Mohr et al., 2010). Concentrations of persulfate and H_2O_2 were 5 mM (1190 mg/L and 170 mg/L, respectively) for all experiments. While these oxidant concentrations are in excess compared to the concentration of 1,4-dioxane, they are much lower than the concentrations typically used for standard field ISCO applications. These lower concentrations are employed to enhance cost effectiveness.

3.10.2 Batch Experiments

The degradation of 1,4-dioxane by iron-filings-activated persulfate was measured in batch reactors. Solutions of 10 mM $Na_2S_2O_8$ and 1 mM 1,4-dioxane were mixed 1:1 (v:v) in a glass flask. Iron filings were added to the mixture to yield a solid-liquid ratio of 1:10 (w/w). The flask was sealed with parafilm and placed on a rotary shaker table at approximately 200 rpm at a room temperature of 30±1°C. Subsamples (2 ml) were collected over the course of the batch experiment in glass vials, and placed in an ice-water bath to quench further reaction. The samples were centrifuged for 1 minute to separate iron filing particles, and the supernatant was transferred to a glass tube, cooled to ~0°C in an ice-water bath, and immediately analyzed for the concentrations of 1,4-dioxane, persulfate, sulfate, ferrous ion, total iron, and pH. Each subsample comprised only a very small portion of the total reactor volume (approximately 1%) and, therefore, the sampling process was assumed to have no significant impact on the solid-liquid ratio or the relevant reactions.

The batch experiments included several control treatments. The purpose of the first control was to determine 1,4-dioxane degradation by persulfate in the absence of iron filings. For comparison purposes, 1,4-dioxane degradation by H_2O_2 was also examined. The second control was to determine 1,4-dioxane degradation in the presence of iron filings but absence of persulfate. Another set of controls was designed to determine separately the reactivity of persulfate and sulfate with the iron filings in the absence of 1,4-dioxane. The final control, 1,4-dioxane solution with no oxidant or iron filings, tested for loss of 1,4-dioxane due to volatilization, photochemical decomposition, or other potential mass-loss processes during the course of the batch experiments.

1,4-Dioxane concentration was measured using gas chromatography (Shimadu GC-14A, Columbia, MD) equipped with a SPB^{TM}-624 capillary column (Supelco, 30m×0.53 mm×3µm) and a flame ionization detector. Splitless direct injection was used with injector temperature of 200°C. The temperature program was set to start at 40°C and then ramp to 110°C at 10°C/min. Detector temperature was 250°C. A modified iodide spectrophotometry method of Liang et al. (2008) was used to determine persulfate ($S_2O_8^{2-}$) and H_2O_2 concentrations. KI salt was dissolved in a 5 g/L $NaHCO_3$ solution to the concentration of 100 g/L. Samples were mixed with the KI-$NaHCO_3$ solution at a ratio of 1:19 (v:v). Absorptivity of the solution was measured after a 20 minute holding time with spectrophotometry (Hach DR2800, Loveland, CO) at a wavelength of 400 nm. Interference by ferric iron in solution on the absorptivity of the persulfate or H_2O_2 complex was corrected via independent analysis for the solution-phase concentration of ferric iron and

associated relative absorptivity. Sulfate, ferrous ion, and total iron were measured with spectrophotometry using the Ba^{2+}-based USEPA SulfaVer4 method (HACH module No.8051), 1,10-phenanthroline-based method (No.8146), and FerroVer method (No.8008), respectively. The ferric iron concentration was calculated as the difference between total iron and ferrous ion concentrations. The pH of the samples was measured by a Beckman 510 pH meter (Brea, CA).

3.10.3 Column Experiments

The columns used in the experiments were constructed of 316-stainless steel. They have a 2.2-cm inner diameter and are either 25-cm or 7-cm long. Porous frits were placed on each end of the column to promote uniform flow and retain the porous media. All tubing, frits, and connectors were constructed of stainless steel.

The 25-cm column was dry packed with a 20-cm length of iron filings, capped at each end with 2.5 cm of sand. The vertically oriented packed column was then flushed with CO_2 to displace air, and then saturated with deaerated water using a single-piston precision-flow HPLC pump (Gilson, Acuflow Series II). The column was then oriented horizontally for the experiments.

A solution of 5 mM persulfate or a mixed solution of 5 mM persulfate and 0.5 mM 1,4-dioxane was injected into the column at a constant flow rate of either ~1 or ~0.1 ml/min, equivalent to pore-water velocities of ~30 or ~3 cm/h. After 7~9 pore volumes of injection, the influent was switched to water. Effluent samples were collected in glass tubes emplaced in an ice-water bath to quench the reaction, and weighed. The samples were then immediately analyzed for concentrations of 1,4-dioxane, persulfate, sulfate, ferrous ion, total iron, and pH, accordingly. The concentrations of persulfate and 1,4-dioxane in the reservoir were measured before, during, and after each experiment to monitor for potential loss.

Control experiments were conducted using identical procedures. One set of experiments was conducted to measure the potential reactivity of 1,4-dioxane to the iron filings in the absence of persulfate. Another experiment was conducted to evaluate the transport and degradation of persulfate in silica sand. Finally, experiments were conducted with hydrogen peroxide as the oxidant in place of persulfate.

3.10.4 Ancillary Studies

Specific experiments were conducted to investigate the impact of combining persulfate and iron-filings on aqueous and solid-phase geochemistry. Iron filings (15 g) were added to flasks containing either 150 ml of 5 mM $Na_2S_2O_8$ solution or 150 ml of nano-pure water. The flasks were sealed with parafilm and shaken at 200 rpm (30±1°C). Subsamples (10 ml) were collected from the flasks at 1 h and 24 h, and analyzed for aqueous-phase concentration of persulfate, sulfate, Fe^{2+}, total iron, and pH following the procedures described above. Concentrations of metals in the subsamples were analyzed using inductively coupled plasma mass spectrometry (ICP-MS, ELAN DRC-II, Perkin Elmer, Shelton, CT). The calibration solution was prepared in 1% nitric acid from multi-element stock solutions such as those available from AccuStandard (New Haven, CT). Immediately after the 10-ml subsample was drawn from the flask, the remainder of the solution in the flask was discarded and the iron filings were rinsed more than 10 times with de-ionized water. The iron filings were then dried in pure N_2 atmosphere under room temperature. The dried iron filings were analyzed with SEM-EDS (S-3400N SEM with UltraDry EDS, Thremo-scientific,

Madison, WI) for surface element composition, and with XRD (D8 Advance, Bruker AXS, Madison, WI) to identify minerals formed on the surface.

Formation of radicals was examined employing electron paramagnetic resonance spectroscopy. Two ml of the reaction solution (supernatant with suspended fine iron particles if iron filings were present) was mixed with the spin trapping agent DMPO to a final DMPO concentration of ~0.1 M. The mixed solution was immediately placed in capillaries with 1 mm ID, and analyzed with an X-band EPR spectrometer (Elexsys E500, Bruker, Woodlands, TX) equipped with the rectangular resonator operating in TE_{102} mode. The spectra were recorded at room temperature, at the microwave frequency of 9.340 GHz, microwave power of 2 mW, and magnetic field modulation amplitude of 1 G.

4. RESULTS AND DISCUSSION

4.1 Ozone Oxidant Demand Impact Stabilized by Cyclodextrin Results and Discussion

4.1.1 Ozone transformation of HPβCD

A broadband positive-ion ESI FT-ICR mass spectrum for synthetic groundwater treated with 250 mg/L HPβCD and 2 mg/L O_3 is shown in Figure 4.1.1. We observed a successive addition of 2-hydroxypropyl groups (up to ten 2-hydroxypropyl groups per molecule) to singly- and doubly-charged HPβCD ions. Singly-charged ions were predominantly observed as sodium adducts ([M+Na]+), whereas doubly-charged ions are detected as metal adducts including calcium, magnesium, lithium and potassium as illustrated in Figure 4.1.2. The elemental composition assignments were confirmed by accurate mass measurement from high-resolution FT-ICR MS, which was performed for the O_3-treated (i.e., with ozone) and O_3-untreated (i.e., without ozone) groundwater samples prepared with identical concentrations of HPβCD to investigate the effect of ozonation on the HPβCD concentration. Interestingly, we observed that ozonation partially decreases the abundance of all observed HPβCD ions, and this is illustrated in Figure 4.1.3. Note that peak heights are scaled to the largest peak in the mass spectrum (i.e., the more abundant internal standard peak in the lower spectrum indicates decreased peak height and HPβCD abundance). Additionally, no HPβCD ion signals were completely removed, and formation of new HPβCD reaction/oxidation products was not observed, which suggests complete transformation of each glucose molecule within HPβCD without detection of intermediate products. Negative-ion mode FT-ICR mass spectra were monitored for HPβCD reaction products as well (data not shown). This partial transformation also suggests that much of the HPβCD remained un-transformed. Figure 4.1.4 shows the variation in the HPβCD ion abundance in groundwater with and without O_3 treatment for a range of HPβCD concentrations HPβCD (5-500 mg/L; 7-688 M) and O_3 (0.5-2 mg/L; 0.024-0.096 M) exposure concentrations. Overall, O_3 treatment partially decreases the observed HPβCD abundance. The fluorescence analysis results showed similar results (data not shown). This partial transformation may support HPβCD biodegradation by initiating transformation and providing substrate for microbes. Without this O_3 transformation, it is expected that cyclodextrins are generally resistant to biological decay for a period of at least a few months (Wang et al., 1998).

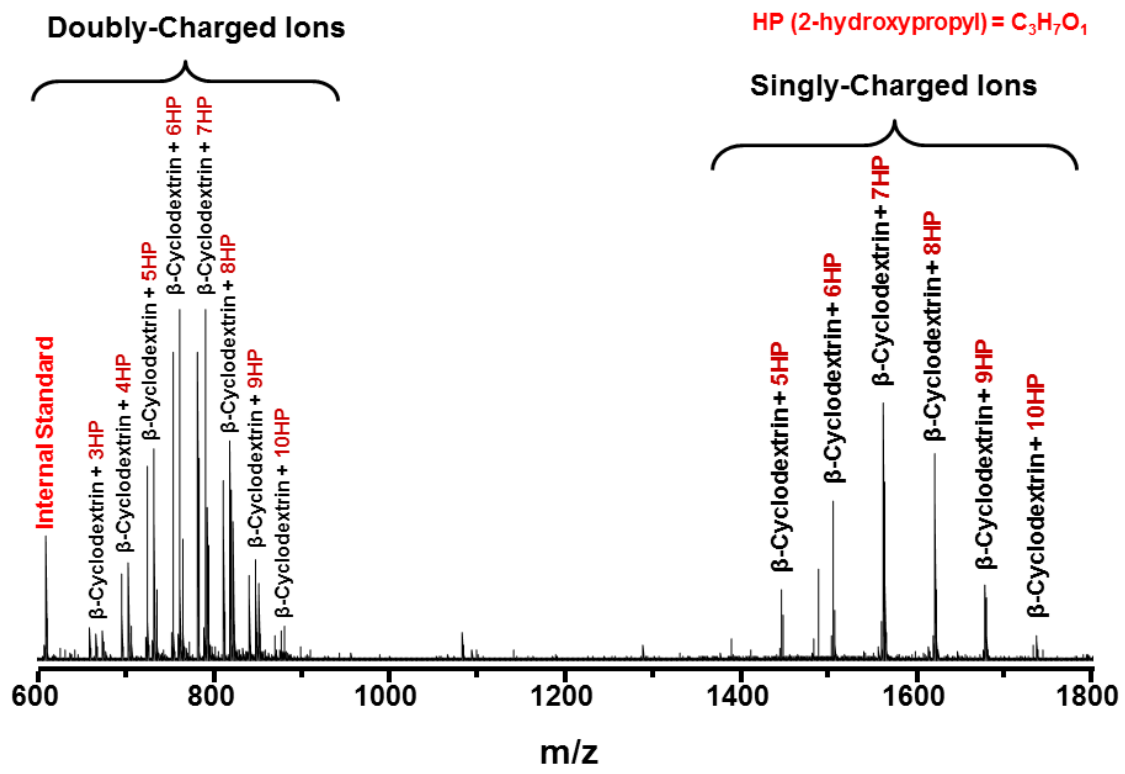

Figure 4.1.1. Broadband ESI FT-ICR mass spectrum for HPβCD (250 mg/L; 344 M) in groundwater with 2 mg/L (0.096 M) O_3.

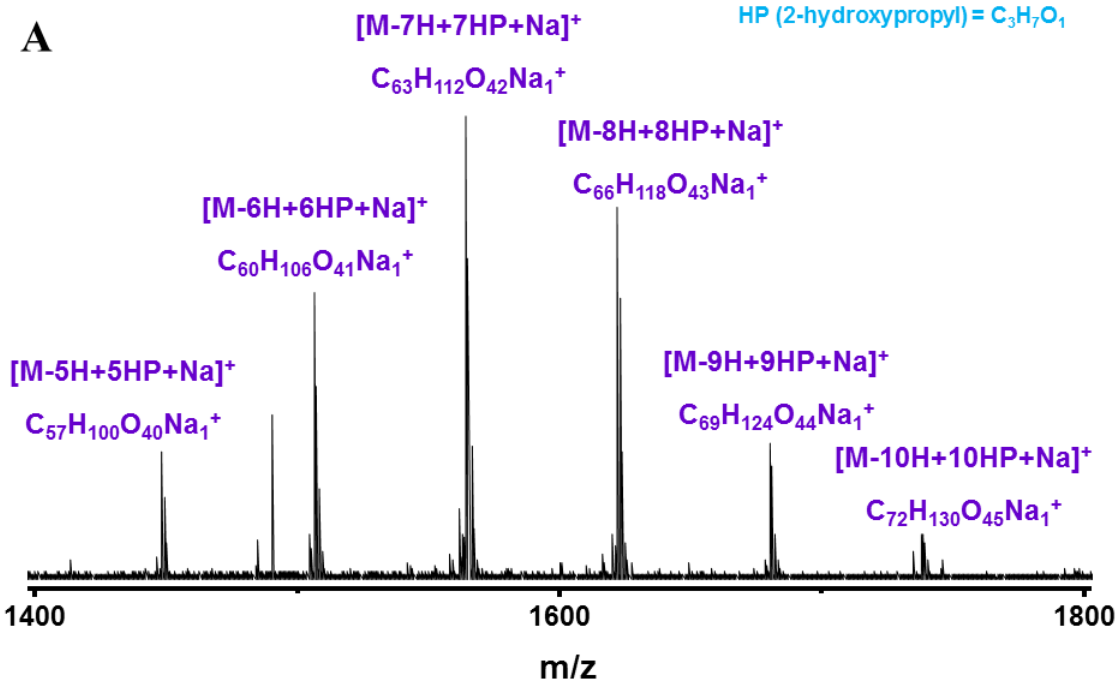

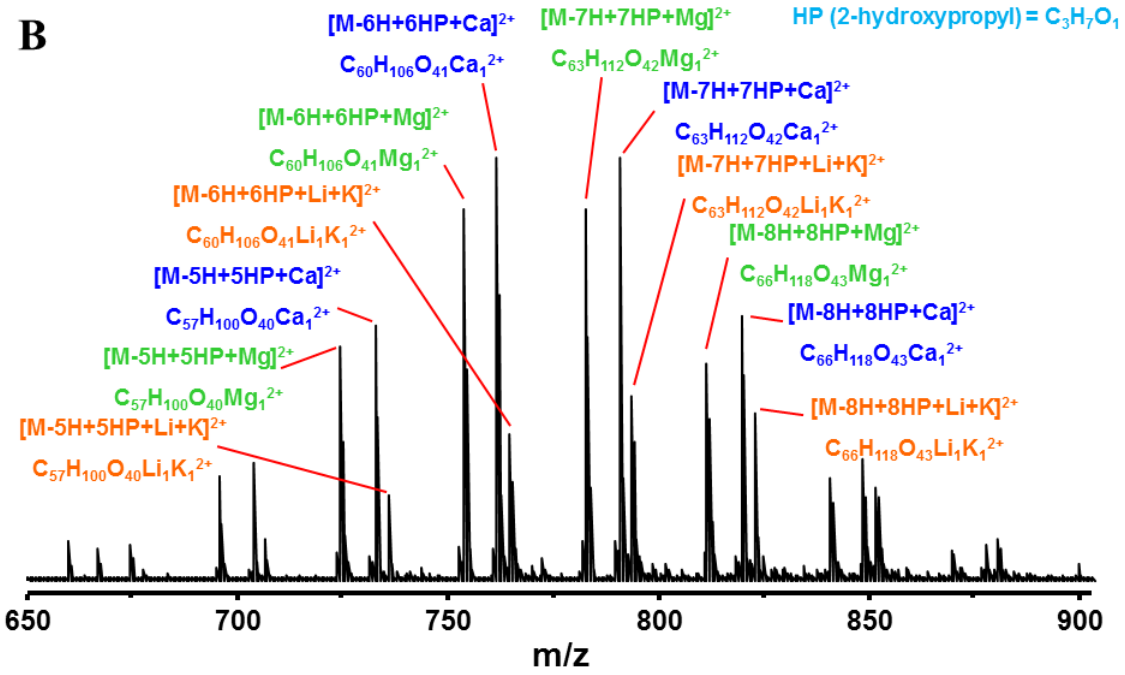

Figure 4.1.2**.** (A) FT-ICR mass spectrum for HPβCD (expanded from Figure 4.1.1) with mass scale expanded segment illustrating singly-charged ions. The observed sodium adducts ([M+Na]+) show serial addition of 2-hydroxypropyl groups. (B) Mass scale expanded segment illustrating doubly-charged ions.

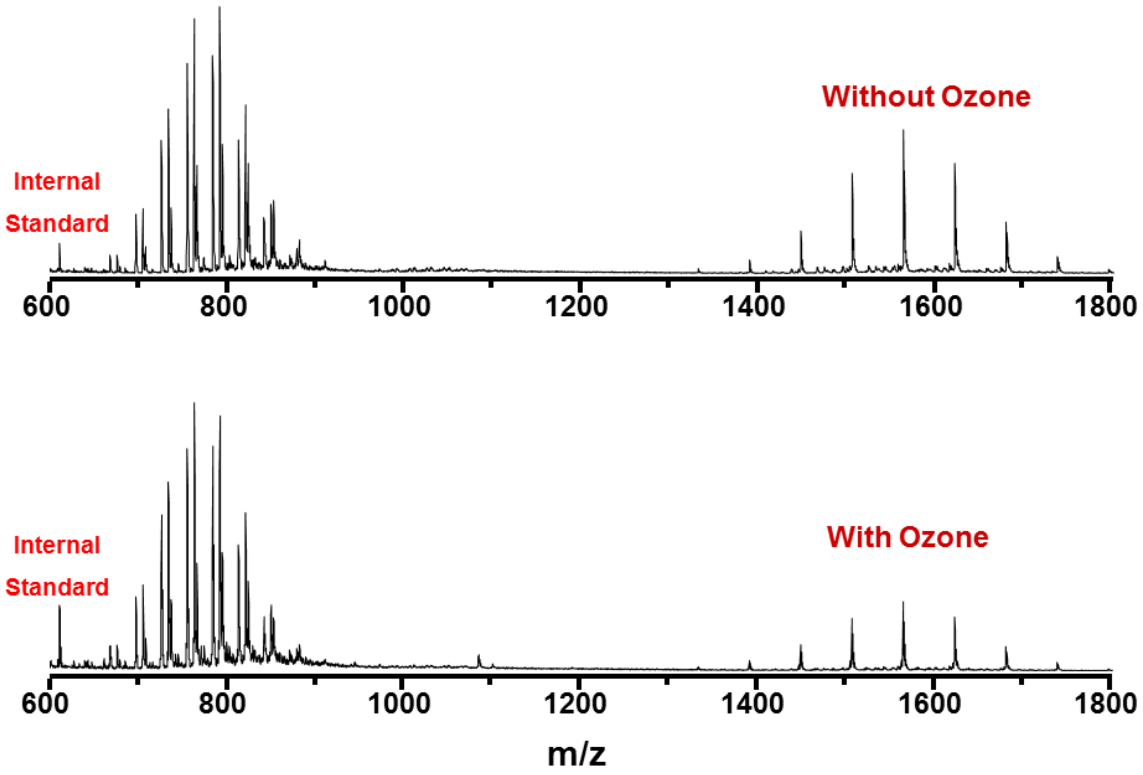

Figure 4.1.3**.** Linear ion trap mass spectrum for HPβCD showing transformation of HPβCD (originally 250 mg/L; 344 M) upon exposure to 2 mg/L (0.096 M) O_3 in groundwater by comparison of mass spectra with and without O_3 exposure. Peak heights are scaled to largest peak. However, internal standard peak heights and concentrations are identical.

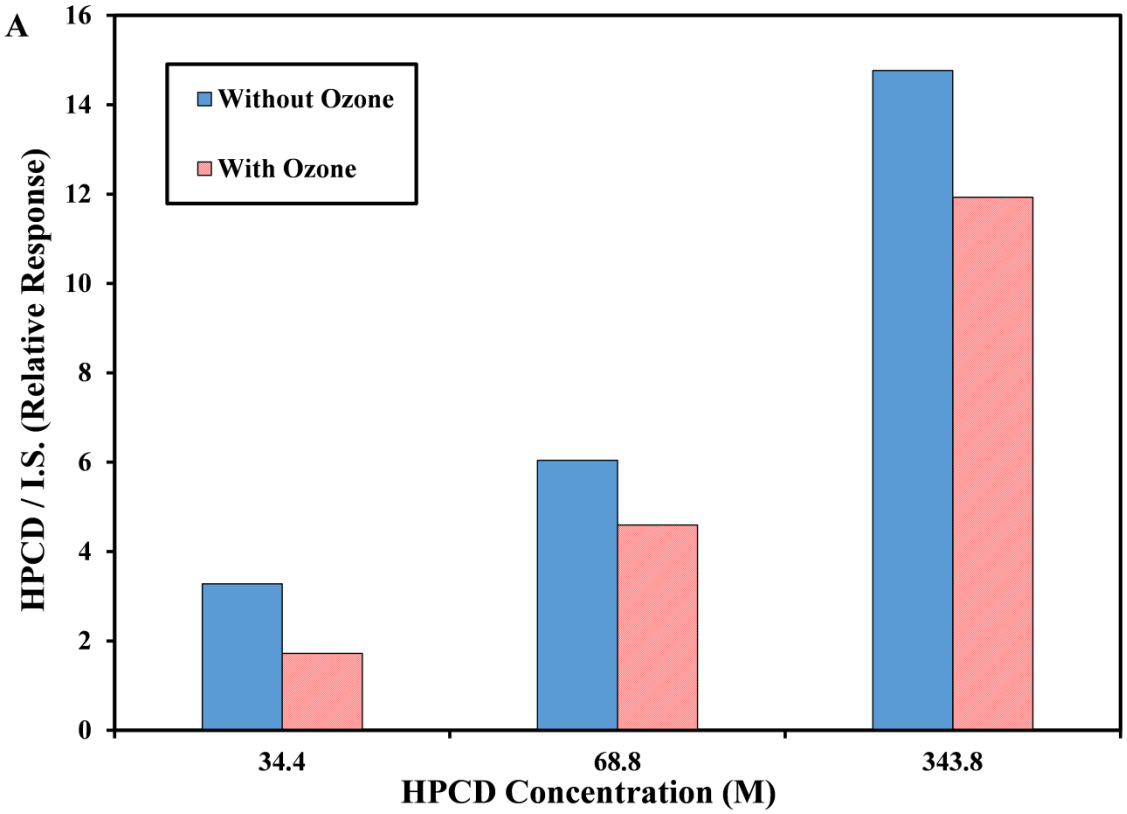
A
Without Ozone
With Ozone
HPCD / I.S. (Relative Response)
0
2
4
6
8
10
12
14
16
34.4
68.8
343.8
HPCD Concentration (M)

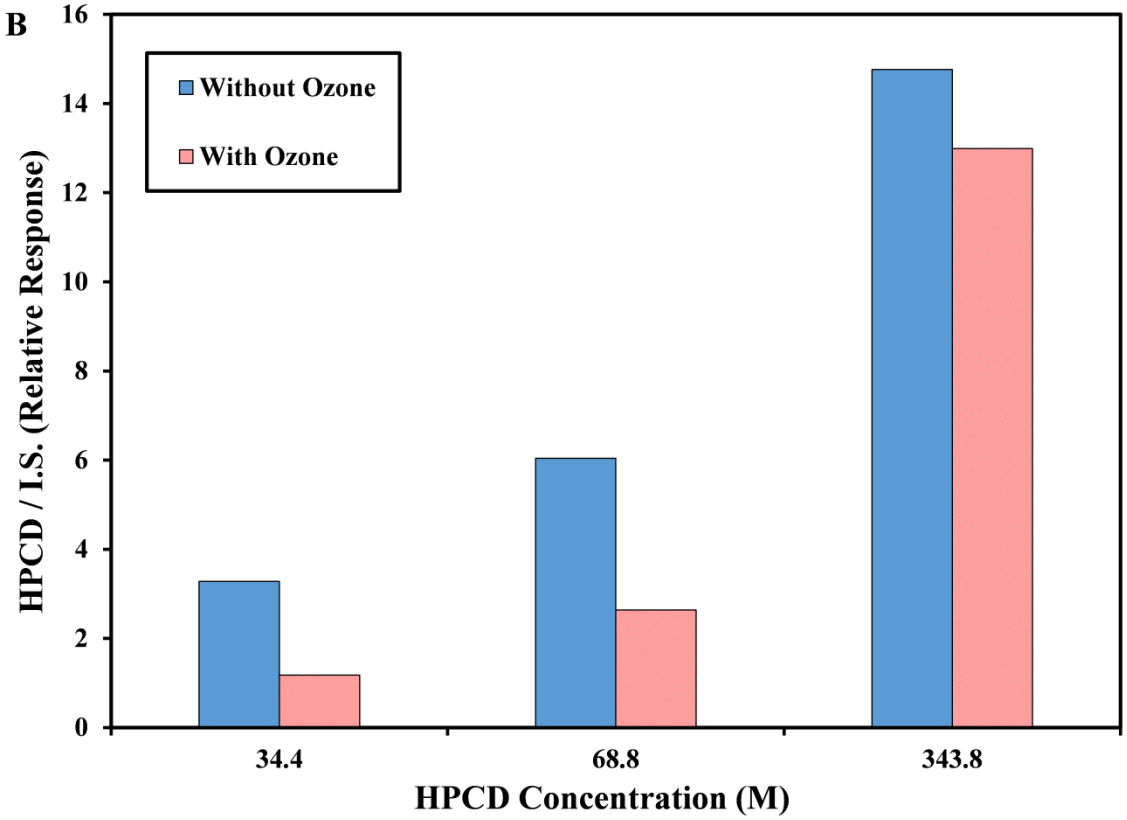
B
Without Ozone
With Ozone
HPCD / I.S. (Relative Response)
0
2
4
6
8
10
12
14
16
34.4
68.8
343.8
HPCD Concentration (M)

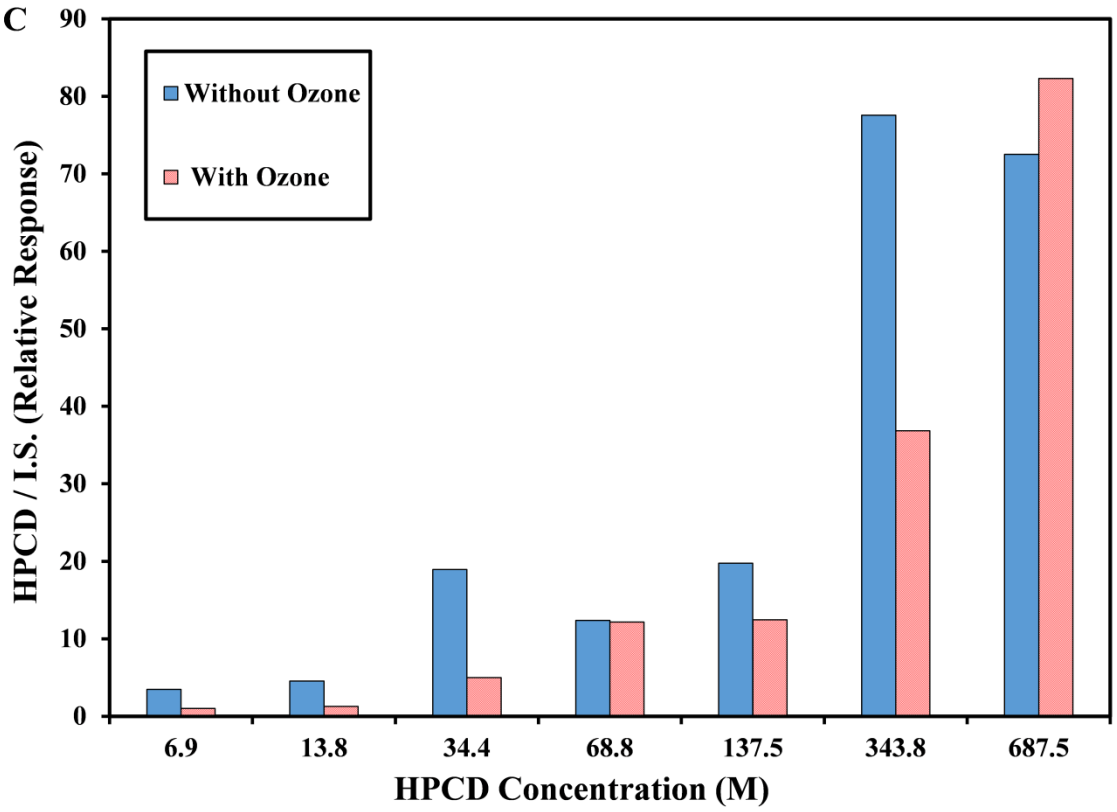

Figure 4.1.4**.** Linear ion trap relative quantitation of HPβCD with and without (A) 0.5 (0.024 M), (B) 1 (0.048 M), and (C) 2 mg/L (0.096 M) O_3 concentrations (I.S. = internal standard).

4.1.2 Ozone decomposition and stabilization within HPβCD inclusion complex

O_3 decomposition followed pseudo 1st-order reaction kinetics in the synthetic groundwater (without any complexation agents) and in groundwater containing HPβCD (Figure 4.1.5a). Dissolved O_3 rapidly reacted with the synthetic groundwater solution, and had a half-life of 0.5-1.3 hours (k = 0.526-1.42 hours^{-1}) (Table 4.1.1). O_3 was still measurable, persisted in solution longer, and had a smaller decay rate coefficient when HPβCD was present. The half-life of O_3 in groundwater solutions with HPβCD to O_3 mole ratios of 17.5:1 and 34.6:1 increased to 6.73 (k = 0.103 hours^{-1}) and 14.75 hours (k = 0.047 hours^{-1}), respectively. The O_3 half-life and HPβCD to O_3 mole ratio were linearly related for the O_3 decay experiments (Figure 4.1.5b), and the results from linear regression analyses are also presented (R^2=0.99). The increase in half-life with increases in HPβCD suggests that O_3 reactivity was decreased or delayed due to formation of an inclusion complex between O_3 and HPβCD. When the O_3 was more abundant than HPβCD (1:14.5 HPβCD to O_3 mole ratio), the half-life of O_3 was 0.37 hours (k = 1.894 hours^{-1}), which was not significantly different from the experiments with groundwater only (without HPβCD) (Table 4.1.1). Additional evidence for the formation of a HPβCD:O_3 complex was discovered as a shift in UV-vis spectroscopy wavelength scan results for solutions containing HPβCD and O_3 compared to unmixed solutions at similar concentrations (Jung et al., 2013; Liang et al., 2007a).

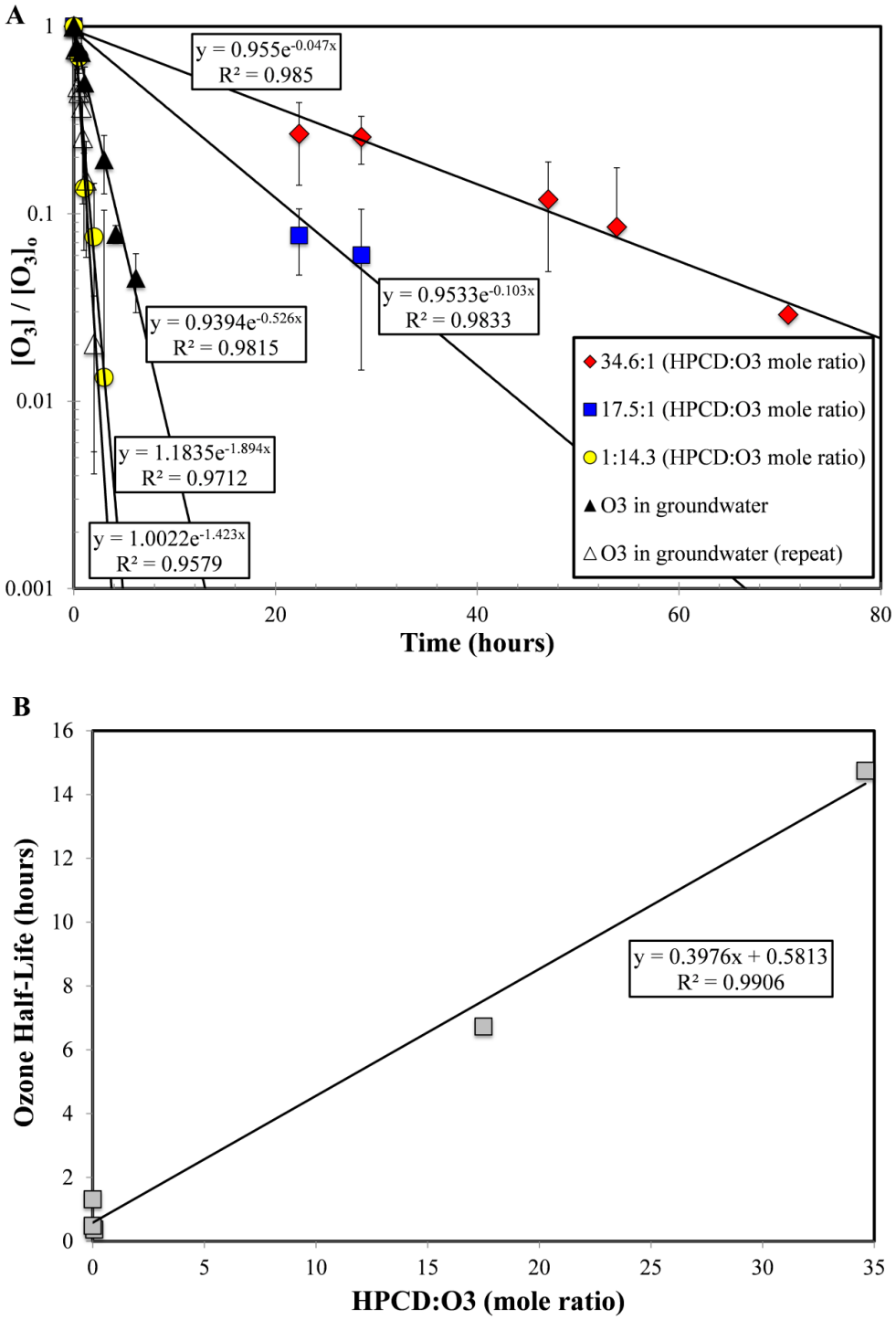

Figure 4.1.5. (A) O_3 concentration decay in groundwater solutions containing varying HPβCD to O_3 molar ratios. The lines are regression results assuming pseudo 1st order (exponential) decay, and error bars represent the 95% confidence interval for triplicates. (B) O_3 half-life times plotted as a function of HPβCD:O_3 molar ratio, and the line presents the linear regression analysis.

Table 4.1.1**.** Comparison of O_3 concentration decay pseudo 1st order rate constants (k) and half-life times in synthetic groundwater solutions with varying HPβCD to O_3 mole ratios. "O_3 in groundwater" contains no HPβCD.

Description	k ($hours^{-1}$)	O_3 Half-Life (hours)
O_3 in groundwater	0.53	1.32
O_3 in groundwater (repeat)	1.42	0.49
1:14.5 (HPβCD:O_3)	1.89	0.37
17.5:1 (HPβCD:O_3)	0.10	6.73
34.6:1 (HPβCD:O_3)	0.05	14.8

4.1.3 Ozone delayed release from the HPβCD inclusion complex

The cumulative O_3 mass release from the HPβCD complex and delayed reactivity of O_3 in groundwater with the potassium indigo trisulfonate indicator solution was investigated for solutions starting with a HPβCD to O_3 molar ratio of 34.6:1 and 9.4:1 (Figure 4.1.6a), which displays the cumulative increase of free O_3 concentration over time determined by the continuous oxidation of potassium indigo trisulfonate over time by O_3 upon release from the inclusion complex. Control experiments (without O_3) confirmed that indigo concentration did not change with HPβCD addition (i.e. no indigo- HPβCD complex) and the concentration of indigo did not change over time without O_3 (data not shown). The initial O_3 added was 0.5 mg/L, and upon addition of HPβCD the O_3 concentration decreased due to inclusion complex formation. The results from experiments containing HPβCD, O_3, and indigo potassium trisulfonate show increasing cumulative O_3 reactivity over time, which typically approached yet did not reach the initially present amount of O_3. These results suggest that the O_3 did form an inclusion complex with HPβCD, and over time the O_3 was released from the HPβCD cavity over approximately the first 75 hours. After which, the indigo reagent appears to begin decomposing (data not shown). Several additional experiments were conducted over a wide range of HPβCD and initial O_3 concentrations, and Figure 4.1.6b presents a compilation of delayed release experiments, which indicate, for each case, that O_3 concentrations in water constantly increases over time. The increase in free O_3 over time confirms that the inclusion complex is a reversible process, and that the O_3 reactivity is at least partially conserved. The released O_3 would be available for reaction with contaminants as indicated by the observed indigo transformation. Indigo is a model contaminant in this proof of concept evaluation. The results support the hypothesis that the partitioning of O_3 into the HPβCD cavity can, in fact, delay the reactivity of O_3 in groundwater solutions.

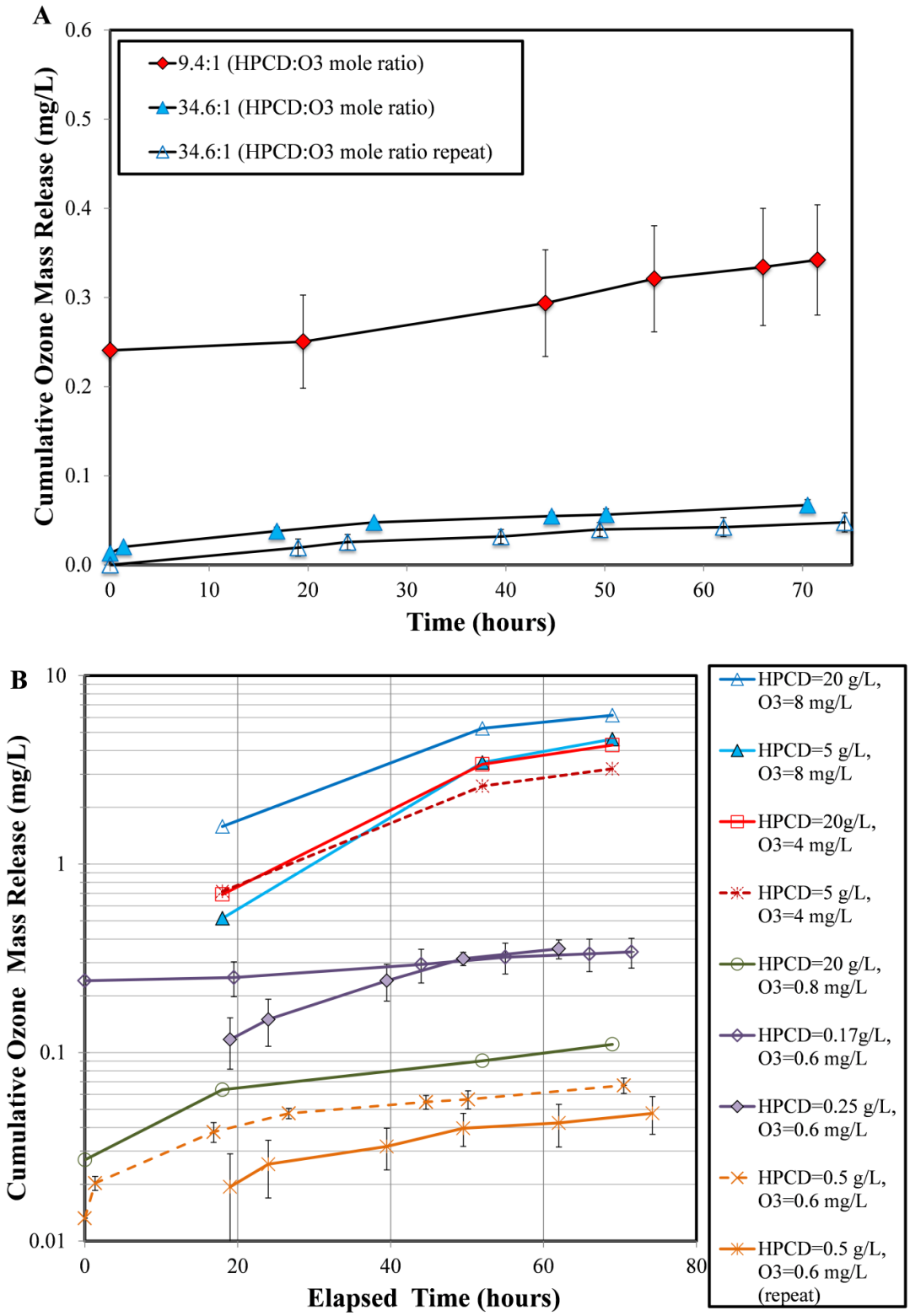

Figure 4.1.6. Delayed O_3 reactivity with potassium indigo trisulfonate in HPβCD solution starting with (A) 34.6μM:1μM and 9.4μM:1μM HPβCD to O_3 ratios, and (B) a compilation of several experiments over various HPβCD to O_3 ratios. Error bars (where present) represent the 95% confidence intervals.

4.1.4 Effect of HPβCD and organic matter on oxidant demand

Enhancement of the O_3 lifespan, longevity, and reaction specificity is essential to the development of an ISCO method for recalcitrant subsurface contaminants. Hydroxide radicals produced by O_3 are generally considered relatively nonspecific, and will react with water as well as solid-soil materials. Clayton et al. provide a review of O_3 reactions with organic matter, metal oxides, and dissolved solutes. For example, manganese and iron oxide catalysis of O_3 decay of contaminants has been suggested, at least in the gas phase (Clayton et al., 2011). Thus, the impact of HPβCD:O_3 complex formation on reaction specificity was also examined by testing the influence of the inclusion complex formation on the O_3 reactions with naturally occurring reduced species associated with soils. Experiments investigating the effects of HPβCD on the O_3 oxidant demand were conducted using AFP44 sediment. O_3 oxidant demand was quantified in grams O_3 per kilogram sediment with and without HPβCD. Under the experimental conditions tested, a system containing HPβCD and O_3 at a 34.6:1 mole ratio was able to decrease the O_3 oxidant demand of AFP44 sediment by approximately 55% when compared to the system without HPβCD (Figure 4.1.7a). These results are consistent with our original hypothesis that HPβCD can improve the reaction specificity of O_3 by forming the inclusion complex that results in decreasing the oxidant consumption by aquifer solids.

Examination of O_3 facilitated delivery ISCO also requires evaluation of potential O_3 oxidant demand variability and controls over O_3 oxidant demand magnitudes. In an attempt to examine the effect of SOM on the O_3 oxidant demand, the standard method for quantifying the $KMnO_4$ oxidant demand was modified for O_3, and tested on all three sediments. The O_3 oxidant demand results are consistent with the standard method for permanganate. Both the O_3 oxidant demand (Figure 4.1.7b) and $KMnO_4$ oxidant demand (data not shown) results had an increasing linear trend between the oxidant demand and SOM content and CEC. The results confirm that O_3 reacts with both aqueous hydroxide ions and sediment organic matter. SOM is a major source of O_3 oxidant demand, and O_3 likely reacts with other high surface area (high CEC) soil minerals (i.e., metal oxides), and this further supports the notion that O_3 oxidant demand can be reduced by separating O_3 from solid surface interactions using an inclusion complex with HPβCD. Similarly, the HPβCD:O_3 complex may potentially limit O_3 access to reactive species in the aqueous phase (e.g., radical scavengers). Based on these results, one can expect the oxidant demand to increase with increasing SOM content, whereas, other oxidizable minerals may also contribute. There are few prior reports of O demand and the methods may be significantly different from those used herein (Huling and Pivetz, 2006). However, the reported values are similar to those reported herein (Huling and Pivetz, 2006; Masten and Davies, 1997). Although these results support our understanding of the variability and controls over oxidant demand, it is important to note that laboratory-scale results may not directly translate to site-specific, field-scale values (Mumford et al., 2004; Xu and Thomson, 2009).

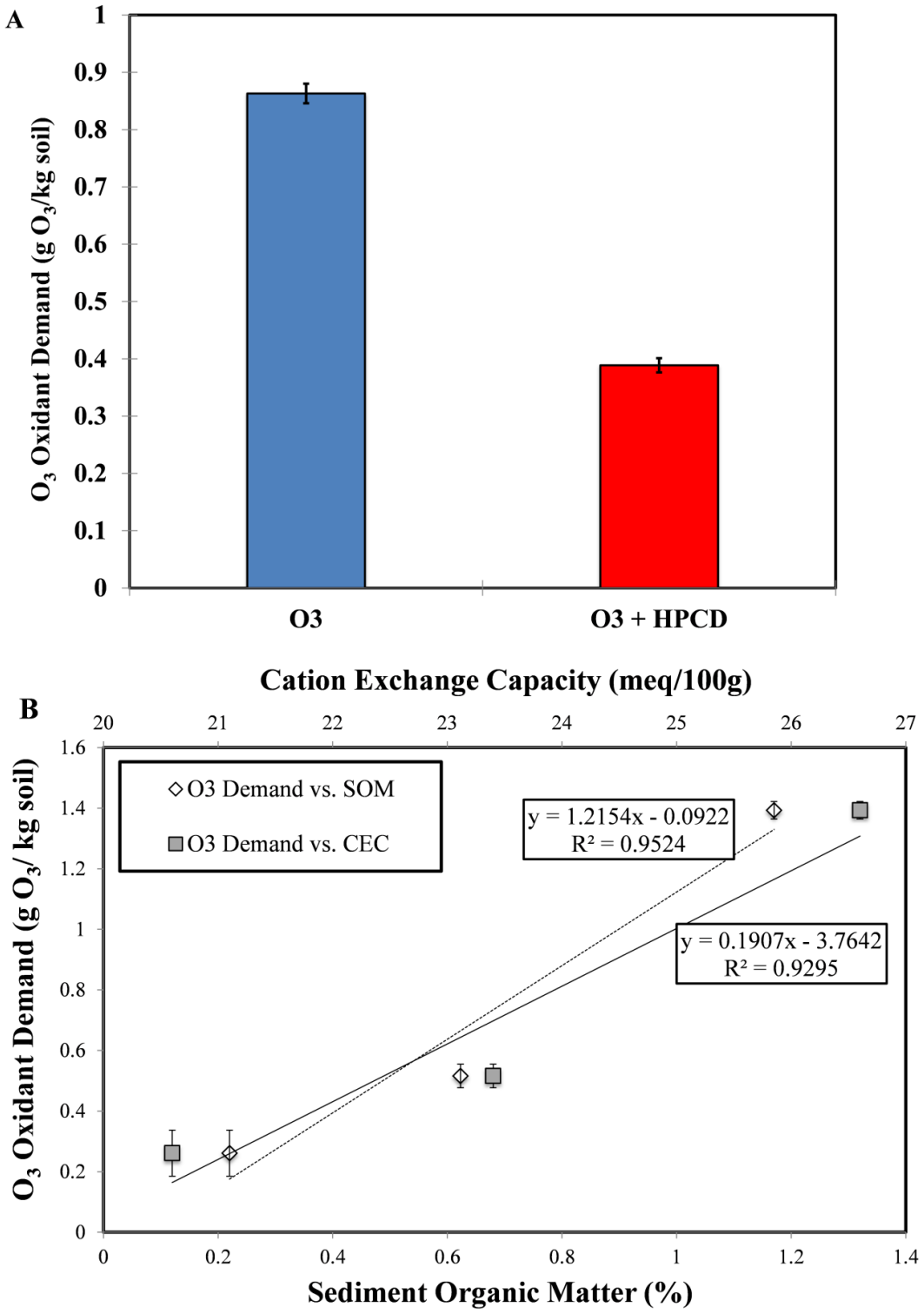

Figure 4.1.7. (A) O_3 NOD of AFP44 non-bioamended sediment for groundwater solutions containing O_3 with and without HPβCD (34.6:1 HPβCD to O_3 mole ratio). The initial O_3 concentration for ONOD experiments for HPβCD was 1.5 mg/L. (B) O_3 natural oxidant demand (ONOD) as a function of SOM and CEC for the AFP44, Amended-1, and Amended-2 soils. The lines represent the regression analyses, and the error bars indicate 95% confidence intervals.

4.2 Oxidant Demand and Scavenging of 1,4-Dioxane Decay Results and Discussion

4.2.1 Influence of groundwater chemistry on 1,4-dioxane degradation

Both control tests showed minimal mass-loss of 1,4-dioxane in 48 hours (data not shown). The results for 1,4-dioxane degradation by siderite-activated persulfate-H_2O_2 in ultrapure water and groundwater are presented in Figure 4.2.1. There was approximately 35% 1,4-dioxane loss for the system in the presence of groundwater at 48 hours. In contrast, approximately 50% degradation was attained for the system with ultrapure water. The results indicate considerable impact of the background groundwater constituents on the removal of 1,4-dioxane. 1,4-Dioxane degradation was essentially identical in ultrapure water (~31%) and groundwater (~29%) after 4 hours of reaction. However, the degradation rates deviated greatly thereafter.

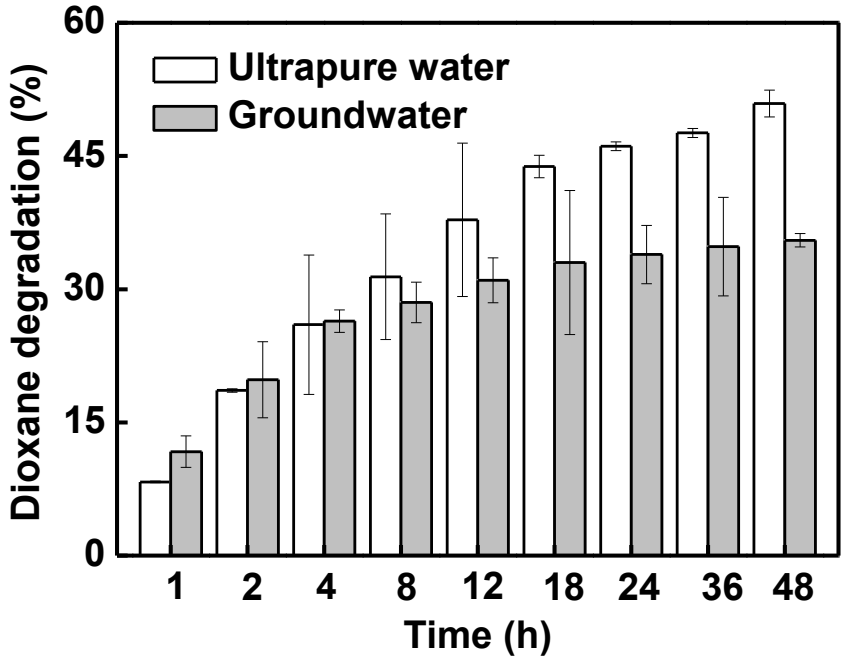

Figure 4.2.1**.** 1,4-Dioxane degradation by the siderite-activated persulfate and H_2O_2 in ultrapure water and groundwater.

1,4-Dioxane degradation exhibited a two-stage reaction pattern, with a high rate of degradation in the first 4 hours followed by a relatively slow rate of degradation. Pseudo-first-order reaction rate constants for 1,4-dioxane degradation with and without groundwater are 0.064±0.001 and 0.068±0.001 h^{-1} for the initial degradation stage, indicating similar degradation efficiency during this period. Conversely, the rate constants were 0.006±0.001 and 0.016±0.001 h^{-1} for the later stage. The results indicate that the presence of groundwater resulted in approximately 3 times slower degradation after the first 4 hours.

The reduction of the rate of 1,4-dioxane degradation in the presence of groundwater was most likely caused by activation inhibition and/or the radical scavenging effect as several ions are abundant in the groundwater sample used herein. They are typical constituents for most

groundwaters. Specific experiments were conducted to illuminate the impact of specific ions on 1,4-dioxane degradation, the results of which are presented in the following sections.

Table 4.2.1. Pseudo-first-order reaction rate constant k and half-life $t_{1/2}$ for 1,4-dioxane degradation in siderite-activated H_2O_2 and persulfate.

Aqueous phase	Rate constant k (h^{-1})		Half-life $t_{1/2}$ (h)	
	Rapid[a]	Slow[b]	Rapid	Slow
Ultrapure water	0.068	0.016	10.2	43.3
Groundwater	0.064	0.006	10.8	115.5

[a] Rate constant k for siderite-activated binary oxidant system was calculated by rapid reaction period

[b] Rate constant k for siderite-activated binary oxidant system was calculated by slow reaction period

4.2.2 Influence of selected anions on the degradation of 1,4-dioxane

Chloride (Cl^-), sulfate (SO_4^{2-}), and bicarbonate (HCO_3^-) ions were studied, since they are the most abundant anions in the groundwater used in the previous section. They are also three typical anionic constituents in groundwater. The degradation of 1,4-dioxane in the presence of chloride, sulfate, and bicarbonate, respectively, is illustrated in Figure 4.2.2a. The addition of chloride ion produced no significant impact on 1,4-dioxane degradation. However, 1,4-dioxane removal was significantly inhibited with the addition of sulfate and bicarbonate ions, with degradation reduced by ~35% and 66%, respectively, compared to ultrapure water.

It is hypothesized that the inhibition effect observed is related to the scavenging of hydroxyl and sulfate radicals by the added ions. The scavenging ability is expected to decrease in the following order (for equal concentration): bicarbonate > sulfate > chloride (Kochany and Lipczynska-Kochany, 1992; Liang et al., 2006; Lipczynska-Kochany et al., 1995). It is also reported that chloride might have a greater impact on Fenton processes than bicarbonate and sulfate (Riga et al, 2011). However, a chloride concentration of 100 mM (3.5 g/L) was used in that study, higher than what is typical for most groundwaters.

Additional experiments were conducted with different concentrations of bicarbonate ion. The inhibition effect increased with the increase of bicarbonate concentrations from 0 to 2 mM (Figure 4.2.2b). Moreover, 1,4-dioxane degradation efficiency was significantly inhibited with as low as 0.2 mM bicarbonate present. No further significant increase in inhibition was observed above 0.2 mM bicarbonate. Further inhibition was limited due to the limited amount of radicals present.

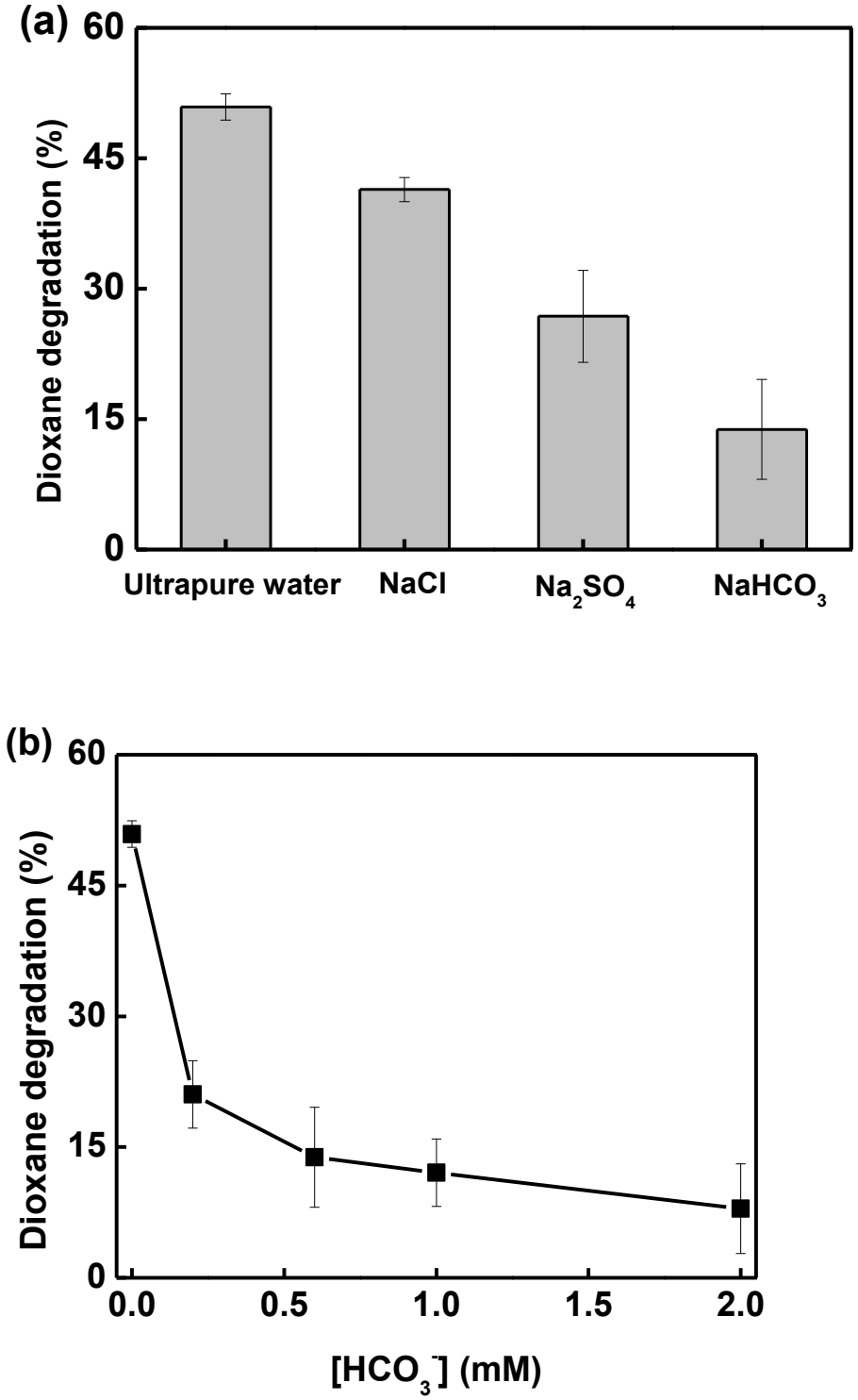

Figure 4.2.2. 1,4-Dioxane degradation by the siderite-activated persulfate and H_2O_2 after 48 h reaction (a) the effects of Cl^-, SO_4^{2-}, and HCO_3^- on the degradation efficiency; (b) the influence of HCO_3^- concentration on the degradation efficiency.

4.2.3 Influence of selected cations on the degradation of 1,4-dioxane

The degradation of 1,4-dioxane in the presence of potassium (K^+), calcium (Ca^{2+}), and magnesium (Mg^{2+}), respectively, is illustrated in Figure 4.2.3a. 1,4-dioxane degradation was inhibited with the addition of potassium, calcium, and magnesium ions, with degradation reduced by ~35%, 59%, and 28%, respectively. It is noteworthy that the observed inhibition is particularly strong for calcium.

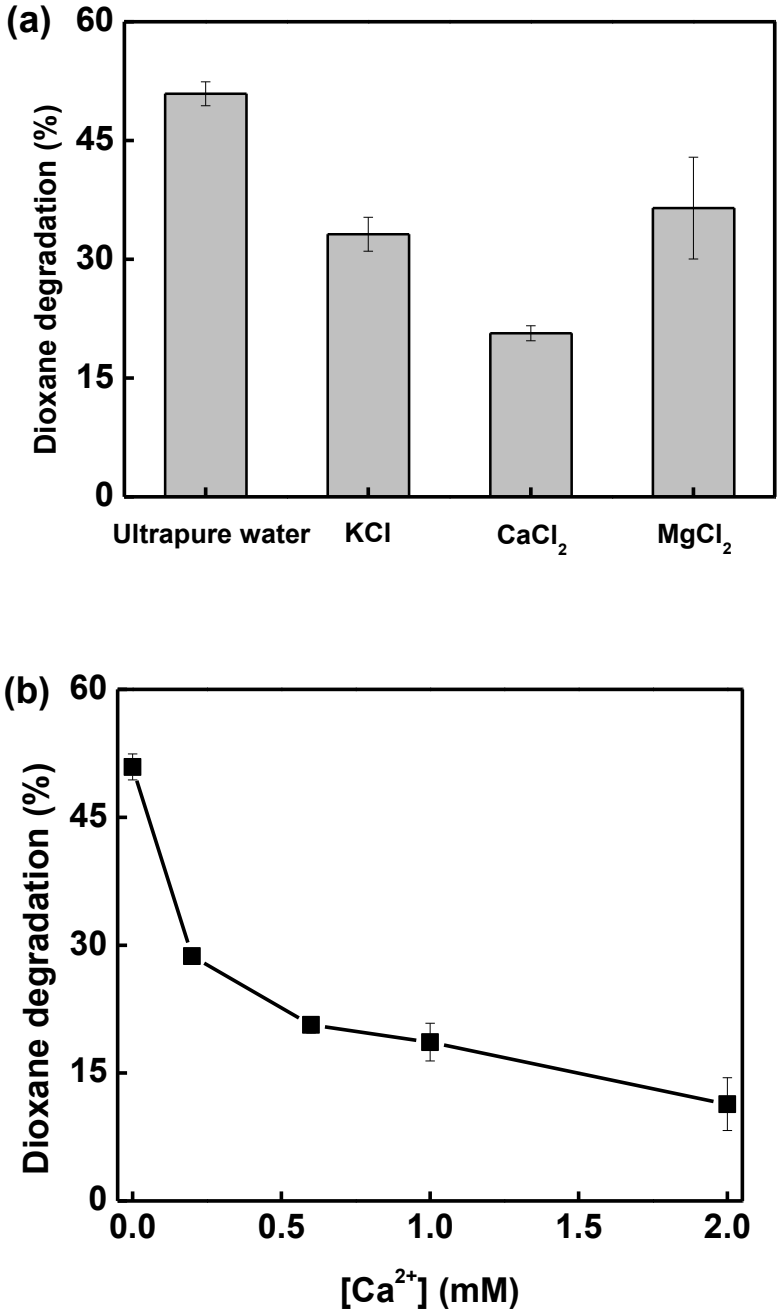

Figure 4.2.3. 1,4-Dioxane degradation by the siderite-activated persulfate and H_2O_2 after 48 h reaction (a) the effects of K^+, Ca^{2+}, and Mg^{2+} on the degradation efficiency; (b) the influence of Ca^{2+} concentration on the degradation efficiency.

One possibility is that potassium, calcium, and magnesium ions might consume oxidant without generation of effective radicals, and lead to less oxidant available for the oxidative degradation of 1,4-dioxane. For example, calcium might consume persulfate to generate $CaSO_4$ without the generation of sulfate radicals. Calcium is a typical cationic constituent in groundwater, and its concentration can reach hundreds of milligram per liter in high salinity groundwater.

Additional experiments were conducted with different concentrations of calcium ion. The inhibition effect increased with the increase of calcium concentrations from 0 to 2 mM (Figure 4.2.3b). There was a considerable decrease in degradation efficiency when calcium concentration increased from 0 to 0.2 mM. However, the decrease in efficiency was more modest when the concentration exceeded 0.2 mM.

4.3 Cyclodextrin Inclusion Complex Measurement Results and Discussion

4.3.1 Direct Spectrophotometric Measurement Method

Absorbance changes have been used to investigate aqueous complexation (Jung et al., 2013; Liang et al., 2007a). UV absorbance values generally changes upon addition of HPβCD to solutions of TCA, TCE, 1,4-dioxane, or O_3, which indicates that each of these systems forms inclusion complexes. Results in Supplementary Data illustrate the UV absorbance as a function of wavelength data with and without HPβCD. Figure 4.3.1 and 4.3.2 show the Benesi-Hildebrand plots and Scott's plots, respectively, used to determine stoichiometry and K values. The linear regressions (R^2=0.99-0.84) for O_3, TCA, and TCE experiments in these two plots (Benesi-Hildebrand and Scott's plot) indicated a 1:1 stoichiometry for inclusion complexation. The average inclusion constants from Benesi-Hildebrand plots for O_3, TCE, and TCA were 0.5 mM^{-1}, 3.5 mM^{-1}, and 2.6 mM^{-1}, respectively. The average values from Scott's plot for O_3, TCE, and TCA were 1.7 mM^{-1}, 3.8 mM^{-1}, and 2.6 mM^{-1}, respectively. Table 4.3.1 presents the resulting K mean and standard deviation values from the UV spectroscopic method calculated from both types of plots at different ionic strengths (i.e., DI water, 50 mM NaCl, and 100 mM of NaCl) and pH (i.e., values 6 and 9). Figure 4.3.1 and 4.3.2 also include data from experiments conducted at different ionic strengths for TCE, which can also be compared to results of the experiments conducted with DI water. Salinity variation experiments were also conducted for TCA and 1,4-dioxane for binding constant value determination (Table 4.3.1). However, the impact of salt additions on O_3 complexation were not presented due to the reactivity of O_3 with chloride ions to form molecular chlorine. Increasing salinity showed an increase in the inclusion constants for TCE and TCA. Table 4.3.1 also lists the inclusion constants for TCE and TCA at pH 9, and there was an increase in binding constant mean values with the pH increase (from pH 6 to 9) for TCE and TCA. Inclusion constant values for O_3 at pH 9 were unobtainable, likely because of rapid O_3 reaction with hydroxide and OH• radical production. At pH 6 and 9 in DI water, there was no complexation observed for 1,4-dioxane with HPβCD. However, complexation was repeatedly observed and K was determined for HPβCD:1,4-dioxane upon addition of NaCl up to 100 mM. Eight of the ten experiments (i.e., except TCE at pH 9 and O_3 at pH 6) had Benesi-Hildebrand and Scott's plot results that were statistically similar, which suggests a significant similarity between these methods. The minor deviations observed between these two methods are expected given experimental variability. The level of similarity of the Benesi-Hildebrand and Scott's plot results suggest comparability between these methods.

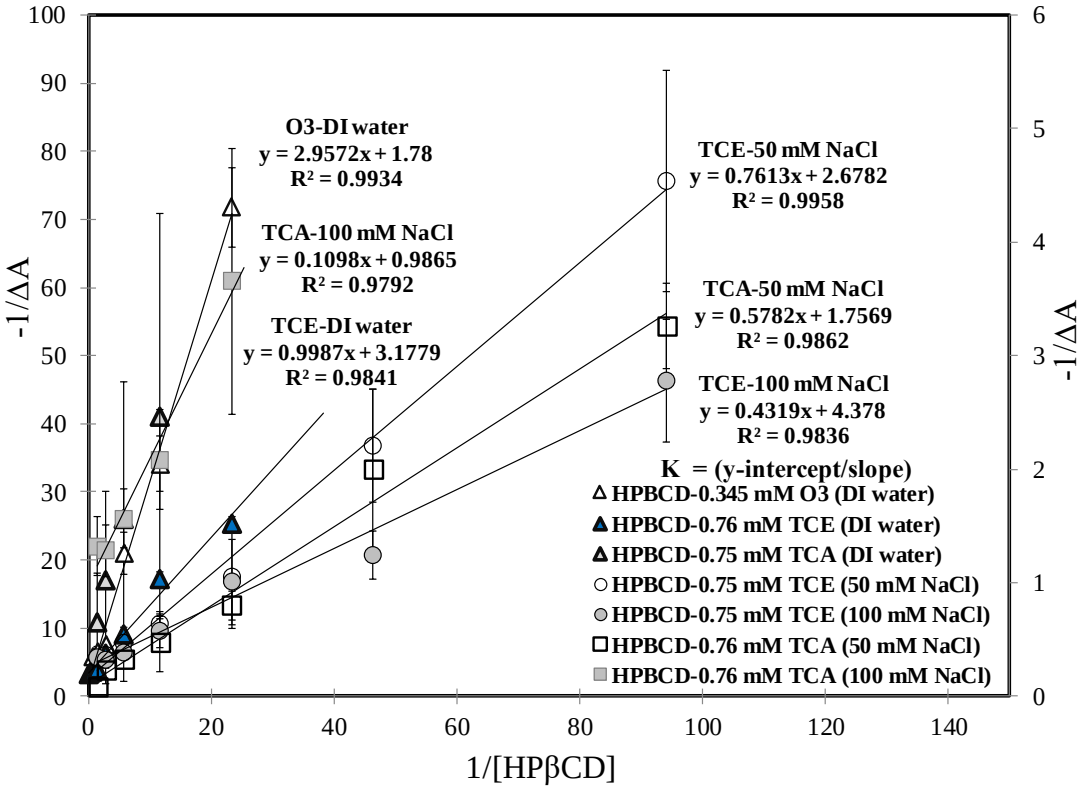

Figure 4.3.1**.** Benesi-Hildebrand plot for O_3, TCA, and TCE (in DI water and two salt concentration solutions). HPβCD:TCA (100 mM NaCl) is on the secondary axis, symbols indicate mean values, error bars are standard deviations, and lines present regression results used for binding equilibria analysis.

Table 4.3.1**.** Binding constant (K) results measured from UV spectroscopy (i.e., direct method). Symbol dash (-) means there was no measureable complexation, and mean and standard deviation values are presented.

		HPβCD:TCA		HPβCD:TCE		HPβCD:1,4-dioxane		HPβCD:O_3	
pH	NaCl (mM)	Benesi-Hildebrand	Scott's Equation	Benesi-Hildebrand	Scott's Equation	Benesi-Hildebrand	Scott's Equation	Benesi-Hildebrand	Scott's Equation
6	0	2.6 ± 0.4	2.6 ± 1.4	3.5 ± 1.5	3.8 ± 1.7	-	-	0.5 ± 0.4	1.7 ± 0.2
6	50	7.5 ± 1.1	5.7 ± 2.5	3.9 ± 2.8	7.2 ± 0.8	-	-	-	-
6	100	9.9 ± 3.8	15.8 ± 2.1	6.5 ± 1.8	9.1 ± 2.8	2.9 ± 2.1	3.8 ± 2.2	-	-
9	0	3.8 ± 1.1	7.1 ± 1.7	7.1 ± 1.9	9.5 ± 1.1	-	-	-	-

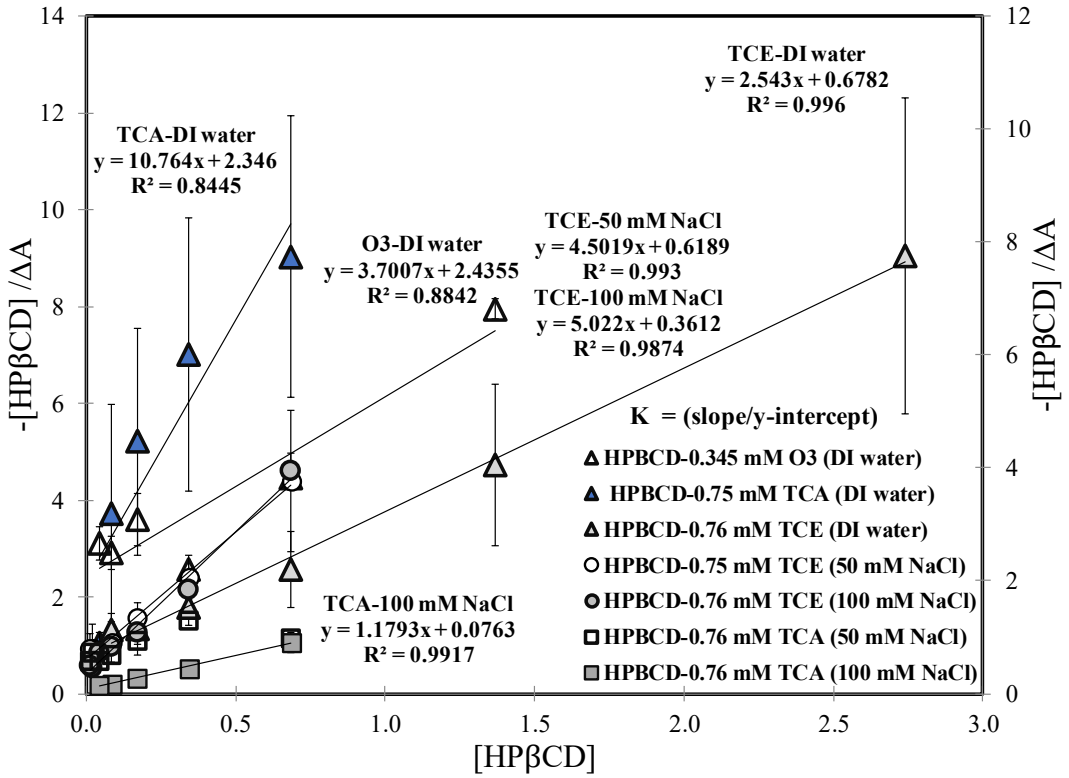

Figure 4.3.2**.** Scott's plot for O_3, TCA, and TCE (in DI water and two salt concentration solutions). The HPβCD with TCE-DI water, TCE-100 mM NaCl, and TCA with 50 and 100 mM NaCl results are on the secondary axis. Symbols indicate mean values, error bars are standard deviations, and lines present regression results used for binding equilibria analysis.

4.3.2 Competitive Complex Measurement Method

TNS was selected as the competitive guest compound, because the complexation of TNS with HPβCD with quantification by fluorescence spectroscopy is well known (Kondo et al., 1976). Figure 4.3.3 presents the changes in fluorescence intensity with constant TNS (10 µM or 1 µM) as a function of change in HPβCD and γ-CD concentration to determine I_0, as the maximum fluorescence intensity for a given TNS concentration with increasing CD concentrations, which indicates the maximum amount of TNS can fit into the HPβCD or γ-CD cavity. The parameter I_0 is required to quantify how much TNS can be replaced from HPβCD or γ-CD cavity by guest molecule when guest molecule and TNS are present in the same solution. Results indicate that the change in fluorescence intensity became stable above ~3-4 mM of HPβCD. I_0 was 209 fluorescence intensity when 10 µM of TNS were added to HPβCD, and I_0 was 27 fluorescence intensity when 1 µM of TNS were added to HPβCD. Similarly for γ-CD, I_0 was 5.4 for 1:1 complex formation with 1 µM of TNS. The fluorescence intensity of TNS did not change with γ-CD as much as it changed with HPβCD, because the cavity volume of γ-CD (0.427nm^3) is two fold larger than the cavity volume of HPβCD (0.261 nm^3) (Yang et al., 2006).

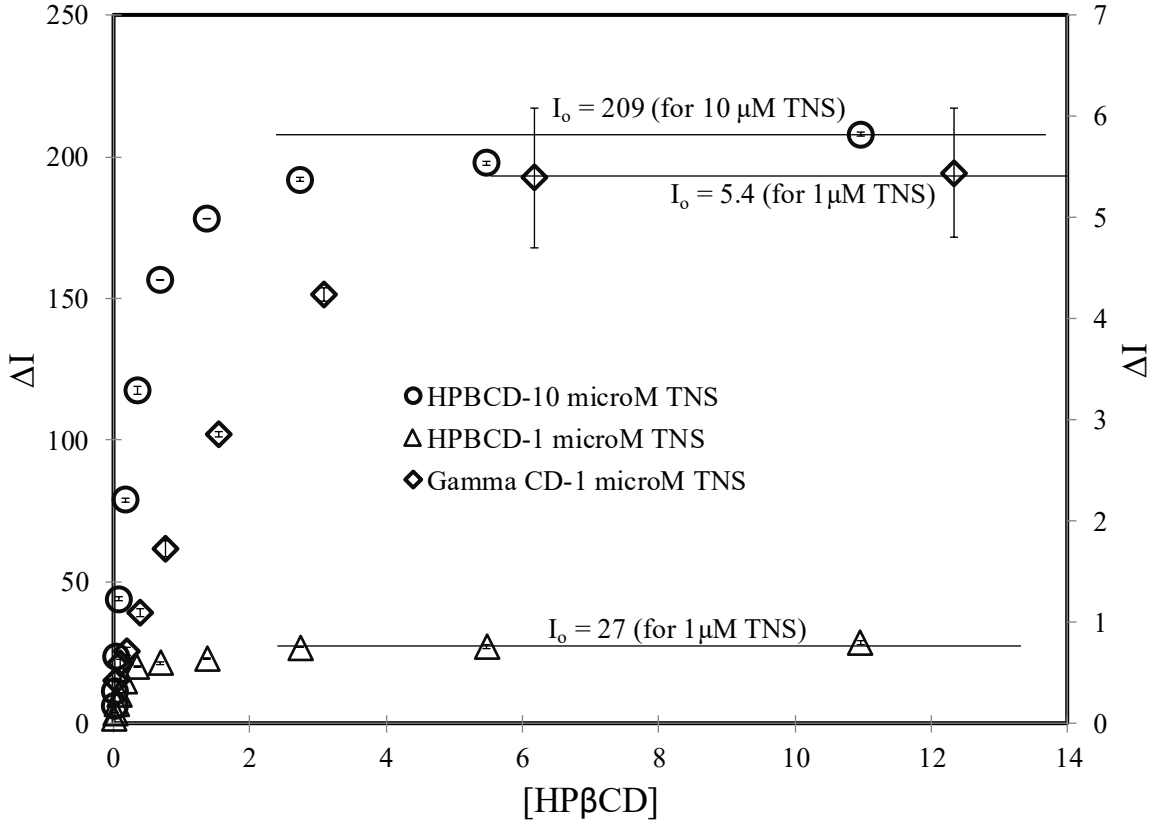

Figure 4.3.3**.** Change in fluorescence intensity of TNS as a function of increasing HPβCD concentration (mM) for determination of I_0 (maximum fluorescence intensity). Symbols indicate mean values, error bars are standard deviations, and γ-CD 1 μM TNS data are on the secondary axis.

Figure 4.3.4 is the Benesi-Hildebrand plot of 1/ΔI versus 1/[HPβCD] or 1/[γ-CD] for experiments with TNS and HPβCD or γ-CD without additional competing guest compounds. The increasing trends of the data were well described with linear regression analysis as in Figure 4.3.4 (R^2 = 0.98 - 0.99), which confirms 1:1 stoichiometry of TNS with both CDs. The guest concentrations for the experiments presented here were low enough to avoid other complexation stoichiometries. The mean K values for HPβCD:TNS complexes were 4.2 mM^{-1} at pH 6 and 5.7 mM^{-1} at pH 9, and the K for γ-CD:TNS was 0.8 mM^{-1} (at pH 6) (Table 4.3.2). These results are comparable to previously reported K values for HPβCD:TNS (4.5 mM^{-1}) and γ-CD:TNS (0.11 mM^{-1}) (Johnson and Reinsborough, 1992).

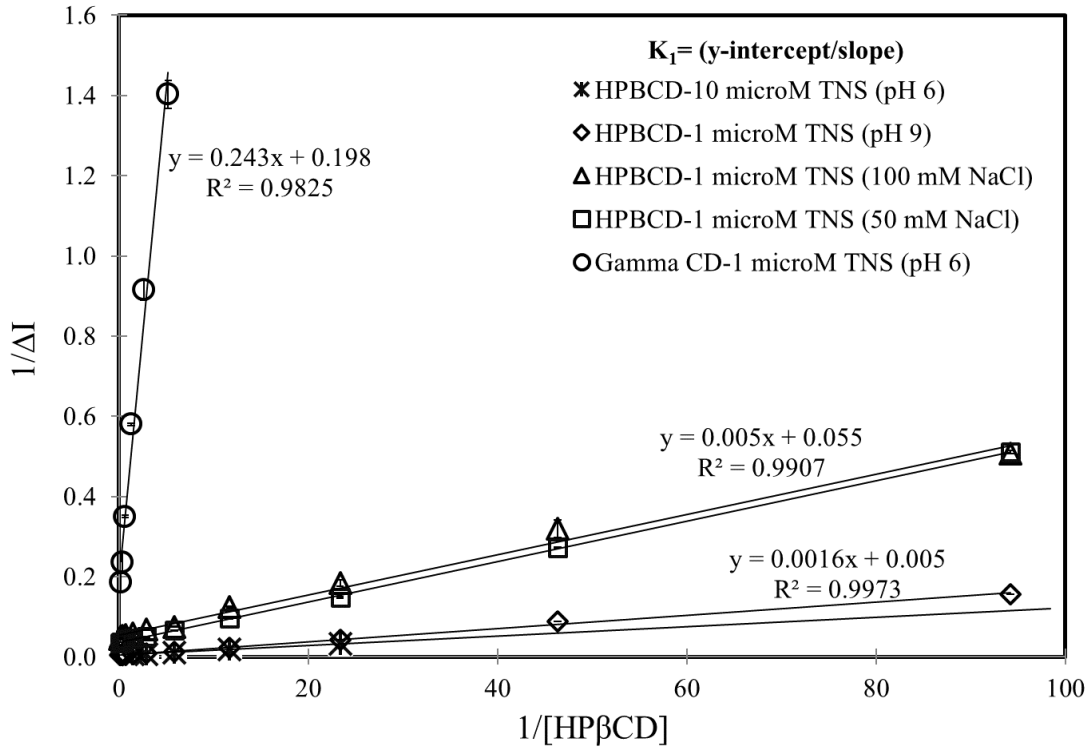

Figure 4.3.4**.** Benesi-Hildebrand plot for TNS complexation with HPβCD within different pH and salt concentration solutions, and for TNS complexation with γ-CD in DI water. Symbols indicate mean values, error bars are standard deviations, and lines present regression results used for binding equilibria analysis.

Table 4.3.2**.** Binding constant (K) results measured by the fluorescence spectroscopy (i.e., competitive method) with TNS and direct method results for TNS complexation. Symbol dash (-) indicates there was no measureable complexation, and mean and standard deviation values are presented.

pH	NaCl (mM)	HPβCD:TNS	HPβCD:TCA	HPβCD:TCE	HPβCD:1,4-dioxane	HPβCD:O_3
6	0	4.2 ± 0.3	1.8 ± 0.5	3.0 ± 1.6	-	0.6 ± 0.3
6	50	7.4 ± 0.1	2.1 ± 0.5	3.6 ± 0.3	-	-
6	100	11.9 ± 1.4	8.4 ± 0.6	7.7 ± 0.4	2.3 ± 0.6	-
9	0	5.7 ± 1.0	3.8 ± 0.6	5.5 ± 1.5	-	1.2 ± 0.5

Experimental results including 1/ΔI versus 1/[HPβCD] at pH 9 and at two different ionic strengths (100 mM and 50 mM of NaCl) used for determining K of HPβCD:TNS are also shown in Figure 4.3.4 for comparison to experiments conducted in DI water. K values for TNS increased with increasing initial pH values from 6 to 9, and there was also a significant difference observed in binding constant of HPβCD:TNS with increasing ionic strength (i.e., NaCl addition). The mean binding constant increased from 4.2 mM^{-1} (DI water) to 7.4 mM^{-1} at 50 mM of NaCl and also

increased to 11.9 mM^{-1} at 100 mM (Table 4.3.2). The increases observed in K measured with increases in initial pH value may be related to the salt additions used to modify the initial pH. This increasing binding constant trend with increasing salinity is similar to the observations obtained for TCE and TCA (Table 4.3.1). These K_1 values for TNS with HPβCD were then used to determine K_2 values using data from experiments containing HPβCD, TNS, and an additional competitive guest compound (Equation 6).

The plot of $Q_1Q_2/(Q_2-Q_1)$ versus Q_2, which is the ratio of free TNS to the CD bound TNS in absence and presence of additional guest molecule is shown in Figure 4.3.5. The data indicate increasing trends except for the γ-CD experiment. Linear regression results with R^2= 0.88-0.99 confirm inclusion complex formation and indicated 1:1 stoichiometries of HPβCD:O_3, HPβCD:TCE, and HPβCD:TCA. The resulting mean K values for TCE, TCA, and O_3 with HPβCD at pH 6 were 3.0 mM^{-1}, 1.8 mM^{-1}, 0.6 mM^{-1}, respectively (Table 4.3.2). However, the negative slope indicated for the γ-CD:TCA resulted in negative K values estimates, which suggests that there may not be a complex, or the γ-CD inclusion complexation may be near the lower limit for these measurement methods.

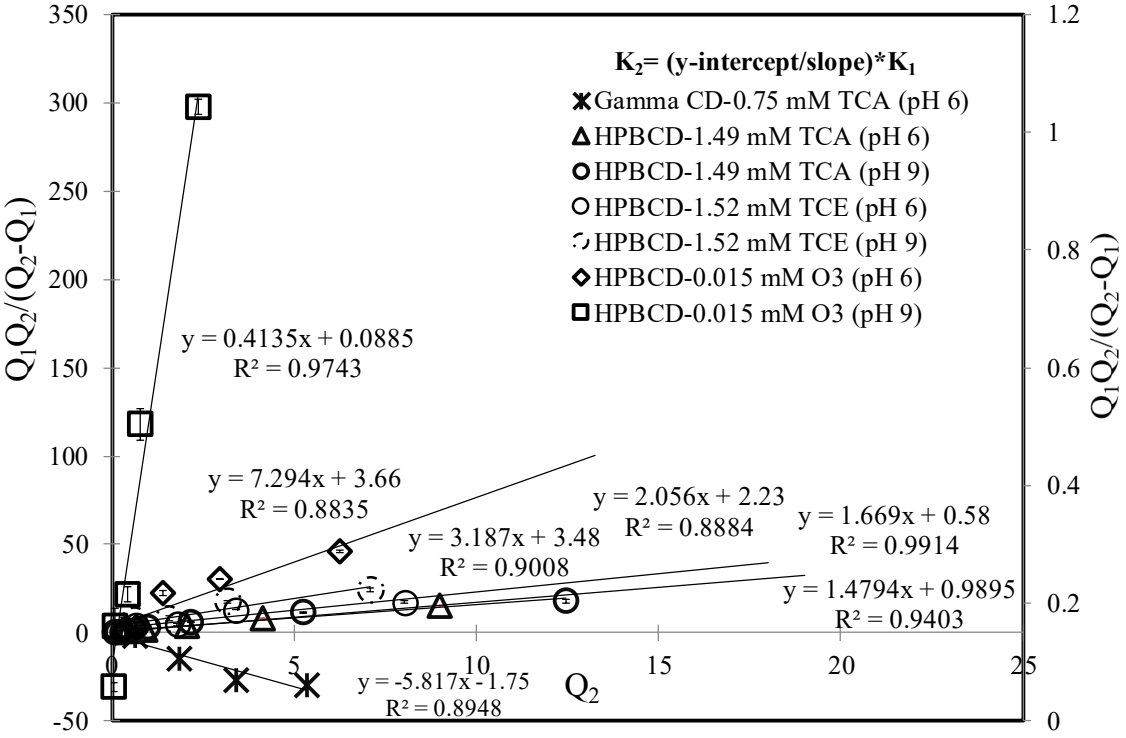

Figure 4.3.5**.** Plot of $Q_1Q_2/(Q_2-Q_1)$ versus Q_2 for TCA, O_3, and TCE with HPβCD at pH values 6 and 9 and for TCA with γ-CD at pH 6. Symbols indicate mean values, error bars are standard deviations, and lines present regression results used for binding equilibria analysis.

Data from experiments at initial pH 9 for comparison with those at initial pH 6 are presented in Figure 4.3.5. Linear regression results indicate 1:1 stoichiometries of TCE, TCA, and O_3 with HPβCD at pH 9. The mean K values of TCE, TCA, and O_3 at pH 9 were 5.5 mM^{-1}, 3.8 mM^{-1}, and 1.2 mM^{-1}, respectively (Table 4.3.2), and these values were increased compared to those for experiments conducted at initial pH 6 (noted above), which may be attributed to changes

in pH and/or NaOH concentrations used to alter the pH. The trends in K values increasing with initial pH values are consistent for both the direct and competitive methods (Table 4.3.1 and 4.3.2).

Figure 4.3.6 is the plot of $Q_1Q_2/(Q_2-Q_1)$ versus Q_2 for TCA and TCE competitive complexation in the presence of TNS. Linear regression, with R^2= 0.82-0.97 (except TCA with 50 mM of NaCl which has a low R^2) confirmed complexation and 1:1 stoichiometry (Figure 4.3.6). The binding constant mean values determined for TCE and TCA with HPβCD in DI water were 3.0 mM^{-1} and 1.8 mM^{-1}, respectively; at 50 mM of NaCl were 3.6 mM^{-1} and 2.1 mM^{-1}, respectively; and at 100 mM of NaCl were 7.7 mM^{-1} and 8.4 mM^{-1}, respectively (Table 4.3.2). These values generally increased with increasing salinity, which was also the trend observed for TNS and TCE and TCA using the UV spectroscopy method (Tables 4.3.1 and 4.3.2). Acquiring K values for HPβCD:O_3 at different NaCl concentrations, was not possible because O_3 reacts with Cl.

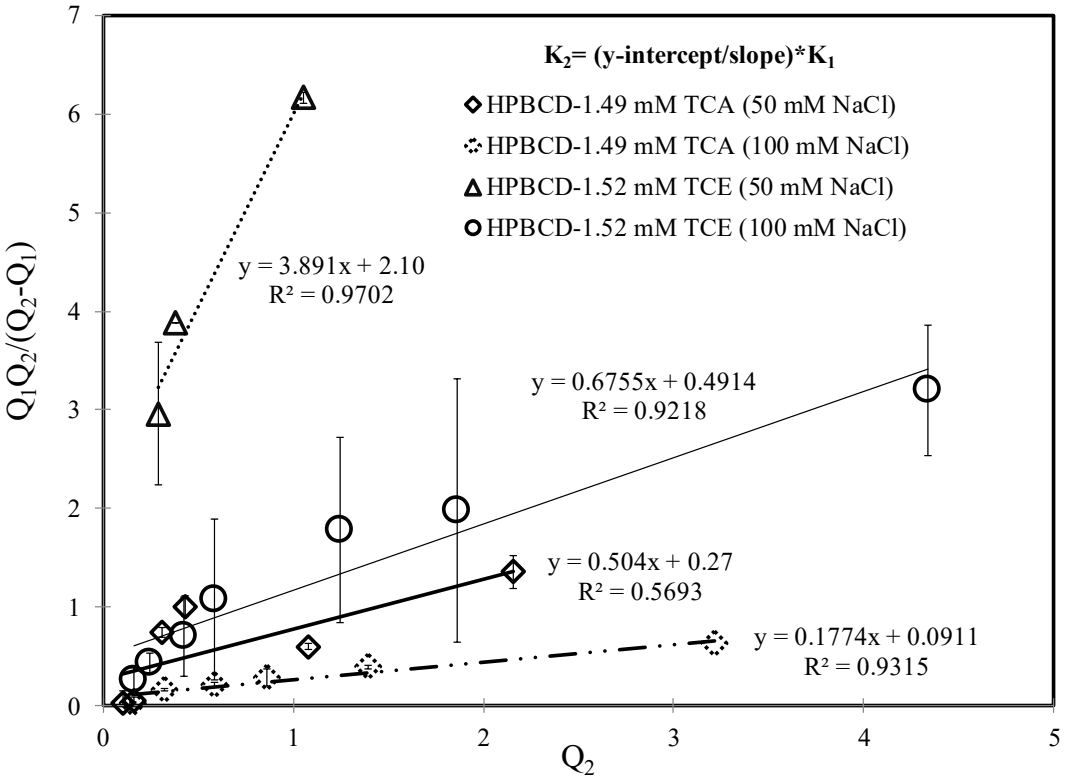

Figure 4.3.6**.** Plot of $Q_1Q_2/(Q_2-Q_1)$ versus Q_2 for TCE and TCA within two different salt concentration solutions. Symbols indicate mean values, error bars are standard deviations, and lines present regression results used for binding equilibria analysis.

Figure 4.3.7 presents HPβCD:1,4-dioxane complexation data from a series of experiments in DI water, 50 mM NaCl, and 100 mM NaCl. There was a decreasing slope observed for HPβCD:1,4-dioxane in DI water and 50 mM of NaCl, which resulted in negative K value estimates indicated no measureable complexation of 1,4-dioxane with HPβCD. However, this decreasing trend was reversed, and there was an increasing slope observed for HPβCD:1,4-dioxane with 100 mM of NaCl, which indicated complexation of 1,4-dioxane with HPβCD was only measureable at the higher salt content. The mean K for HPβCD:1,4-dioxane was 2.3 mM^{-1} in 100

mM of NaCl (Table 4.3.2). This binding constant is comparable to the 2.9 and 3.8 mM^{-1} mean values obtained using the direct methods (i.e., Benesi-Hildebrand and Scott's plot) and the overlapping standard deviations suggest that the estimates are statistically similar. For both direct and competitive methods, K was only measureable upon addition of salt at a concentration of 100 mM NaCl (Table 4.3.1 and 4.3.2). We attribute this to a negligible, or a not measureable, amount of complexation at low salinity due to the relatively high polarity and solubility of 1,4-dioxane compared to TCE and TCA. This suggests that complexation may have been enabled with increased salt concentration due to "salting out" effects and creating a sufficient decrease in 1,4-dioxane compound aqueous solubility.

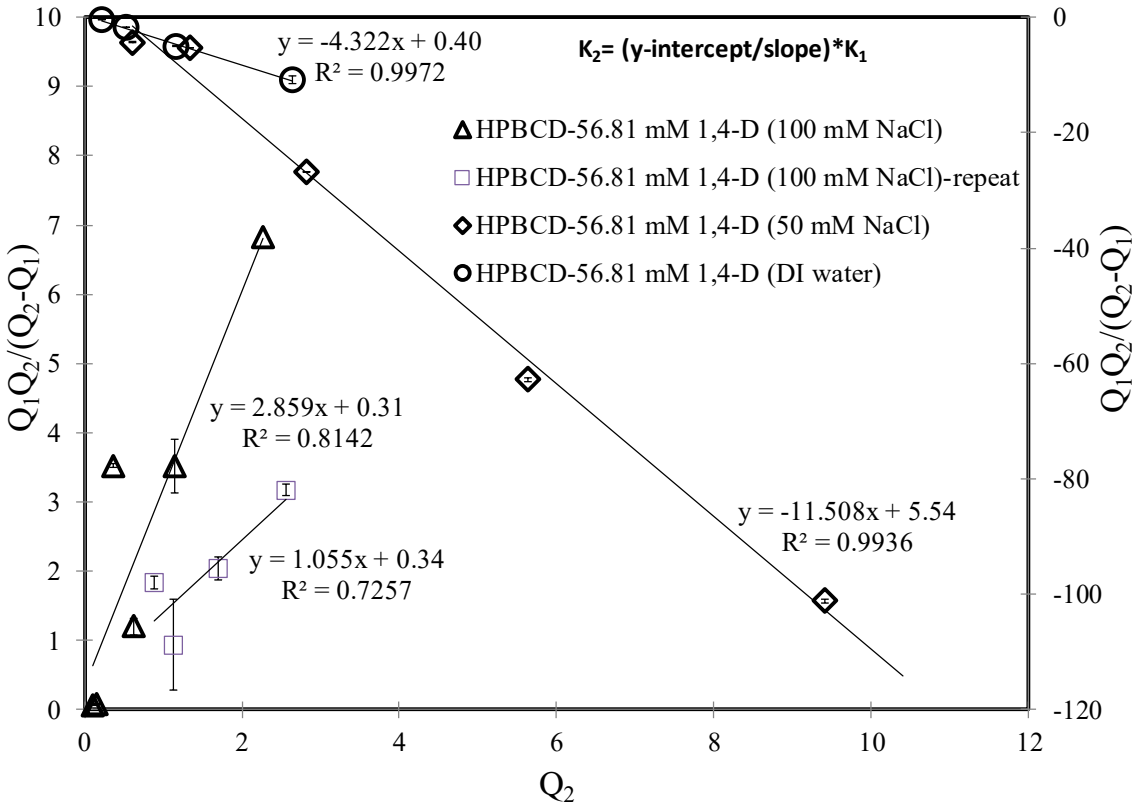

Figure 4.3.7. Plot of $Q_1Q_2/(Q_2-Q_1)$ versus Q_2 for 1,4-dioxane within DI and two other salt concentrations. Data sets for HPβCD with 1,4-dioxane at 100 mM and 50 mM of NaCl are on the secondary axis. Symbols indicate mean values, error bars are standard deviations, and lines present regression results used for binding equilibria analysis.

4.3.3 Methods Comparison and Implications

Mean K measurement results obtained from the UV direct method (Table 4.3.1) were comparable to results from competitive method (Table 4.3.2). Both competitive and direct spectroscopic methods provided reasonable and consistent K values and confirmed 1:1 stoichiometry, which supports validity of the results and applicability of the spectroscopic methods. The standard deviation values presented in the tables and figure error bars provide quantification of both the bulk K estimation and sample analysis variability, respectively. This variability was significant and was, at times, on the order of the mean values. However, the most

appropriate or sensitive methods can be selected for measuring binding constants based on physical and chemical properties of ligand and substrate. For example, using spectrometry analysis, compounds with low solubility and distinct UV absorbance ability will tend to provide more reasonable measurement results (Connors, 1987). O_3 and TCE have low solubilities and have distinct UV absorbance peaks (see Supplementary Data), whereas TCA has a low solubility and no specific absorbance peaks. On the other hand, 1,4-dioxane is highly soluble, and it does not have distinct UV absorbance peaks. O_3 and TCE are sensitive to both competitive and direct methods. For TCA and 1,4-dioxane, the competitive methods are more accurate than the direct method. Generally, the direct, or UV, method had larger standard deviation values compared to the competitive method for the compounds evaluated herein.

The measured binding constant values did vary between each of the guest compounds investigated herein. However, the variability was not unexpected or anomalous given the variability in the composition and structures of the guest compounds. In general the mean values for K did not vary by orders of magnitude for the compounds investigated, and excluding TNS the mean values in Table 4.3.2 tend to vary by factors of <2 to 5, and K value variability between compounds can be over multiple orders of magnitude. In fact, the binding constant values measured herein did typically fall above the mean but within a previously published statistical distribution (i.e., mean K = 0.5 mM^{-1}, and the 1st standard deviation K above the mean = 4 mM^{-1}) for HPβCD with several different types of chemicals (Connors, 1997). The vast majority of guest compounds investigated for inclusion complexation with HPβCD have been hydrophobic organics (e.g., pharmaceuticals). However, researchers have recently discovered that several different types of compounds, including ionic organics, can complex with CD in aqueous systems (Ondo et al., 2011), which is consistent with the 1,4-dioxane complexation results at elevated salt content. Even though it is not an organic molecule, results presented herein confirms that O_3 does also form inclusion complexes with HPβCD. Partitioning of O_3 into the HPβCD cavity may also be attributed to the water expulsion and hydrophobic partitioning mechanisms (noted previously), because of the relative hydrophobicity and low aqueous solubility of O_3.

The binding constant results reported herein also do not vary significantly from prior reports for some of the same compounds assuming 1:1 binding was observed and considered in the binding constant determination. For example, Shirin et al. (Shirin et al., 2003) used ^{1}H NMR titration method and reported the TCE stability constant range was 3 – 120 M^{-1} for β-CD, and this large range varied by the type and degree of substitution within β-CD molecules. Yang et al. (Yang et al., 2006) reported the binding constant of TCE with various CDs both individually and within contaminant mixtures using GC-FID. They found the binding constant of HPβCD:TCE was 0.119 mM^{-1} for TCE alone and 0.143 mM^{-1} for multiple contaminant systems. The previously reported average K of TCE with HPβCD was lower than binding constant observed herein for HPβCD:TCE (Shirin et al., 2003; Yang et al., 2006). The binding constant of TCE determined in this study was consistent with a 1:1 complex formation of HPβCD:TCE, whereas these prior studies mentioned above used different methods analysis and assumed 1:2 complex formation. Upon data reanalysis of the binding constant of HPβCD:TCE Shirin et al. (Shirin et al., 2003) reported with the assumption of 1:1 complexation, the K value is larger (i.e., K = 2.1 mM^{-1}), which is comparable to the K measured for HPβCD:TCE herein.

Estimated K values for γ-CD were not obtained for O_3 or any contaminants considered herein. The cavity volume of HPβCD (0.262 nm^3) is almost two-fold smaller than cavity volume

of γ-CD (0.426 nm^3). Although, the cavity volume is larger for γ-CD, K values were able to be determined for HPβCD and not for γ-CD using these spectroscopic methods, which suggests that the smaller cavity of HPβCD has a stronger attraction presumably due to the increased hydrophobicity with lower volume for water molecules and hydrogen bonding in the cavity. Additionally, the guest compound molar volume variability is relatively low compared to the variability in the K values, and would not likely be a controlling factor for the measured variability in K values between guest compounds.

Figure 4.3.8 is a plot of the binding constant values at different salinities and/or ionic strengths for contaminants considered in this investigation, and results from both direct and competitive methods are also presented for comparison. Comparing values for a particular guest compound illustrates the similarity of the two methods compared in Figure 4.3.8 (i.e., UV for direct method and FL or fluorescence for the competitive method with TNS). The direct and competitive methods had statistically similar results for both 1,4-dioxane and TCE, whereas the methods varied significantly for TCA upon salt additions. The trend of increasing binding constants with NaCl (noted earlier) concentration is evident and consistent. Increasing salt concentration in the solution likely caused a decrease in guest aqueous solubility (i.e., salting out) (Blanford, 2014; Schwarzenbach et al., 2003). Solubility of O_3 (10 mg L^{-1}) is lower than TCE (1083 mg L^{-1}) and TCA (1550 mg L^{-1}), and the solubility for 1,4-dioxane is much larger than TCA. The trend, in Figure 4.3.8, mentioned above for binding constant values (1,4-dioxane<TCA<TCE) is the opposite of the trend for the guest compound aqueous solubility (1,4-dioxane>TCA>TCE). Typically, hydrophobicity of organics is inversely correlated to aqueous solubility (Schwarzenbach et al., 2003), and hydrophobicity correlates with partitioning of guests into CD molecules (Blanford, 2014). O_3 and TNS did not follow the trend of K value inversely related to aqueous solubility, which was likely due to the ionic properties of these compounds. Even though the solubility of O_3 is approximately two orders of magnitude lower than TCE, the K value for O_3 was consistently lower than that of TCE. However, aqueous solubility of many compounds typically has an inverse relationship between the binding constant of CD complex formation (Blanford et al., 2014; Boving and McCray, 2000). Decreasing solubility increases the binding constant values for partitioning into the hydrophobic cavity of HPβCD, and this was likely the cause of the increases in K with increasing salinity. Thus, solubility and/or hydrophobicity of guest compounds has a significant impact on binding constant values for HPβCD complexation.

The development of these spectroscopic methods for aqueous complex binding constant measurement has implications for water treatment and groundwater remediation applications, as well. This work illustrates multiple binding constant measurement methods that are easily applied in the laboratory. Binding constants are the thermodynamic equilibrium data needed to quantify aqueous complexes, and they are commonly used within reactive solute transport models (i.e., if equilibrium geochemistry is considered), geochemical models (i.e., aqueous complex speciation), or other engineering design calculations (i.e., reagent application) for design of groundwater contamination remediation.

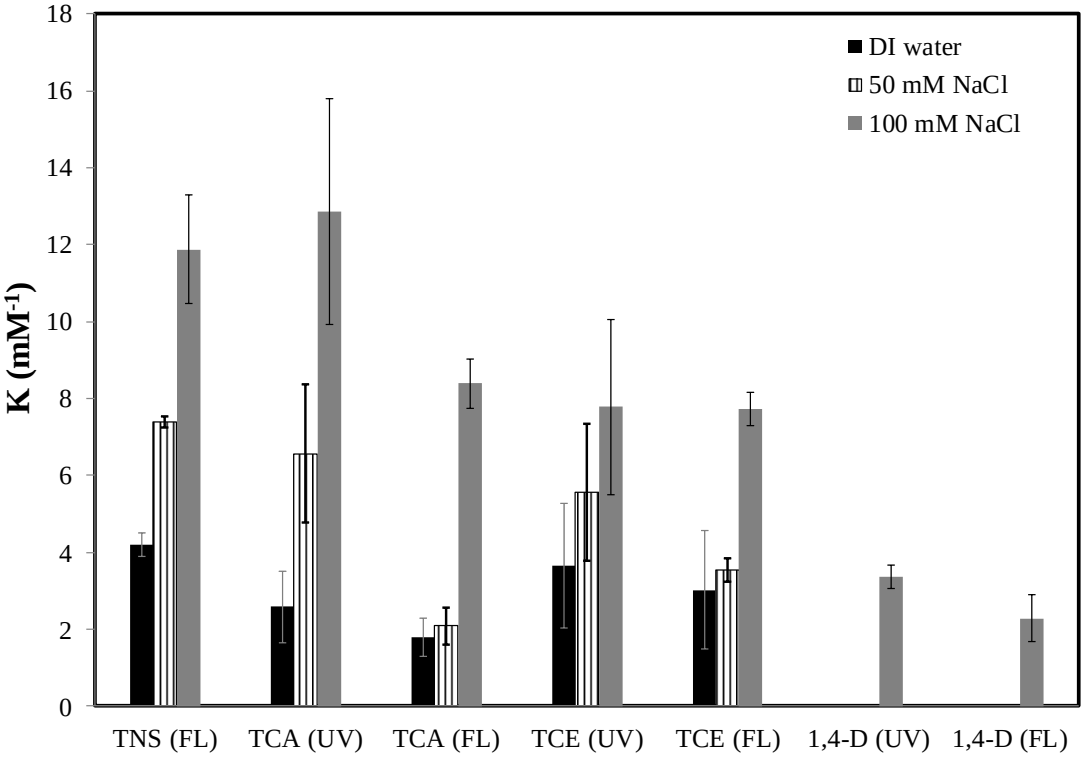

Figure 4.3.8**.** Comparison of binding constant values for inclusion complexation with HPβCD measured using the two spectroscopic methods for each guest compound with variation in solution salt concentration. FL and UV refer to fluorescence (i.e., indirect method and direct method for TNS) and UV spectroscopy (i.e., direct method), respectively. Bars indicate mean values, and error bars represent standard deviations.

Application of this technology for 1,4-dioxane and co-contaminants in wastewater or groundwater systems is especially attractive as typical remediation methods are not effective for transformation of 1,4-dioxane. As noted previously, bioremediation is inhibited with chlorinated co-contaminants (Mahendra et al., 2013), which are generally found in groundwater with 1,4-dioxane. Oxidation with low-strength oxidants such as permanganate is ineffective, and sorption and volatilization are ineffective for removal to low concentrations (DiGuiseppi and Whitesides, 2007; Mohr et al., 2010; Zenker et al., 2003). Chemical oxidation using O_3 represents one of the only methods to rapidly destroy 1,4-dioxane and co-contaminants to the low concentrations targeted by regulators.

4.4 Cyclodextrin Enhanced Ozonation of 1,4-Dioxane Results and Discussion

4.4.1 Effect of cyclodextrin on contaminant transformation kinetics

Oxidant addition was required to remove 1,4-dioxane contamination from aqueous solutions. Control experiments for each contaminant in single (with and without HPβCD) and multiple component experiments without O_3 did not have a decreasing concentration trend (i.e., no significant removal), and varied above/below the initial concentration with ~3% or less variability (see Supplementary Data), which confirmed that volatilization losses over the experimental period

of a few hours were negligible over the range of contaminant concentrations used. However, Figure 4.4.1 presents relative concentration versus time data and regression results for the transformation of 1,4-dioxane over time using O_3 with and without HPβCD for three different oxidant to contaminant ratios for the single contaminant experiments. This illustrates that 1,4-dioxane concentrations decreased exponentially over time upon exposure to O_3. Because the initial O_3 concentration was always much greater than the contaminants and the reaction kinetic data were obtained in less than 200 minutes, the O_3 was always in excess throughout the experiments. Thus, the data where well described with pseudo 1st order kinetics, regression results had relatively high R^2 values (especially with zero intercept), and the regression slopes indicated the transformation rate constant values. These trends of pseudo 1st order kinetics were also observed for experiments conducted with TCE and TCA (see Supplementary Data).

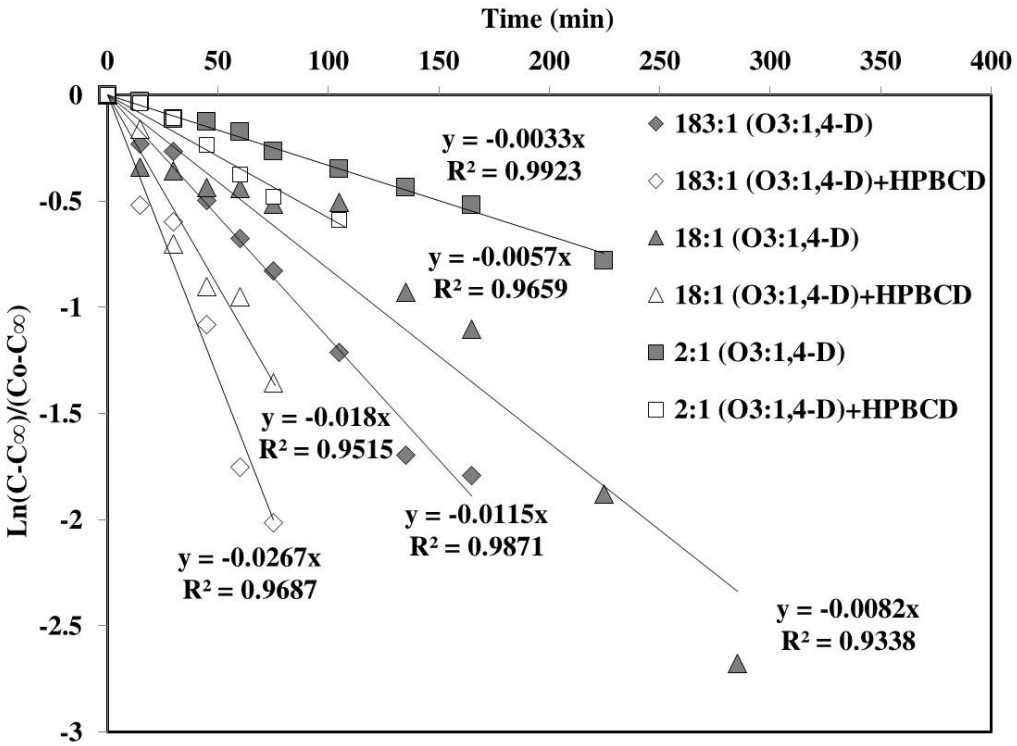

Figure 4.4.1**.** Transformation kinetics of 1,4-dioxane using O_3 with and without HPβCD in single contaminant systems at various oxidant to contaminant ratios. Lines present regression results used for pseudo 1st order kinetic analysis. Symbols indicate mean values, and error bars indicate 95% confidence intervals.

Oxidation product compounds were identified upon review of mass spectra and chromatogram results (see Supplementary Data). Evaluation of reaction pathways and mechanisms is beyond the scope of this investigation. However, the organic acids, aldehydes, and diethylene glycol daughter products identified are similar to those that have been reported by prior research focused on 1,4-dioxane transformation mechanisms. For example, Barndok et. al. (Barndok et al., 2014a) observed ethylene glycol and oxalic acids as byproducts of O_3 transformation of 1,4-dioxane. Klecka et. al. (Klecka, 1986) mentioned that organic acids and aldehydes with low molecular weight are usually generated as reaction products through ozonation of 1,4-dioxane, and Adams et. al. (Adams et al., 1994) found 1,3-dioxolane as a byproduct during oxidation of 1,4-dioxane by O_3 with H_2O_2. Comparability of the reaction products with prior investigations

confirms that 1,4-dioxane was removed through oxidation, and suggests that 1,4-dioxane degradation likely followed the ethylene glycol intermediate formation pathway typical of AOP using O_3 (Barndok et al., 2014a).

The rate constants increased with HPβCD compared to experiments without HPβCD, which was not expected. This confirms that the presence of HPβCD increased the reaction kinetics for O_3 with 1,4-dioxane. Two possible explanations for this are that HPβCD reactions with O_3 enhanced oxidation of 1,4-dioxane and O_3 reactivity with 1,4-dioxane was enhanced through increased proximity due to inclusion complexation formation with HPβCD. There is evidence of partial reactivity between O_3 and HPβCD (Dettmer et al., 2017), but this would likely consume O_3 reactivity unless additional organic radicals are formed. As noted above, the formation of ternary complexes (i.e., pollutant-cyclodextrin-iron) have been used to explain enhanced contaminant degradation through increased proximity of reactants (Liang et al., 2007a; Lindsey et al., 2003a; Veignie et al., 2009).

It has been observed that O_3 and organic compounds both can partition into the HPβCD hydrophobic cavity (Dettmer et al., 2017; Khan, 2018; McCray et al., 2000). Table 4.4.1 contains binding constants previously reported in Khan et al. and the fractional amount of each guest complexed within HPβCD for the experimental conditions reported herein, indicates a similar partitioning fraction for O_3 (20%) compared to TCE (10%) and TCA (35%). However, 1,4-dioxane partitioning was negligible or not able to be measured without salinity increases. The mechanism that is generally accepted for inclusion-complex formation within the HPβCD cavities is hydrophobic partitioning and displacement of water molecules from the cavity (Connors, 1997), and this reversible partitioning is generally considered to be caused by a weak attraction force with rapid equilibration within seconds (Nakatani and Hiromi, 1984), which presumably would not impact reaction kinetics. Formation of clathrate inclusion complexes within HPβCD including O_3, TCE, TCA, and 1,4-dioxane may result in a ternary complex where both O_3 and contaminants enter the HPβCD cavity, which might have increased reaction rate constants possibly through increases in reactant proximity, reactions with HPβCD, and/or modification of HPβCD cavity chemical composition. Reactant proximity may have even been altered outside of the cavity as reactants compete for complexation.

The difference in reactivity within the cavity also could be possible if the resident water is released from the cavity upon complex formation, which would alter the decay of O_3 with removal of hydroxide. A lack of hydroxide ions within the cavity would suggest direct ozonation of contaminants as the mechanism, and both direct oxidation and indirect oxidation with OH• radical formation would occur outside the cavity. Composition differences within the cavity compared to bulk water would cause changes in reactivity with and without HPβCD for compounds that form HPβCD inclusion complexes. The occurrence of both reactants inside the cavity may also lower the activation entropy of the reaction. If hydroxide radical formation was inhibited within the cavity, direct oxidation by O_3 might become the dominant mechanism.

Table 4.4.1. Binding constant values (Khan, 2018) and guest fraction complexed for each of the salinity and initial pH conditions examined in the kinetics experiments. STDEV refers to the standard deviation.

pH	NaCl (mM)	HPβCD:TCA		HPβCD:TCE		HPβCD:1,4-dioxane		HPβCD:O_3	
		Fraction of Guest Complexed within Cyclodextrin Cavity							
		Mean	STDEV	Mean	STDEV	Mean	STDEV	Mean	STDEV
6	0	0.35	± 0.00	0.42	± 0.10	-	-	0.18	± 0.11
	50	0.58	± 0.05	0.52	± 0.11	-	-	-	-
	100	0.72	± 0.07	0.61	± 0.05	0.41	± 0.04	-	-
9	0	0.52	± 0.11	0.63	± 0.05	-	-	-	-
pH	NaCl (mM)	HPβCD:TCA		HPβCD:TCE		HPβCD:1,4-dioxane		HPβCD:O_3	
		Inclusion Complex Binding Constant (mM^{-1})							
		Mean	STDEV	Mean	STDEV	Mean	STDEV	Mean	STDEV
6	0	2.6	± 0.0	3.6	± 1.4	-	-	1.1	± 0.8
	50	6.6	± 1.3	5.6	± 2.3	-	-	-	-
	100	12.9	± 4.1	7.8	± 1.8	3.4	± 0.6	-	-
9	0	5.4	± 2.3	8.3	± 1.7	-	-	-	-

TCE and TCA are generally found in the groundwater contaminant mixtures at most 1,4-dioxane contaminated sites, and oxidation evaluation with these co-contaminants was evaluated to assess the potential for treatment inhibition. Mirroring the single contaminant system, multicomponent experiments were conducted, and the results showed the transformation of 1,4-dioxane, TCE, and TCA followed pseudo 1st order reaction kinetics for both O_3 with and without HPβCD (see Supplementary Data). In the multiple contaminant experiments, the compound most rapidly destroyed was TCE, followed by 1,4-dioxane and then TCA using O_3 without HPβCD. TCE transformation was too rapid to measure in the single component for both O_3 with and without HPβCD at oxidant:contaminant ratios of 1830:1 and 18:1 for the multicomponent experiments. The addition of HPβCD, in multicomponent experiments, did not result in a significant increase in the 1,4-dioxane transformation rate coefficient, which may be attributed to competition between contaminants for inclusion complexation formation and competition between oxidation reactions.

The rate constant for 1,4-dioxane using O_3 without HPβCD was seven times greater in multiple contaminant systems than single contaminant systems (Supplementary Data). One possible cause of the enhancement of the transformation rate constant in multiple contaminant systems is the potential formation of organic and/or chloride radicals in multiple contaminant systems, which would have been absent in single contaminant system experiments conducted with DI water. Partitioning of 1,4-dioxane into the HPβCD cavity may have also increased with chloride reaction product formation, and this could have increased 1,4-dioxane and O_3 reactivity. The TCA transformation rate constant in the multiple contaminant system was four times lower than that of the single contaminant system.

Rate constant results were generally comparable to prior work. Masten and Hoigne (Masten and Hoigne, 1992) reported 0.103 min^{-1} for ozonation of TCE, and this is comparable to the 0.2 min^{-1} determined here. For 1,4-dioxane ozonation, Kwon et al. (Kwon et al., 2012) reported 0.0036 min^{-1}, Tian et al. (Tian et al., 2014) reported 0.0026 min^{-1}, and both of these compare well with the results at the lower oxidant to contaminant ratio (Supplementary Data). Barndok et al. reported a larger rate constant of 1.2 min^{-1} for 1,4-dioxane oxidation (Barndok et al., 2014a), which was likely greater than the observed rate constant in the present study likely due to the industrial wastewater chemical composition (i.e., higher salinity). Eberle et al. (Eberle et al., 2016) reported significantly lower rate constant values for 1,4-dioxane oxidation using PAP. This phosphate buffered oxidant mixture exhibited values of $5x10^{-5}$ min^{-1} and $3x10^{-4}$ min^{-1} for 10:1 and 100:1 oxidant to contaminant ratios (Eberle et al., 2016). The total oxidant requirement and reactivity can be contaminant specific (Masten and Hoigne, 1992), and in presence of multiple compounds, the selectivity of oxidant to contaminant may vary from that of the single compound system. Moreover, it has been previously observed that adding multiple contaminants can enhance the reaction rate constant by forming organic radicals (Freshour et al., 1996). The results presented herein suggest that the ozonation reactions are not inhibited due to the presence of any of these common co-contaminants even though microbial decay of 1,4-dioxane tends to be inhibited in the presence of chlorinated co-contaminants (Zhang et al., 2016).

4.4.2. Effect of initial pH value on contaminant transformation kinetics

Variability of pH can significantly alter ozonation reaction kinetics of recalcitrant contaminants including 1,4-dioxane (Barndok et al., 2014b), and depending on the contaminant structure, and susceptibility to direct or indirect ozonation upon OH• radical formation, pH increases can promote or inhibit contaminant transformation reaction rates (Masten and Hoigne, 1992). To evaluate potential initial pH effects, experiments were conducted (in multiple contaminant systems at 4.7:1 oxidant to contaminant ratio) with various initial pH conditions. Figure 4.4.2 presents comparisons of rate constant variability as a function of initial pH for 1,4-dioxane, TCE, and TCA using O_3 with and without HPβCD. Transformation kinetics for each of the contaminants at each of the initial pH values followed pseudo 1^{st} order reaction kinetics using O_3 with and without HPβCD (see Supplementary Data).

The rate constants for TCA transformation did not have significant change as a function of initial pH. 1,4-Dioxane, transformation rate constants increased with increasing initial pH using O_3 (Figure 4.4.2a), which is consistent with prior work (Barndok et al., 2014a; Tian et al., 2014). Increasing transformation of 1,4-dioxane with increasing initial pH was attributed to the increased hydroxide concentrations, which supports OH• radical production and increased reactivity (e.g., oxidation potential) compared to the direct reactivity of O_3 (Kwon et al., 2012; Masten and Hoigne, 1992; Tian et al., 2014). However, the rate constant variability with pH for 1,4-dioxane and TCA was not very significant compared to the TCE rate constant variability. Tian et al. also examined 1,4-dioxane ozonation rate constants for alkaline pH, they found rate constants did not increase between pH 7-10 as between pH 10-12 (Tian et al., 2014), and the rate constant they reported at neutral pH (0.0026 min^{-1}) was comparable to the rate constant presented in Figure 4.4.2. Tian et al. also measured a value of 0.15 min^{-1} at pH 10, which is comparable to the pH 10 value of 0.1 min^{-1} from Figure 4.4.2. Upon HPβCD addition, all three contaminants had decreases in transformation rate constants with increases in initial pH (Figure 4.4.2b), which suggests direct oxidation could dominate over OH• radical production within the HPβCD cavity. Kwon et al. also investigated the kinetics for 1,4-dioxane transformation using different AOPs focusing on

degradation by OH• radicals (Kwon et al., 2012). They observed that O_3 alone can degrade 1,4-dioxane at a rate constant of 0.0036 min^{-1}, which is also comparable to the observation in present study. Kwon et al. observed an increase in the rate constant from pH 4 to pH 10 using $O_3/H_2O_2/UV$ (Kwon et al., 2012), and this was consistent with the results of this investigation. They also observed that pH during ozonation reactions decrease to <4 without buffering even if they are initiated at various other initial pH values up to 10.

Transformation rate constants for TCE decreased with increasing initial pH, which was observed for both O_3 with and without HPβCD (Figure 4.4.2). The increase in the transformation rate constant for TCE at low initial pH was attributed to increased O_3 stability at low pH (i.e., lower concentration and reactivity with hydroxide). TCE tends to favor the direct reaction between O_3 and the double bond of TCE compared to the OH• radical reactivity with TCE, because the OH• radical tends to be consumed by the electron withdrawing group Cl^- attached to TCE (Masten and Hoigne, 1992; Sunder and Hempel, 1997). Transformation rate constants for TCE using O_3 with HPβCD were not significantly different compared to O_3 without HPβCD, which further suggests direct oxidation could dominate over OH• radical production within the HPβCD cavity.

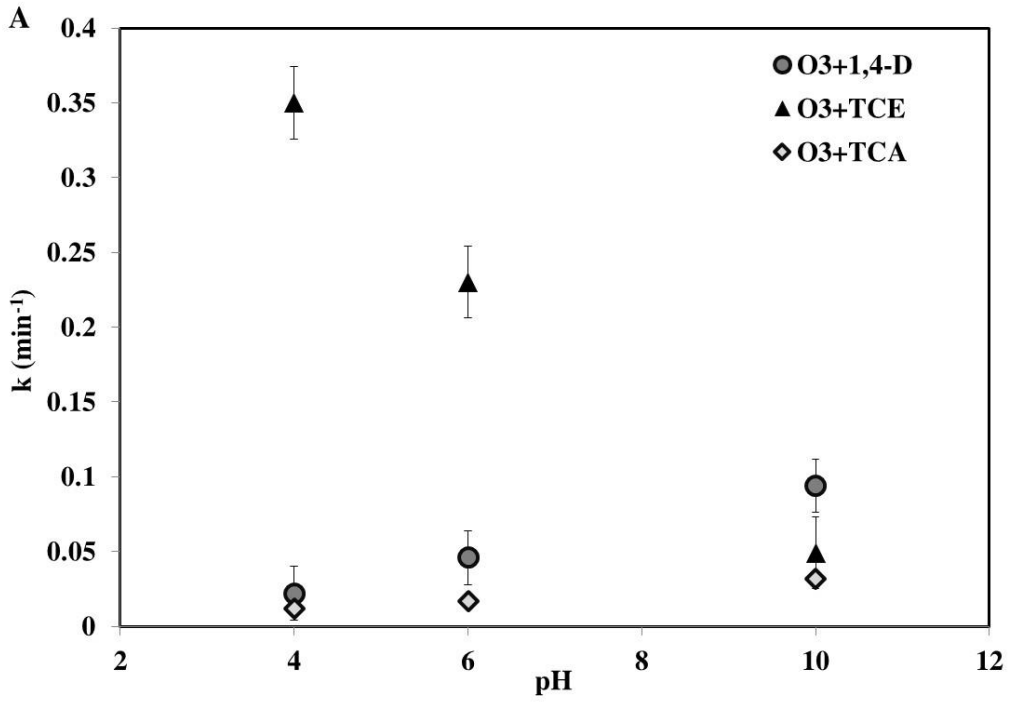

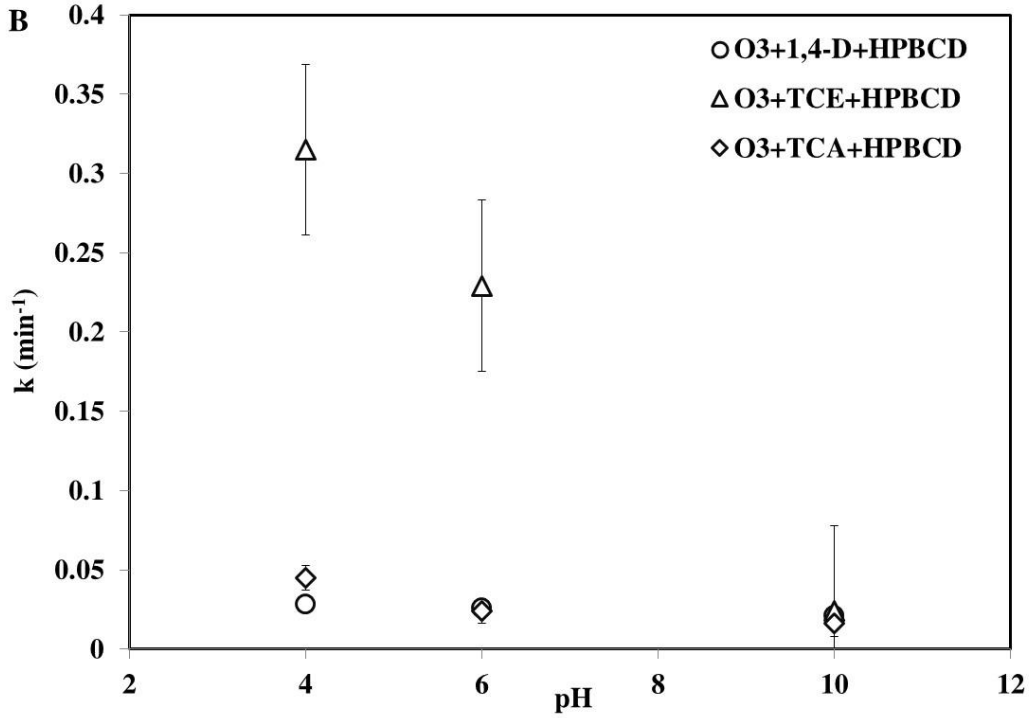

Figure 4.4.2**.** (A) Impact of initial pH on transformation rate constants for 1,4-dioxane, TCE, and TCA using O_3 without HPβCD in multiple contaminant systems (4.7:1 oxidant to contaminant ratios). (B) Impact of initial pH on transformation rate constants for 1,4-dioxane, TCE, and TCA using O_3 with HPβCD in multiple contaminant systems (4.7:1 oxidant to contaminant ratios). Symbols are mean values and error bars are 95% confidence intervals.

4.4.3. Effect of salinity on contaminant transformation kinetics

Chloride is known as a ozonation radical scavenger, and additions have been shown to inhibit oxidation of 1,4-dioxane and other contaminants (Eberle et al., 2016; Kishimoto et al., 2007; Tsitonaki et al., 2010), and rate constant decreases with Cl additions were expected. Figure 4.4.3a is a plot of transformation rate constants for 1,4-dioxane using O_3 with and without HPβCD as a function of NaCl composition in the single contaminant systems using O_3 with and without HPβCD. Results showed that as salinity and/or ionic strength in the solution increased the 1,4-dioxane transformation rate constants also increased. The results indicate that transformation rate constants for 1,4-dioxane using O_3 without HPβCD in single contaminant system were over 8 and 6 times greater upon addition of 100 mM of NaCl for experiments without and with HPβCD, respectively. With increases in salinity, the electrical conductivity and ionic strength increases, which can also enhance oxidation reactions (Barndok et al., 2014b).

Another potential reason for the greater transformation rate constant for 1,4-dioxane using O_3 with increasing NaCl addition concentrations may be the possible production of chloride radicals, which could have acted as an additional oxidant for 1,4-dioxane decay. Chloride ions can be oxidized to Cl•, which rapidly combines with another chloride in water forming $Cl_2•^-$ (chlorine radical) (Anipsitakis et al., 2006). Also, chloride ions could enhance production of OH• or organic radicals in the presence of O_3, which may have enhanced the transformation of 1,4-dioxane using O_3. Depending on the target pollutant, the formation of chlorine radicals may impede or improve the pollutant degradation rate (Zhang et al., 2014; Zhang et al., 2013). Chlorine oxidation of 1,4-

dioxane in presence and absence of H_2O_2 was observed previously, and degradation of 1,4-dioxane during chlorination was also documented (Klecka, 1986). The authors mentioned the formation of hypochlorous acid in presence of aqueous chlorine, which was the main oxidant that facilitated the degradation of 1,4-dioxane (Klecka, 1986).

With addition of 100 mM of NaCl, the transformation rate constants for 1,4-dioxane using O_3 with HPβCD increased by 88% from the analogous experiments without HPβCD (as noted above), which may be also attributed to as enhanced 1,4-dioxane partitioning into the HPβCD cavity at this greater salt content (Table 4.4.1). A figure in Supplementary Data illustrates the UV absorbance versus wavelength for solutions of HPβCD, 1,4-dioxane, and 1,4-dioxane with HPβCD for DI water and 100 mM NaCl solutions. Changes in absorbance with HPβCD addition and the isosbestic cross over point both indicate that 1,4-dioxane forms an inclusion complex with HPβCD. Recent binding constant data for 1,4-dioxane complexation with HPβCD suggest that NaCl may enhance complexation (Khan, 2018), and they found that binding constants become more quantifiable with increased NaCl concentrations. Increasing salt content generally decreases aqueous solubility (i.e., salting out) of organic compounds (Blanford, 2014; Setschenow, 1889), which increases partitioning of low-polarity compounds into the hydrophobic HPβCD cavity (Table 4.4.1). The increase in reactivity due to NaCl additions supports the theory that NaCl additions increase concentrations of 1,4-dioxane within the HPβCD cavity, as this would bring more contaminant into closer proximity to O_3 within the cavity. This increased inclusion complexation may also explain in part the variations in rate constants with pH as HCl was used to decrease the aqueous solution initial pH. These results also corroborate the potential for formation of ternary complexes of 1,4-dioxane:O_3:HPβCD, which could increase reaction rates with increased proximity of reaction reactants. These results also suggest that the ionic strength of typical groundwater would not be a substantial limiting factor when applying O_3 alone or O_3 with HPβCD to treat 1,4-dioxane contaminated groundwater, or wastewater, especially when chlorinated contaminants such as TCE and TCA are present.

Figure 4.4.3b provides a summary plot and a comparison of the effect of salts and radical scavengers on transformation rate constants for 1,4-dioxane, TCE, and TCA in single and multiple contaminant systems in presence and absence of HPβCD. Figure 4.4.3b also shows that the 1,4-dioxane rate constant increased from single to multicomponent experiments, and increased additionally with addition of NaCl (as noted above). The 1,4-dioxane rate constant also increased with HPβCD addition, and the largest rate constant for 1,4-dioxane was with HPβCD, co-contaminants, and NaCl. The results suggest that rate constants increase with NaCl concentrations, which could be due to enhanced partitioning into the HPβCD cavity or the potential Cl• radical formation (as noted above). Similarly, the observed rate constant increases with addition of co-contaminants may be due to the release of chlorine radicals upon transformation of chlorinated co-contaminants or formation of organic radicals.

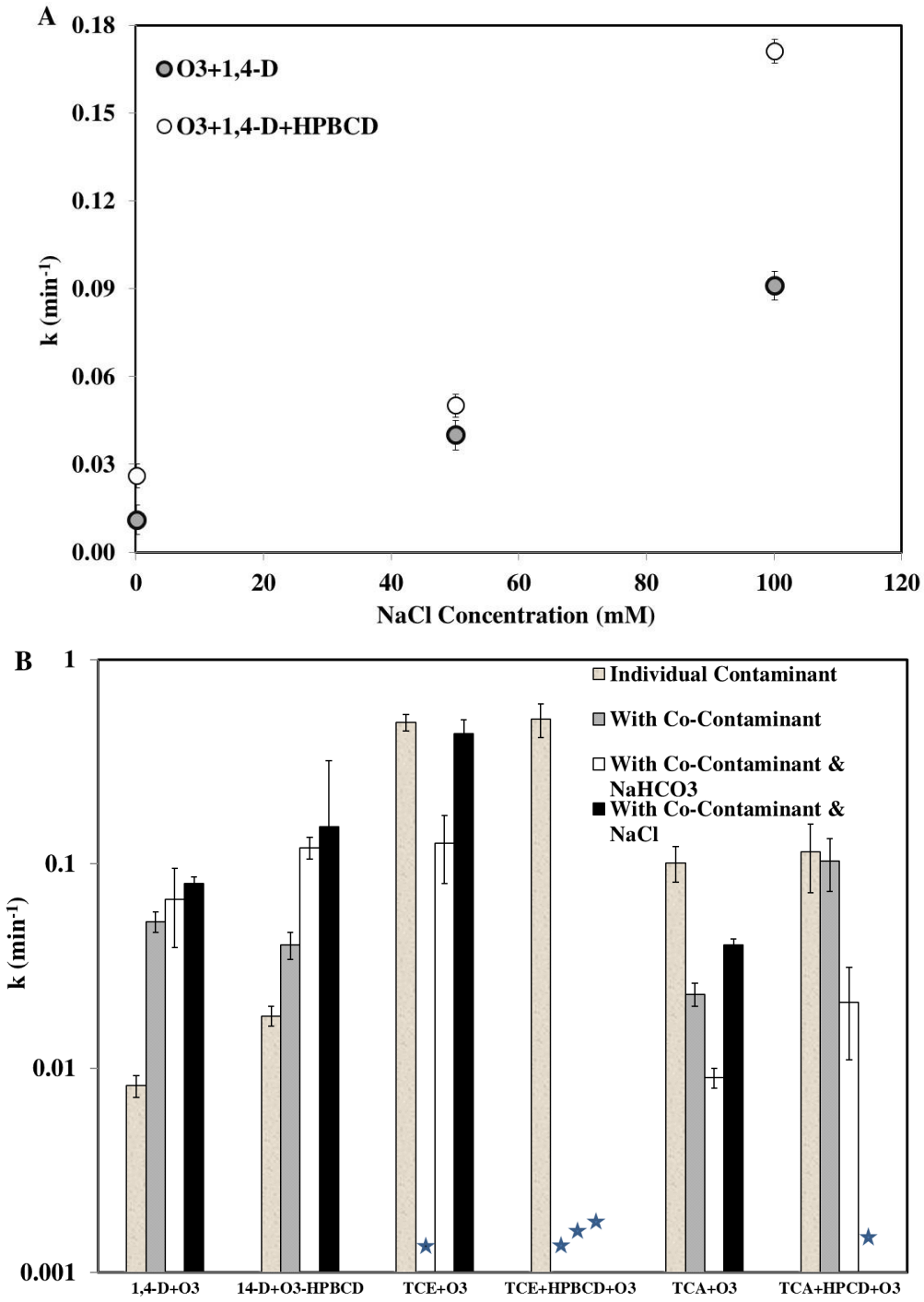

Figure 4.4.3**.** (A) 1,4-Dioxane transformation kinetics rate constant versus NaCl concentration using O_3 with and without HPβCD without co-contaminants. (B) Comparison of transformation rate constants for contaminants using O_3 (18:1 mole ratio) with and without HPβCD in single contaminant system, in multiple contaminant system, in presence of NaCl, and in presence of $NaHCO_3$. Stars indicate experiments that reacted too quickly to measure rate constants, symbols and bars indicate mean values, and error bars indicate 95% confidence intervals.

Bicarbonate, as a generally ubiquitous aqueous ion (Stiff, 1971), can also inhibit oxidation as a radical scavenger or quencher (Barndok et al., 2014a; Glaze and Kang, 1988; Hoigne et al., 1985; Zhou et al., 2013), and it has also been considered a stronger radical scavenger than chloride (Yan et al., 2016). Thus, the effect of bicarbonate additions on 1,4-dioxane, TCE, and TCA overall transformation using O_3 alone and O_3 with HPβCD were investigated in multiple contaminant systems (18:1 oxidant to contaminant ratio) and the results are shown in Figure 4.4.3b. Transformation rate constants decreased for both TCE and TCA with $NaHCO_3$ addition compared to DI water experiments even though reactions were not completely inhibited. In contrast, the transformation rate constants in presence of $NaHCO_3$ were greater than transformation rate constant for 1,4-dioxane using O_3 in DI water, and slightly lower than transformation rate constants in presence of NaCl for 1,4-dioxane using O_3 without HPβCD. With addition of $NaHCO_3$, the salinity and the pH of the solution increased slightly (up to pH=7.4). The change in salinity likely had a more significant impact on the rate constant increase for 1,4-dioxane compared with DI water experiments (see Figure 4.4.3a). Both NaCl and $NaHCO_3$ salts tend to increase the binding constants of contaminants with HPβCD due to salting out (Khan, 2018). Adding $NaHCO_3$ increased the transformation rate constant of 1,4-dioxane using O_3 with HPβCD, which indicated that HPβCD inclusion complex formation reduced $NaHCO_3$ radical scavenging effects (i.e., increased reaction specificity). Potential separation of O_3 and OH• radicals from potential scavengers, transition to direct ozonation, and increasing oxidant and contaminant proximity may have contributed to this observation. This 1,4-dioxane oxidation rate enhancement upon bicarbonate addition was also recently reported elsewhere (Barndok et al., 2014a), and prior research has observed that in presence of radical scavengers, inhibition of oxidation reaction can be minimized if both contaminant and oxidant can separate from scavengers within the bulk aqueous solution by partitioning onto a surface (Chen and Carroll, 2016; Freshour et al., 1996). The results presented herein indicates a similar effect of decreased radical scavenging when O_3 and contaminants partition into the HPβCD cavity.

These reported rate constants and examination of their variability are often useful for simulating reactive transport in the subsurface (Carroll et al., 2009). Although these results support our understanding of O_3 based ISCO, it is important to note that the laboratory-scale results presented herein may not directly translate to field-scale conditions. It has been commonly observed that rate constants determined at the laboratory scale can be significantly greater than field-scale values. Additionally, ISCO effectiveness may be significantly impacted by subsurface heterogeneities (Brusseau et al., 2011; Marble et al., 2010).

4.5 Peroxone Activated Persulfate Treatment of 1,4-Dioxane Results and Discussion

4.5.1 Oxidation of 1,4-dioxane, TCA, and TCE in single-contaminant systems

In single-contaminant aqueous phase experiments, the 1,4-dioxane concentration decreased exponentially over time (Figure 4.5.1). The reaction rates increased with oxidant concentration and are well described by pseudo-first-order kinetics (Table 4.5.1).

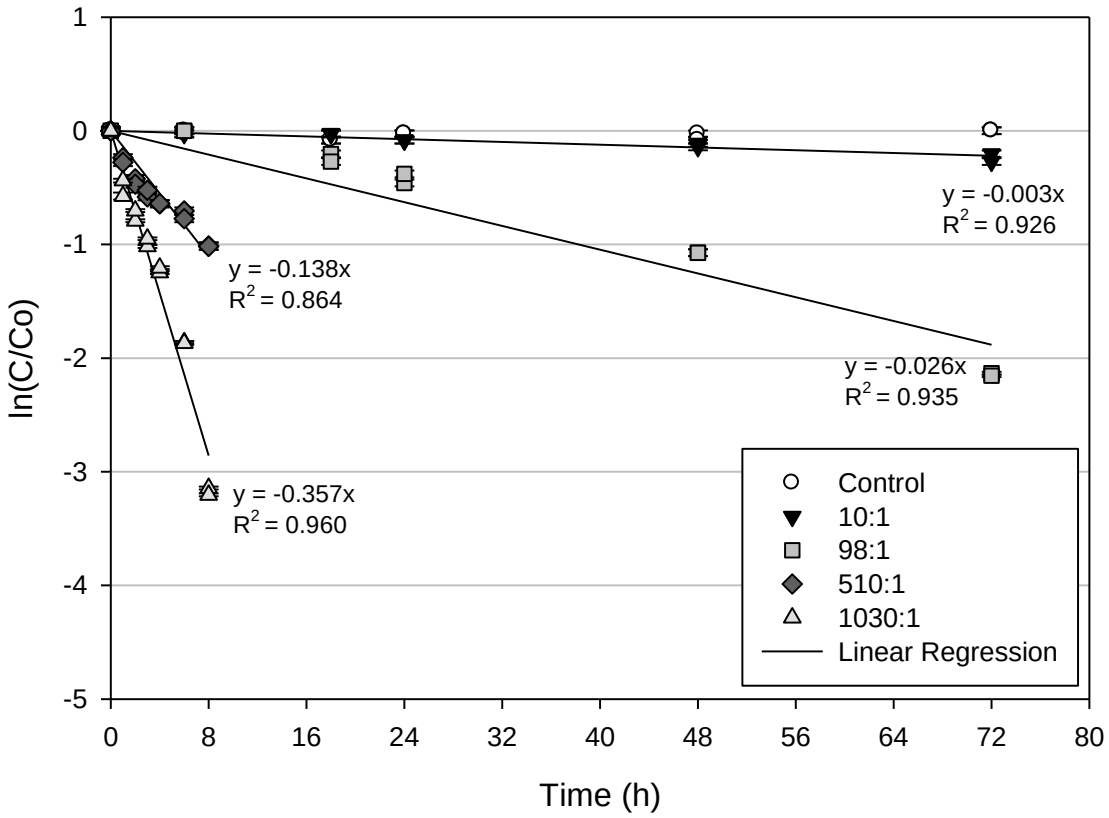

Figure 4.5.1. Oxidation of 1,4-dioxane by PAP. Four oxidant:contaminant ratios were investigated. The 10:1 reaction was shown to continue for at least 312 h (supporting information). The reaction for the most concentrated oxidant formulations, 510:1 and 1030:1, was so rapid that a second 24 h experiment, with a denser sampling interval, was conducted to capture degradation in those systems. Error bars of some data points are obscured by the datum point symbol.

Table 4.5.1. Oxidation of 1,4-dioxane, TCA, and TCE by PAP in single-contaminant systems. TCE and 1,4-dioxane experimental duration was 72 h. TCA experimental duration was 312 h. #A 312 h duration 1,4-dioxane experiment using a 10:1 ratio was also run and confirmed the results observed in the 72 h experiment (supporting materials). *Reaction rate was rapid (t ½ < 6h) during the initial 72 h experiment such that a second 24 h experiment with a denser sampling interval was used for rate calculations and confirmed the results observed in the 72 h experiment.

Molar Ratio	Contaminant Concentration (mg/L)	Contaminant Concentration (mM/L)	Persulfate (g/L)	Persulfate (mM/L)	k_1 (h^{-1})	t ½ (h)	R^2
1,4-Dioxane							
1030:1*	3.6	0.041	10.1	42.4	0.357	1.9	0.960
990:1	3.8	0.043	10.1	42.4	-	<6h	-
510:1*	3.6	0.041	5.0	21.0	0.138	5.0	0.864
490:1	3.8	0.043	5.0	21.0	0.152	4.6	0.879
98:1	3.8	0.043	1.0	4.2	0.020	34.7	0.939
10:1#	3.6	0.041	0.1	0.42	0.003	231	0.972
10:1	3.8	0.043	0.1	0.42	0.003	231	0.926
1,1,1-TCA							
1900:1	5.9	0.044	19.9	83.6	0.063	11.0	0.980
960:1	5.9	0.044	10.1	42.4	0.042	16.5	0.982
480:1	5.9	0.044	5.0	21.0	0.029	23.9	0.976
TCE							
110:1	5.3	0.040	1.0	4.2	0.445	1.6	0.971
53:1	5.3	0.040	0.5	2.1	0.273	2.5	0.980
25:1	5.3	0.040	0.25	1.0	0.127	5.5	0.995
10:1	5.3	0.040	0.1	0.4	0.067	10.3	0.974

Table 4.5.2**.** Oxidation of 1,4-dioxane by PAP under various ionic strengths. The duration of this experiment was 8 hours.

Molar Ratio	1,4-Dioxane (mM/L)	Sodium Persulfate (mM/L)	Disodium phosphate (mM/L)	Calcium Chloride (mM/L)	Ionic Strength (M/L)	pH final	k_1 (h^{-1})	t ½ (h)	R^2
500:1	0.042	21	4.3	0	0.076	7.5	0.156	4.4	0.928
500:1	0.042	21	4.3	0.7	0.078	7.4	0.141	4.9	0.916
500:1	0.042	21	4.3	7	0.097	5.8	0.103	6.7	0.968
500:1	0.042	21	4.3	70	0.286	5.1	0.065	10.7	0.962

Table 4.5.3**.** Observed versus predicted PAP oxidation rates in the multi-contaminant system. Total PAP concentration: 4.2 mM (as persulfate). The predicted values are calculated from the rate/molar ratio relationships shown in Figure 4.5.2 derived from the single-contaminant systems.

VOC	Molar Ratio	Contaminant Concentration (µM/L)	Predicted		Observed	
			$k_1(h^-)$	t ½ (h)	$k_1(h^-)$	t ½ (h)
1,4-Dioxane	280:1	14.8	0.092	7.5	0.057	12.2
1,1,1-TCA	450:1	9.4	0.018	38.5	0.010	69.3
TCE	410:1	10.3	1.763	0.4	0.231	3.0
Total	120:1	34.5				

For the 990:1 system, the reaction was so rapid that more than 50% of the 1,4-dioxane had already been degraded after the first sampling interval (6 h). By the second sampling time (18 h), no detectable 1,4-dioxane remained. For the 490:1 system 1,4-dioxane degraded beyond the limit of detection by the 24 h sampling. Due to the rapid reaction rates ($t_{½}$ < 6h) during the initial 72 h experiment, a second 24 h experiment with a denser sampling interval was used for rate calculations and confirmed the results observed in the 72 h experiment. For reference, the molar oxidant:contaminant ratio of undiluted PAP used commercially to treat VOC contaminated aquifers is about 6 to 10 time more concentrated than that used in the 990:1 system.

Oxidation slowed with decreasing oxidant:contaminant ratios and was the slowest ($t_{1/2}$ = 231 h) for the 10:1 system with only 20% reduction in 1,4-dioxane concentration observed after 72 h. A follow-up experiment showed that oxidation was continuous for at least 312 h (Supplementary Data) and the pseudo-first order reaction rate was k_1 = 0.003 h^{-1}. These data demonstrate that it is possible to degrade 1,4-dioxane even with dilute PAP solutions (10:1) and that the degradation process proceeds for at least 13 days. The apparent longevity of the PAP oxidant offers the possibility of injecting pulses of PAP solution into a 1,4-dioxane contaminated aquifer and exploiting its lasting reactivity to reach deep into the polluted area, assuming that the batch test result can be replicated under field conditions.

PAP degraded both TCE and TCA at 25 ^oC (Supplementary Data). Of these two 1,4-dioxane co-contaminants, TCE was much faster degraded than TCA. The fact that TCA can be readily oxidized by PAP is an advantage over thermally activated persulfate oxidation of TCA,

which prior studies have shown is recalcitrant to oxidation at ambient temperatures (20-30 ^{o}C) (Gates-Anderson et al., 2001; Gu et al., 2011; Huang et al., 2005; Liang et al., 2003; Waldemer et al., 2007; Xu et al., 2014). As for 1,4-dioxane, the rate of VOC degradation increased with increasing oxidant:contaminant ratios and the reaction kinetics are pseudo-first-order over the range of oxidant:contaminant ratios investigated (Table 4.5.1).

1,4-Dioxane was destroyed by PAP about 13 times slower than TCE, but eight times more rapidly than TCA. This observation is illustrated by plotting the degradation rate (k_1) for each of the three contaminants against the corresponding molar oxidant:contaminant ratio (Figure 4.5.2). The coefficient of determination (R^2) for all three correlations is high ($\geqq$0.894), which indicates that the rate of oxidation for each contaminant is predictable from the oxidant concentration within the range tested.

Besides contaminant concentrations, ORP and pH were monitored throughout the single-contaminant experiments (Supplementary Data). ORP ranged from 200 to 600 mV and generally increased with increasing oxidant:contaminant ratios (Supplementary Data). The ORP fluctuated in some of the control solutions (deionized water). This was attributed to memory effects of the ORP probe.

The initial pH ranged from 7.3 to 8.6, and was directly related to the amount of buffered PAP added to the solution. The pH fell throughout the course of the experiment (by up to 3.3 pH) indicating the production of protons. The decrease in pH was most pronounced in the TCE system and smaller (0.2 to 1.2 pH) in the case of 1,4-dioxane and TCA. Similar drops in pH during persulfate oxidation of organics have been documented in several other persulfate systems (Block et al., 2004; Huang et al., 2002; Huang et al., 2005; Liang et al., 2003; Liang et al., 2011). The reason for decreasing pH values over time is the production of sulfate, an extremely weak conjugate base, which can lead to production of sulfuric acid (Kolthoff & Miller 1951). The severity of pH drop in both laboratory and field systems is a function of the buffering capacity and the oxidant dosage.

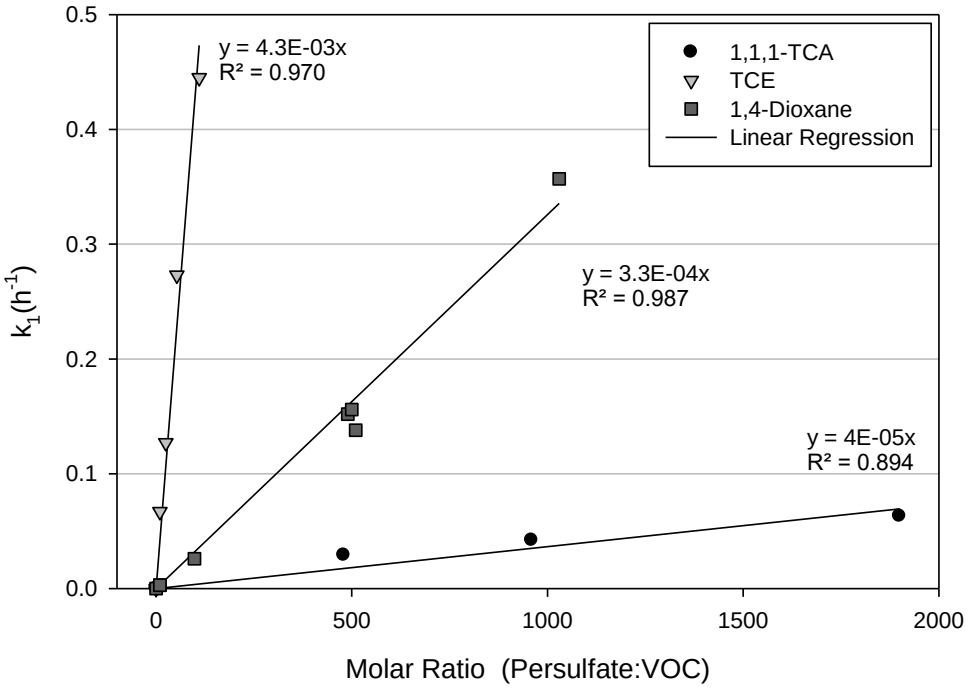

Figure 4.5.2. The degradation rates (k_1) for TCA, 1,4-dioxane, and TCE are plotted against the molar oxidant:contaminant ratio. The data indicate that the rate of oxidation for each contaminant is predictable within the range tested.

4.5.2 Effect of Ionic Strength on 1,4-Dioxane Oxidation

Table 4.5.2 shows the results of the ionic strength experiment. The higher the ionic strength of the solution, the slower the 1,4-dioxane degradation. Substantial 1,4-dioxane inhibition was observed when the ionic strength exceeded 0.2 M/L. This is most likely due to the increased presence of radical scavenging chloride ions. Chloride has been shown to inhibit persulfate oxidation of other contaminants such as TCE and MTBE at similar temperatures and concentrations (Huang et al., 2002; Liang et al., 2007b; Tsitonaki et al., 2010). Further, with increasing initial calcium chloride concentration, the pH of the solution decreased. This is most likely due to increased displacement of phosphate from solution through the formation of calcium monohydrogen phosphate ($CaHPO_4$), resulting in decreased buffering capacity. This would also account for a cloudy precipitate observed in the higher $CaCl_2$ concentration solutions (7 and 70 mM/L). The lower pH in these systems may have also contributed to the observed slower reaction rates. However, future work explicitly examining the effects of pH on PAP oxidation of 1,4-dioxane is needed. The results of this experiment suggest that the ionic strength of typical groundwaters would not be a substantial limiting factor when applying PAP to treat 1,4-dioxane in the field. However the effects of ionic strength might need to be considered when working in brackish waters.

4.5.3 Oxidation in Multi-Contaminant System

Mirroring the results of the single-contaminant experiments, the compound most rapidly destroyed was TCE, followed by 1,4-dioxane and then TCA, of which 60% was degraded after 96 h of exposure to PAP. The concentration of each compound decreased exponentially over time (Figure 4.5.3). The corresponding reaction rates and half-lives are summarized in Table 4.5.3. Observed half-lives ranged from 3.0 h for TCE to 69.3 h for TCA, with 1,4-dioxane at 12.2 h.

The rates observed in the multi-contaminant experiment were compared to those obtained for each compound in the single-contaminant experiments. Since the reaction rates are dependent on the initial oxidant concentration, the linear equations shown in Figure 4.5.2 were used to predict the rates of each compound at the molar oxidant:contaminant ratios used in the multi-contaminant experiment. For 1,4-dioxane and TCA the rates were interpolated, where as for TCE the rate was extrapolated.

The predicted oxidation rate constants and half-lives for all three contaminants are shown in Table 4.5.3. The data indicates that the observed rate (0.057 h^{-1}) of 1,4-dioxane oxidation in the multi-contaminant system was 38% slower (0.092 h^{-1}) than that predicted based on the single-contaminant experiments. Similarly, the oxidation of TCA and TCE in a multi-contaminant system was slower than predicted from the single-contaminant system by 44% and 87%, respectively (Figure 4.5.2).

As observed during the single-contaminant oxidation experiments, the pH decreased by 1.2 pH, while the ORP rose from 240 mV to 380 mV (Supplementary Data). The persulfate concentration remained two orders of magnitude higher than the initial VOC concentrations throughout the experiment, justifying the use of a pseudo-first-order rate model.

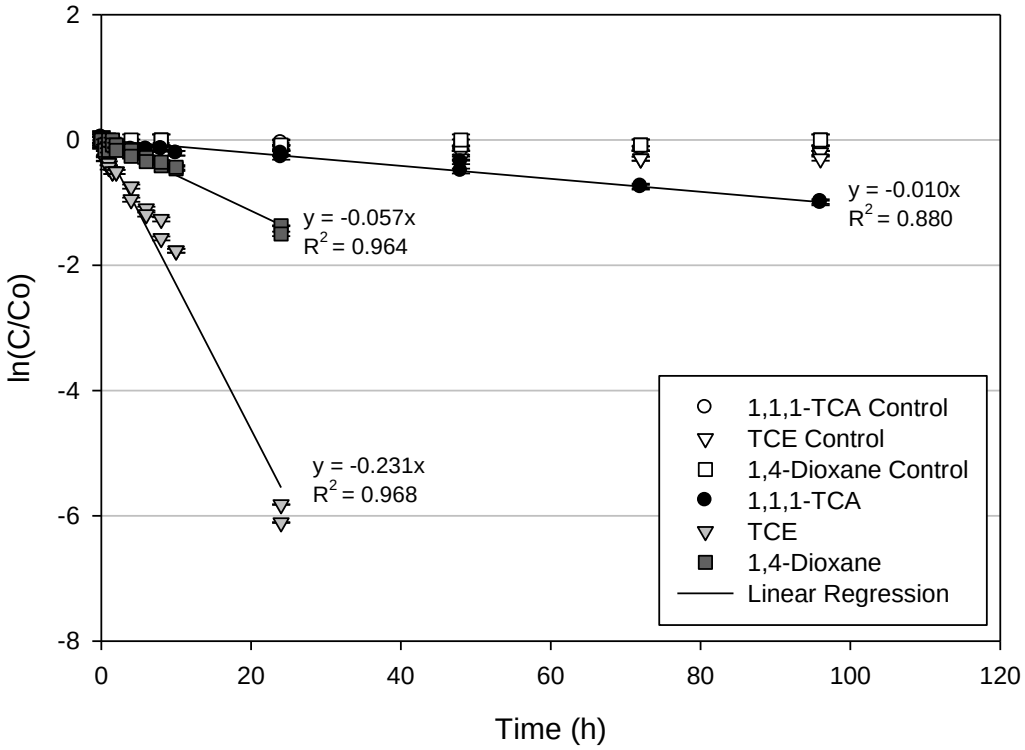

Figure 4.5.3. Simultaneous oxidation of 1,4-dioxane, TCE, and TCA by PAP. The initial concentration of each of the three compounds was approximately 1.3 mg/L. The total molar concentration of all the compounds combined was 0.035 mM. Based on this concentration, the total VOC oxidant:contaminant ratio was approximately 120:1. Error bars of some data points are obscured by the datum point symbol.

4.6 Siderite Activated Peroxide & Persulfate Contaminant Treatment Results and Discussion

4.6.1 Effect of Temperature on TCE Degradation

The control tests for TCE and DCA in ultrapure water (Figure 4.6.1) and ultrapure water + siderite (Supplementary Data) show minimal TCE mass loss during the experiment. Conversely, approximately 10% DCA loss was observed in the presence of siderite.

The temperature effect on TCE degradation in the SO and the STO systems was investigated at temperatures varying from 10 to 50 ^{o}C. The results indicate that greater TCE degradation was achieved for higher temperatures (Figure 4.6.1a and b). These results are anticipated based on the impact of higher temperatures on diffusive mixing, pH, and activation. As observed in Figure 4.6.2, the pH was lower at higher temperatures for the STO system (Figure 4.6.2). Lower pH favors the hydrogen peroxide-persulfate-based oxidation process. Furthermore, heat enhances persulfate-oxidant activation. Therefore, higher temperatures enhanced the magnitude of degradation.

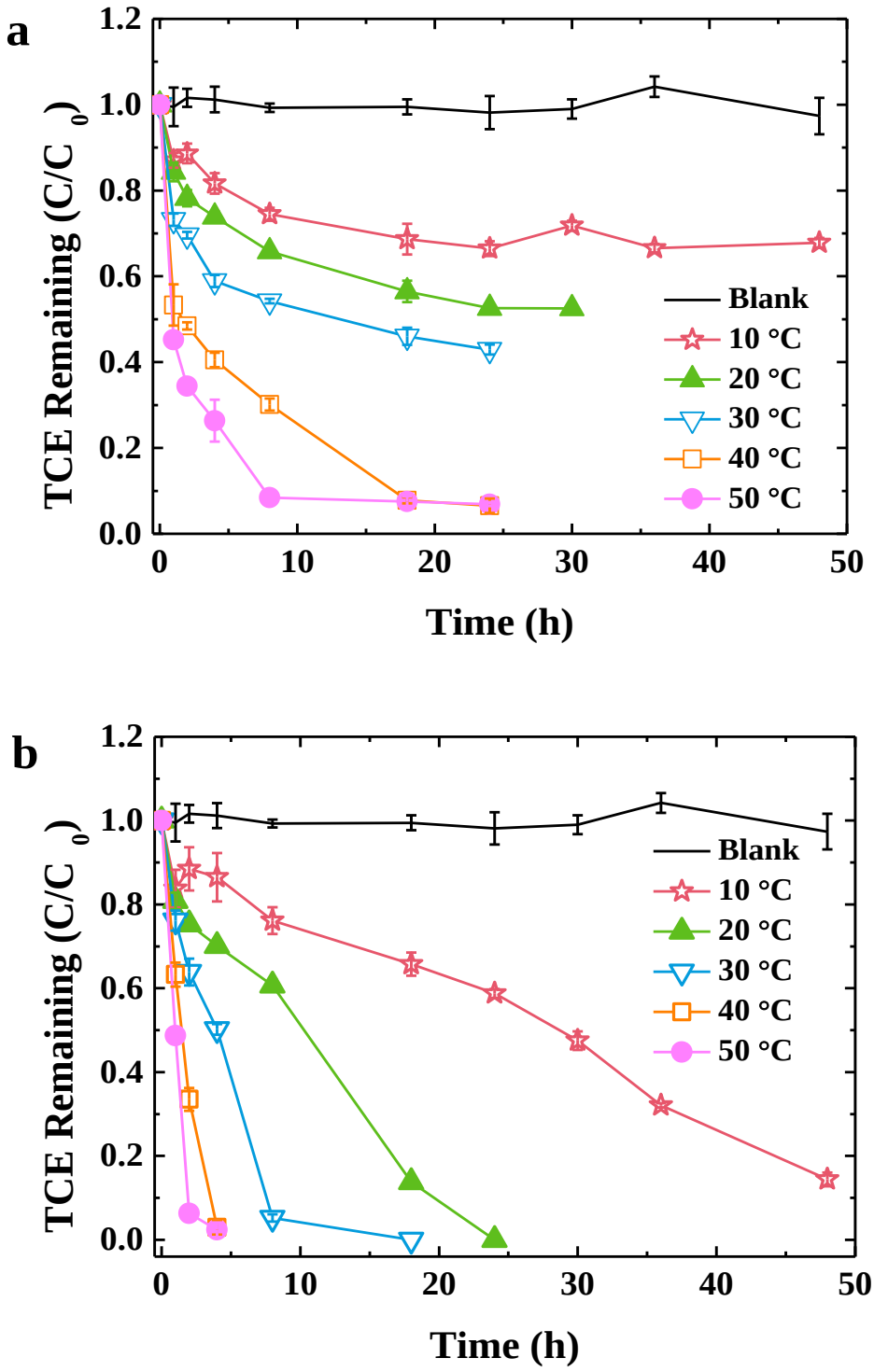

Figure 4.6.1. TCE degradation under different temperatures a) the SO system (siderite-catalyzed hydrogen peroxide oxidant); b) the STO system (siderite-catalyzed hydrogen peroxide and persulfate).

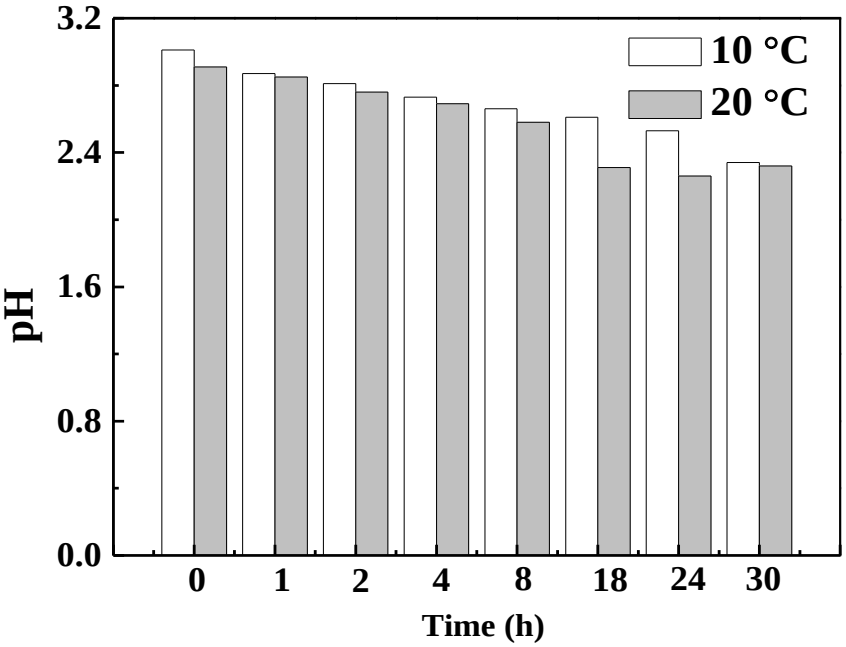

Figure 4.6.2**.** The pH change during TCE degradation under different temperatures for the STO system.

Table 4.6.1**.** Kinetic equations for TCE degradation in different oxidation systems.

System	Reaction Period	Temperature (^oC)	Regression equation	R^2	k_{obs} [a] (h^{-1})
SO [b]	Rapid-stage	10	y = -0.076x + 0.014	0.90	0.076
SO	Rapid-stage	20	y = -0.123x - 0.016	0.95	0.123
SO	Rapid-stage	30	y = -0.208x - 0.054	0.83	0.208
SO	Rapid-stage	40	y = -0.362x - 0.089	0.85	0.362
SO	Rapid-stage	50	y = -0.533x - 0.087	0.93	0.533
SO	Slow-stage	10	y = -0.011x - 0.161	0.93	0.011
SO	Slow-stage	20	y = -0.018x - 0.237	0.98	0.018
SO	Slow-stage	30	y = -0.044x - 0.311	0.95	0.044
SO	Slow-stage	40	y = -0.116x - 0.420	0.99	0.116
SO	Slow-stage	50	y = -0.242x - 0.496	0.98	0.242
STO [c]	Entire reaction	10	y = -0.034x + 0.025	0.90	0.034
STO	Entire reaction	20	y = -0.104x + 0.014	0.94	0.104
STO	Entire reaction	30	y = -0.361x + 0.212	0.92	0.361
STO	Entire reaction	40	y = -0.899x + 0.304	0.96	0.899
STO	Entire reaction	50	y = -1.383x + 0.221	0.93	1.38

[a] K_{obs} is the pseudo first-order rate constant

[b] SO: siderite-catalyzed hydrogen peroxide oxidant

[c] STO: siderite-catalyzed binary oxidants (hydrogen peroxide and persulfate)

The radical generation mechanisms in the SO and STO systems has been delineated in our previous studies (Yan et al., 2015). For the SO system, the decomposition rate of hydrogen peroxide is rapid in the first 2 hours of the reaction, resulting in high production of HO· at the beginning of the reaction, followed by a period of reduced decomposition rate. Therefore, a two-stage kinetic reaction process was identified: the rapid-stage (first 2 hours of the reaction) and the slow-stage (reaction after 2 hours). In the STO system, the existence of persulfate slowed the decomposition rate of hydrogen peroxide (Yan et al., 2015). Thus a single first-order rate equation was applied to the entire reaction period. Pseudo-first-order reaction rate constants for TCE degradation under multiple temperatures are presented in Table 4.6.1.

The rate constants obtained from the data were applied to the Arrhenius equation Eq. (13) and (14) to calculate the activation energy (E_a, kJ/mol).

$$k = Ae^{-E_a/RT} \tag{13}$$

$$\ln k = \ln A - \frac{E_a}{RT} \tag{14}$$

where k is the rate constant, A is the Arrhenius constant, R is the ideal gas constant (0.0083 KJ/mol·K), and T is the absolute temperature (K). The activation energy can be calculated from the slope of the ln K~1/T relationship (Eq. (14), Figure 4.6.3). The activation energy for the SO system (rapid-stage, slow-stage) and the STO system were 37.7, 60.8, and 72.9 kJ/mol, respectively. For the SO system, the activation energy of the slow-stage was almost two times larger than for the rapid-stage. This is related to the relative amounts of hydrogen peroxide available in the two stages. For the STO system, although the existence of persulfate slightly increased the energy barrier of the reaction compared to the traditional Fenton-like reaction (the SO system), it significantly decreased the decomposition rate of hydrogen peroxide (Yan et al., 2013). Thus, it takes longer to deplete oxidant in the STO system, compared with the SO system. In the STO system, as the reaction proceeded, the heat released from hydrogen peroxide decomposition acted as an internal energy source to promote the reaction, which enhanced the contaminant degradation efficiency. Dichloroacetic acid and formic acid were reported as TCE degradation byproducts in our previous work (Yan et al., 2015).

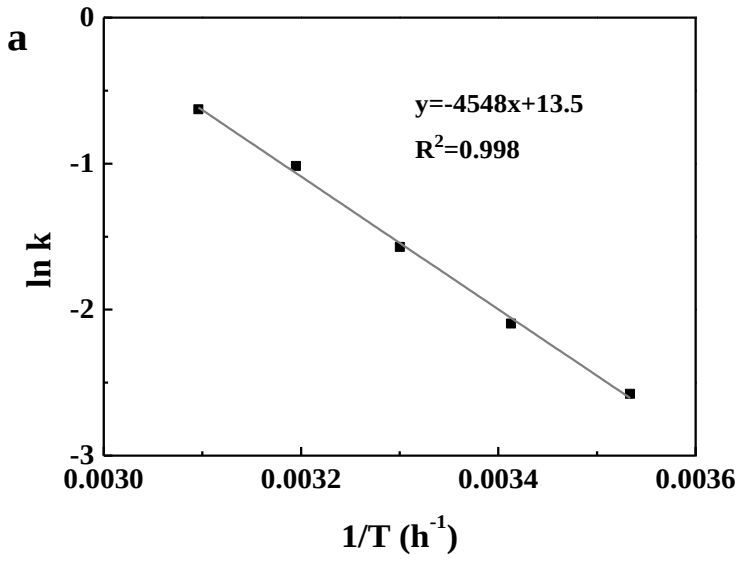

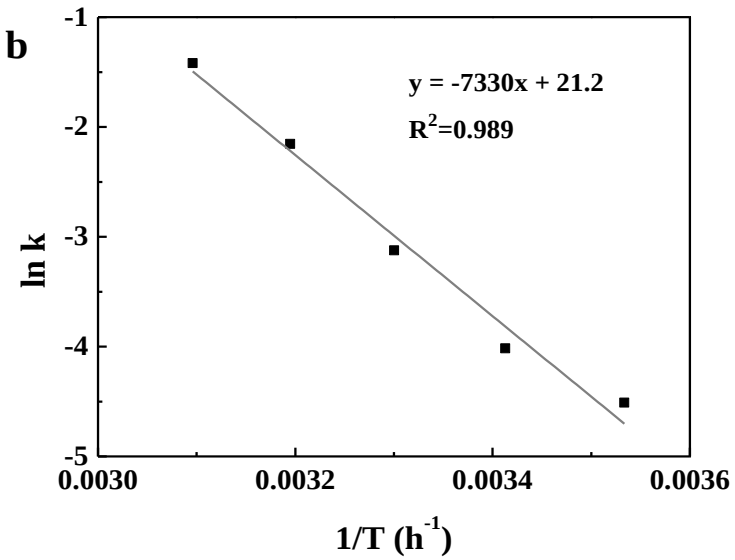

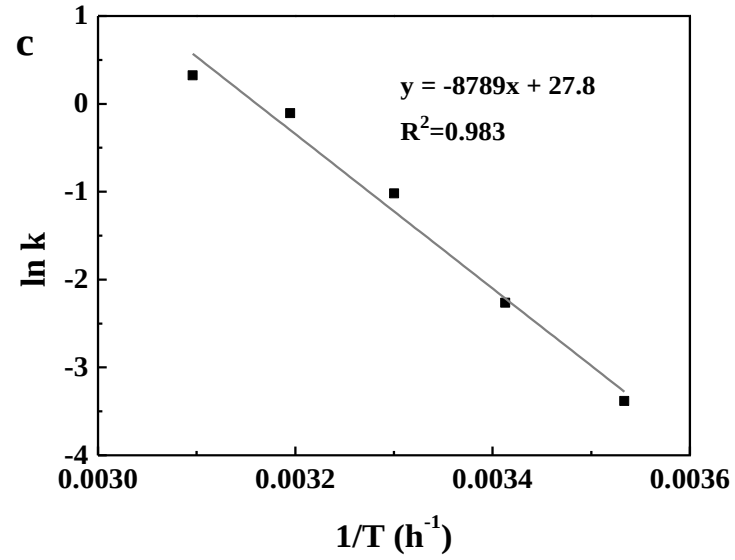

Figure 4.6.3**.** The activation energy for TCE degradation a) first 2 hours of reaction for the SO system; b) after 2 hours of reaction for the SO system; c) entire reaction period for the STO system.

4.6.2 The Influence of Phosphate on TCE Degradation Thermodynamics

The influence of $H_2PO_4^-$ on the degradation of TCE in the SO and the STO systems under multiple temperatures was tested (Figure 4.6.4a and b). The results illustrate that increasing the temperature leads to higher TCE degradation in the presence of $H_2PO_4^-$ within the temperature range used herein.

For the SO system, the presence of $H_2PO_4^-$ had minimal impact on TCE degradation under low temperature condition (10 ^oC). As the temperature increased, the degradation of TCE was inhibited in the presence of $H_2PO_4^-$ compared to the reaction without $H_2PO_4^-$. The $H_2PO_4^-$ in the

system could complex with Fe^{2+}, leading to the conversion of iron species (Eq. (15) and (16)) (Ratanatamskul et al. 2010).

$Fe^{2+} + H_2PO_4^- \rightarrow FeH_2PO_4^+$ (15)

$Fe^{3+} + H_2PO_4^- \rightarrow FeH_2PO_4^{2+}$ (16)

$FeH_2PO_4^+$ may still have the potential to activate hydrogen peroxide. However, $FeH_2PO_4^{2+}$ has limited ability to activate hydrogen peroxide. Therefore, the overall activation ability decreased. Moreover, the competition between the organic contaminant and $H_2PO_4^-$ in reaction with HO· could also decrease the degradation efficiency.

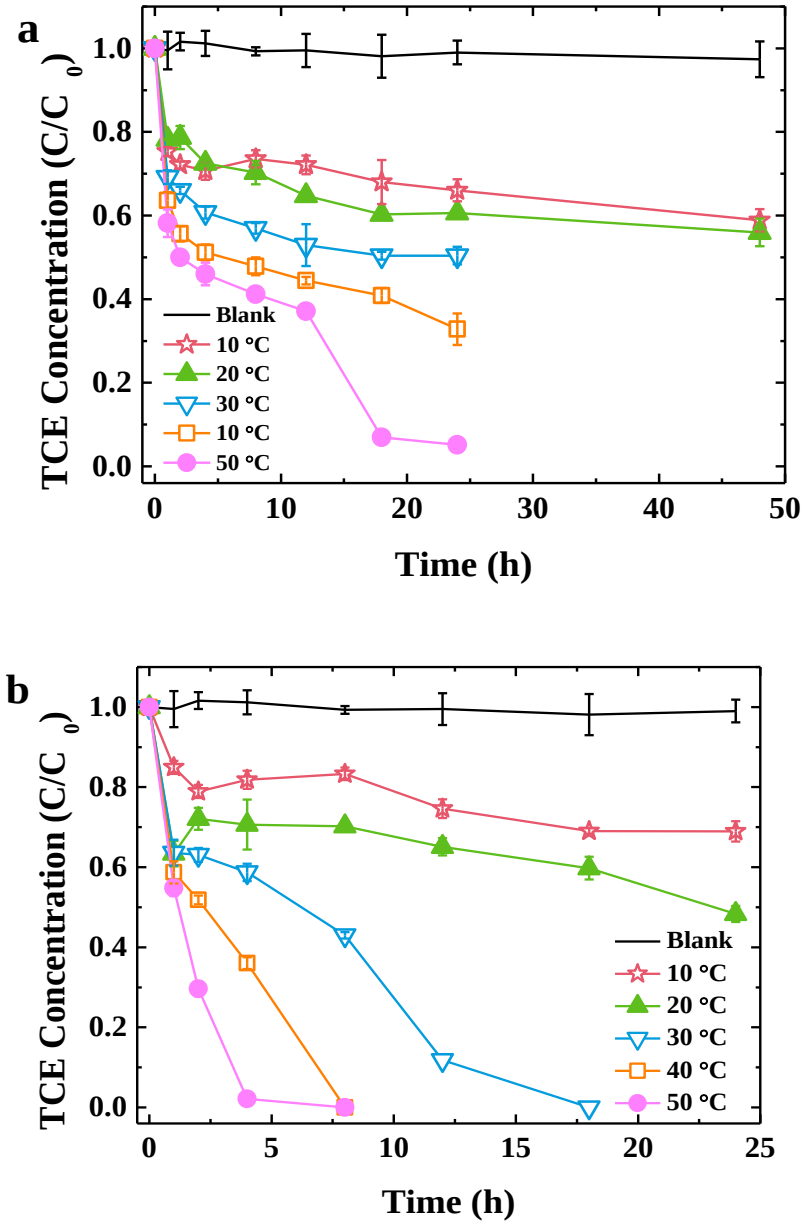

Figure 4.6.4. The effect of $H_2PO_4^-$ on TCE degradation under different temperatures a) the SO system; b) the STO system.

For the STO system, the inhibition effect of $H_2PO_4^-$ was present under all temperatures. Greater inhibition was observed at lower temperatures. The results are likely caused by a greater relative impact of radical scavenging by the salt at lower temperature due to the lower amount of radicals produced.

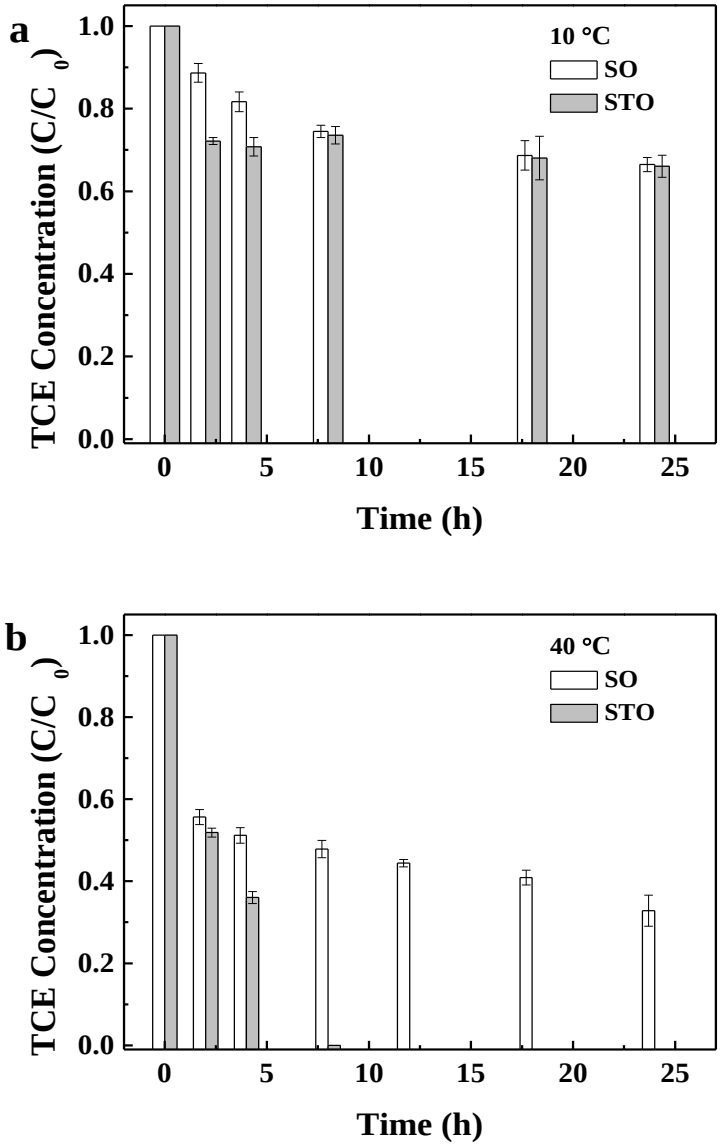

Figure 4.6.5**.** The impact of $H_2PO_4^-$ on TCE degradation in the SO and STO systems under different temperatures a) 10 ^oC; b) 40 ^oC.

The results illustrate that the SO and the STO systems exhibited different inhibition mechanisms under different temperatures. Therefore, a low (10 ^oC) and a high (40 ^oC) temperature were selected to explore the mechanism of the temperature-depended inhibition in the SO and the STO systems. Figure 4.6.5a and b show TCE degradation in single and binary oxidant systems with the existence of $H_2PO_4^-$ under two temperatures. At 10 ^oC, the STO system was more sensitive to the existence $H_2PO_4^-$. The oxidation ability of the STO system was strongly inhibited, resulting TCE degradation efficiency lower than the SO system. At 40 ^oC, the influence of $H_2PO_4^-$ on the STO system became minimal. However, the SO system exhibited strong inhibition. The

results reveal that $H_2PO_4^-$ inhibits the degradation by consuming the generated radical. Different from the SO system, oxidant decomposition and radical generation are relatively slow in the STO system. Under low temperature, the degradation efficiency of the STO system was limited by the limited decomposition ability of persulfate. In addition, the reduced inhibition effect as increasing the temperature reveals the important role of resultant $SO_4^{-}\cdot$ in the STO system.

4.6.3 Effect of Temperature on DCA Degradation

The DCA degradation in the SO and STO systems under different temperatures was investigated (Figure 4.6.6a and b). Figure 4.6.6a indicates that the SO system had limited DCA degradation, as compared to the control group. In addition, temperature has minimal influence on DCA degradation in the SO system. For the STO system, raising the temperature leads to greater DCA degradation (Figure 4.6.6b), similar to TCE. More than 95% DCA was degraded within 48 hours at 20 ^oC and above. Mass balance calculations, based on measured DCA and Cl^- concentrations, show 100% Cl balance, indicating no degradation product accumulated.

The DCA exhibited significantly different degradation behavior in the SO and the STO systems. The results indicate that the activated-hydrogen peroxide process (Fenton-like process) has very limited ability for DCA degradation. The addition of only a small amount of persulfate improves the degradation efficiency significantly. The results of a previous study showed that most hydrogen peroxide was decomposed at the beginning of the reaction in the SO system (Yan et al., 2015). However, the reaction rate between DCA and $HO\cdot$ is limited compared to the self-quenching rate of $HO\cdot$, which will be further discussed in the next section. Furthermore, the addition of persulfate could reduce hydrogen peroxide decomposition rate and produce $SO_4^{-}\cdot$, and thus improve the degradation. In addition, the solution pH should also influence degradation efficiency. During the experiment, the pH of the SO system was ~7, and the pH of the STO system was ~3 (Supplementary Data). Under low pH condition, more ferrous ion would dissolve into solution from the siderite, therefore enhancing the activation activity. Therefore, DCA degradation mechanisms are different between the SO and the STO systems.

A first-order rate equation was applied, and pseudo-first-order reaction rate constants for DCA degradation under multiple temperature conditions in the STO system are shown in Table 4.6.2. The activation energy can be calculated from the slope of ln K~1/T relationship (Figure 4.6.7). The calculated activation energy for DCA degradation in the STO system was 62.3 kJ/mol.

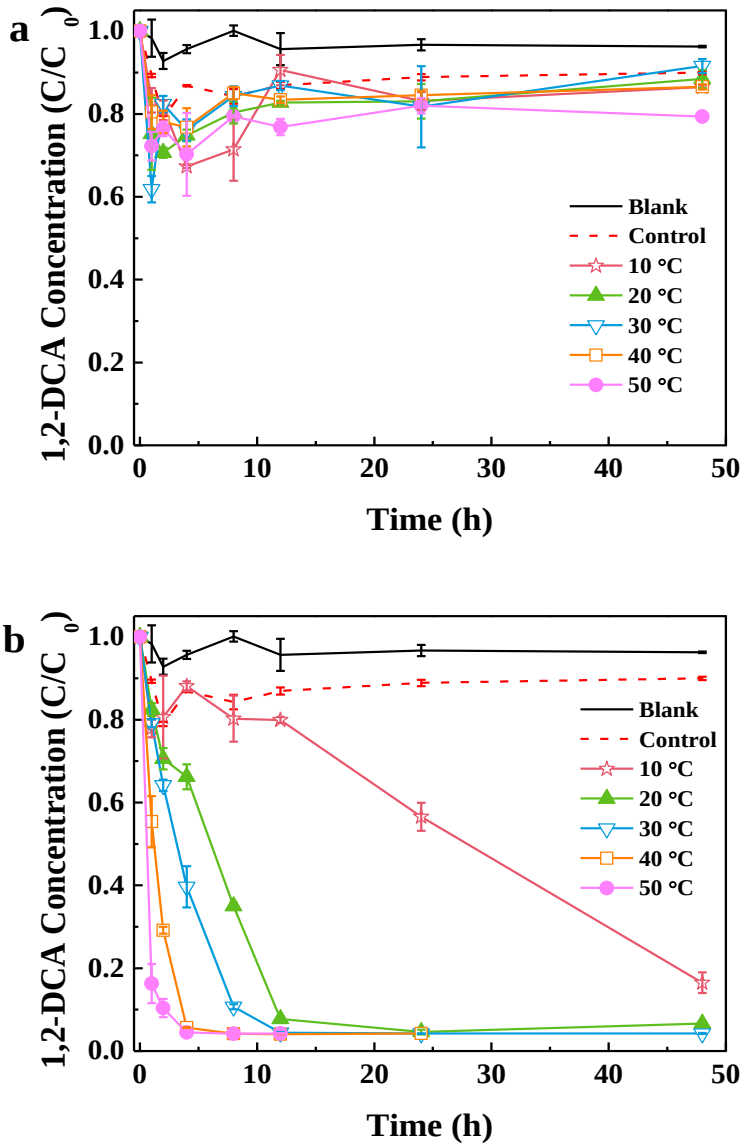

Figure 4.6.6. DCA degradation under different temperatures a) the SO system; b) the STO system.

Table 4.6.2. Kinetic equations for DCA degradation in the STO system.

Temperature (°C)	Regression equation	R^2	k_{obs} [a] (h^{-1})
10	y = -0.034x + 6.198	0.92	0.034
50	y = -0.197x + 6.333	0.92	0.197
30	y = -0.380x + 6.279	0.99	0.380
40	y = -0.723x + 6.299	0.99	0.723
50	y = -1.035x + 5.983	0.89	1.035

[a] K_{obs} is the pseudo first-order rate constant

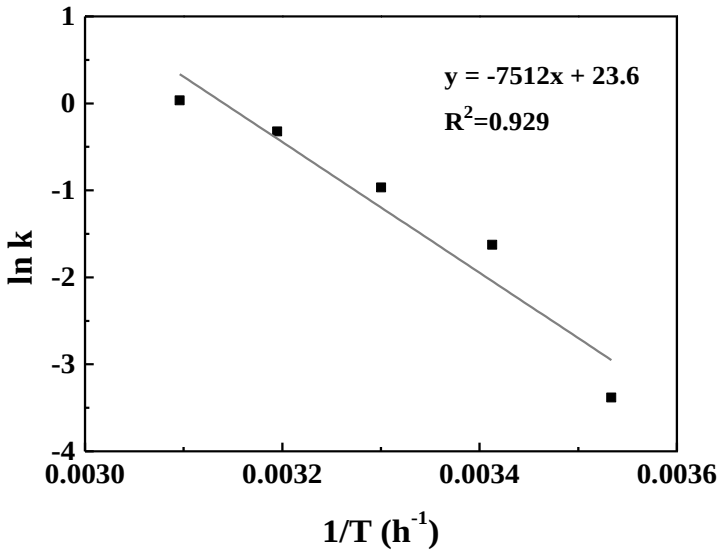

Figure 4.6.7**.** The activation energy for DCA degradation in the STO system.

4.6.4 The Performance of the Iron-Activated Advanced Oxidation Under Different Contaminant Conditions

Based on the results above, TCE and DCA had different degradation efficiencies in the SO system. TCE is an unsaturated chlorinated aliphatic hydrocarbon, whereas DCA is a saturated chlorinated aliphatic hydrocarbon. Different structure might influence the degradation pathway. The reaction rate constant of HO· and TCE is $(3.3–4.3)\times10^9$ $mol^{-1}s^{-1}$ (Eq. (17)).

$$HO\cdot + ClCH{=}CCl_2 \rightarrow \cdot CCl_2CHClHO \quad (17)$$

The self-quenching rate constant of HO· is $\sim5.3\times10^9$ $mol^{-1}s^{-1}$ (Eq. (18)) (Chen et al., 2001).

$$2HO\cdot \rightarrow H_2O_2 \quad (18)$$

The reaction between DCA and HO· is reported (Eq. (19) and (20)) (Randazzo et al., 2011), and the reaction rate constant is $\sim2\times10^8$ $mol^{-1}s^{-1}$ (Lal et al., 1988; Minakata et al., 2009).

$$2HO\cdot + ClCH_2\text{-}CH_2Cl \rightarrow ClCH_2COOH + H^+ + Cl^- + H_2 \quad (19)$$

$$4HO\cdot + ClCH_2\text{-}CH_2Cl \rightarrow HOOCCOOH + 2H^+ + 2Cl^- + 2H_2 \quad (20)$$

The self-quenching rate constant of HO· is almost the same as the reaction rate constant of TCE and HO·, but over one order of magnitude larger than the reaction rate constant of DCA and HO·. Therefore, the SO system is generally effective for treating certain amount of TCE but not effective for degrading DCA.

The degradation efficiencies of TCE and DCA were almost the same in the STO system, which was also proved by the similar activation energy. The points of zero charge of siderite is

5.3±0.1. The STO system has pH ~3. Acidic condition prevents the adsorption and thus improve the effectiveness of degradation. Furthermore, the STO system being superior to the SO system for DCA treatment might also have contributed to the production of $SO_4^{-\cdot}$, and the sustainable release of radicals.

4.7 Aqueous Ozone Transport and Oxidant Demand Reactivity Results and Discussion

4.7.1 Comparing batch and column experiment

The equilibrium batch experiments were conducted to quantify the degradation rate constant of O_3 reacting with hydroxide in water at three different salt concentrations in bulk water without sediment. Figure 4.7.1 presents the results of the batch experiments with mean values for natural log of the concentration normalized by the initial concentration (C/Co) versus reaction elapsed time. Standard deviation error bars indicate experimental variability. Linear regression was able to describe the results, which confirms that the reaction follows pseudo first order degradation kinetics and the slope of the regression equation is the rate constant for O_3 decay. The figure also compares the DI water experiments to the results of experiments conducted in 50 and 100 mM NaCl, and the results indicate that the slope, or degradation rate constant, increases with increasing salt concentration. The degradation rate constant for O_3 with 100 mM NaCl was 70% higher compared to DI water and for O_3 with 50 mM NaCl 45% higher compared to DI water. This trend was likely due to the reactivity of O_3 with chloride ions to form molecular chlorine or potential chloride radical formation (as noted above). Reaction kinetics of O_3 in groundwater with pH 7.8 (batch experiment) was 0.036 min^{-1}. These results were within the range of reaction kinetics of O_3 reported in the previous literature (0.03 to 0.18 min^{-1}) (Gardoni et al., 2012).

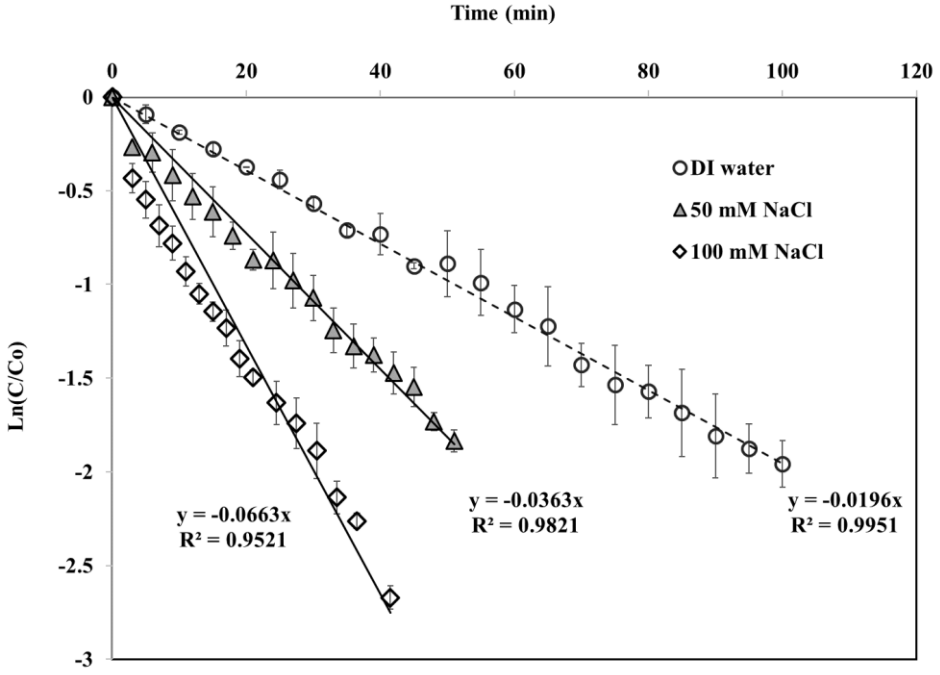

Figure 4.7.1. Degradation kinetics of O_3 in three different salt concentrations in batch experiment.

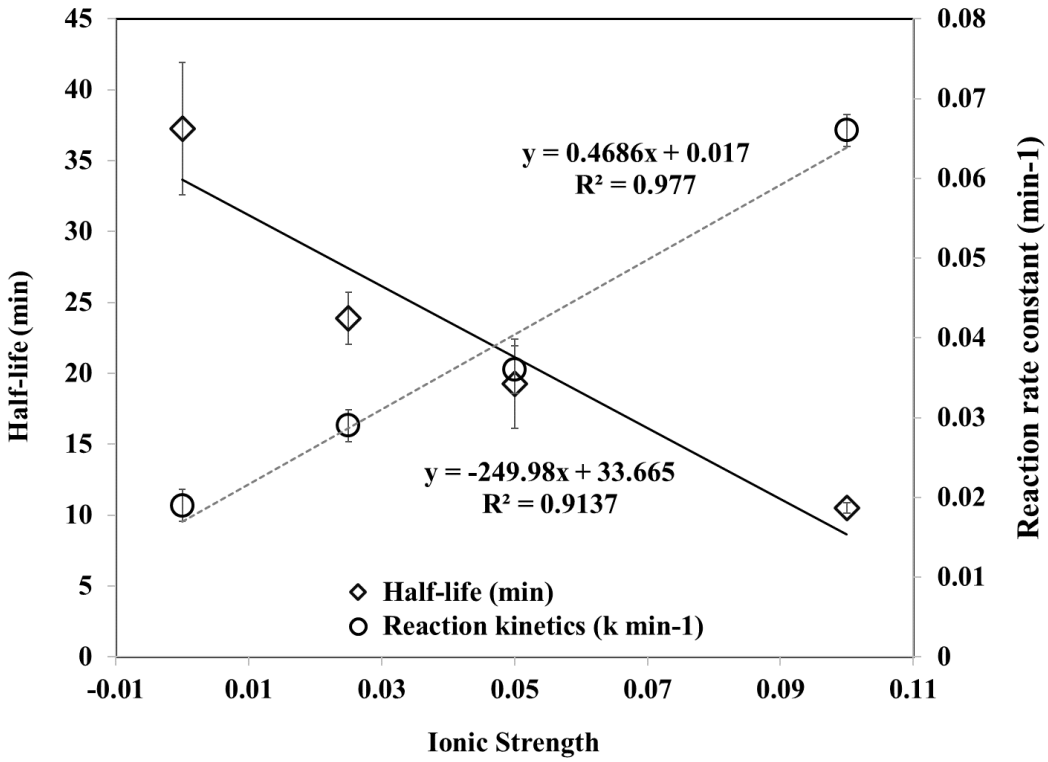

Figure 4.7.2. Relationship of reaction rate constant and half-life of O_3 with ionic strength (mM).

Figure 4.7.2 presents the O_3 decay rate constant and half-life versus ionic strength (mM) for the experiments conducted with different NaCl concentrations. An additional data point for ionic strength (0.025 mM) was included from a recent paper (Dettmer et al., 2017). These results indicate a proportional trend observed between ionic strength and reaction rate constants. Interestingly, all the experiments, except the one from Dettmer et al., only included NaCl to vary ionic strength, and the Dettmer et al. study included various salts to mimic a synthetic groundwater. The trend of rate constant increasing with ionic strength was consistent despite this variation in the type of salt used to alter ionic strength. This trend has implications for prediction of O_3 reaction rate constants and aqueous O_3 reactive lifetime in natural water systems where water chemistry and ionic compositions may be variable.

The batch reaction rate constants measured DI water experiments were also compared to reaction rate constants estimated from O_3 tracer test results where experiments included both O_3 reactive decay in water and also solute transport processes. To determine rate constants using tracer breakthrough column experiment data, we considered the effluent recovered mass relative to the injected mass to be analogous to the C/Co. This was determined from moment analysis and plotted as a function of mean arrival time of the O_3 tracer plume also determined using moment analysis. The exponent value obtained from exponential regression of these data represents the bulk plume decay rate constant for these solute transport experiments.

4.7.2 Non-reactive tracer transport and hydrodynamic parameters

Representative measured and model simulated breakthrough curves were plotted as relative concentration (C/Co) versus pore volume or hydraulic residence time for non-reactive tracer (i.e.,

PFBA) experiments. Test results shown in Figure 4.7.3 through 4.7.5 are for experiments conducted using the 20, 60, and 152 cm columns, respectively. The measured breakthrough curves had sharp and symmetrical concentration changes on arrival and elution curves, indicating ideal transport behavior in the homogeneously packed columns. No measurable sorption or degradation was observed as retardation factor was 0.987 – 1.03 (determined from moment analysis mean travel times) and mass recovery was ~100% based on moment analysis effluent integration. Comparison of breakthrough curves for different flow rates and different distances indicated no significant changes in solute transport behavior between these variable experimental conditions. This indicates that the variability in flow rates or transport distances did not have any impact on hydrodynamic transport behavior of the nonreactive tracer PFBA. The simulation produced with the nonreactive solute transport model provided good matches to the measured data, and these simulations were used to estimate dispersion coefficients.

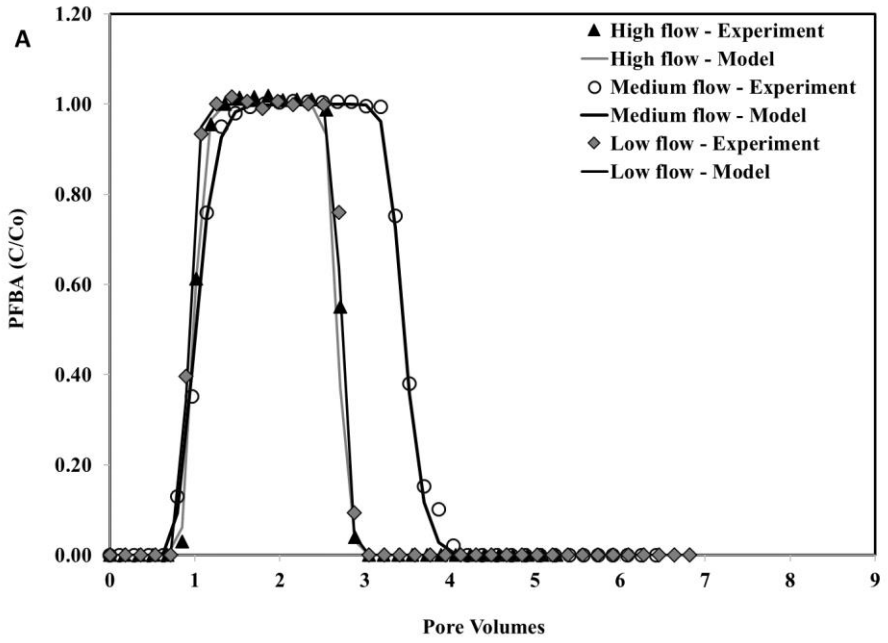

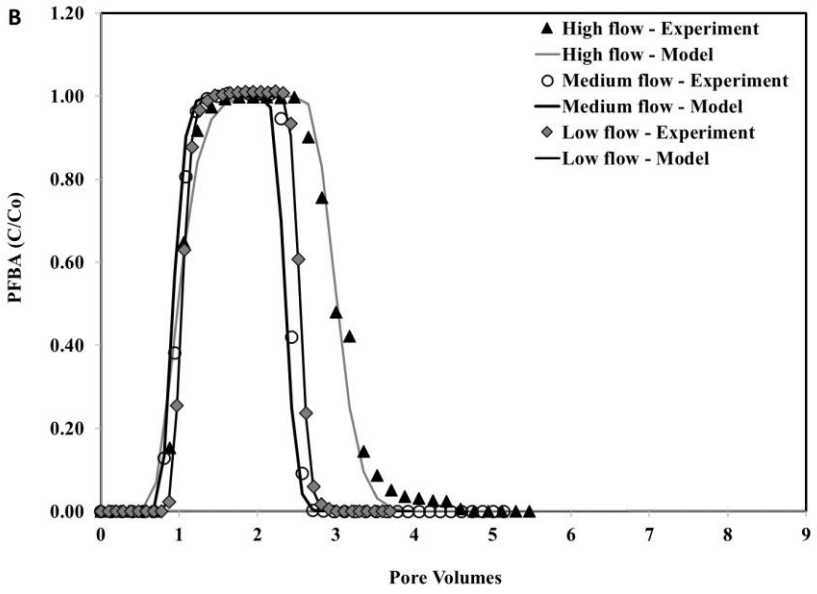

Figure 4.7.3. Breakthrough curve of PFBA in 20 cm column from experiment (two repeats-Figure A and B) and reactive transport model fitted data.

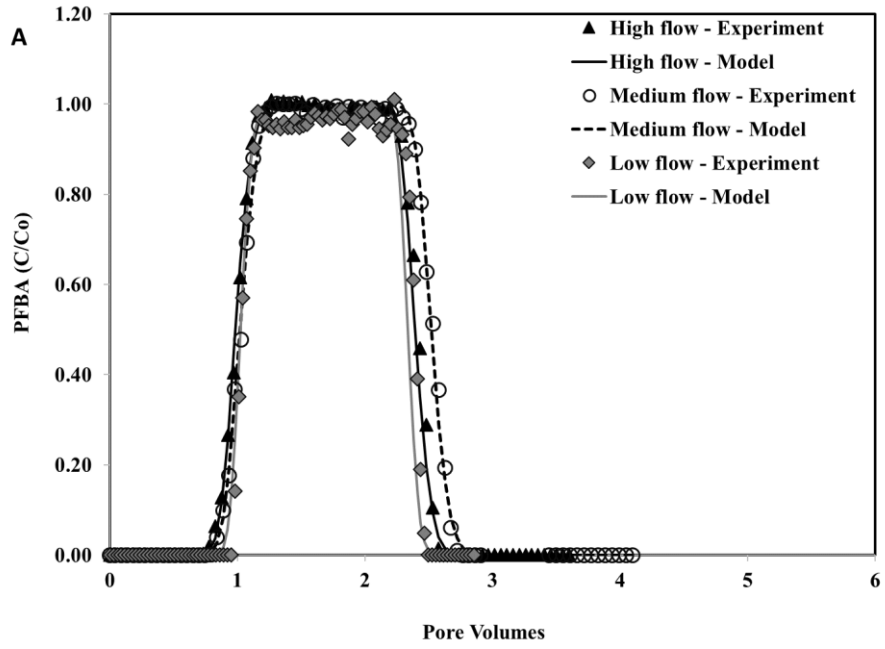

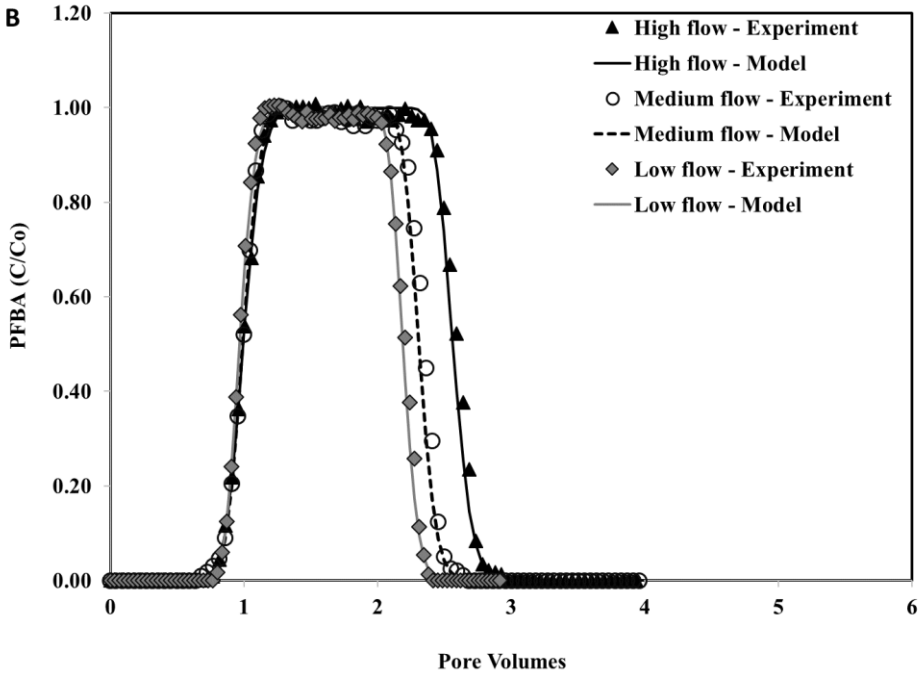

Figure 4.7.4. Breakthrough curve of PFBA in 60 cm column from experiment (two repeats-Figure A and B) and reactive transport model fitted data.

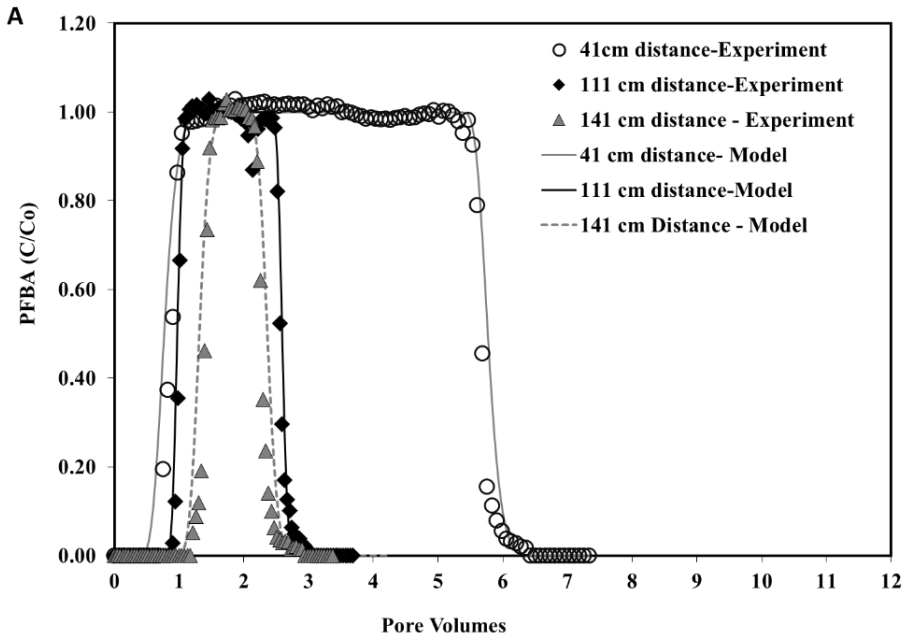

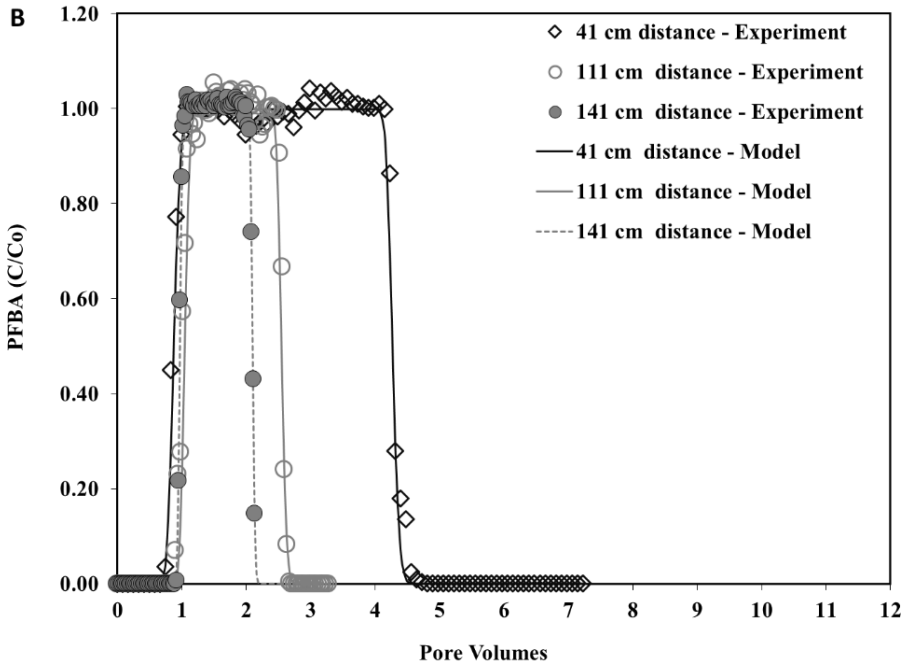

Figure 4.7.5. Breakthrough curve of PFBA in 152 cm column from experiment (two repeats- Figure A and B) and reactive transport model fitted data.

Table 4.7.1 presents the model-estimated hydrodynamic parameters (Peclet number and dispersion coefficient for the three different pore water velocities and three different columns with different lengths). For the 20 cm and 60 cm column length, there was an increasing trend in dispersion coefficient with increasing pore water velocity, which was expected. For 152 cm long column with 3 different collection ports (i.e., 41 cm, 111 cm, and 141 cm) and single pore water velocity (0.827 cm/min), the dispersion coefficient (0.023 ± 0.007 cm^2/min) did not show any significant trend, which was also expected.

Table 4.7.1. Estimated Peclet number and dispersion coefficient results from modeling PFBA tracer experiments.

20 cm column				
Parameters	**Variables**	**Low Flow**	**Medium Flow**	**High Flow**
Peclet number ((L*v)/D)	**Pe**	6650	2433	3063
Porewater velocity = [Q/(A*n)]	**V** (cm/min)	0.88 ± 0.0	1.7 ± 0.05	2.7 ± 0.14
Dispersion coefficient = [(L*v)/Pe]	**D** (cm^2/min)	0.004 ± 0.0001	0.02 ± 0.01	0.04 ± 0.02

60cm column				
Parameters	**Variables**	**Low Flow**	**Medium Flow**	**High Flow**
Peclet number	**Pe**	24420	12000	11100
Pore water velocity = [Q/(A*n)]	**V** (cm/min)	0.86 ± 0.32	1.64 ± 0.06	2.71 ± 0.27
Dispersion coefficient = [(L*v)/Pe]	**D** (cm^2/min)	0.002 ± 0.001	0.009 ± 0.0002	0.014 ± 0.002
152cm column				
Parameters	**Variables**	**Port A (41 cm distance)**	**Port B (111 cm)**	**Port C (141 cm)**
Peclet no.	**Pe**	3382	91575	38775
Pore water velocity = [Q/(A*n)]	**V** (cm/min)	0.83	0.83	0.83
Dispersion coefficient = [(L*v)/Pe]	**D** (cm^2/min)	0.01 ± 0.009	0.001 ± 0.0005	0.003 ± 0.0007

4.7.3 Ozone transport behavior in saturated porous media and model fitting

Table 4.7.2 presents a comparison of the transport parameters including decay rate constants and retardation factors (both from moment analysis of the experimental data and from the transport modeling) for O_3 under the column experiment conditions including various column lengths and pore water velocities. The moment analysis results determined that O_3 had retardation factors (Table 4.7.2) that were consistently larger than one and larger than PFBA, which had retardation factors that were consistently approximately one. This indicates that aqueous O_3 underwent a small yet measureable amount of sorption.

Measured breakthrough curves (normalized concentration versus pore volumes) for O_3 transport in different column with different column length and different flow rates are also presented along with model simulation results shown in Figure 4.7.6 through 4.7.8 are for experiments conducted using the 20, 60, and 152 cm columns, respectively. The O_3 breakthrough curves were not as sharp as the nonreactive tracer results, which also suggests that some sorption occurred and influenced O_3 transport. The experimentally determined and model estimated retardation factors were not generally statistically different despite variability in the mean values. For O_3 tracer transport within the 152 cm column (Figure 4.7.8), concentration variability, spreading, and tailing were observed to be more significant than was observed for any of the other column data sets. This additional variability was attributed to differences in the column experimental setup. PVC was used to construct the 152 cm column (the other columns were stainless steel), which may have had some reactivity with O_3. Additionally, the larger diameter, glass wool at influent end, and differences in sampling port construction may have contributed to the experimental variability.

Table 4.7.2. Dispersion coefficient and degradation rates of O_3 from CXTFIT model for 20 cm, 60 cm, and 152 cm column.

Column Length	Pore water velocity (cm/min)		Retardation factor (Experiment)	Retardation factor (Model)	k (min^{-1}) Moment analysis	k (min^{-1}) Model
20 cm column	0.88 ± 0.0		1.69 ± 0.49	1.83 ± 0.57	0.03 ± 0.013	0.06 ± 0.01
	1.72 ± 0.05		1.47 ± 0.47	1.58 ± 0.44		0.06 ± 0.01
	2.73 ± 0.14		1.49 ± 0.21	1.63 ± 0.57		0.04 ± 0.009
60 cm column	0.86 ± 0.32		1.56 ± 0.15	1.50 ± 0.17	0.02 ± 0.002	0.03 ± 0.005
	1.64 ± 0.06		1.45 ± 0.19	1.40 ± 0.27		0.02 ± 0.007
	2.71 ± 0.27		1.63 ± 0.30	1.56 ± 0.38		0.03 ± 0.006
152 cm column	41 cm	0.83 cm/min	1.95	1.67	0.02	0.03
	111cm		1.07	0.72		0.01
	141 cm		1.13	0.94		0.01

Experimental O_3 tracer transport breakthrough data were matched and well-described by the modeling results. Dispersion coefficients determined from the PFBA nonreactive tracer modeling were also used for the O_3 tracer experiment modeling. Comparison of these experimental and modeling results also illustrate that the peak relative concentrations were generally lower than 1 (PFBA tracer peaks were consistently at 1), and Figure 4.7.5 and Figure 4.7.6 indicate that concentration peaks decreased from 1 (C/Co) with decreasing flow velocities, which indicates that additional decay of O_3 occurred with increasing contact time during transport in the column. The alternative interpretation is that O_3 decay can be minimized by maximizing groundwater flow velocity, which would also maximize oxidant transport distance in the subsurface. This behavior was quantified through O_3 decay rate constant parameter estimation, which is summarized in Table 4.7.2 with mean and standard deviation values. Despite the minor variability, the model and experimentally derived values were comparable, and generally the values for the 20 cm (k varies from 0.034 to 0.056 min^{-1}), the 60 cm (k varies from 0.018 to 0.027 min^{-1}) and the 152 cm (k varies from 0.011 to 0.025 min^{-1}) columns were comparable even though there were significant variations in transport length and pore water velocity. Overall, the column experiment and modeling derived rate constant values for O_3 were comparable for the 5 different transport distances with 7 different pore water velocities. In addition, the observed degradation rate constant of O_3 from moment analysis and from the modeling were comparable to each other and comparable to batch experiment.

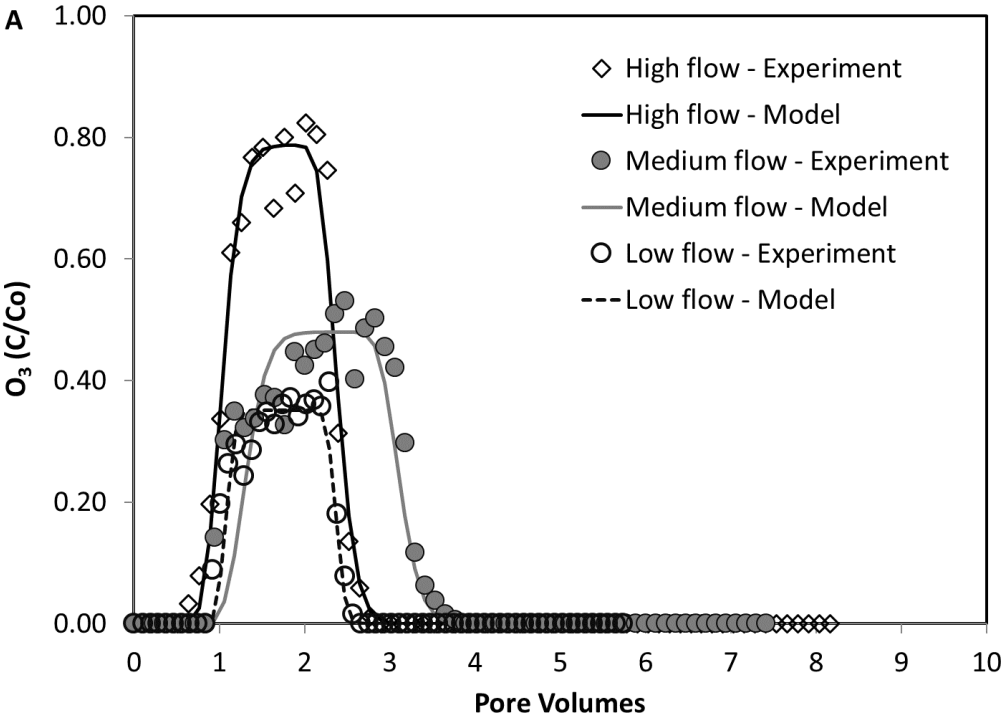
A
1.00
0.80
0.60
0.40
0.20
0.00
O3 (C/Co)
0
1
2
3
4
5
6
7
8
9
10
Pore Volumes
High flow - Experiment
High flow - Model
Medium flow - Experiment
Medium flow - Model
Low flow - Experiment
Low flow - Model

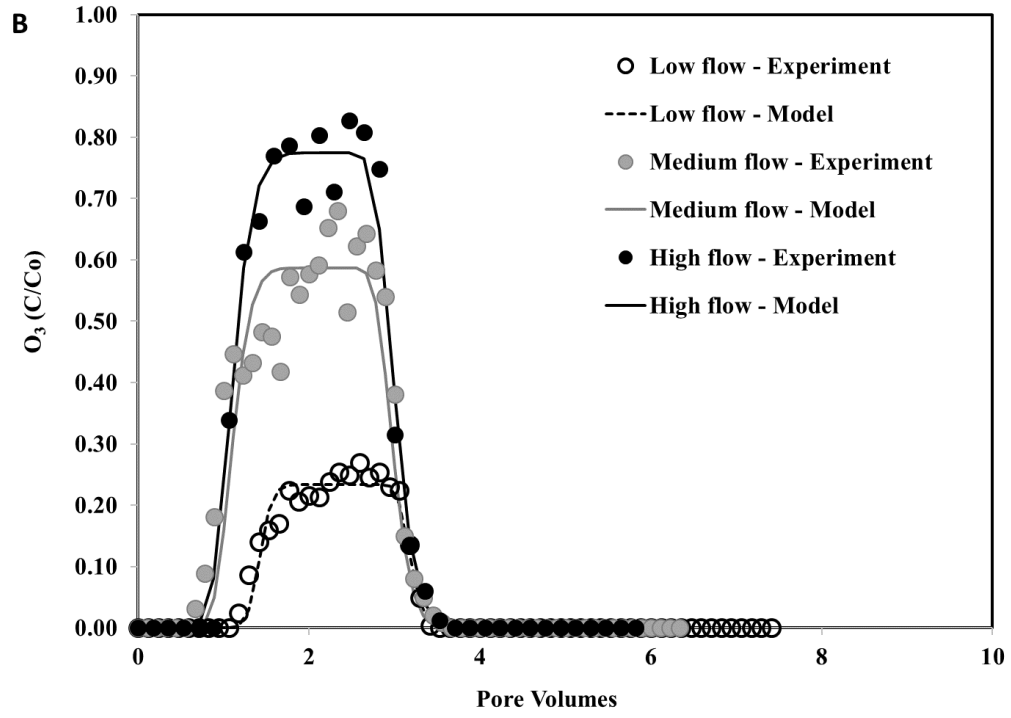
B
1.00
0.90
0.80
0.70
0.60
0.50
0.40
0.30
0.20
0.10
0.00
O3 (C/Co)
0
2
4
6
8
10
Pore Volumes
Low flow - Experiment
Low flow - Model
Medium flow - Experiment
Medium flow - Model
High flow - Experiment
High flow - Model

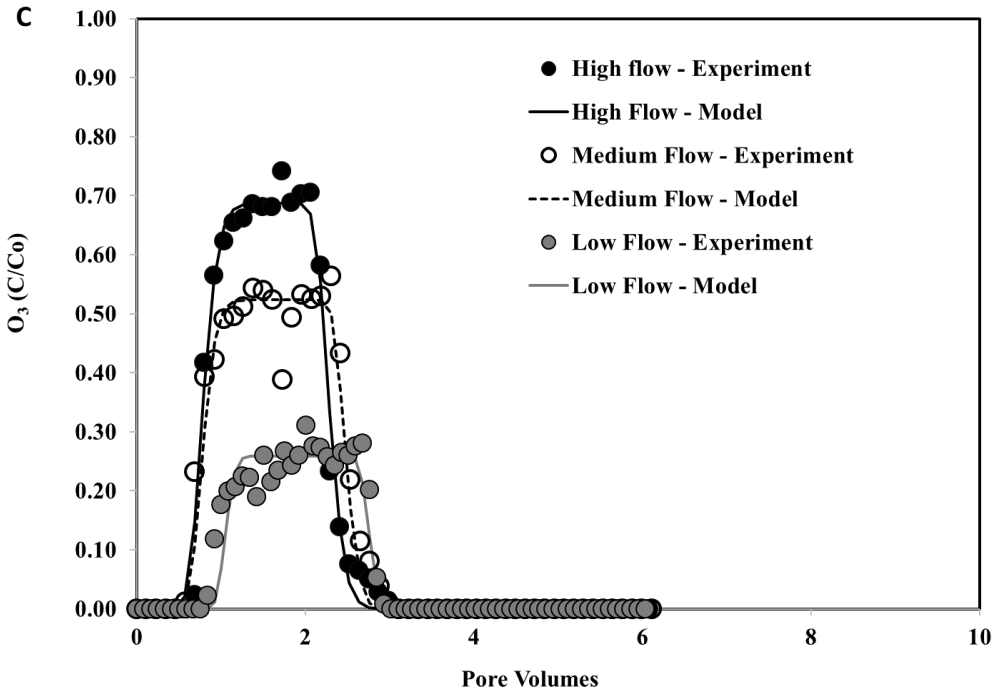

Figure 4.7.6. Ozone breakthrough curves (from 3 repeats-Figure A, B, and C) at different flow rates from experiment and reactive transport model fitted data for 20 cm column.

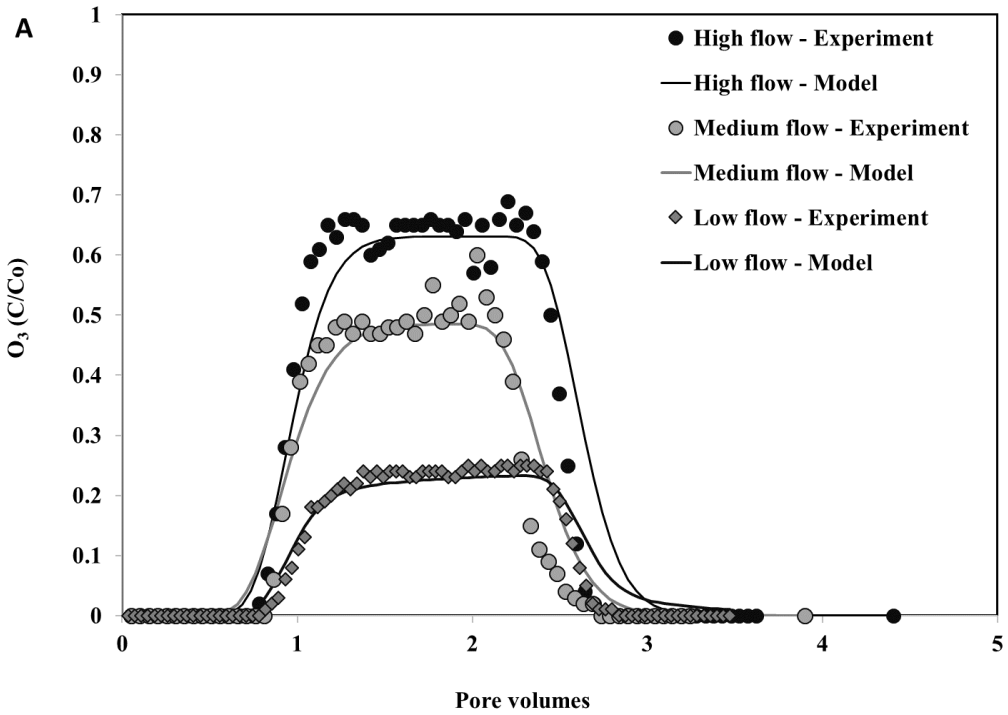

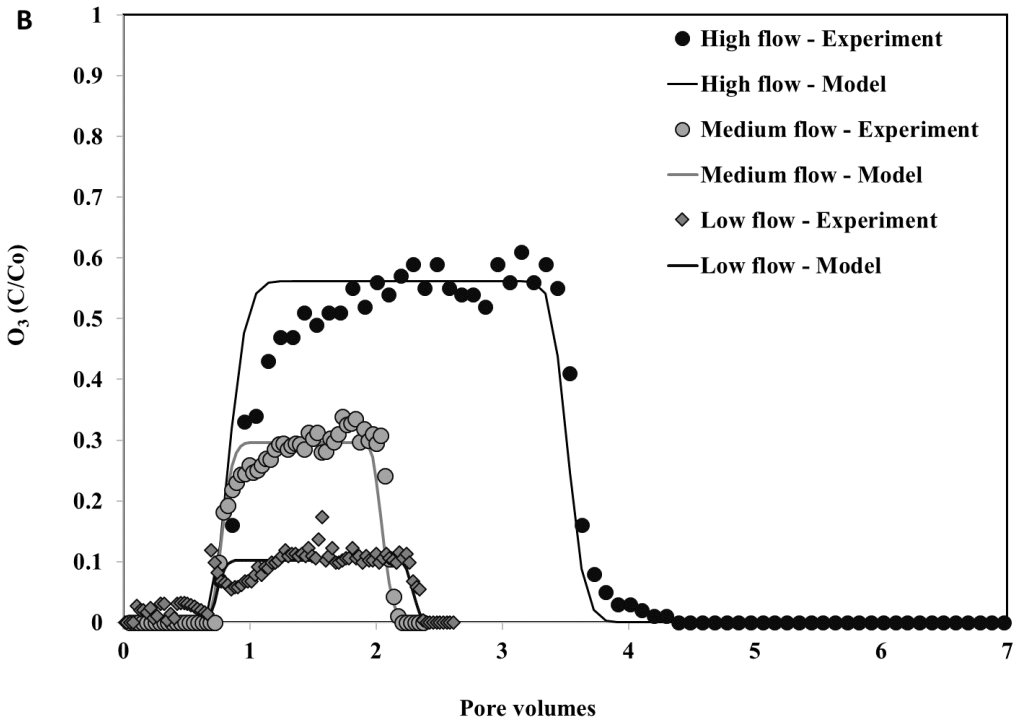

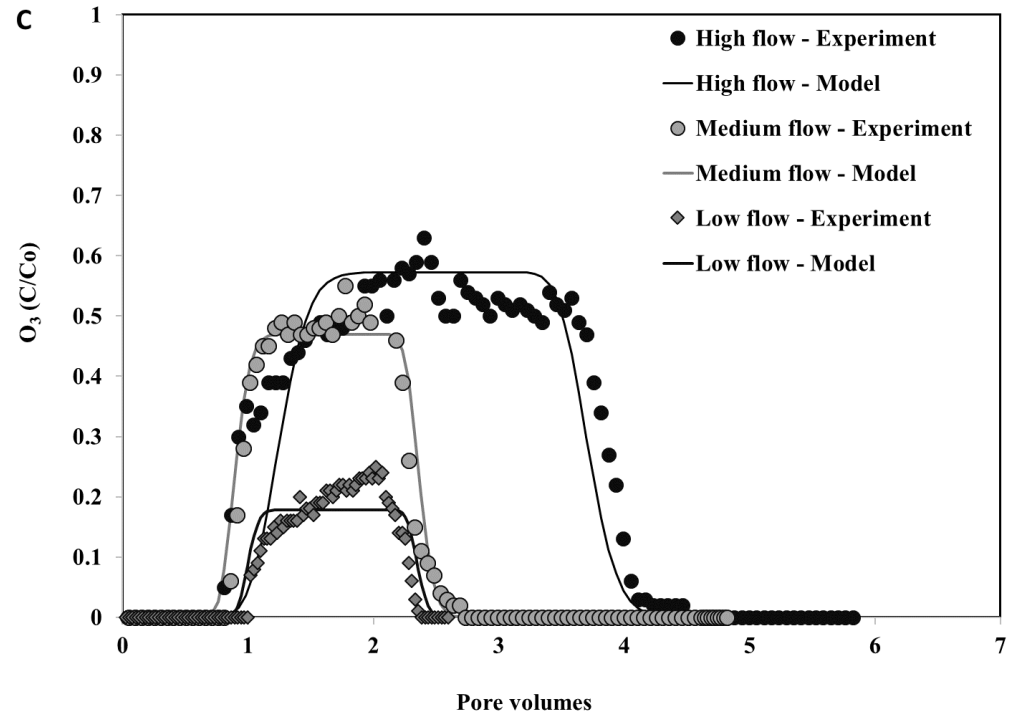

Figure 4.7.7. Ozone breakthrough curves (from 3 repeats-Figure A, B, and C) at different flow rates from experiment and reactive transport model fitted data for 60 cm column.

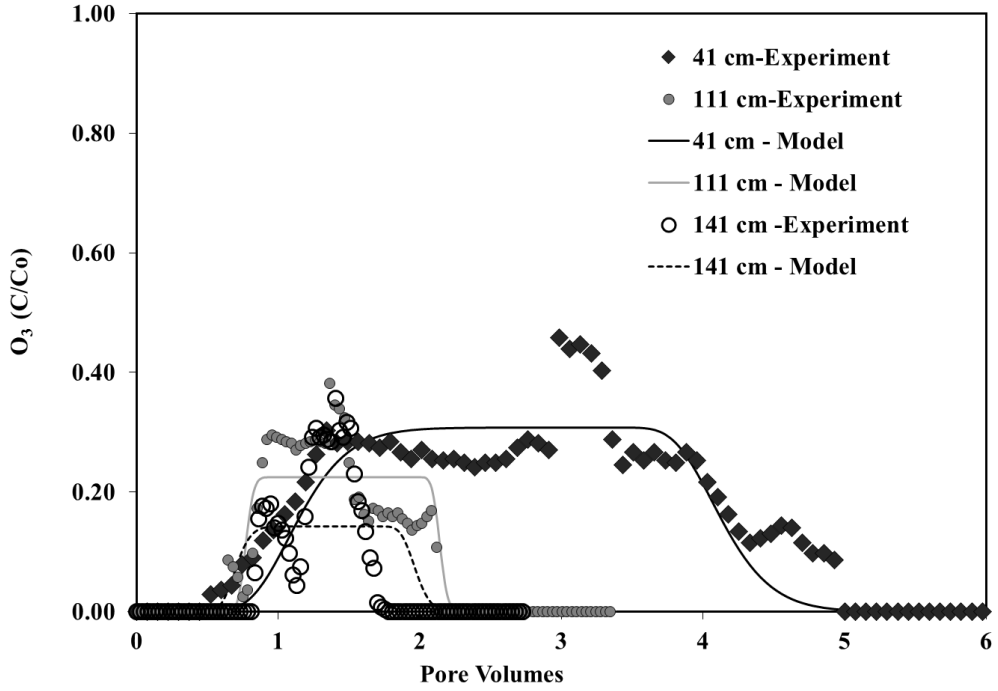

Figure 4.7.8. Breakthrough curve of O_3 in 152 cm column from experiment and reactive transport model fitted data.

As noted above, the experiments quantify O_3 transport and decay behavior at three different pore water velocities for 20 cm and 60 cm long column, respectively. Yet, transport distance was constant while velocity was varied for each of these systems. Whereas transport and decay behavior of O_3 was measured for only one pore water velocity (i.e., one experiment) with measurements at three different transport distances within the 152 cm column. Table 4.7.2 shows that all of these experiments resulted in similar aqueous-phase O_3 pseudo 1st order reaction rate constants. The consistency in these rate constants suggests that degradation rate constant of O_3 does primarily depend on the contact time. Contact time was altered with pore water velocity in the columns with only one sampling port (i.e., constant length), and it was altered in the 152 cm column under constant velocity by sampling at three different ports each with a different transport length to evaluate transport over a longer time. Additionally, these results indicate that solute transport processes, such as dispersion or adsorption, did not have a significant impact on the O_3 concentration attenuation, which was dominated by the degradation reactions with hydroxide in water.

Further comparison of the tracer test estimation of O_3 rate constants measured within water saturated porous media during solute transport can be made by comparing these results with the results of the O_3 rate constants obtained from bulk water batch experiments. The batch experiment rate constant was 0.019 ± 0.002 min^{-1}, which was consistent with the rate constants obtained for experiments in the 60 cm and 152 cm columns, respectively. The initial concentrations for the batch experiments were similar to the input concentrations of column experiments. However, the batch experiments were conducted in well-mixed reactors with negligible solute transport

processes, and the tracer experiments were likely impacted by both solute transport processes and O_3 decay reactions, which were accounted for in the modeling but not in the moment analysis rate constant estimates. These results support the previously noted observation that, for the porous media used herein, solute transport processes, such as dispersion or adsorption, did not have a significant impact on the O_3 concentration attenuation. Prior work observed the half-life of gaseous O_3 in sandy soil was 40 minutes, which is comparable to the present column studies (33 ± 13 min). Also, the reaction kinetics for gaseous O_3 in sandy soil was 0.017 min^{-1} (Choi et al., 2002), which was also comparable to present research. This suggests that O_3 decay kinetics may not be significantly different for aqueous or gas-phase injections.

These results illustrate the consistency and predictability of O_3 decay kinetics, and suggest that O_3 decay is the dominant process impacting concentrations in these experimental systems. The Accusand quartz sand used for these experiments is highly inert (i.e., low organic matter and metal oxide content), and seems to have negligible oxidant demand. Additionally, the uniformity of the grain size for this porous media contributed to the minimal dispersion impacts on concentrations. Although O_3 sorption was observed, the decay of O_3 had a more significant impact on the transport and attenuation such that the bulk aqueous decay kinetics were comparable to the bulk concentration decay during transport through porous media. These results suggest that O_3 decay and transport can be well characterized if the sediment oxidant demand and dispersion can be characterized for a particular site. These results also suggest that maximizing groundwater flow velocity during O_3 injection can be used to maximize transport distance for reagent delivery.

4.8 Transport and Peroxone Activated Persulfate Treatment of 1,4-Dioxane Results and Discussion

4.8.1 Batch Scale Experiments

Batch scale experiments were used to determine the degradation of 1,4-dioxane using OxyZone® in the presence of homogenized silica quartz sand under varying oxidant: contaminant ratios, derive reaction kinetics, and compare the results with those of Eberle et al. (Eberle et al., 2016), who studied aqueous phase kinetics in the absence of sediment.

Table 4.8.1**.** Oxidation of 1,4-dioxane over 16 days (384 hours) at the oxidant:contaminant ratio of 250:1.

k_1 (h^{-1})	0.0213
$T_{1/2}$ (h)	33
R^2	0.97

The first set of batch studies covered oxidant: contaminant (OxyZone® to 1,4-dioxane) molar ratios ranging from 100:1, 250:1, 500:1, and 1000:1 and lasted 24 hours (Supplementary Data). The experiment was carried out to determine the optimal oxidant: contaminant ratio for the subsequent kinetics study. At high ratios (≥500:1), 1,4-dioxane is comparatively quickly destroyed. At 250:1 or lower, 1,4-dioxane destruction is sufficiently slow to monitor it over an extended period, i.e. about two weeks. Based on these results, a 250:1 ratio was chosen to conduct

the following kinetics study. For comparison, the initial OxyZone® oxidant: contaminant ratio is 7,400:1 before it is being injected into the column or injected into a polluted aquifer under field test conditions.

The second set of batch experiments kept the oxidant:contaminant ratio fixed at 250:1 but extended the reaction period to 16 days (Figure 4.8.1). The control experiment proved that no significant degradation took place in the absence of oxidant, whereas the 1,4-dioxane concentration dropped to below detection limit when exposed to oxidant after 192 hours (Figure 4.8.1). By plotting the relative concentrations at each time point (Figure 4.8.2) and using the slope of the best-fit line for solving Eqns. 2 and 3, the reaction rate and half-life time was determined (Table 4.8.1).

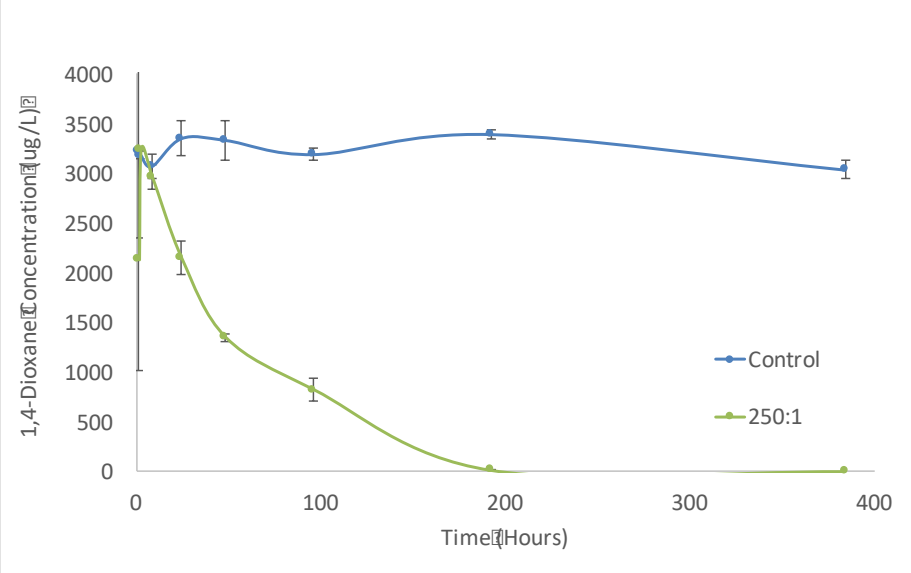

Figure 4.8.1**.** Batch scale oxidation of 1,4-dioxane over time oxidant:contaminant ratio of 250:1.

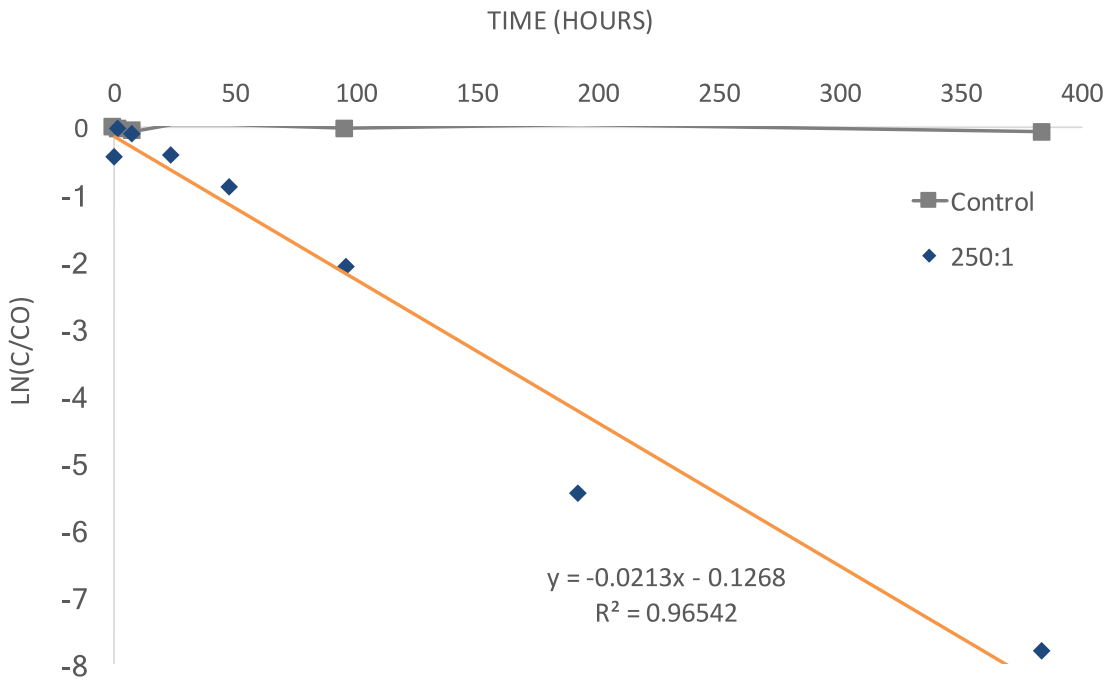

Figure 4.8.2**.** Ln(C/Co) over time for the 16-day period at the oxidant:contaminant ratio 250:1.

4.8.2 Column Experiments

Column scale tests were conducted to obtain an understanding of 1,4-dioxane treatment under dynamic, flow through conditions. An initial conservative tracer test indicates that the column was packed homogenously and that preferential flow was of no concern (Figure 4.8.3).

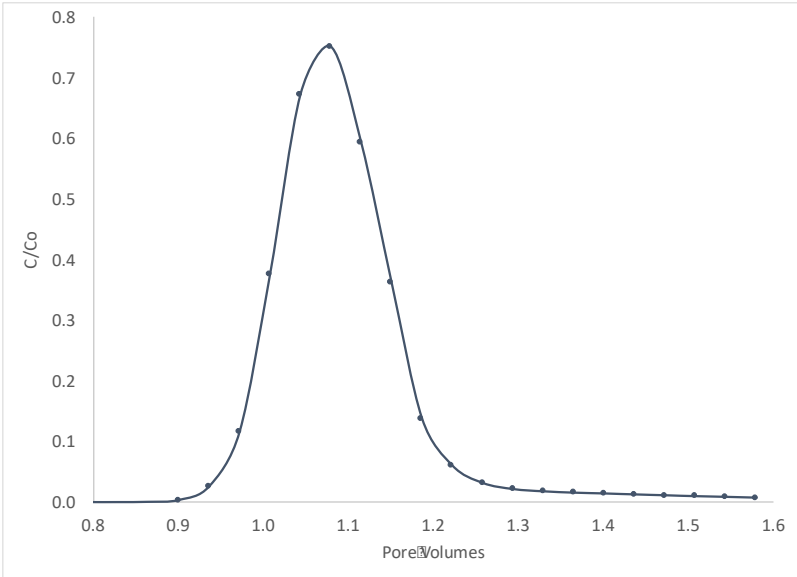

Figure 4.8.3**.** Conservative tracer breakthrough curve.

4.8.2.1 Treatment Scenario I - Slug injection in two ports

Two tests were conducted, differing only in the time it took to inject 100 ml (about 0.05 PV) pulses of oxidant each into two ports (A and C; diagram in methods). During the first test (Test I), the oxidant was injected quickly, i.e. within 25 minutes. The test ran for 12 hours or just under 1.5 pore volumes. There are two peaks in the EC data, at 0.55 PV and 0.95 PV respectively, which signal the breakthrough of the two separate pulses (Figure 4.8.4). Inflow 1,4-dioxane concentration was 268 µg/L. At 0.4 PV, the concentration rose to 376 µg/L (Figure 4.8.4). This anomaly is also reflected in the ORP and pH data (Figure 4.8.5). Following the breakthrough of the oxidant, as indicated by the rise in EC, the ORP values rose to 276.5 mV, while 1,4-dioxane concentration decreased (to as low as 215 µg/L, or 0.55 C/Co). The pH decline appears inversely related to the rise in ORP (Figure 4.8.5). The pH of the system starts at near neutral and eventually stabilizes at around 6.4.

The zeroth moment (M_0) moment describes the oxidant mass recovery. For Scenario I, Test I, only 7.66 grams of OxyZone® was recovered in the effluent, or 51% of the total mass injected. However, the EC readings were elevated still at the end of the experiment (Figure 4.8.4), indicating that an unknown fraction of the oxidant had not eluted from the column.

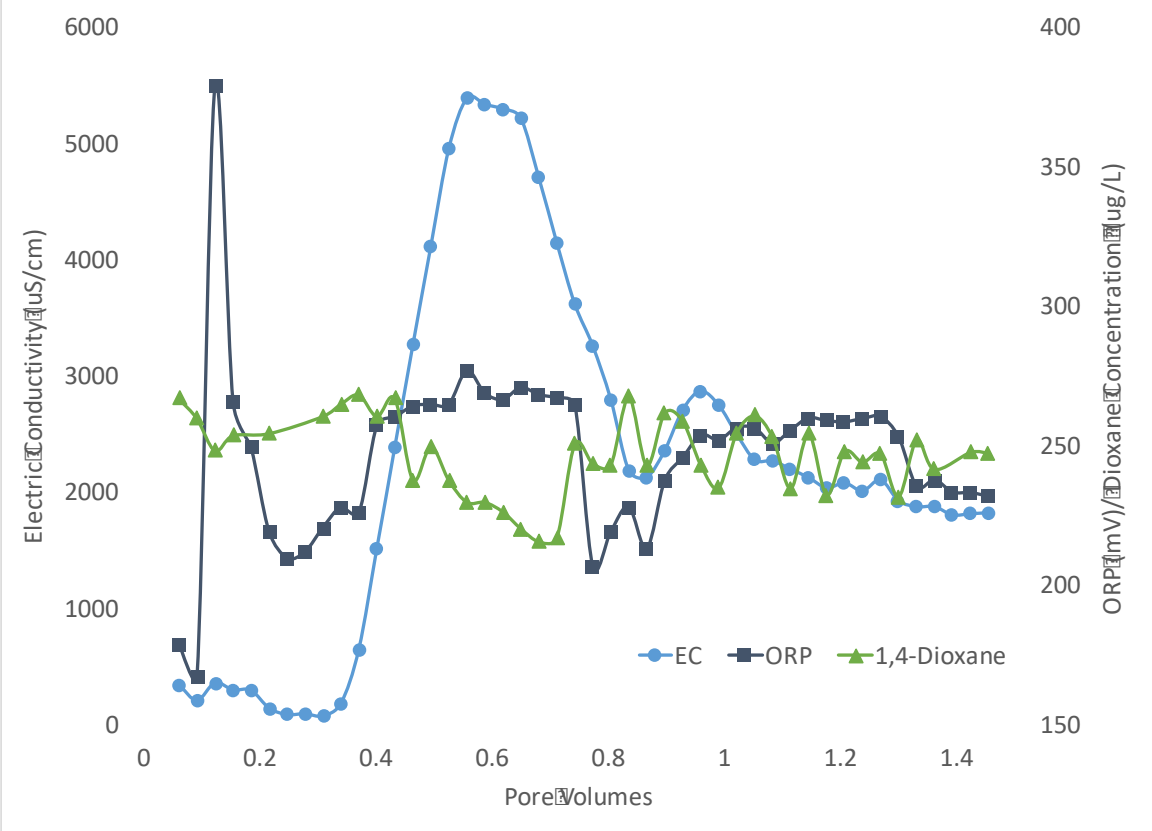

Figure 4.8.4**.** Results from Scenario I Test I experiments, ORP, EC, and 1,4-dioxane concentration.

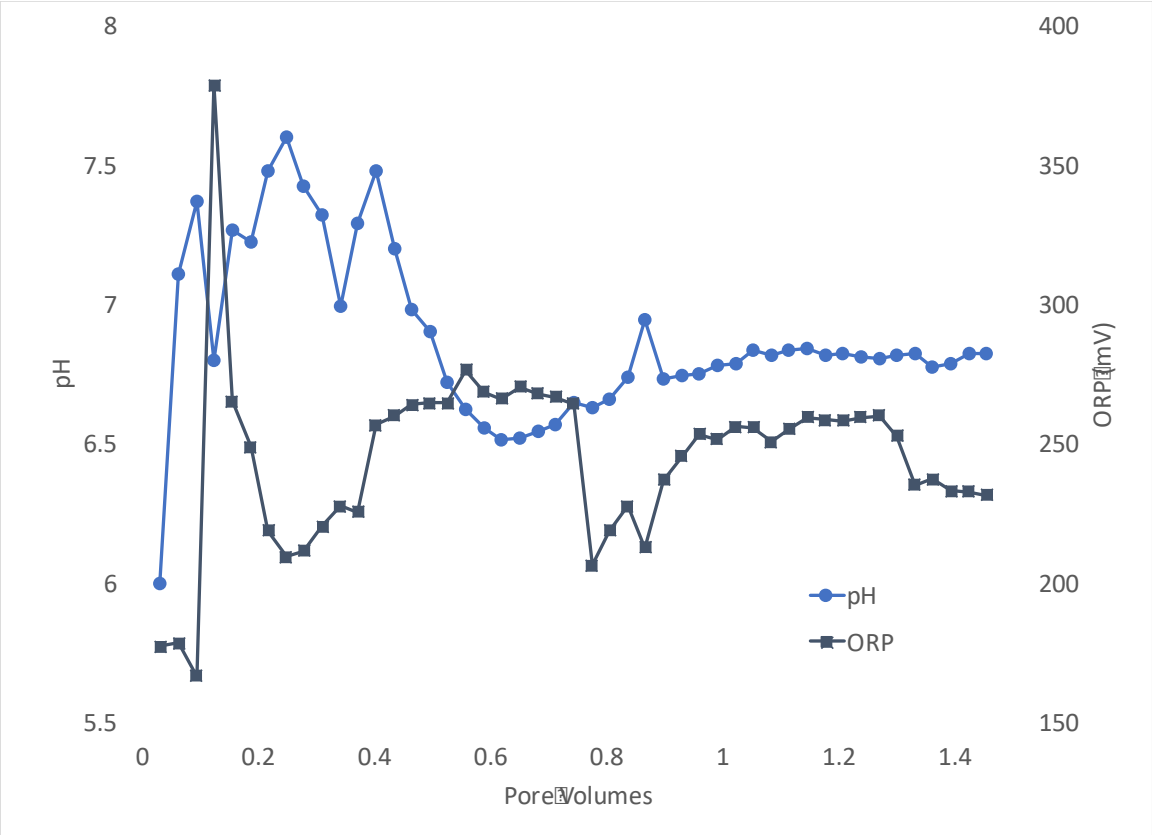

Figure 4.8.5**.** Results from Scenario I Test I experiments, pH and ORP.

Based on the 1,4-dioxane concentration data during the breakthrough of the first pulse of oxidant solution (pore volumes 0.4 to 0.7), the 1,4-dioxane degradation rate constant was k= 0.08 h^{-1} (Figure 4.8.6). The breakthrough of the second pulse had no distinct effect on the 1,4-dioxane concentration and therefore no rate was calculated from this data set.

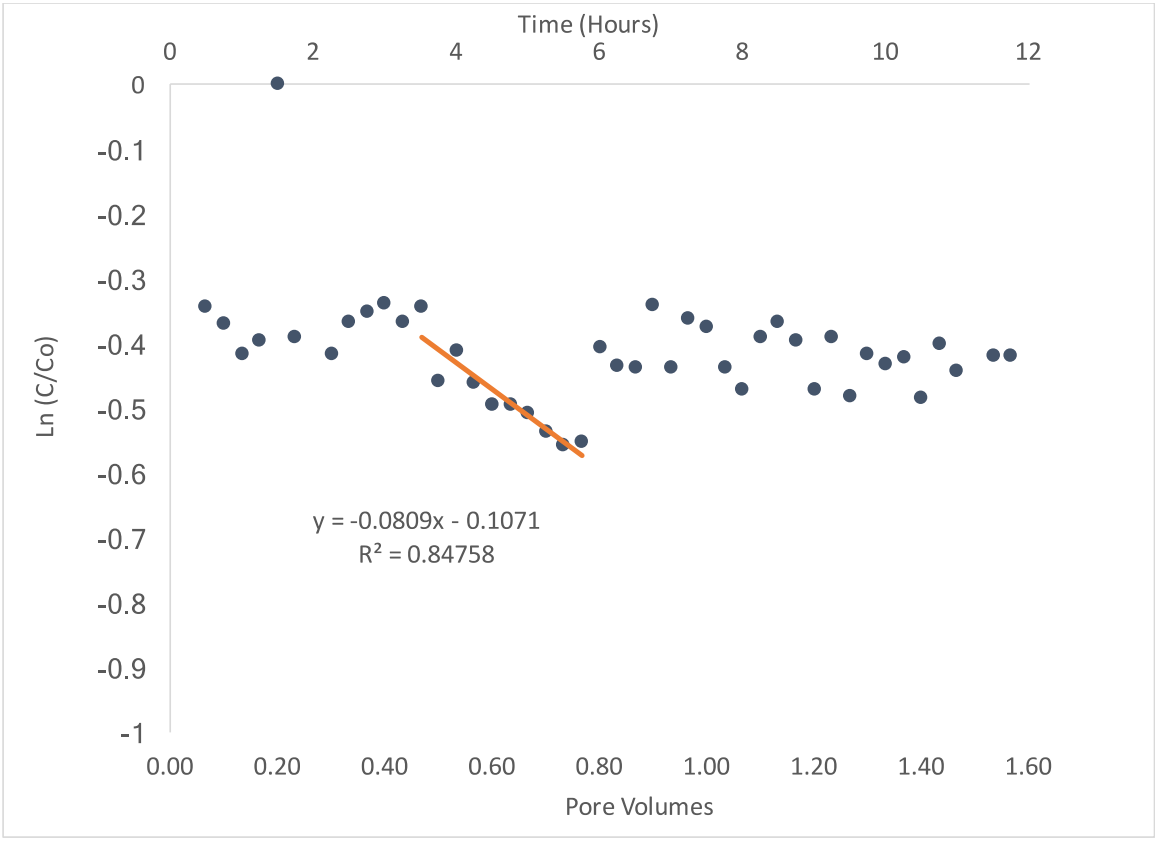

Figure 4.8.6**.** Scenario I, Test 1: The 1,4-dioxane degradation rate constant was calculated as k= 0.0809 h^{-1}.

During the second trial of scenario I (Test II), experimental conditions were identical to Test I with the exception that the oxidant injection time was twice as long (50 min). The experiment continued for 16 hours, or about 2 pore volumes. As for Test I, the pH falls from initially 7.0 to between 6.0 and 6.5 while the ORP rises from less than 240 to maximal 443 mV (Figure 4.8.7). Interestingly, also as before, there is a distinct anomaly shortly after oxidant injection, i.e. pore volume 0.2, where pH sharply drops to <5.0 and ORP sharply rises to 475 mV. Both variables then return to near-base values.

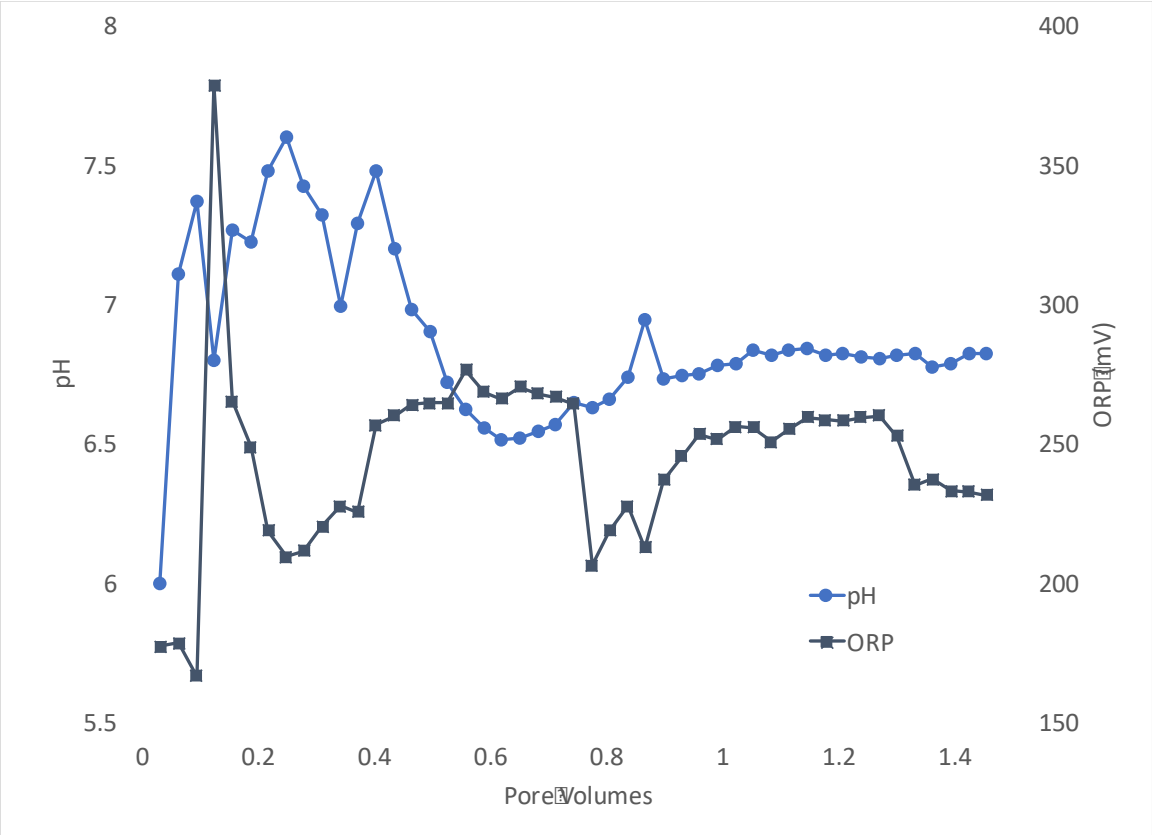

Figure 4.8.7. Results from Scenario I Test II experiments, pH and ORP.

Figure 4.8.8 shows the 1,4-dioxane column effluent concentrations, which, for comparison, was plotted against ORP and EC. The EC peaks at 0.58 PV and 0.96 PV at respective values of 2990 µS/cm and 5230 µS/cm. These peaks clearly reflect the breakthrough of two pulses. The EC peak value of the second pulse, breaking through at a later time, is about twice as high as the earlier peak, suggesting that some overlap of the two pulses has occurred. Even at the end of the experiment, i.e. after 2 PV, the EC did not return to the initial 0.3 µS/cm. A similar behavior was observed for the ORP data, which remained high even after the oxidant should have completely left the column system if behaving as a conservative solute. This indicates that some of the oxidant remained behind in the column, only slowly leaching out. This assessment is corroborated by the M_0 results, which shows an oxidant mass recovery of 10.26 g, or 76%.

It is noted that the breakthrough of the second oxidant pulse did not result in much higher ORP readings, i.e. unlike EC, the ORP is not additive in case pulses overlap. The 1,4-dioxane concentration decreased from 302 µg/L to 188 µg/L, (C/Co=0.62), when ORP and EC were at their respective maximum values at about 1 PV. Even after 1,4-dioxane concentration rose again afterwards, it never reached the influent concentration and remained below 250 µg/L for the remainder of the experiment. The apparent continued contaminant destruction during the later stages of the experiment correlates with the continued presence of oxidant in the column, as indicated by the still elevated EC readings at the end of the experiment. This observation is similar to that made during Test 1.

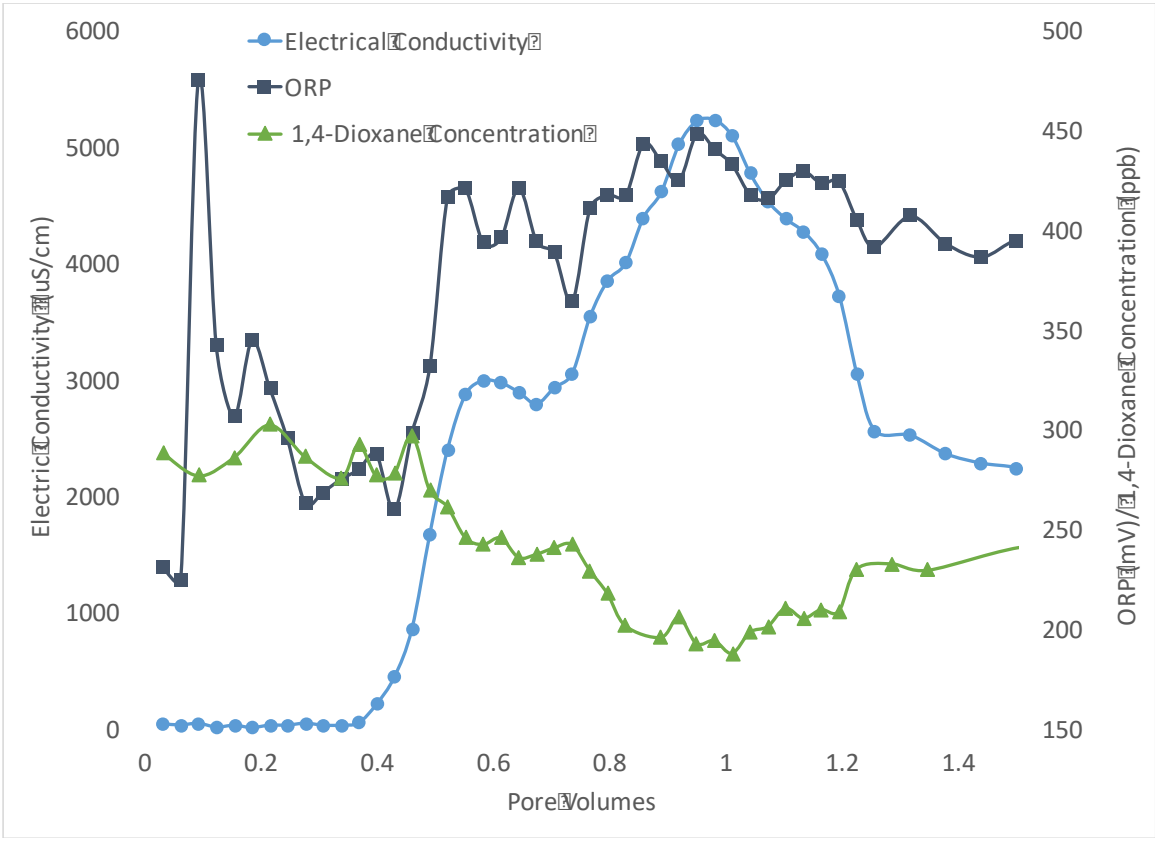

Figure 4.8.8**.** Results from Scenario I Test II: Electric conductivity and ORP readings with 1,4-dioxane concentrations.

The 1,4-dioxane degradation rate constants were calculated for the breakthrough of the first and second pulse (Figure 4.8.9). The rate constants were similar with the breakthrough of the second pulse having a rate constant that was only slightly higher (0.243 h^{-1}) than the first one (0.2 h^{-1}).

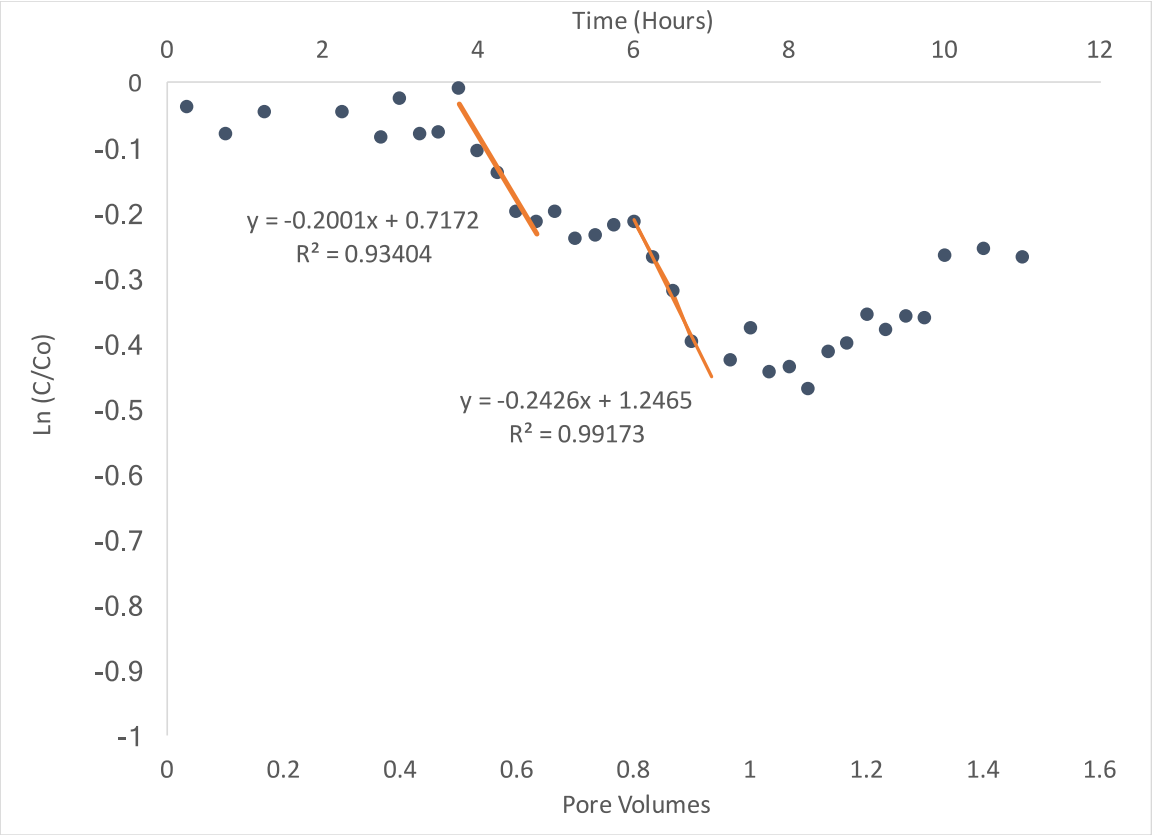

Figure 4.8.9**.** Results from Scenario I Test II: Pseudo first order reaction rate constants calculated from the breakthrough data of the first and second pulses.

4.8.2.2 Treatment Scenario II – Single pulse injection

The second treatment scenario simulated the injection of one pulse of OxyZone® directly into the base of the column. The duration of the experiment was 2.4 PV (approximately 20 hours). The same overall volume (200 mL) of oxidant solution was injected as in the Treatment Scenario I test. Figure 4.8.10 compares breakthrough curves for OxyZone® and sodium chloride.

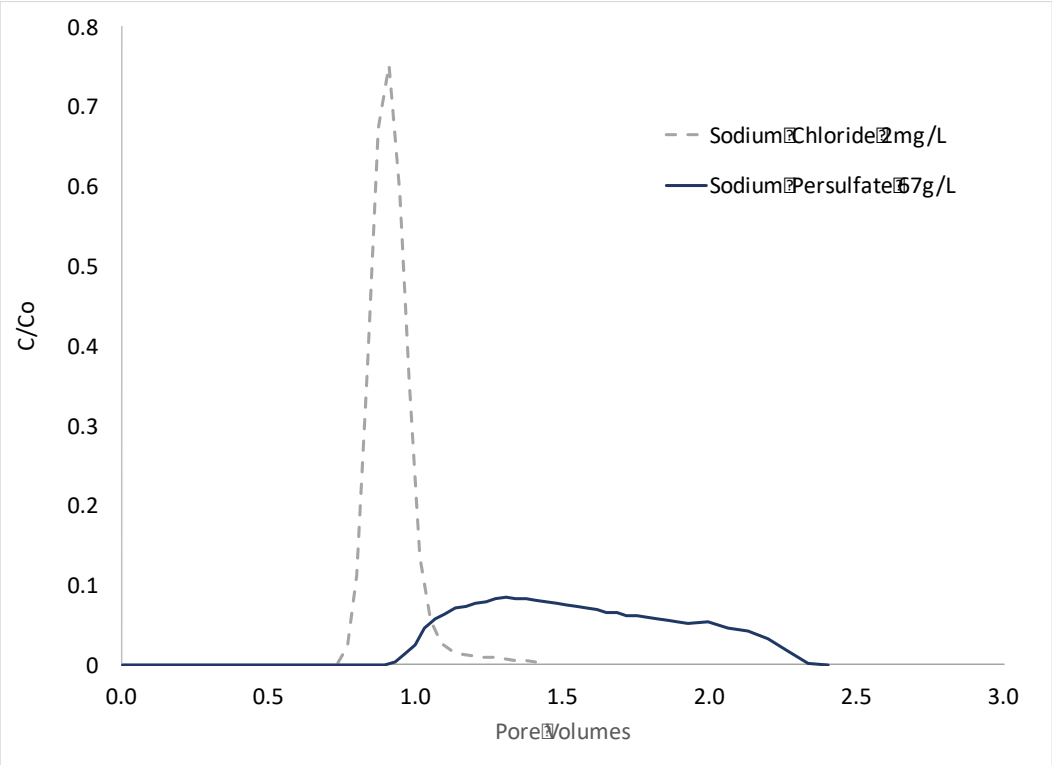

Figure 4.8.10. Treatment Scenario II – Single pulse injection: Comparison between breakthrough curves for OxyZone® and sodium chloride tracer.

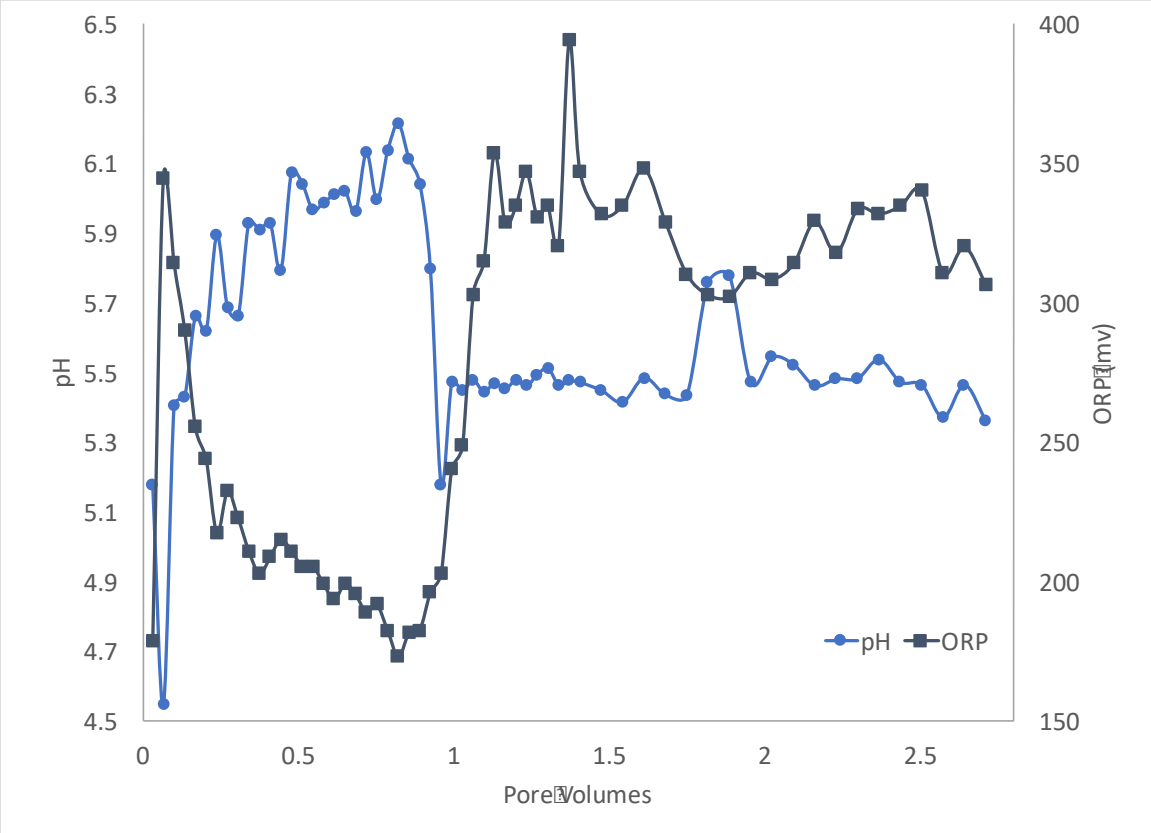

Figure 4.8.11. Results from Scenario II: ORP and pH of pulse flow oxidation.

Figure 4.8.12 shows the 1,4-dioxane concentrations, plotted for comparison against ORP, and EC data. The initial 1,4-dioxane concentration was 287 µg/L. At 1 PV, the concentration dropped to <10 µg/L and decreased to below the limit of detection (3 µg/L) by 1.9 PV. The concentration of 1,4-dioxane remained low until the end of the experiment (2.8 PV). This prolonged oxidation is mirrored in the ORP and EC data. This test was concluded when ORP and EC fell back to baseline levels, which was at the 3 PV mark. At that time, the 1,4-dioxane concentration was still more than 80% lower than the corresponding column influent concentration. Finally, unlike Scenario I experiments, no sharp changes were observed in ORP and pH during the earliest stages of the experiment (Figure 4.8.11).

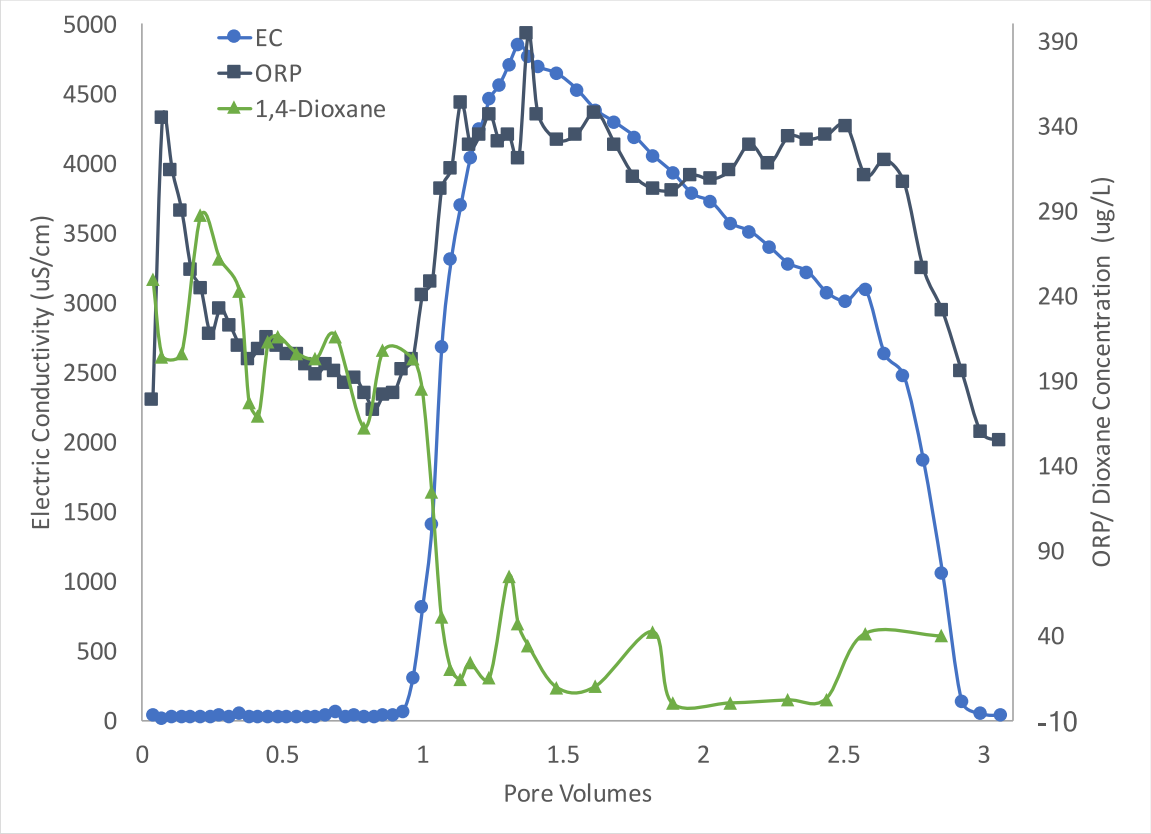

Figure 4.8.12**.** Results from scenario II: 1,4-dioxane concentration. The EC and ORP data were included for comparison.

A linear trend line was fitted through leading edge of the 1,4-dioxane breakthrough curve (Figure 4.8.13). The oxidation rate for this experiment was the highest of any of the experiments, with a rate constant of 1.5389 h^{-1}. The pseudo-first order reaction rate constants for all tests are summarized in Table 4.8.2.

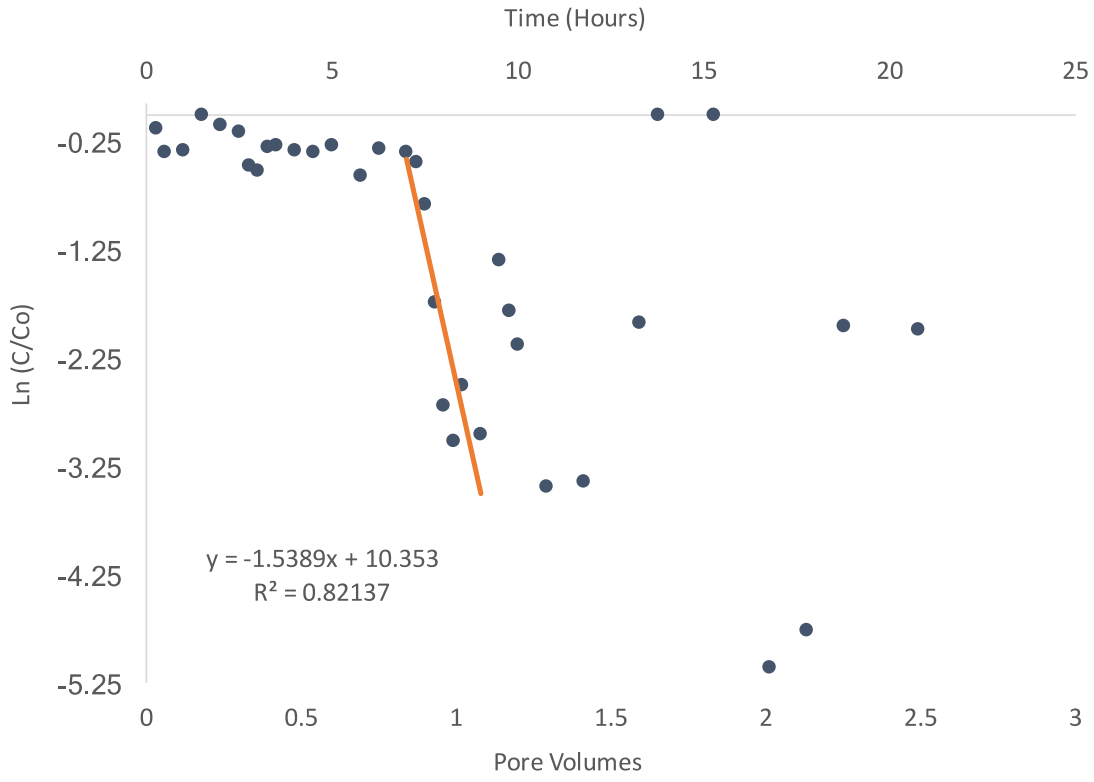

Figure 4.8.13**.** Results from Scenario II: Ln(C/Co) for pseudo-first order reaction rate constant.

Table 4.8.2**.** Reaction rate constants for all column experiments. Note that Test 2a and 2b refer to the reactions rates extrapolated from the first and second pulse breakthrough.

	Scenario I – Test 1	Scenario I – Test 2a	Scenario I – Test 2b	Scenario II
k_1 (h^{-1})	0.081	0.20	0.24	1.54
$T_{1/2}$ (h)	8.57	5.97	6.99	0.45
R^2	0.85	0.83	0.83	0.82

4.8.3 Discussion

The principal objective of this study was to investigate the degradation of 1,4-dioxane by an oxidant (OxyZone®) under dynamic, flow through conditions that mimic the *in situ* treatment of groundwater plumes. Initial batch experiments were conducted to determine 1,4-dioxane degradation rates in the presence of porous material under static conditions. The reaction rates of 1,4-dioxane oxidation with OxyZone® in the presence of sediment were determined.

At an oxidant: contaminant ratio 250:1 and in the presence of porous material, the pseudo-first order rate constant was 0.021 h^{-1} with a half-life of 33 hours. The observed rate was approximately 2.5 times lower than compared to Eberle et al. (Eberle et al., 2016), who investigated rates in the absence of porous material. This finding implies that the degradation of 1,4-dioxane by OxyZone® proceeds more slowly when injected into a porous matrix relative to

treating aqueous phase contamination, as one might be required when treating extracted groundwater *ex-situ*.

At real-world contaminated sites, 1,4-dioxane is predominantly present in a dissolved state, forming elongated plumes of contaminated water. Hence, *in situ* treatment would likely require the injection of a solution containing a reactive agent, such as OzyZone. On this backdrop, two different oxidant injection schemes were tested (*Scenarios I and II*).

The column's basic flow properties were first investigated with a conservative tracer test. The normal distribution of the tracer breakthrough curve indicated that flow field is homogenous and not likely influenced by preferential pathways (Figure 4.8.3).

4.8.3.1 Scenario I Experiments

The greatest decline in 1,4-dioxane concentration was observed during Scenario I – Test II, when column effluent concentration dropped to C/Co=0.62 during the time when mixed with oxidant solution. Even after 1,4-dioxane concentration rose again to about C/Co=0.82, after most of the oxidant had already washed out of the column, it never reached the influent concentration for the remainder of the experiment. This suggests that the remaining oxidant fraction continued to destroy the dissolved contaminant past the time expected for a solute traveling at the speed of groundwater. The reason for the apparent retardation of the persulfate was not further investigated, but it is beneficial for the *in situ* treatment and prolonged oxidation time.

The Scenario I column experiments also demonstrated that it is more advantageous to slowly inject the oxidant solution into the contaminated flow field. That is, quick injection concentrates the pulse within a relatively small fraction of the porous space and therefore exposes the reactive agent to only a small fraction of dissolved contaminant. Although the moment analysis suggests that the injectate is subject to retardation and tailing (Figure 4.8.10), i.e. the oxidant is traveling slower than the plume, the absolute difference in travel time in this column system is not large enough to cause major mixing with 1,4-dioxane present in pores not filled with the oxidant. This was indicated by similar arrival times of the EC peaks relative to that of a conservative solute. Hence, contaminant destruction is confined to a limited fraction of the pore space. However, when injected slowly, the oxidant solution is mixed into a larger fraction of pore space, resulting in more contaminant destruction. This is expressed in the prolong period of much lower 1,4-dioxane concentration in the column effluent during Scenario I – Test II relative to Test 1.

The Scenario I test also demonstrated that the pH decline correlates with a rise in ORP (Figure 4.8.4 and Figure 4.8.7). This result was expected because as the oxidant advances (indicated by the rising ORP), sulfate (SO_4^{2-}) is produced. Sulfate is a weak conjugate base, which leads to the production of sulfuric acid (Kolthoff and Miller, 1951). The formation of sulfuric acid is partially encountered by the phosphate buffer, which is part of the OxyZone® formulation. However, sufficient acid is produced to lower the pH to less than 6.5. In general, the pH value during persulfate treatment is a function of the solution's buffering capacity and the oxidant dosage.

Unlike EC readings, which have been found additive when two pulses overlap (Figure 4.8.5 and Figure 4.8.8), ORP readings were not much higher during the same period. In terms of

increasing the strength of the oxidant solution, this result indicates that there is no immediate benefit by overlapping pulses of similar strength. However, it should be possible to increase the ORP by injecting fresh oxidant solution into the porous medium where oxidant strength has dropped by either consumption or dilution.

Similar to prior research by Eberle et al. (Eberle et al., 2016), the degradation of 1,4-dioxane was modeled with pseudo-first order kinetics. The rate of degradation for Scenario I ranged from 0.088 h^{-1} to 0.116 h^{-1} at an oxidant: contaminant ratio of 250:1. For a system without porous media but at the same oxidant: contaminant ratio, Eberle et al. (Eberle et al., 2016) predicted a rate of k=0.2906 h^{-1}, which is 2.5 times greater than found in this study. This result underlines the importance of accounting for the porous material and its properties when planning for an injection of oxidant into a polluted aquifer.

4.8.3.2 Scenario II Experiments

In terms of degrading 1,4-dioxane, the injection of one pulse at the base of the column was the most successful treatment scenario, resulting in complete destruction of the contaminant over a prolonged period of time (Figure 4.8.12). The rate of destruction was larger than any other experiment (Table 4.8.2). In fact, the projected rate for 1,4-dioxane degradation with OxyZone® at 7,400:1 oxidant: contaminant ratio would be k=7.44 h^{-1} (Eberle et al., 2016). The projected rate reaction calculated in this study with the same oxidant: contaminant ratio is k=1.539 h^{-1}, which is 4.83 times slower than reported by Eberle et al. (Eberle et al., 2016). On the background of the mixing argument made when discussing the effectiveness of fast versus slow injection (Scenario I - Tests 1 and 2), it seems counterintuitive that the injection of one pulse should result in better contact with the contaminant in solution; however, the Scenario II experiment was different in two regards. First, the pulse was injected farthest away from the effluent and therefore traveled longer through the column than under Scenario I. This prolonged residence time in the column magnified the dispersion of the pulse, as indicated by the long spread of the breakthrough curve in relation to the conservative tracer (Figure 4.8.12). Dispersion and mixing provided better contact of the oxidant with 1,4-dioxane, hence greater treatment. Second, the pulse was injected more slowly, relative to Scenario I at the rate of 4 mL/minute. The slow injection distributed the pulse over a larger fraction of the column pore volume. Together, this injection scheme resulted in prolonged and faster treatment, as measured by the pseudo first order reaction rate.

Also, unlike Scenario I experiments, no sharp changes were observed in ORP and pH during the earliest stages of the experiment. This finding suggests that the anomalies during Scenario I are most likely caused by the act of injecting oxidant solution directly into the column, rather than the column inlet. Although not further investigated, it must be assumed that the hydraulic pressure from quickly injecting oxidant solution into a saturated confined column momentarily disturbed the flow system and possibly pushed a small, but noticeable amount of oxidant solution deeper into the column. This would explain why the observed anomaly occurs well before the expected breakthrough of the bulk oxidant.

Although identical volumes were used in both tests (0.1 PV each), the conservative tracer resulted in a sharp peak, while the OxyZone® breakthrough was drawn out. This is partially due to the time it took for injecting the NaCl pulse (33 min) versus 45 min for the OxyZone®. The

recovered mass of OxyZone® (M^0) was 76.67% while the center of mass (M^1) was located at 1.5 PV. Also, the OxyZone® displayed a right-skewed distribution, which suggest significant tailing of solute.

A hypothesis was tested to determine if the density of OxyZone® was responsible for the drawn out breakthrough curves seen during column scale tests. A second sodium chloride tracer test was conducted, but with a concentration of 67 g/L NaCl and a density of approximately 1.05 g/cm^3 (Supplementary Data). This density was chosen to mimic the density of OxyZone®. The data showed that the movement of OxyZone® through porous media is partially density driven, i.e. the shape of the breakthrough curve was similar to the Oxyzone one and distinctively different from the low concentration NaCl tracer test (Concentration NaCL = 2 g/L; Density = 1.0). The density driven advection slowed down the movement of the OxyZone® in the column system and prolonged the contact time with the 1,4-dioxane contaminant, increasing its destruction.

4.9 1,4-Dioxane Treatment Using Persulfate Activated By Iron Filings Results and Discussion

4.9.1 Batch Experiments

The surface chemistry of the iron filings was analyzed with SEM-EDS and XRD, and the results are presented in Supplementary Data. O, Fe, and C are the three major elements on the surface of the iron filings. Oxygen was introduced as the iron filings were oxidized by O_2 in the air. Carbon is a common element in the source steel. Low levels of silicon were identified, which is attributed to dust introduced during collection and transportation of the iron filings. A small quantity of manganese was also observed, likely due to its use as an additive for alloy steels. XRD results showed that magnetite with chemical formula of Fe_3O_4 is the major form of oxidized iron on the surface of the iron filings.

The results of the 1,4-dioxane degradation batch experiments conducted in the absence of iron filings are presented in Figure 4.9.1. 1,4-Dioxane loss for the control, due to volatilization, photochemical decomposition, or other processes, is minimal. This is consistent with the fact that 1,4-dioxane has low vapor pressure at room temperature (~4.0 Kpa at 20°C; (Verschueren, 1985)) and is chemically stable under ambient conditions. In contrast, 1,4-dioxane underwent significant degradation in the presence of persulfate (no iron filings) with an approximately 70% loss in the first 300 h. As the reaction proceeded, sulfate was detected and the concentration increased over time. The combined concentration of sulfate and persulfate was close to the initial persulfate concentration during the entire experiment, showing complete mass balance for sulfur and indicating that sulfate was the only measurable product of persulfate decomposition.

The reaction is assumed to follow first order kinetics given that the oxidant is present in great excess (molar ratio of oxidant to 1,4-dioxane is 10:1). First-order reaction rate constants for 1,4-dioxane and persulfate decomposition were calculated to be 0.006 h^{-1} (Table 4.9.2) and 0.00033 h^{-1} (Supplementary Data), respectively. By the end of the reaction, the molar decomposition ratio is calculated to be 0.5:1 (1,4-dioxane:persulfate) (Figure 4.9.1), indicating high efficiency for persulfate degradation of 1,4-dioxane. In contrast, degradation of 1,4-dioxane was minimal when H_2O_2 was used as the oxidant, with a first-order reaction rate constant of

0.0003 h^{-1} (Table 4.9.2). Approximately 35% of H_2O_2 was lost from solution after 300 h (Supplementary Data). This result shows that H_2O_2 is less efficient for 1,4-dioxane degradation and has lower stability than persulfate.

Table 4.9.1. Compounds and elements on the surface of the iron filings based on XRD and SEM-EDS tests.

Chemical name or formula	Mole Quantity (%)
Elements identified with SEM-EDS	
Oxygen (O)	61.97±0.28
Iron (Fe)	26.72±0.10
Carbon (C)	9.29±0.14
Silicon (Si)	1.06±0.02
Manganese (Mn)	0.37±0.04
Copper (Cu)	0.24±0.03
Sulfur (S)	0.12±0.01
Aluminum (Al)	0.09±0.01
Chromium (Cr)	0.09±0.01
Calcium (Ca)	0.05±0.01
Compounds identified with XRD	
Iron diiron (III) oxide, Magnetite (Fe_3O_4)	50
Iron titanium oxide ($Fe_{1.696}Ti_{0.228}O_3$)	26
Magnesium diiron (III) oxide ($MgFe_2O_4$)	17
Iron manganese (IV) oxide ($FeMnO_3$)	7

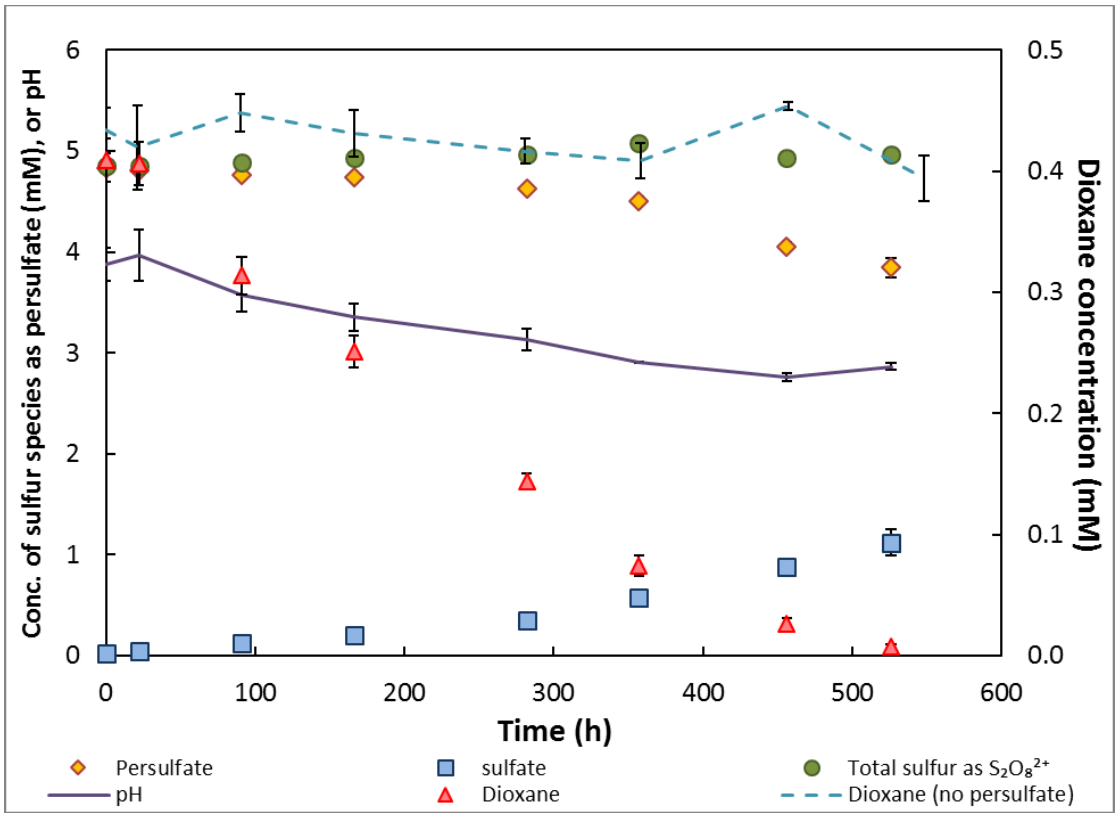

Figure 4.9.1. Degradation of 1,4-dioxane by persulfate in the absence of iron filings in batch reactor system. Error bars show mean ± standard deviation (range may be smaller than the symbol).

Table 4.9.2. Pseudo-first-order reaction rate constant k and half-life $t_{1/2}$ for 1,4-dioxane degradation in batch experiments.

Reactants	Rate constant k (h^{-1})	Half-life $t_{1/2}$ (h)
Dioxane only	0.00008	8664
Dioxane + H_2O_2	0.00029	2390
Dioxane + Fe filings	0.0014	495
Dioxane + persulfate	0.0060	116
Dioxane + persulfate + Fe filings[a]	0.016	43

[a] calculation is based on the data for the second reaction stage ($t \geq 0.5$ h, proposed surface reaction)

The results of the 1,4-dioxane degradation experiments conducted with the addition of iron filings are presented in Figure 4.9.2. There was approximately 10% loss of 1,4-dioxane in the absence of persulfate (Figure 4.9.a). This is in contrast to the no measurable loss observed for the control with no iron filings added. These contrasting results indicate that the iron filings apparently produced a small degree of 1,4-dioxane degradation. 1,4-Dioxane degradation in open aqueous

systems in the presence of micron- (~44 µm) or nano-sized (~1 µm) particles of ZVI has been reported (Shin et al., 2012; Son et al., 2009). Such degradation was caused by dissolved oxygen oxidation catalyzed by the ZVI. The pseudo-first-order reaction rate constants, *k*, vary from 0.03 to 0.18 h^{-1}, depending on the experimental setup, particle size, and solid-liquid ratio. The *k* for 1,4-dioxane degradation with iron filings in this study is 0.0014 h^{-1} (Table 4.9.2). The significantly smaller value determined for our experiments is to be expected given the significantly greater reactive surface areas associated with the micron- or nano-ZVI compared to the iron-filing particles used herein.

1,4-Dioxane concentrations decreased rapidly in the presence of combined persulfate and iron filings, and approximately 70% of the 1,4-dioxane was removed within 50 h (Figure 4.9.2a). 1,4-Dioxane degradation was significantly faster in the presence of iron filings, wherein 70% reduction in 1,4-dioxane required 300 hours in the absence of iron filings. 1,4-Dioxane degradation exhibited a two-stage reaction pattern in the presence of iron filings. An extremely high reaction rate was observed in the first 0.5 h of contact, with 30% of 1,4-dioxane removed. After 0.5 h, degradation of 1,4-dioxane slowed and followed first-order kinetics with a *k* of 0.016 h^{-1} (Table 4.9.2 and Supplementary Data). Approximately 85% of the persulfate was lost from bulk solution within the first 0.5 h, resulting in production of a substantial amount of sulfate. This rapid loss of persulfate and concomitant production of sulfate contrasts greatly with the results observed for the experiment conducted without the iron filings (Figure 4.9.1). The results for 1,4-dioxane, persulfate, and sulfate all demonstrate that the iron filings produced rapid activation of persulfate.

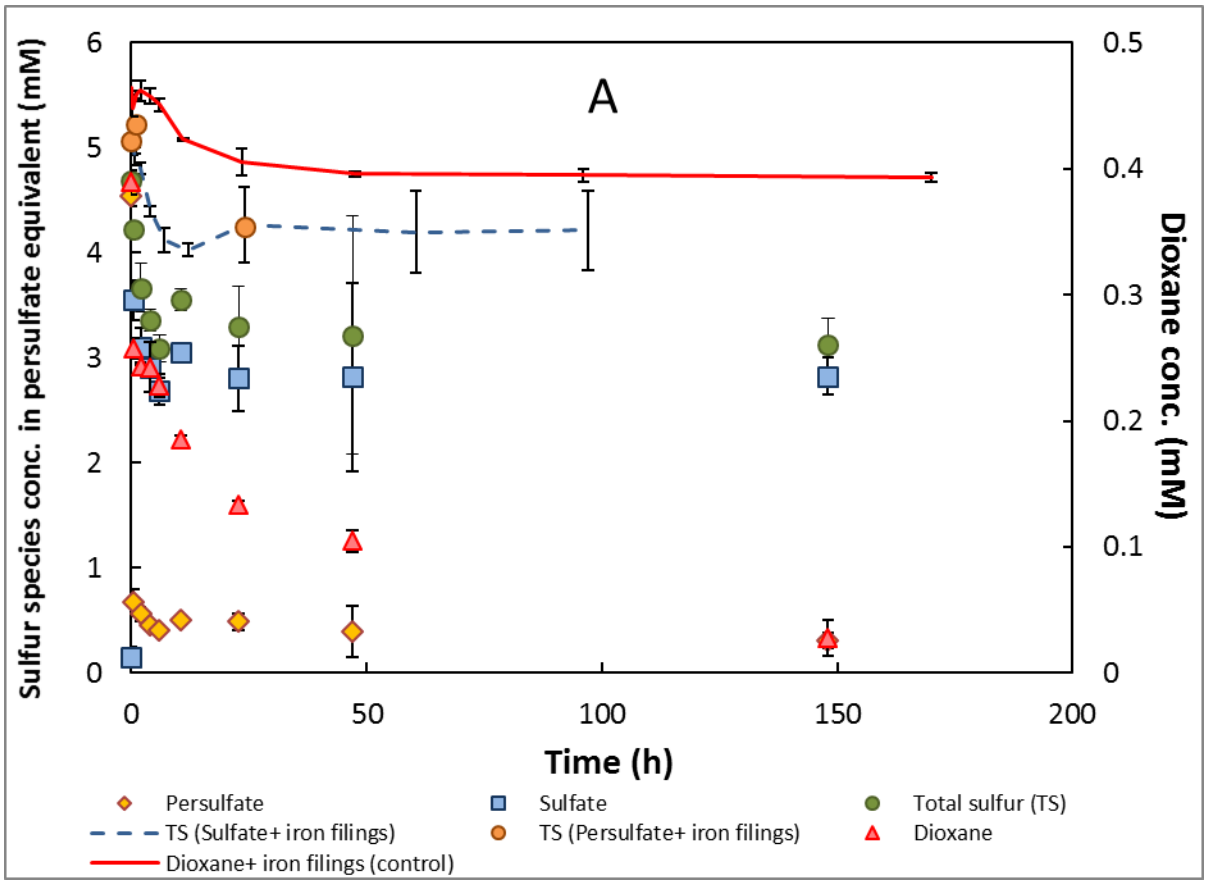

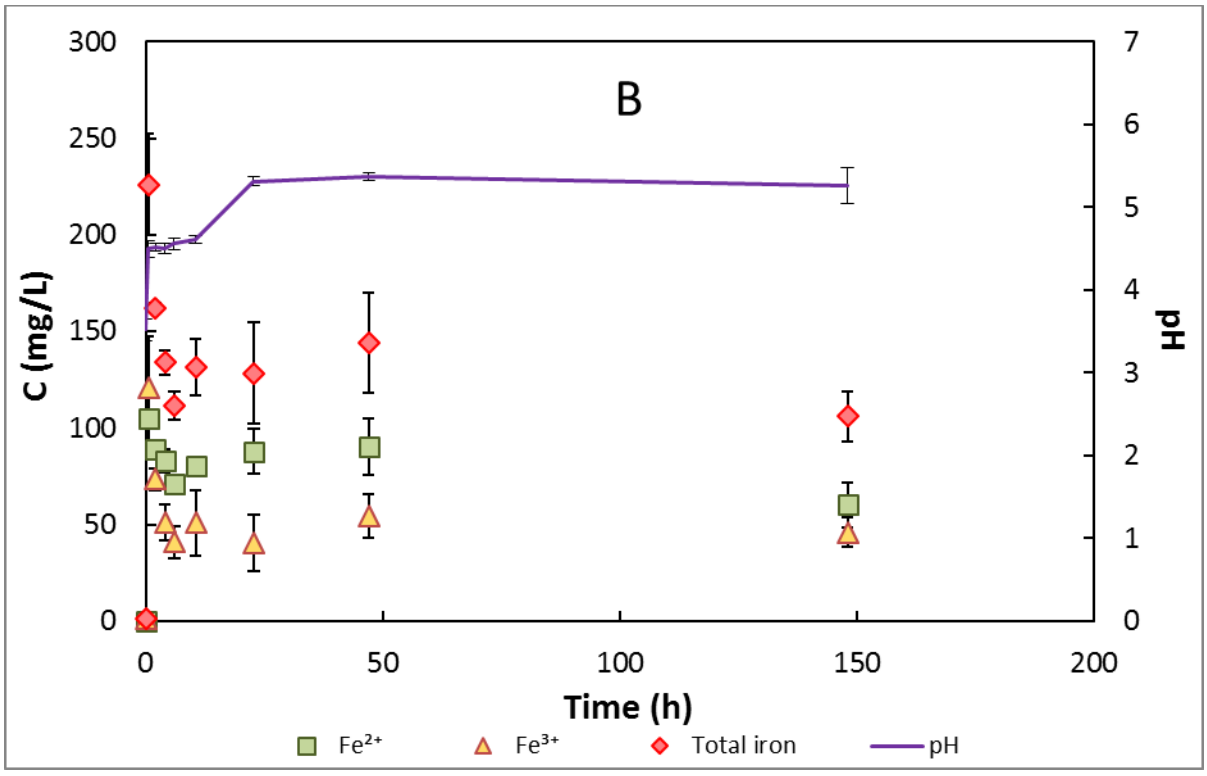

Figure 4.9.2. Degradation of 1,4-dioxane in the presence of iron filings in batch reactor system. Controls of persulfate + iron filings, sulfate + iron filings, and 1,4-dioxane + iron filings are also included. (A) Concentration of sulfur species and 1,4-dioxane versus time. (B) Concentration of iron species and pH versus time.

The concentration of total sulfur in bulk solution decreased after the reaction was initiated, and there was a loss of approximately 30% in total sulfur by the end of the experiment. Recall that there was no measurable loss of total sulfur for the experiment conducted with no iron filings present. Loss of sulfur from solution was also observed for the control tests wherein iron filings were added to sulfate (10 mM) or persulfate (5 mM) solutions with no 1,4-dioxane present (Figure 4.9.2a). It is hypothesized that the sulfur loss observed for the iron-filings experiments is related to transfer of sulfur from bulk solution to the iron filings surface.

Enrichment of sulfur on the surface of the iron filings was observed with SEM-EDS after 1-h contact between iron filings and persulfate solution (Figure 4.9.3a and Figure 4.9.3b). This sulfur species existed in a form that could not be removed by repeated flushing with deionized water, showing that it was bound in some manner to the iron filing surface. Consistent with the SEM-EDS observations, the XRD analysis indicated the presence of minerals in the form of $Fe_2(SO_4)_3$ and $FeSO_4$ on the iron filing surface after 1-h contact with persulfate. Enrichment of sulfur on the solid surface was not observed for the original iron filing sample or the control sample shaken with water for 24 h. In addition, after 24-h contact, the sulfur species associated with the iron filing surface observed for the 1-hr sample disappeared, which was accompanied with a decrease in the relative abundance of Fe (Figure 4.9.3b).

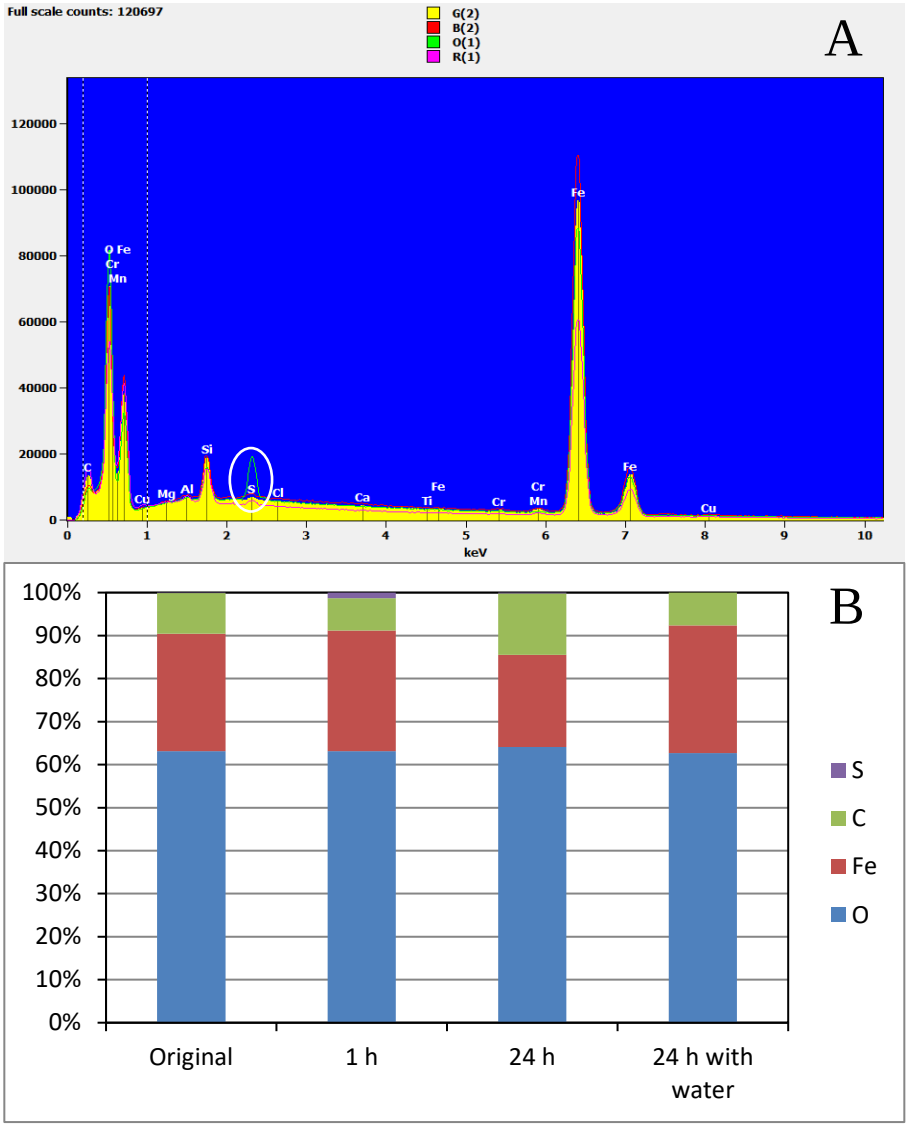

Figure 4.9.3. Elements and their relative abundance on iron filing surface for activation of persulfate. (A) SEM-EDS spectra of the iron filing surface. G(2), original iron filings; O(1), after 1 h reaction; R(1), after 24 h reaction; B(2), after 24 h mixing with water. (B) Relative abundance of the four major elements on iron filing surface.

Solution pH increased for the batch experiment, which is expected due to consumption of persulfate, the source of H^+, in the presence of iron filings. Large amounts of both ferrous and ferric iron were released to the aqueous phase as a result of reaction between persulfate and iron filing surface (Figure 4.9.2b). The metals and their concentrations in bulk solution measured by ICP-MS are presented in Supplementary Data. Release of Fe was also observed by ICP-MS and the concentration was close to the total Fe concentration measured spectrophotometrically. Soluble manganese with concentration higher than 5 mg/L was also detected. In contrast, contact of the iron filings with water (no persulfate) for 24 h had little impact on iron filing surface element composition and caused minimal release of metals (Supplementary Data).

4.9.2. Miscible-Displacement Experiments

Transport of persulfate in the column packed with sand was ideal, with no measurable retardation or mass loss (Supplementary Data). In contrast, persulfate exhibited retardation (breakthrough at approximately 3 pore volumes) and significant mass loss (~85%) during transport in the iron filings (Figure 4.9.4a). Sulfate production was observed, with breakthrough occurring at approximately 1 pore volume, much earlier than persulfate (Figure 4.9.4a). This is because transformation of persulfate to sulfate was quick and adsorption of sulfate by iron filings was minimal, as indicated by the results of the batch experiment (Figure 4.9.2a). An initial plateau in sulfate concentration was observed at approximately C/C_0 of 0.55. A subsequent rise in sulfate concentration occurred coincident with persulfate breakthrough. The pH of the effluent was approximately 5.5 at the time of persulfate injection, increased to 9.5 for two pore volumes, and then returned to the initial value coincident with persulfate breakthrough. Significant increases in both ferrous and ferric iron were also observed coincident with persulfate breakthrough. This release of Fe to the aqueous phase was not a result of the decrease in pH, given that Fe concentrations were lower than 1 mg/L in the effluent at the beginning of injection when the pH was also initially lower.

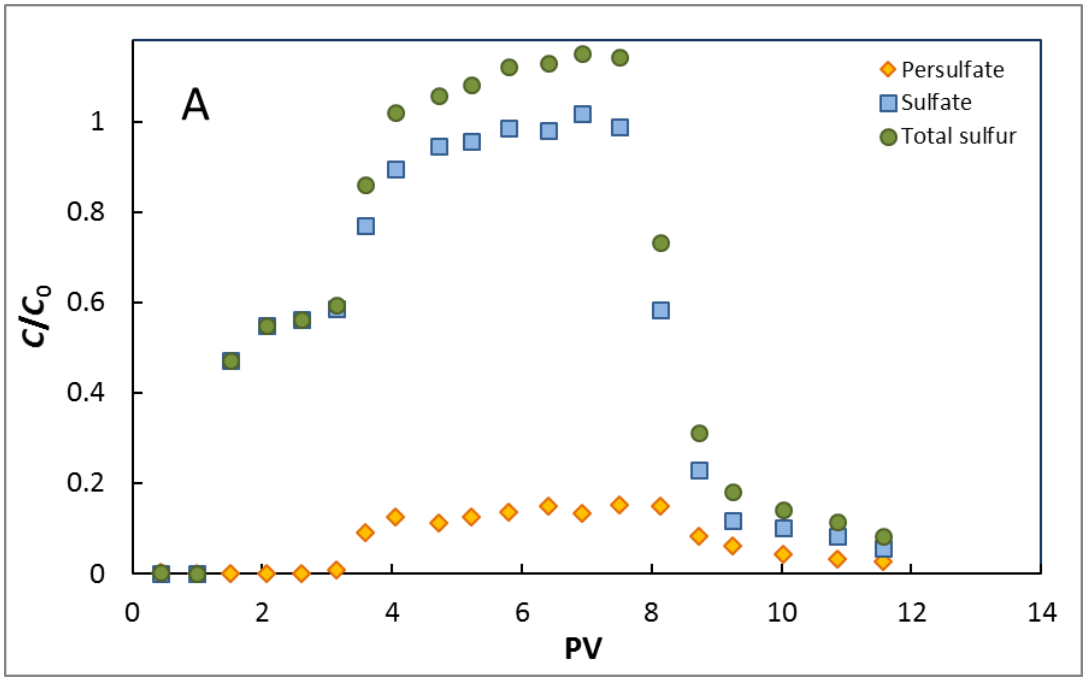

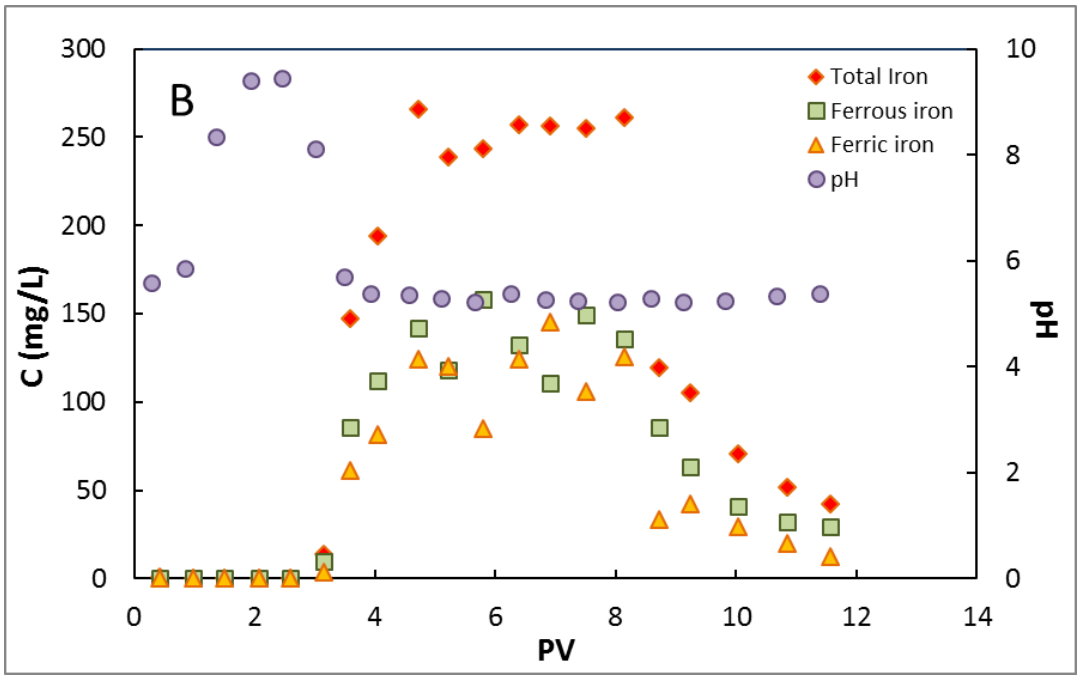

Figure 4.9.4. Breakthrough curves of persulfate in iron filing column and the related solution chemistry (no 1,4-dioxane present). Influent persulfate concentration is 5 mM. The pore-water velocity is 31 cm/h. (A) Breakthrough curves of persulfate, sulfate, and total sulfur. (B) Concentration of iron species and pH in the effluent.

1,4-Dioxane transport in the iron filing column was ideal in the absence of oxidants, with no retardation or mass loss (Supplementary Data). The observed no mass loss for this column experiment, for which the hydraulic residence time (t_r) was approximately 7 h, is consistent with the results of the batch experiment wherein no loss of 1,4-dioxane occurred within ~6 h after mixing with iron filings (Figure 4.9.2a). There was also minimal mass loss of 1,4-dioxane in the presence of persulfate for the experiment conducted at the pore-water velocity of 31 cm/h (t_r = 0.6 h) (Figure 4.9.5a). However, the transport behavior of the sulfur species was essentially identical to that observed for the experiment conducted without 1,4-dioxane (Figure 4.9.4a), indicating excellent reproducibility.

Approximately 10% of the 1,4-dioxane injected was degraded when the pore-water velocity was lowered to 3 cm/h (t_r = 6.7 h) (Figure 4.9.5a). Patterns of iron species production and pH change in the effluent (Figure 4.9.5b) were similar to the experiment conducted without 1,4-dioxane (Figure 4.9.4b). By assuming 1,4-dioxane degradation follows first-order kinetics, a reaction rate constant k of 0.018 h^{-1} is obtained for pore-water velocity of 3 cm/h by solving the first-order kinetics equation:

$$C = C_0 e^{-kt_r} \quad (21)$$

$$t_r = L/v \quad (22)$$

$$v = 4Q/(\pi D^2 n) \quad (23)$$

where C (mM) is the mean 1,4-dioxane concentration in the effluent at steady state, C_0 (mM) is the 1,4-dioxane concentration in the influent, L (cm) is the length of the iron filing bed, v (cm/h) is the mean pore-water velocity, Q is flow rate (mL/h), D is the inner diameter of the column (cm), and n

is porosity. The *k* determined from the column experiment is essentially identical to the *k* obtained for the second reaction stage of the batch experiment (0.016 h^{-1}).

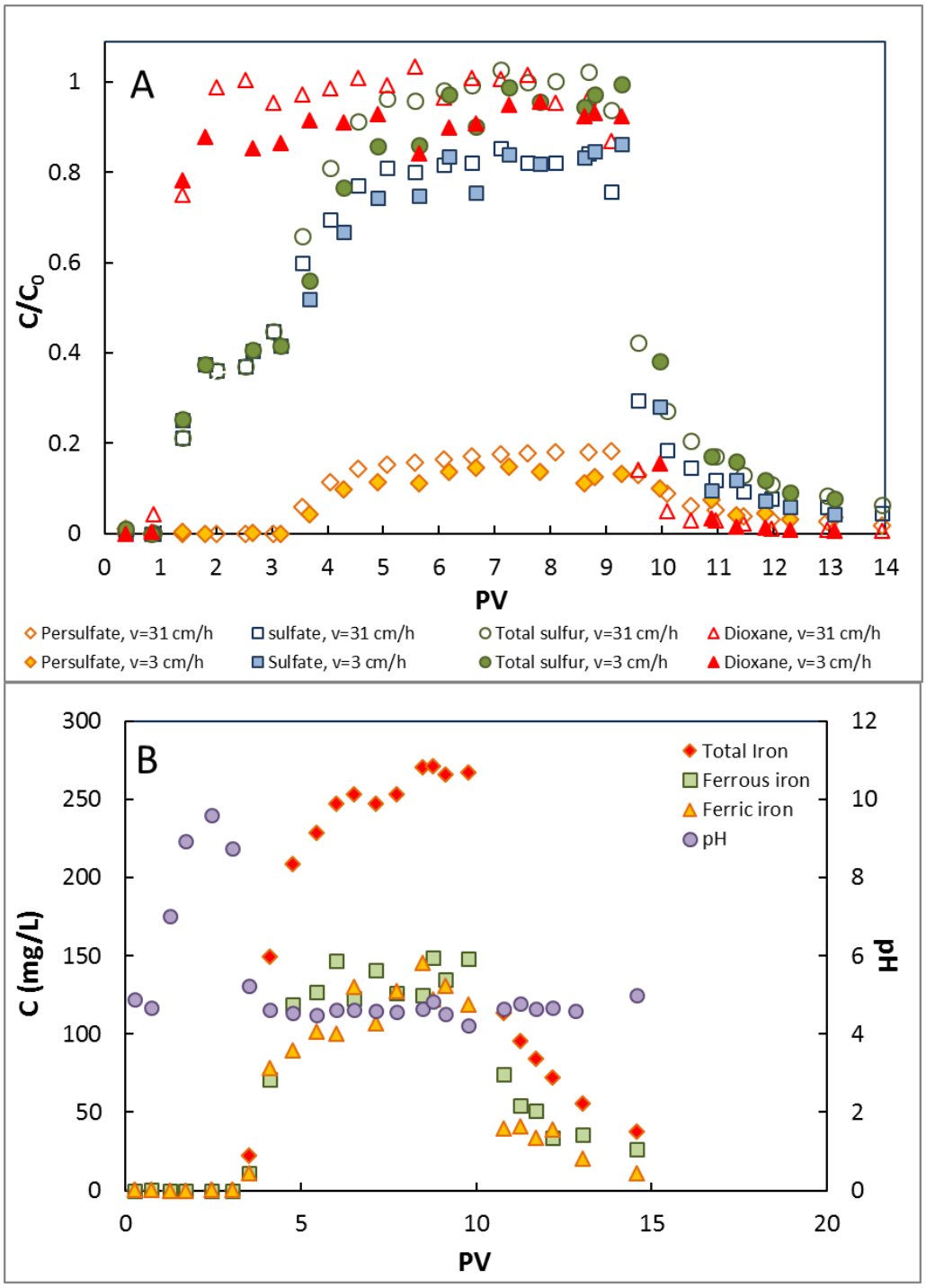

Figure 4.9.5. Degradation of 1,4-dioxane by persulfate in iron filing column and the related solution chemistry. Influent persulfate and 1,4-dioxane concentrations are 5 mM and 0.5 mM, respectively. (A) Breakthrough curves of persulfate, sulfate, total sulfur and 1,4-dioxane at pore-water velocities of 31 and 3 cm/h. (B) Concentration of iron species and pH in the effluent at the pore-water velocity of 3 cm/h.

When H_2O_2 was used in the column experiment, no breakthrough of H_2O_2 or degradation of 1,4-dioxane was observed for either pore-water velocity (Supplementary Data). Release of ferrous or ferric ion into the bulk aqueous phase was minimal compared to the case of persulfate (two order of magnitude lower), and also no significant variation of pH was observed (Supplementary Data). The results are consistent with the fact that H_2O_2 is not stable and readily self-decomposes. These results suggest that persulfate is superior to H_2O_2 for oxidative removal of 1,4-dioxane using iron-filing-based PRB.

4.9.3 Free Radical Analysis

The results obtained from the experiment conducted specifically to characterize free-radical formation are presented in Supplementary Data. Both DMPO-OH and DMPO-SO_4 signals were observed in the EPR spectrum measured for the persulfate solution, which shows the presence of both HO• and $SO_4^{\bullet -}$ radicals. This is consistent with prior observations (Fang et al., 2013b; Yan et al., 2015). The DMPO-SO_4 signal diminished quickly over time, accompanied by a slight increase in the DMPO-OH signal, due to conversion of DMPO-SO_4 adduct to DMPO-OH (Davies et al., 1992; Zalibera et al., 2009).

The persulfate-1,4-dioxane solution with iron filings present exhibited a much more complicated EPR spectrum than the others (Figure 4.9.6a). Radicals other than HO• and $SO_4^{\bullet -}$, such as a spin adduct with H (DMPO-H) and a carbon-centered radical (DMPO-R), were observed (Figure 4.9.6b). Such radicals could be intermediate radicals generated during decomposition of 1,4-dioxane. The signal of these radicals diminished over time and the DMPO-OH signal intensity also decreased, as shown by repetitive scanning on the same sample for 30 min (Figure 4.9.6b).

The above results demonstrate that significant quantities of radicals are generated immediately upon combining persulfate and the iron filings. The very fast rate of 1,4-dioxane degradation observed during the first 0.5 hour of the batch experiment is attributed to this surfeit of radicals in solution. However, the data presented in Figure 4.9.6b indicate that the concentration of radicals in solution decreases rapidly over 0.5 h. Additionally, EPR analysis of samples from the batch experiment shows that radical presence is minimal after 0.5 h (Supplementary Data). This is consistent with the fact that the persulfate concentration decreased by 85% within 0.5 h (Figure 4.9.2), which thereby significantly reduced the source of radicals. The continued, albeit slower, degradation of 1,4-dioxane in the absence of significant free-radical levels after 0.5 h indicates the existence of a second reaction process. This process is hypothesized to comprise a surface reaction mechanism. Such a mechanism is supported by the SEM-EDS and XRD results discussed above, which show a temporary accumulation of sulfur species on the iron filings surface. This mechanism is also hypothesized to be responsible for the retardation of persulfate, two-stage increase in sulfate concentration, and significant release of iron to the aqueous phase observed for the column experiments.

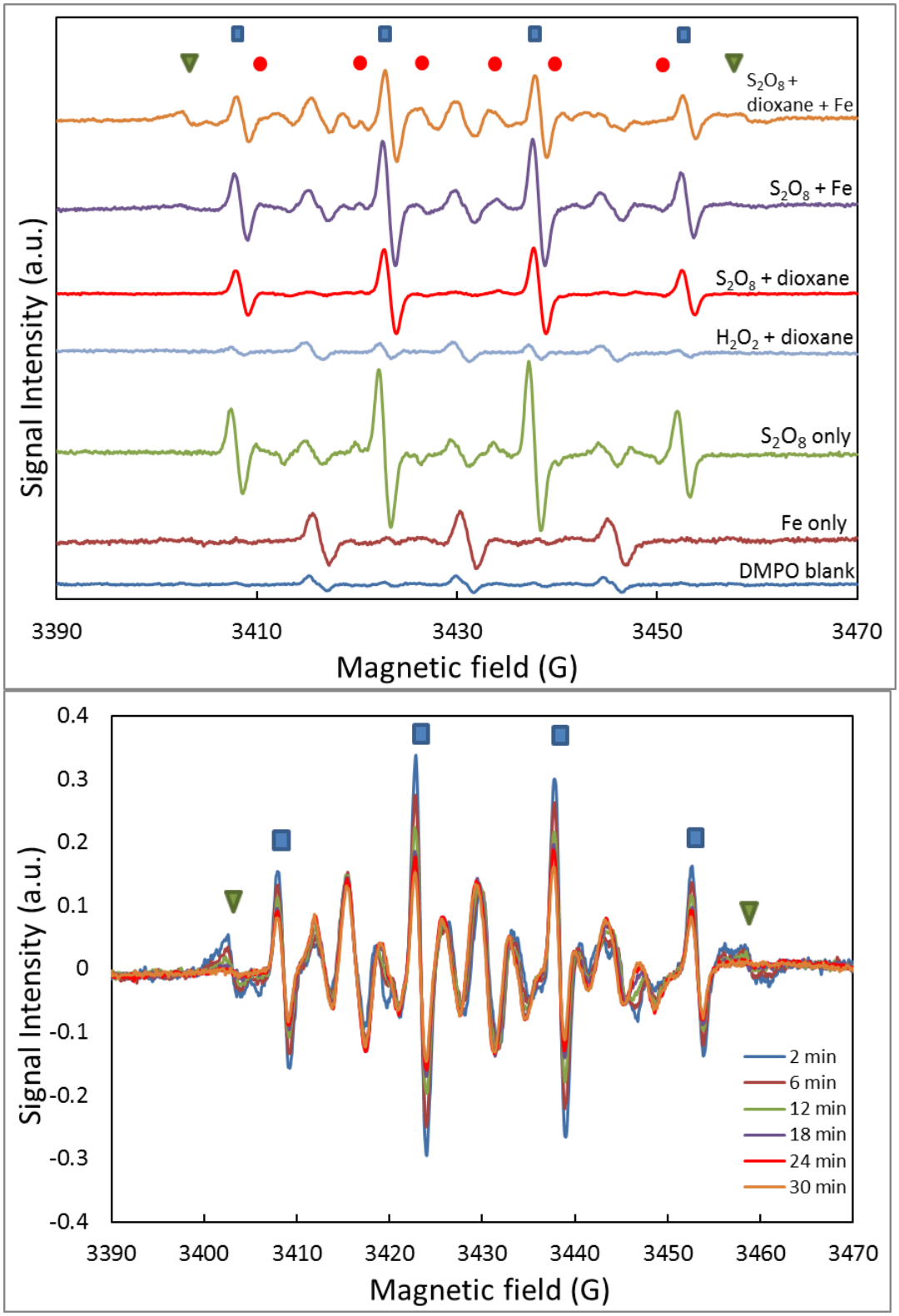

Figure 4.9.6. Electron paramagnetic resonance (EPR) spectra. (A) EPR spectra for different reaction combinations at the start of reaction (~2 min). (B) EPR spectra versus time for supernatant of persulfate-1,4-dioxane-iron filing batch experiment. ■ DMPO-OH; ● DMPO-SO_4; ▼ DMPO-H or DMPO-R.

5. CONCLUSIONS AND IMPLICATIONS FOR FUTURE RESEARCH/IMPLEMENTATION

As noted in the Abstract, the purpose of this project is to develop advanced ISCO as a viable technology for recalcitrant organic contaminants, such as 1,4-dioxane, by enhancing the solubility, stability, and transportability of strong oxidants (e.g., activated persulfate and O_3), which will enable effective *in situ* treatment of 1,4-dioxane and other recalcitrant contaminants. Several delivery enhancement alternatives have been initially considered, and three have been developed. The first is the co-injection of oxidants with delivery agents, and O_3 complexed with cyclodextrin is an example of this system. If oxidants complex or partition into a delivery-agent molecule, the amount of oxidant that can be delivered to the plume can increase. Additionally, stabilization of reagent reactivity during facilitated transport may increase specificity of oxidation for compounds of concern and reduce oxidant consumption due to natural oxidant demand of subsurface sediments. The second is the co-injection of mixtures of oxidants including OxyZone® or perozone activated persulfate (i.e., O_3, hydrogen peroxide, persulfate, and phosphate buffers). These two methods involve the use of aqueous solutions that can be injected into groundwater plumes and used to develop an aqueous flow-through treatment system. An additional application uses solid materials to stabilize and catalyze oxidants. The system developed herein uses iron (either filings or minerals in sediments) to catalyze persulfate. A potential application of these research results is as a permeable reactive barrier for *in situ* treatment of contaminated groundwater plumes.

5.1 Conclusions Related to Objectives

Several discoveries and many findings have occurred through the research conducted for this project. Of the nine studies reported herein (citation information along with additional project publications listed in the Appendices), the conclusions are summarized in the bulleted list below with relevance to the project objectives:

Ozone Oxidant Demand Impact Stabilized by Cyclodextrin Conclusions

- (Obj. 2 and 5) This investigation discovered that HPβCD was only partially degraded by O_3 and the HPβCD:O_3 inclusion complex formation was confirmed. This complex stabilized O_3, significantly increased the lifespan of O_3 in groundwater solutions containing HPβCD, and the O_3 half-life enhancement was linearly related to the HPβCD to O_3 molar ratio. The O_3 half-life in solutions containing 34.6μM HPβCD to 1 μM O_3, increased by as much as 40-fold, relative to HPβCD -free solutions. The same HPβCD:O_3 system also showed a 55% decrease in oxidant demand compared to a similar system without HPβCD. Lastly, the SOM and CEC were directly proportional to the oxidant demand for AFP44 sediment amended with biosolids. This study demonstrates that the application of HPβCD to groundwater solutions containing O_3 can enhance the oxidant lifespan, prolong oxidant reactivity, and oxidant delivery. HPβCD:O_3 inclusion complex formation delayed O_3 decay in groundwater, and reaction specificity may be increased by decreasing oxidant demand.

Oxidant Demand and Scavenging of 1,4-Dioxane Decay Conclusions

- (Obj. 2 and 3) 1,4-Dioxane was successfully degraded by the siderite-activated binary H_2O_2-persulfate system. However, the rate of degradation was slower in the presence of groundwater and typical groundwater constituents compared to ultrapure water. Chloride, sulfate, bicarbonate, potassium, calcium, and magnesium ions that are present in groundwater inhibited the oxidative

degradation of 1,4-dioxane. The inhibition was particularly strong for bicarbonate and calcium ions. The results of this work indicate that the scavenging effect of ions may be another contributor to total oxidant demand (TOD) that should be considered. This may be especially critical for bicarbonate and calcium, which are frequently detected in groundwater at concentrations higher than 0.2 mM (usually 1-2 mM).

Cyclodextrin Inclusion Complex Measurement Conclusions

- (Obj. 2, 3, and 5) Multiple spectroscopic methods including UV and fluorescence for direct and competitive complexation, of O_3, 1,4-dioxane, and chlorinated co-contaminants (TCE and TCA) with HPβCD and γ-CD, produced comparable binding constant results although method applicability and accuracy can vary with guest compound analysis properties. Although we were not able to measure any K values for γ-CD with contaminants examined herein, we found that TCE and TCA both complex with HPβCD at pH 6 and 9. 1,4-Dioxane complexation with HPβCD was not measureable within DI water, whereas the 1,4-dioxane complexation with HPβCD was measureable at increased salinity levels (i.e., 100 mM NaCl), and O_3 complex K values with HPβCD were measured at pH 6 and 9. All three contaminants (TCE, TCA, and 1,4-dioxane) and TNS had higher K values with increased salt concentrations. With changes in salinity and ionic strength, the polarity of the aqueous system changes, which in turn alters guest aqueous solubility and complexation within the hydrophobic CD cavity. This study also confirmed 1:1 stoichiometries for all of the HPβCD complexes, and guest aqueous solubility seemed to be a controlling factor for K values.

Cyclodextrin Enhanced Ozonation of 1,4-Dioxane Conclusions

- (Obj. 1, 2, 3, and 5) This study has shown that aqueous O_3, delivered with and without HPβCD, was capable of degrading 1,4-dioxane, TCE, and TCA to nondetectable concentrations. The results showed that 1,4-dioxane is only slightly more recalcitrant to degrade compared to chlorinated co-contaminants, TCE and TCA, and in the multiple contaminant systems, TCA was more recalcitrant to degrade using O_3 than 1,4-dioxane. The removal rate constants of contaminants increased in the multiple contaminant systems (which is the typical scenario at many contaminated sites) and upon addition of NaCl due to HPβCD increased partitioning and/or the possible formation of multiple radicals such as chloride radicals and organic radicals. Additionally, the contaminant pseudo 1^{st} order decay rate constants for 1,4-dioxane with O_3 in HPβCD increased compared to the rate constants without HPβCD suggesting that complexation impacts the oxidation reactions due to changes in reactivity within the clathrate cavity. This suggests enhanced treatment and oxidative reactivity, which may be attributed to the formation of ternary complexes including HPβCD, oxidant, and contaminant.

- (Obj. 1, 2, 3, and 5) Oxidation of contaminants can be either limited or promoted under some aquatic chemistry conditions including variability in pH, NaCl, or bicarbonate ion concentrations. The removal rate constants for TCE decreased with increasing initial pH. Otherwise, pH did not have a significant impact on rate constants. However, the removal rate constant for 1,4-dioxane did increase with increasing initial pH, in the presence of salts including NaCl and $NaHCO_3$, and in presence of chlorinated co-contaminants using O_3 with and without HPβCD. With HPβCD, all three contaminants had decreases in removal rate constants with increases in initial pH. This was attributed to decreased O_3 stabilization within HPβCD with increased O_3 transformation to OH• radicals compared to lower pH values. Both the contaminants and O_3 form complexes with HPβCD, which increases the potential for direct oxidation of contaminants by O_3 rather than OH•.

$NaHCO_3$ addition did not act as a radical scavenger for 1,4-dioxane removal in HPβCD solutions. These results suggest that the increased proximity of reaction reactants associated with inclusion complex formation has the potential to enhance reaction rates and specificity, and they have implications for both above-ground treatment and ISCO of contaminants using O_3 especially where co-contaminants are present.

Peroxone Activated Persulfate Treatment of 1,4-Dioxane Conclusions

- (Obj. 1, 2, 3, and 5) PAP is capable of degrading 1,4-dioxane, TCE, and TCA in aqueous phase experiments at ambient temperatures (25 ^oC). The destruction of TCA at ambient temperature sets PAP apart from the thermally activated persulfate approach, which shows little effectiveness degrading this compound at ambient temperatures. TCE was the contaminant most rapidly oxidized, with 1,4-dioxane and TCA following in order of decreasing destruction rates. Overall, these results indicate that 1,4-dioxane is more difficult to degrade than chlorinated ethenes, but more susceptible to oxidation compared to chlorinated ethanes. Since all three contaminants often co-occur, monitoring the progress of the oxidative treatment with PAP must be measured against the compound with the slowest degradation rate; TCA in this study. The destruction rates and half-lives obtained from single-contaminant systems were faster than those observed in a multi-contaminant system. However, the observed decrease in degradation rates in a multi-contaminant system was less than an order of magnitude slower than that of the single-contaminant systems, which still allows for rapid treatment of mixed-waste contaminant systems.

- (Obj. 3) Finally, the experimental results clearly demonstrate that it is possible to degrade 1,4-dioxane with dilute solutions of PAP (10:1) and that the degradation process is continuous for at least 13 days, which was the ultimate duration of our laboratory experiments. This finding is particularly important because it supports PAP as a potential long-term *in situ* treatment alternative for 1,4-dioxane polluted groundwater plumes.

Siderite Activated Peroxide & Persulfate Contaminant Treatment Conclusions

- (Obj. 2 and 4) This study investigated TCE and DCA degradation performance by the SO and the STO systems under multiple temperature conditions. TCE degradation efficiency was higher in the STO system than the SO system under all of the experiment temperature conditions. Higher temperature resulted in higher TCE degradation efficiency. For the SO system, the TCE degradation kinetic and thermodynamic parameters were identified by two stages, due to the hydrogen peroxide decomposition behavior. The activation energy for TCE removal in the SO system (first 2 hours, after 2 hours reaction) and the STO system were 37.7, 60.8, and 72.9 kJ/mol, respectively. The higher activation energy of the STO system caused by the higher energy needed for the decomposition of persulfate. The $H_2PO_4^-$ had a temperature-dependent inhibitory effect on the SO and the STO systems. For the SO system, the $H_2PO_4^-$ had minimal impact on TCE degradation under low temperature condition (10 ^oC) but exhibited increased influence as temperature increased. The STO system exhibited the opposite tendency, illustrating the different reaction mechanism between the two systems. Minimal amount of DCA was degraded in the SO system at the various temperatures. However, the DCA degradation efficiency was significantly enhanced in the STO system. The calculated activation energy for DCA removal in the STO system was 62.3 kJ/mol. These results show the binary activated hydrogen peroxide-persulfate system has a strong potential to oxidize chlorinated aliphatic hydrocarbons and good application prospects for *in situ* treatment of groundwater.

Aqueous Ozone Transport and Oxidant Demand Reactivity Conclusions

- (Obj. 1 and 5) O_3 dissolved in water followed pseudo-first order reaction kinetics for both batch (bulk water) and column, solute-transport experiments. Degradation rate constants of O_3 in DI water determined from column experiment results and reactive transport model parameter estimation were consistent and were comparable to batch experiments. Degradation rate constants have proportional relationship with NaCl concentrations within the aqueous solution. O_3 decay in both batch and solute transport experiments was controlled by the contact time. Increasing flow rates increased O_3 mass recovery and increasing distances decreased O_3 mass recovery. However, degradation rate constants remained nearly constant for different flow rates and distances, which suggests that solute transport processes (including diffusion and dispersion) for the inert sand pack used herein did not have a significant impact on the O_3 concentration attenuation. This suggests that, despite aqueous solubility limitations and rapid reactivity with water, aqueous O_3 transport distance from an injection well can be increased with groundwater flow velocities, which may not be the case for gaseous O_3 injection immiscible fluid flow and buoyancy constraints.

Transport and Peroxone Activated Persulfate Treatment of 1,4-Dioxane Conclusions

- (Obj. 2, 4, and 5) Peroxone activated persulfate oxidation of 1,4-dioxane was achieved in both batch and column scale experiments using OxyZone as the oxidizing agent. In batch scale experiments, 1,4-dioxane was degraded at the rate of 0.0213 h^{-1} at the molar oxidant: contaminant ratio of 250:1. In the three column experiments, the degradation rates varied from 0.0808-1.5389 h^{-1}. The column experiments compared multiple pulsed oxidant injection to continuous injection, and the results of the pulsed injections suggested that oxidation continued long after the end of oxidant injection. These data is supported by the prolonged contaminant oxidation that takes place in both batch and column scale experiments. This research supports the development of ISCO of 1,4-dioxane in groundwater plumes. OxyZone's persistence in the system enhances ISCO capabilities by minimizing the volume of oxidant needed for remediation.

1,4-Dioxane Treatment Using Persulfate Activated By Iron Filings Conclusions

- (Obj. 1, 2, and 4) Successful activation of persulfate was achieved by using iron filings in both batch and column experiments. The activation process comprises two stages, including a first stage of rapid decomposition of persulfate and a second stage of rate-limited surface reaction. Comparison of the pseudo-first-order reaction rate constants for 1,4-dioxane degradation shows significantly higher reaction rates in the presence of iron filings, indicating the effectiveness of iron filing in activating persulfate and facilitating 1,4-dioxane degradation.

5.2 Implications for ISCO Applications at Contaminated Groundwater Sites

5.2.1 Potential ISCO Applications at Contaminated Groundwater Sites

The technical and economic feasibility of AOP application for ISCO remediation of 1,4-dioxane or other groundwater contaminants is likely to be highly site specific and dependent on many factors. Currently, the most common method used to remediate 1,4-dioxane involves *ex situ* treatment using AOP (e.g., O_3 and H_2O_2). Contaminated groundwater must be extracted, treated, and then reinjected or redistributed. Overall, *ex situ* treatment is costly, can be highly inefficient, and *in situ* approaches should be considered for the remediation of 1,4-dioxane plumes (as with other types of contaminants). *In situ* chemical oxidation can be an effective method for remediation of source zones contaminated by several classes of organic compounds. We have shown that AOP reagents can be used to remediate 1,4-dioxane contaminated groundwater.

However, such reagents are typically short-lived, and therefore may only be applicable to source area treatment. Increasing oxidant longevity can also increase the feasibly ISCO for groundwater plumes.

These limitations may be reduced by co-injecting O_3 with a complexing agent (i.e., cyclodextrin), which facilitates the transport of O_3 into groundwater plumes to increase its longevity and transportability and thereby enhances the effective subsurface treatment volume. It is anticipated that this will in turn decrease the cost and time required to remediate such contaminated sites. The proposed oxidant-facilitated transport technology would increase the size of the reaction zone associated with each injection well, which decreases well drilling/construction costs. In addition, the technology would enhance the persistence of the oxidant in the system. Both of these effects will improve overall treatment effectiveness of the ISCO application. For some sites, pump and treat could be discontinued with this application if monitored natural attenuation were to become viable upon removal of the source area (lowering the cost relative to pump and treat). One significant cost benefit would result from not needing to pump, transport, store, and dispose of groundwater with a transition to *in situ* treatment.

For treatment of groundwater plumes, the application mode could involve creation of a flow-through reactive barrier within the subsurface, through which the plume would transport and be remediated without extraction. Injection of ISCO reagents into a series of vertical wells spaced perpendicular to the mean direction of groundwater flow would create a reactive treatment of the plume. The groundwater plume would be treated as it migrates through this *in situ* reaction zone. Pump and treat could be discontinued with this application, as plume containment and treatment would be achieved through ISCO injection (lowering the cost relative to pump and treat). The reactive zone would be maintained through low-flow ongoing gravity-fed injection of oxidant. The facilitated transport, oxidant stabilization, and *in situ* activation technologies developed herein enhance the transportability of the oxidants, which increases the uniformity and distance of coverage. This will increase the effectiveness of the reactive barrier, and also reduce the number of wells and attendant costs required to maintain continuous coverage. The flow-through treatment barrier or curtain approach could be applied at the down-gradient edge of a groundwater plume, and it could also be applied at the down-gradient edge of a source zone.

Co-injection of HPβCD with O_3 into groundwater can increase the O_3 transport distance by more than an order of magnitude, which could be used to maintain the above noted reactive flow-through treatment for groundwater contamination plumes. As H_2O_2 stabilization using organic-acid stabilizers has been demonstrated previously (Watts et al., 2007), this O_3:HPβCD complex may also support ISCO using perozone reactions. Use of HPβCD or other reactants could be used to enhance delivery, but since O_3 has been shown here to effectively treat both 1,4-dioxane and co-contaminants, no other reactants would be required for contaminant treatment. O_3 can be generated on-site from atmospheric air, and only electricity supply would be needed for continuous groundwater treatment.

In situ activation of persulfate can be used to enhance its effectiveness for ISCO. Without activation, aqueous persulfate is quite stable with a half-life of approximately 600 days (Liu et al., 2014), which suggests a significant potential for injection into the subsurface, transport into groundwater plume areas, and use for ISCO. Co-injection of oxidants such as PAP uses the oxidants to activate persulfate, and the addition of buffers such as the formulation termed

OxyZone can delay and stabilize persulfate activation (i.e., *in situ* activation) to enhance transportability while extending the lifetime of the oxidant reactivity. We have also shown that *in situ* activation of persulfate can be achieved with iron (and other species) present and naturally occurring in aquifer materials.

Activation of persulfate can be also used to enhance its reactivity for efficient contaminant oxidative transformation, and subsurface amendments may be emplaced *in situ* to target zones requiring increased reactivity. Targeted subsurface amendments could be used as a reactive barrier for *in situ* groundwater treatment to decrease contaminant flux released from either sources or at plume boundaries (Marble et al., 2014). These amendments could include either organic or inorganic catalysts of persulfate (Anipsitakis and Dionysiou, 2004; Chen and Carroll, 2016; Liu et al., 2014; Zhong et al., 2015).

Iron activated persulfate treatment of 1,4-dioxane was shown herein to be effective within a PRB application. The PRB bed length required for field application of the persulfate-enhanced PRB can be calculated based on assumed first-order reaction kinetics and using the reported *k* of 0.018 h^{-1}. Assuming the persulfate is perfused uniformly within the PRB, and given a typical groundwater velocity of 0.3 m/d, the estimated bed lengths (L in equation (2)) are 1.6, 2.1, and 3.2 m for 1,4-dioxane removal rates of 90%, 95%, and 99% (C/C_0 = 0.1, 0.05, and 0.01), respectively. These thicknesses are in the range of bed lengths typically used for PRB applications. It is significant to note that the persulfate concentration used herein, ~1 g/L, is an order of magnitude lower than the concentrations typically used in standard field ISCO applications. It is also interesting to note that the *k* (0.018 h^{-1}) is comparable to the values (0.03~0.12 h^{-1}) obtained with micron- or nano-ZVI in batch experiments (Shin et al., 2012; Son et al., 2009), indicating that the persulfate-enhanced PRB has the potential to achieve a 1,4-dioxane removal efficiency similar to nano-ZVI. These results illustrate the potential of the persulfate-enhanced PRB for *in situ* remediation of 1,4-dioxane contaminated groundwater.

5.2.2 Estimated Reagent Cost Comparison

Cost analysis of these novel 1,4-dioxane treatment technologies was not included in the scope of work, but we can provide some cost information for preliminary consideration. A recent 1,4-dioxane treatment publication described the commercial HiPOx treatment system at AFP44 in terms of reagent costs (DiGuiseppi et al., 2016). The average flow rate was 1891 gpm, and the average annual reagent cost was the sum of $60,000 for H_2O_2 and $5,000 in O_3 generation, which equated to $\$2.73 \times 10^{-4}$ per gallon total, $\$2.52 \times 10^{-4}$ per gallon for H_2O_2, and $\$2.1 \times 10^{-5}$ per gallon for O_3. The annual O&M for the AFP44 system was $1.2 million, which suggests that the cost for this ex situ, pump and treat system was $0.00505 per gallon (Table 5.1).

Table 5.1. Summary of treatment system cost dollars per gallon assuming a 184 mole ratio for treatment of 0.01 mg/L 1,4-dioxane contamination.

In Situ OxyZone® (~5 mg/L $Na_2S_2O_8$)	$ 0.00016
In Situ 1 mg/L O_3 & 50 mg/L HPβCD	$ 0.05246
In Situ 5 mg/L $Na_2S_2O_8$	$ 0.00008
Ex Situ HiPOx AFP44 (DiGuiseppi et al. 2016)	$ 0.00505

In situ treatment reagent cost can be estimated if we assume negligible pumping cost with a gravity fed delivery system. Assuming a site with 10 μg/L 1,4-dioxane is targeting treatment at 184 oxidant:contaminant mole ratio, we can estimate the cost of oxidant needed to treat the contaminated aquifer on a per gallon basis. In terms of cost comparison, we can compare the "per gallon" cost estimates for the AFP44 ex situ system to in situ treatment using PAP, persulfate, and HPβCD co-injected with O_3 (Table 5.1). The O_3 cost includes an initial capital investment for the O_3 generation equipment, which can be purchased for ~$5000 for a small system. There is a small electricity cost in the range of $0.05 per gallon treated. HPβCD technical grade is $5.90 per pound. The additional cost of adding HPβCD at 50 mg/L is $2.46x10^{-3} per gallon. For a total HPβCD co-injection with O_3, the reagent cost amounts to $5.25x10^{-2} per gallon of aquifer water. Sodium persulfate costs approximately $1.85 per pound. Assuming the same 184 oxidant:contaminant mole ratio, sodium persulfate without activator can be injected at 5 mg/L for $7.7x10^{-5} per gallon of aquifer water. OxyZone® would include the same concentration of sodium persulfate with the addition of hydrogen peroxide and buffer totaling $1.53x10^{-4} per gallon treated. Note that the water treatment volume for ISCO could be much lower than pump and treat because of significant inefficiencies including dilution caused by pumping at plume boundaries for hydraulic control.

6. LITERATURE CITED

Abe, A., 1999. Distribution of 1, 4-dioxane in relation to possible sources in the water environment. Science of the total environment, 227(1): 41-47.

Acero, J.L., Haderlein, S.B., Schmidt, T.C., Suter, M.J.F. and Von Gunten, U., 2001. MTBE oxidation by conventional ozonation and the combination ozone/hydrogen peroxide: Efficiency of the processes and bromate formation. Environmental Science & Technology, 35(21): 4252-4259.

Adams, C.D., Scanlan, P.A. and Secrist, N.D., 1994. Oxidation and Biodegradability Enhancement of 1,4-Dioxane Using Hydrogen-Peroxide and Ozone. Environmental Science & Technology, 28(11): 1812-1818.

Adamson, D.T., Anderson, R.H., Mahendra, S. and Newell, C.J., 2015. Evidence of 1,4-Dioxane Attenuation at Groundwater Sites Contaminated with Chlorinated Solvents and 1,4-Dioxane. Environmental Science & Technology, 49(11): 6510-6518.

Adamson, D.T. et al., 2014. A Multisite Survey To Identify the Scale of the 1,4-Dioxane Problem at Contaminated Groundwater Sites. Environmental Science & Technology Letters, 1(5): 254-258.

Adamson, D.T. et al., 2017. 1,4-Dioxane drinking water occurrence data from the third unregulated contaminant monitoring rule. Science of the Total Environment, 596: 236-245.

Adeel, Z. and Luthy, R.G., 1995. Sorption and Transport Kinetics of a Nonionic Surfactant through an Aquifer Sediment. Environmental Science & Technology, 29(4): 1032-1042.

Ahn, S., Peterson, T.D., Righter, J., Miles, D.M. and Tratnyek, P.G., 2013. Disinfection of Ballast Water with Iron Activated Persulfate. Environmental Science & Technology, 47(20): 11717-11725.

Ahuja, D.K., Bachas, L.G. and Bhattacharyya, D., 2007. Modified Fenton reaction for trichlorophenol dechlorination by enzymatically generated H2O2 and gluconic acid chelate. Chemosphere, 66(11): 2193-2200.

Alcantara-Garduno, M.E., Okuda, T., Nishijima, W. and Okada, M., 2008a. Ozonation of trichloroethylene in acetic acid solution with soluble and solid humic acid. Journal of

Hazardous Materials, 160(2-3): 662-667.
Alcantara-Garduno, M.E., Okuda, T., Tsai, T.Y., Nishijima, W. and Okada, M., 2008b. Experimental and mathematical evaluation of trichloroethylene removal from saturated soil using acetic acid with saturated ozone. Separation and Purification Technology, 60(3): 299-307.
Allan, I.J., Semple, K.T., Hare, R. and Reid, B.J., 2007. Cyclodextrin enhanced biodegradation of polycyclic aromatic hydrocarbons and phenols in contaminated soil slurries. Environmental Science & Technology, 41(15): 5498-5504.
Anderson, R.H., Anderson, J.K. and Bower, P.A., 2012. Co-occurrence of 1,4-dioxane with trichloroethylene in chlorinated solvent groundwater plumes at US Air Force installations: Fact or fiction. Integrated Environmental Assessment and Management, 8(4): 731-737.
Anipsitakis, G.P. and Dionysiou, D.D., 2003. Degradation of Organic Contaminants in Water with Sulfate Radicals Generated by the Conjunction of Peroxymonosulfate with Cobalt. Environmental Science & Technology, 37(20): 4790-4797.
Anipsitakis, G.P. and Dionysiou, D.D., 2004. Radical Generation by the Interaction of Transition Metals with Common Oxidants. Environmental Science & Technology, 38(13): 3705-3712.
Anipsitakis, G.P., Dionysiou, D.D. and Gonzalez, M.A., 2006. Cobalt-Mediated Activation of Peroxymonosulfate and Sulfate Radical Attack on Phenolic Compounds. Implications of Chloride Ions. Environmental Science & Technology, 40(3): 1000-1007.
ASTM, 2010. D7262-10, Standard Test Method for Estimating the Permanganate Natural Oxidant Demand of Soil and Aquifer Solids, West Conshohocken, PA, www.astm.org.
Bader, H. and Hoigné, J., 1981. Determination of ozone in water by the indigo method. Water Research, 15(4): 449–456.
Ball, R.G., 2010. Soil and Water Remediation Method and Apparatus. US Patent No. 7,667,087. Enchem Engineering, Inc., US.
Ball, R.G., 2011. Chemical oxidation method and compounds, US Patent 8,049,056. Enchem Engineering, Inc., US.
Ball, R.G., 2016. Chemical Oxidation Method and Compounds, US Patent No. 9,409,216. Enchem Engineering, Inc., US.
Barbeni, M., Minero, C., Pelizzetti, E., Borgarello, E. and Serpone, N., 1987. Chemical degradation of chlorophenols with Fenton's reagent (Fe2++ H2O2). Chemosphere, 16(10-12): 2225-2237.
Barndok, H., Cortijo, L., Hermosilla, D., Negro, C. and Blanco, A., 2014a. Removal of 1,4-dioxane from industrial wastewaters: Routes of decomposition under different operational conditions to determine the ozone oxidation capacity. Journal of Hazardous Materials, 280: 340-347.
Barndok, H., Hermosilla, D., Cortijo, L., Torres, E. and Blanco, A., 2014b. Electrooxidation of industrial wastewater containing 1,4-dioxane in the presence of different salts. Environmental Science and Pollution Research, 21(8): 5701-5712.
Beckett, M.A. and Hua, I., 2000. Elucidation of the 1, 4-dioxane decomposition pathway at discrete ultrasonic frequencies. Environmental science & technology, 34(18): 3944-3953.
Beltran, F., Acedo, B. and Rivas, J., 1999. Use of ozone and hydrogen peroxide to remove alachlor from surface water. Bulletin of Environmental Contamination and Toxicology, 63(1): 9-14.
Beltrán, F.J., González, M., Ribas, F.J. and Alvarez, P., 1998. Fenton reagent advanced oxidation of polynuclear aromatic hydrocarbons in water. Water, Air, and Soil Pollution, 105(3-4): 685-700.

Bender, M.L. and Komiyama, M., 1978. Cyclodextrin Chemistry. Spring-Verlag, New York.
Bennedsen, L.R., Muff, J. and Søgaard, E.G., 2012. Influence of chloride and carbonates on the reactivity of activated persulfate. Chemosphere, 86(11): 1092-1097.
Bertanza, G. et al., 2013. EDCs, estrogenicity and genotoxicity reduction in a mixed (domestic plus textile) secondary effluent by means of ozonation: A full-scale experience. Science of the Total Environment, 458: 160-168.
Bhuyan, S.J. and Latin, M.R., 2012. BTEX Remediation under Challenging Site Conditions Using In-Situ Ozone Injection and Soil Vapor Extraction Technologies: A Case Study. Soil and Sediment Contamination: An International Journal, 21: 545--556.
Bijan, L. and Mohseni, M., 2005. Integrated ozone and biotreatment of pulp mill effluent and changes in biodegradability and molecular weight distribution of organic compounds. Water Research, 39(16): 3763-3772.
Bizzigotti, G.O., Reynolds, D.A. and Kueper, B.H., 1997. Enhanced solubilization and destruction of tetrachloroethylene by hydroxypropyl-beta-cyclodextrin and iron. Environmental Science & Technology, 31(2): 472-478.
Blanford, W.J., 2014. Model of phase distribution of hydrophobic organic chemicals in cyclodextrin-water-air-solid sorbent systems as a function of salinity, temperature, and the presence of multiple CDs. Journal of Inclusion Phenomena and Macrocyclic Chemistry, 79(1-2): 57-64.
Blanford, W.J. et al., 2001. Cyclodextrin-enhanced vertical flushing of a trichloroethene contaminated aquifer. Ground Water Monitoring and Remediation, 21(1): 58-66.
Blanford, W.J., Gao, H., Dutta, M. and Ledesma, E.B., 2014. Solubility enhancement and QSPR correlations for polycyclic aromatic hydrocarbons complexation with alpha, beta, and gamma cyclodextrins. Journal of Inclusion Phenomena and Macrocyclic Chemistry, 78(1-4): 415-427.
Block, P.A., Brown, R.A. and Robinson, D., 2004. Novel activation technologies for sodium persulfate in situ chemical oxidation. Columbus, OH: Battelle Press, pp. 24-27.
Boving, T.B. and Brusseau, M.L., 2000. Solubilization and removal of residual trichloroethene from porous media: Comparison of several solubilization agents. Journal of Contaminant Hydrology, 42: 51--67.
Boving, T.B. and McCray, J.E., 2000. Cyclodextrin-Enhanced Remediation of Organic and Metal Contaminants in Porous Media and Groundwater. Remediation Journal, 10(2): 59-83.
Boving, T.B., McCray, J.E., Blanford, W. and Brusseau, M.L., 2004. Cyclodextrin Enhanced Remediation at NAB Little Creek, Virginia Beach, VA, Final Report to Environmental Security Technology Certification Program. ESTCP (Department of Defense).
Boving, T.B., Wang, X.J. and Brusseau, M.L., 1999. Cyclodextrin-enhanced solubilization and removal of residual-phase chlorinated solvents from porous media. Environmental Science and Technology, 33(5): 764-770.
Brusseau, M.L. et al., 2011. Impact of In Situ Chemical Oxidation on Contaminant Mass Discharge: Linking Source-Zone and Plume-Scale Characterizations of Remediation Performance. Environmental Science & Technology, 45(12): 5352-5358.
Brusseau, M.L., McCray, J. and Wang, X., 1996. Using cyclodextrin for in situ remediation of petroleum contamination. Abstracts of Papers of the American Chemical Society, 211: 103-ENVR.
Brusseau, M.L., Miller, R.M., Zhang, Y.M., Wang, X.J. and Bai, G.Y., 1995. Biosurfactant-Enhanced and Cosolvent-Enhanced Remediation of Contaminated Media. Surfactant-Enhanced Subsurface Remediation, 594: 82-94.

Brusseau, M.L., Wang, X.J. and Hu, Q.H., 1994. Enhanced Transport of Low-Polarity Organic-Compounds through Soil by Cyclodextrin. Environmental Science & Technology, 28(5): 952-956.

Brusseau, M.L., Wang, X.J. and Wang, W.Z., 1997. Simultaneous elution of heavy metals and organic compounds from soil by cyclodextrin. Environmental Science & Technology, 31(4): 1087-1092.

Burmaster, D.E., 1982. The new pollution: groundwater contamination. Environment: Science and Policy for Sustainable Development, 24(2): 6-36.

Buxton, G.V., Greenstock, C.L., Helman, W.P. and Ross, A.B., 1988. Critical review of rate constants for reactions of hydrated electrons, hydrogen atoms and hydroxyl radicals (· OH/· O− in aqueous solution. Journal of physical and chemical reference data, 17(2): 513-886.

Cai, C., Zhang, H., Zhong, X. and Hou, L., 2014. Electrochemical enhanced heterogeneous activation of peroxydisulfate by Fe–Co/SBA-15 catalyst for the degradation of Orange II in water. Water Research, 66: 473-485.

Capellos, C. and Bielski, B.H.J., 1972. Kinetic systems: mathematical description of chemical kinetics in solution.

Carroll, K.C. and Brusseau, M.L., 2009. Dissolution, cyclodextrin-enhanced solubilization, and mass removal of an ideal multicomponent organic liquid. Journal of Contaminant Hydrology, 106(1-2): 62-72.

Carroll, K.C., Jordan, F.L., Glenn, E.P., Waugh, W.J. and Brusseau, M.L., 2009. Comparison of nitrate attenuation characterization methods at the Uranium mill tailing site in Monument Valley, Arizona. Journal of Hydrology, 378(1-2): 72-81.

Chang, Y.-Y., Roh, H. and Yang, J.-K., 2013. Improving the clean-up efficiency of field soil contaminated with diesel oil by the application of stabilizers. Environmental Technology, 34(June 2014): 1481--1487.

Chaplin, B.P., 2014. Critical review of electrochemical advanced oxidation processes for water treatment applications. Environmental Science: Processes & Impacts 16(6): 1182-1203.

Chen, G. et al., 2001. The mechanism and applicability of in situ oxidation of trichloroethylene with Fenton's reagent. Journal of Hazardous Materials, 87(1-3): 171-186.

Chen, H. and Carroll, K.C., 2016. Metal-Free Catalysis of Persulfate Activation and Organic-Pollutant Degradation by Nitrogen-Doped Graphene and Aminated Graphene. Environmental Pollution, 215: 96–102.

Choi, H., Lim, H.N., Kim, J., Hwang, T.M. and Kang, J.W., 2002. Transport characteristics of gas phase ozone in unsaturated porous media for in-situ chemical oxidation. Journal of Contaminant Hydrology, 57(1-2): 81-98.

Ciotti, C., Baciocchi, R. and Tuhkanen, T., 2009. Influence of the operating conditions on highly oxidative radicals generation in Fenton's systems. Journal of hazardous materials, 161(1): 402-408.

Clayton, W.S., Petri, B.G. and Huling, S.G., 2011. Fundamentals of ISCO Using Ozone. In: R.L. Siegrist (Editor), In Situ Chemical Oxidation for Groundwater Remediation. Springer Science+Business Media, LLC.

Clifford, J.S., Ioannidis, M.A. and Legge, R.L., 2007. Enhanced aqueous solubilization of tetrachloroethylene by a rhamnolipid biosurfactant. Journal of Colloid and Interface Science, 305(2): 361-365.

Coleman, H.M., Vimonses, V., Leslie, G. and Amal, R., 2007. Degradation of 1,4-dioxane in water using TiO2 based photocatalytic and H2O2/UV processes. Journal of Hazardous Materials, 146(3): 496-501.

Connors, K.A., 1987. Binding Constants: The Measurement of Molecular Complex Stability. Wiley-Interscience, New York, 432 pp.
Connors, K.A., 1997. The stability of cyclodextrin complexes in solution. Chemical Reviews, 97(5): 1325-1357.
Crimi, M.L. and Siegrist, R.L., 2003. Geochemical effects on metals following permanganate oxidation of DNAPLs. Ground Water, 41(4): 458-469.
Cronk, G., 2008. Case study comparison of multiple activation methods for sodium persulfate ISCO treatment, pp. 200.
Davies, M.J., Gilbert, B.C., Stell, J.K. and Whitwood, A.C., 1992. Nucleophilic substitution reactions of spin adducts. Implications for the correct identification of reaction intermediates by EPR/spin trapping. Journal of the Chemical Society, Perkin Transactions 2(3): 333-335.
De Laat, J. and Le, T.G., 2005. Kinetics and modeling of the Fe (III)/H2O2 system in the presence of sulfate in acidic aqueous solutions. Environmental science & technology, 39(6): 1811-1818.
De Laat, J. and Le, T.G., 2006. Effects of chloride ions on the iron (III)-catalyzed decomposition of hydrogen peroxide and on the efficiency of the Fenton-like oxidation process. Applied Catalysis B: Environmental, 66(1-2): 137-146.
Deegan, A.M. et al., 2011. Treatment options for wastewater effluents from pharmaceutical companies. International Journal of Environmental Science and Technology, 8(3): 649-666.
Dettmer, A. et al., 2017. Stabilization and prolonged reactivity of aqueous-phase ozone with cyclodextrin. Journal of Contaminant Hydrology, 196: 1-9.
DiGuiseppi, W., Walecka-Hutchinson, C. and Hatton, J., 2016. 1,4-Dioxane Treatment Technologies. Remediation, Winter: 71-92.
DiGuiseppi, W.H. and Whitesides, C., 2007. Treatment Options for Remediation of 1,4-Dioxane in Groundwater. Environmental Engineer, American Academy of Environmental Engineers, 43(2): 1-7.
Draper, W.M., Dhoot, J.S., Remoy, J.W. and Perera, S.K., 2000. Trace-level determination of 1, 4-dioxane in water by isotopic dilution GC and GC-MS. Analyst, 125(8): 1403-1408.
Drzewicz, P., Perez-Estrada, L., Alpatova, A., Martin, J.W. and Gamal El-Din, M., 2012. Impact of Peroxydisulfate in the Presence of Zero Valent Iron on the Oxidation of Cyclohexanoic Acid and Naphthenic Acids from Oil Sands Process-Affected Water. Environmental Science & Technology, 46(16): 8984-8991.
Duwelius, R.F., Yeskis, D.J., Wilson, J.T. and Robinson, B.A., 2002. Geohydrology, Water Quality, and Simulation of Ground-Water Flow in the Vicinity of a Former Waste-Oil Refinery near Westville, Indiana.
Eberle, D., Ball, R. and Boving, T.B., 2016. Peroxone activated persulfate treatment of 1,4-dioxane in the presence of chlorinated solvent co-contaminants. Chemosphere, 144: 728-735.
Edwards, D.A., Luthy, R.G. and Liu, Z.B., 1991. Solubilization of Polycyclic Aromatic-Hydrocarbons in Micellar Nonionic Surfactant Solutions. Environmental Science & Technology, 25(1): 127-133.
EPA, 2008. Fact sheet emerging contaminant- 1,4-Dioxane. In: S.W.a.E. Responsesolid (Editor), Washington, DC.
EPA, 2013a. The third unregulated contaminant monitoring rule (UCMR 3): data summary, Washingt. DC.

EPA, U.S., 2013b. Integrated Risk Information System (IRIS) on 1,4-Dioxane, National Center for Environmental Assessment, Office of Research and Development, Washington DC (2013).
Fang, G.-D. et al., 2013a. Transformation of polychlorinated biphenyls by persulfate at ambient temperature. Chemosphere, 90(5): 1573-1580.
Fang, G., Gao, J., Dionysiou, D.D., Liu, C. and Zhou, D., 2013b. Activation of Persulfate by Quinones: Free Radical Reactions and Implication for the Degradation of PCBs. Environmental Science & Technology, 47(9): 4605-4611.
Ferrarese, E., Andreottola, G. and Oprea, I.A., 2008. Remediation of PAH-contaminated sediments by chemical oxidation. Journal of Hazardous Materials, 152(1): 128-139.
Fountain, J.C., Klimek, A., Beikirch, M.G. and Middleton, T.M., 1991. The Use of Surfactants for Insitu Extraction of Organic Pollutants from a Contaminated Aquifer. Journal of Hazardous Materials, 28(3): 295-311.
French, D., 1957. The Schardinger Dextrins. Advances in Carbohydrate Chemistry, 12: 189-280.
Freshour, A.R., Mawhinney, S. and Bhattacharyya, D., 1996. Two-phase ozonation of hazardous organics in single and multicomponent systems. Water Research, 30(9): 1949-1958.
Furman, O.S., Teel, A.L. and Watts, R.J., 2010. Mechanism of Base Activation of Persulfate. Environmental Science & Technology, 44(16): 6423-6428.
Gandesbery, T., Hetzel, F., Smith, R. and Riege, L., 1998. Ambient concentrations of toxic chemicals in San Francisco Bay sediments. California Environmental Protection Agency, Regional Water Quality Control Board, San Francisco Bay Region.
Garcia-Rio, L. et al., 2006. Evidence for complexes of different stoichiometries between organic solvents and cyclodextrins. Organic & Biomolecular Chemistry, 4(6): 1038-1048.
Gardoni, D., Vailati, A. and Canziani, R., 2012. Decay of Ozone in Water: A Review. Ozone-Science & Engineering, 34(4): 233-242.
Gassie, L.W. and Englehardt, J.D., 2017. Advanced oxidation and disinfection processes for onsite net-zero greywater reuse: A review. Water Research, 125: 384-399.
Gates-Anderson, D.D., Siegrist, R.L. and Cline, S.R., 2001. Comparison of Potassium Permanganate and Hydrogen Peroxide as Chemical Oxidants for Organically Contaminated Soils. Journal of Environmental Engineering, 127(4): 337-347.
Ghosh, P., Samanta, A.N. and Ray, S., 2010. Oxidation kinetics of degradation of 1,4-dioxane in aqueous solution by H2O2/Fe(II) system. Journal of Environmental Science and Health Part a-Toxic/Hazardous Substances & Environmental Engineering, 45(4): 395-399.
Ghoshal, S. and Hill, A.J., 2002. Micellar solubilization of napthalene, and phenanthrene from nonaqueous-phase liquids. Environmental Science & Technology, 36(18): 3901-3907.
Glaze, W.H. and Kang, J.W., 1988. Advanced Oxidation Processes for Treating Groundwater Contaminated with Tce and Pce - Laboratory Studies. Journal American Water Works Association, 80(5): 57-63.
Glaze, W.H., Kang, J.W. and Chapin, D.H., 1987. The Chemistry of Water-Treatment Processes Involving Ozone, Hydrogen-Peroxide and Ultraviolet-Radiation. Ozone-Science & Engineering, 9(4): 335-352.
Gomes, J., Costa, R., Quinta-Ferreira, R.M. and Martins, R.C., 2017. Application of ozonation for pharmaceuticals and personal care products removal from water. Science of the Total Environment, 586: 265-283.
Gu, X. et al., 2011. Oxidation of 1, 1, 1-trichloroethane stimulated by thermally activated persulfate. Industrial & Engineering Chemistry Research, 50(19): 11029-11036.
Hand, S., Wang, B.X. and Chu, K.H., 2015. Biodegradation of 1,4-dioxane: Effects of enzyme inducers and trichloroethylene. Science of the Total Environment, 520: 154-159.

Hartog, N., Griffioen, J. and Van der Weijden, C.H., 2002. Distribution and reactivity of O-2-reducing components in sediments from a layered aquifer. Environmental Science & Technology, 36(11): 2338-2344.
Haselow, J.S., Siegrist, R.L., Crimi, M. and Jarosch, T., 2003. Estimating the total oxidant demand for in situ chemical oxidation design. Remediation Journal, 13(4): 5-16.
He, X., Mezyk, S.P., Michael, I., Fatta-Kassinos, D. and Dionysiou, D.D., 2014. Degradation kinetics and mechanism of β-lactam antibiotics by the activation of H2O2 and Na2S2O8 under UV-254 nm irradiation. Journal of hazardous materials, 279: 375-383.
Hill, R.R., Jeffs, G.E. and Roberts, D.R., 1997. Photocatalytic degradation of 1, 4-dioxane in aqueous solution. Journal of Photochemistry and Photobiology A: Chemistry, 108(1): 55-58.
Hoigne, J. and Bader, H., 1976. The role of hydroxyl radical reactions in ozonation processesin aqueous. Water Research, 10: 377–386.
Hoigne, J. and Bader, H., 1983a. Rate Constants of Reactions of Ozone with Organic and Inorganic-Compounds in Water .1. Non-Dissociating Organic-Compounds. Water Research, 17(2): 173-183.
Hoigne, J. and Bader, H., 1983b. Rate Constants of Reactions of Ozone with Organic and Inorganic-Compounds in Water .2. Dissociating Organic-Compounds. Water Research, 17(2): 185-194.
Hoigne, J., Bader, H., Haag, W.R. and Staehelin, J., 1985. Rate Constants of Reactions of Ozone with Organic and Inorganic-Compounds in Water .3. Inorganic-Compounds and Radicals. Water Research, 19(8): 993-1004.
Huang, K.-C., Couttenye, R.A. and Hoag, G.E., 2002. Kinetics of heat-assisted persulfate oxidation of methyl tert-butyl ether (MTBE). Chemosphere, 49(4): 413-420.
Huang, K.-C., Zhao, Z., Hoag, G.E., Dahmani, A. and Block, P.A., 2005. Degradation of volatile organic compounds with thermally activated persulfate oxidation. Chemosphere, 61(4): 551-560.
Huling, S. and Pivetz, B., 2006. Engineering Issue Paper: In-Situ Chemical Oxidation. Engineering: 1-60.
IARC, 1999. Monograph on 1,4-Dioxane. International Agency for Research on Cancer, Lyon, France.
Ikehata, K. and El-Din, M.G., 2005a. Aqueous pesticide degradation by ozonation and ozone-based advanced oxidation processes: A review (Part I). Ozone-Science & Engineering, 27(2): 83-114.
Ikehata, K. and El-Din, M.G., 2005b. Aqueous pesticide degradation by ozonation and ozone-based advanced oxidation processes: A review (Part II). Ozone-Science & Engineering, 27(3): 173-202.
Ikehata, K., Wang-Staley, L., Qu, X.Y. and Li, Y., 2016. Treatment of Groundwater Contaminated with 1,4-Dioxane, Tetrahydrofuran, and Chlorinated Volatile Organic Compounds Using Advanced Oxidation Processes. Ozone-Science & Engineering, 38(6): 413-424.
Johnson, M.D. and Reinsborough, V.C., 1992. Binding Constants for Cyclodextrin Inclusions by Competitive Spectrofluorometry Involving 6-(P-Toluidino)Naphthalene-2-Sulfonate. Australian Journal of Chemistry, 45(12): 1961-1966.
Jung, Y., Park, J.Y., Ko, S.O. and Kim, Y.H., 2013. Stabilization of hydrogen peroxide using phthalic acids in the Fenton and Fenton-like oxidation. Chemosphere, 90: 812--819.
Khan, N.A., Johnson, M.D., and Carroll, K.C., 2018. Spectroscopic Methods for Aqueous Cyclodextrin Inclusion Complex Binding Measurement for 1,4-Dioxane, Chlorinated Co-

Contaminants, and Ozone. Journal of Contaminant Hydrology.
Kim, H., Yang, S. and Yang, H., 2013. Surfactant-enhanced ozone sparging for removal of organic compounds from sand. Journal of Environmental Science and Health Part a-Toxic/Hazardous Substances & Environmental Engineering, 48(5): 526-533.
Kishimoto, N., 2007. Dependency of advanced oxidation performance on the contaminated water feed mode for ozonation combined with electrolysis using a two-compartment electrolytic flow cell. Journal of Advanced Oxidation Technologies, 10(2): 241-246.
Kishimoto, N. et al., 2008. Ozonation combined with electrolysis of 1,4-dioxane using a two-compartment electrolytic flow cell with solid electrolyte. Water Research, 42(1-2): 379-385.
Kishimoto, N., Yasuda, Y., Mizutani, H. and Ono, Y., 2007. Applicability of ozonation combined with electrolysis to 1,4-dioxane removal from wastewater containing radical scavengers. Ozone-Science & Engineering, 29(1): 13-22.
Klecka, G.M., 1986. Removal of 1,4-dioxane from wastewater. Journal of Hazardous Materials, 13(2): 161-168.
Kochany, J. and Lipczynska-Kochany, E., 1992. Application of the EPR spin-trapping technique for the investigation of the reactions of carbonate, bicarbonate, and phosphate anions with hydroxyl radicals generated by the photolysis of H2O2. Chemosphere, 25(12): 1769-1782.
Kolthoff, I.M. and Miller, I.K., 1951. The Chemistry of Persulfate. I. The Kinetics and Mechanism of the Decomposition of the Persulfate Ion in Aqueous Medium. Journal of the American Chemical Society(73): 3055-3059.
Kondo, H., Nakatani, H. and Hiromi, K., 1976. Interaction of Cyclodextrins with Fluorescent-Probes and Its Application to Kinetic Studies of Amylase. Journal of Biochemistry, 79(2): 393-405.
Korom, S.F., McFarland, M.J. and Sims, R.C., 1996. Reduced sediments: A factor in the design of subsurface oxidant delivery systems. Ground Water Monitoring and Remediation, 16: 100--105.
Kosaka, K., Yamada, H., Matsui, S. and Shishida, K., 2000. The effects of the co-existing compounds on the decomposition of micropollutants using the ozone/hydrogen peroxide process. Water Science and Technology, 42(7-8): 353-361.
Kraybill, H.F., 1978. Carcinogenesis induced by trace contaminants in potable water. Bulletin of the New York Academy of Medicine, 54(4): 413.
Krembs, F.J., Siegrist, R.L., Crimi, M.L., Furrer, R.F. and Petri, B.G., 2010. ISCO for Groundwater Remediation: Analysis of Field Applications and Performance. Ground Water Monitoring and Remediation, 30(4): 42-53.
Kwon, S.C. et al., 2012. Treatment characteristic of 1,4-dioxane by ozone-based advanced oxidation processes. Journal of Industrial and Engineering Chemistry, 18(6): 1951-1955.
Lal, M., Schöneich, C., Mönig, J. and Asmus, K.-D., 1988. Rate constants for the reactions of halogenated organic radicals. International journal of radiation biology, 54(5): 773-785.
Lam, S.W., Hermawan, M., Coleman, H.M., Fisher, K. and Amal, R., 2007. The role of copper (II) ions in the photocatalytic oxidation of 1, 4-dioxane. Journal of Molecular Catalysis A: Chemical, 278(1-2): 152-159.
Landy, D., Mallard, I., Ponchel, A., Monflier, E. and Fourmentin, S., 2012a. Cylcodextrins for remediation technologies. In: J.S.a.D.R. Eric Lichtfouse (Editor), Environmental Chemistry for a Sustainable World Volume 1: Nanotechnology and Health Risk. Springer, pp. 47-81.
Landy, D., Mallard, I., Ponchel, A., Monflier, E. and Fourmentin, S., 2012b. Remediation

technologies using cyclodextrins: An overview. Environmental Chemistry Letters, 10: 225--237.
Larsen, T.A., Lienert, J., Joss, A. and Siegrist, H., 2004. How to avoid pharmaceuticals in the aquatic environment. Journal of Biotechnology, 113(1-3): 295-304.
Latimer, W.M., 1938. Oxidation states of the elements and their potentials in aqueous solutions.
Lee, Y. and Lee, W., 2010. Degradation of trichloroethylene by Fe(II) chelated with cross-linked chitosan in a modified Fenton reaction. Journal of Hazardous Materials, 178(1-3): 187-193.
Lewis, S. et al., 2009. Chelate-Modified Fenton Reaction for the Degradation of Trichloroethylene in Aqueous and Two-Phase Systems. Environmental Engineering Science, 26(4): 849-859.
Liang, C., Wang, Z.-S. and Mohanty, N., 2006. Influences of carbonate and chloride ions on persulfate oxidation of trichloroethylene at 20 C. Science of the total environment, 370(2-3): 271-277.
Liang, C.J. and Bruell, C.J., 2008. Thermally activated persulfate oxidation of trichloroethylene: Experimental investigation of reaction orders. Industrial & Engineering Chemistry Research, 47(9): 2912-2918.
Liang, C.J., Bruell, C.J., Marley, M.C. and Sperry, K.L., 2003. Thermally activated persulfate oxidation of trichloroethylene (TCE) and 1,1,1-trichloroethane (TCA) in aqueous systems and soil slurries. Soil & Sediment Contamination, 12(2): 207-228.
Liang, C.J., Huang, C.F., Mohanty, N., Lu, C.J. and Kurakalva, R.M., 2007a. Hydroxypropyl-beta-cyclodextrin-mediated iron-activated persulfate oxidation of trichloroethylene and tetrachloroethylene. Industrial & Engineering Chemistry Research, 46(20): 6466-6479.
Liang, C.J., Wang, Z.S. and Bruell, C.J., 2007b. Influence of pH on persulfate oxidation of TCE at ambient temperatures. Chemosphere, 66(1): 106-113.
Liang, S.H., Kao, C.M., Kuo, Y.C., Chen, K.F. and Yang, B.M., 2011. In situ oxidation of petroleum-hydrocarbon contaminated groundwater using passive ISCO system. water research, 45(8): 2496-2506.
Lim, H.N., Choi, H., Hwang, T.M. and Kang, J.W., 2002. Characterization of ozone decomposition in a soil slurry: kinetics and mechanism. Water Research, 36(1): 219-229.
Lindsey, M.E., Xu, G., Lu, J. and Tarr, M.A., 2003a. Enhanced Fenton degradation of hydrophobic organics by simultaneous iron and pollutant complexation with cyclodextrins. Science of the Total Environment, 307: 215--229.
Lindsey, M.E., Xu, G.X., Lu, J. and Tarr, M.A., 2003b. Enhanced Fenton degradation of hydrophobic organics by simultaneous iron and pollutant complexation with cyclodextrins. Science of the Total Environment, 307(1-3): 215-229.
Lipczynska-Kochany, E., Sprah, G. and Harms, S., 1995. Influence of some groundwater and surface waters constituents on the degradation of 4-chlorophenol by the Fenton reaction. Chemosphere, 30(1): 9-20.
Liu, H.Z., Bruton, T.A., Doyle, F.M. and Sedlak, D.L., 2014. In Situ Chemical Oxidation of Contaminated Groundwater by Persulfate: Decomposition by Fe(III)- and Mn(IV)-Containing Oxides and Aquifer Materials. Environmental Science & Technology, 48(17): 10330-10336.
Loeb, B.L., 2018. Forty Years of Advances in Ozone Technology. A Review of Ozone: Science & Engineering. Ozone-Science & Engineering, 40(1): 3-20.
Lofrano, G., Pedrazzani, R., Libralato, G. and Carotenuto, M., 2017. Advanced Oxidation Processes for Antibiotics Removal: A Review. Current Organic Chemistry, 21(12): 1054-1067.
Mahendra, S., Grostern, A. and Alvarez-Cohen, L., 2013. The impact of chlorinated solvent co-

contaminants on the biodegradation kinetics of 1,4-dioxane. Chemosphere, 91(1): 88-92.
Marble, J.C. et al., 2014. Application of a Persistent Dissolved-Phase Reactive Treatment Zone for Mitigation of Mass Discharge from Sources Located in Lower-Permeability Sediments. Water Air and Soil Pollution, 225(11).
Marble, J.C., Carroll, K.C., Janousek, H. and Brusseau, M.L., 2010. In situ oxidation and associated mass-flux-reduction/mass-removal behavior for systems with organic liquid located in lower-permeability sediments. Journal of contaminant hydrology, 117(1-4): 82--93.
Masten, S.J., 1991. Ozonation of Vocs in the Presence of Humic-Acid and Soils. Ozone-Science & Engineering, 13(3): 287-312.
Masten, S.J. and Davies, S.H.R., 1997. Efficacy of in-situ ozonation for the remediation of PAH contaminated soils. Journal of Contaminant Hydrology, 28(4): 327-335.
Masten, S.J. and Hoigne, J., 1992. Comparison of Ozone and Hydroxyl Radical-Induced Oxidation of Chlorinated Hydrocarbons in Water. Ozone-Science & Engineering, 14(3): 197-214.
Matthieu, D.E. et al., 2013. Intercalation of trichloroethene by sediment-associated clay minerals. Chemosphere, 90(2): 459-463.
Maurino, V., Calza, P., Minero, C., Pelizzetti, E. and Vincenti, M., 1997. Light-assisted 1, 4-dioxane degradation. Chemosphere, 35(11): 2675-2688.
McCray, J.E., Bai, G., Maier, R.M. and Brusseau, M.L., 2001. Biosurfactant-enhanced solubilization of NAPL mixtures. Journal of Contaminant Hydrology, 48(1-2): 45-68.
McCray, J.E., Boving, T.B. and Brusseau, M.L., 2000. Cyclodextrin-enhanced solubilization of organic contaminants with implications for aquifer remediation. Ground Water Monitoring and Remediation, 20(1): 94-103.
McCray, J.E. and Brusseau, M.L., 1998. Cyclodextrin-enhanced in situ flushing of multiple-component immiscible organic liquid contamination at the field scale: Mass removal effectiveness. Environmental Science & Technology, 32(9): 1285-1293.
McCray, J.E. and Brusseau, M.L., 1999. Cyclodextrin enhanced in situ flushing of multiple-component immiscible organic liquid contamination at the field scale: Analysis of dissolution behavior. Environmental Science and Technology, 33(1): 89-95.
Medley, D.R. and Stover, E.L., 1983. Effects of Ozone on the Biodegradability of Biorefractory Pollutants. Journal Water Pollution Control Federation, 55(5): 489-494.
Mehrvar, M., Anderson, W.A. and Moo-Young, M., 2000. Photocatalytic degradation of aqueous tetrahydrofuran, 1, 4-dioxane, and their mixture with TiO2. International Journal of Photoenergy, 2(2): 67-80.
Mehrvar, M., Anderson, W.A. and Moo-Young, M., 2001. Photocatalytic degradation of aqueous organic solvents in the presence of hydroxyl radical scavengers. International Journal of photoenergy, 3(4): 187-191.
Mehrvar, M., Anderson, W.A. and Moo-Young, M., 2002. Comparison of the photoactivities of two commercial titanium dioxide powders in the degradation of 1, 4-dioxane. International journal of photoenergy, 4(4): 141-146.
Miller, C.J., Rose, A.L. and Waite, T.D., 2012. Hydroxyl radical production by H2O2-mediated oxidation of Fe (II) complexed by Suwannee River fulvic acid under circumneutral freshwater conditions. Environmental science & technology, 47(2): 829-835.
Minakata, D., Li, K., Westerhoff, P. and Crittenden, J., 2009. Development of a group contribution method to predict aqueous phase hydroxyl radical (HO•) reaction rate constants. Environmental science & technology, 43(16): 6220-6227.
Mirzaei, A., Chen, Z., Haghighat, F. and Yerushalmi, L., 2017. Removal of pharmaceuticals from

water by homo/heterogonous Fenton-type processes - A review. Chemosphere, 174: 665-688.
Mohr, T.K.G., 2001. Solvent stabilizers. Santa Clara Valley Water District, San Jose, CA.
Mohr, T.K.G., Stickney, J.A. and DiGuiseppi, W.H., 2010. Environmental Investigation and Remediation: 1,4-Dioxane and other Solvent Stabilizers. CRC Press Taylor & Francis.
Mohr, T.K.G., Stickney, J.A. and DiGuiseppi, W.H., 2016. Environmental investigation and remediation: 1, 4-dioxane and other solvent stabilizers. CRC Press.
Moreira, F.C., Boaventura, R.A.R., Brillas, E. and Vilar, V.J.P., 2017. Electrochemical advanced oxidation processes: A review on their application to synthetic and real wastewaters. Applied Catalysis B-Environmental, 202: 217-261.
Mumford, K.G., Lamarche, C.S. and Thomson, N.R., 2004. Natural Oxidant Demand of Aquifer Materials Using the Push-Pull Technique. Journal of Environmental Engineering, 130(October): 1139--1146.
Nakajima, A., Sasaki, H., Kameshima, Y., Okada, K. and Harada, H., 2007. Effect of TiO2 powder addition on sonochemical destruction of 1, 4-dioxane in aqueous systems. Ultrasonics sonochemistry, 14(2): 197-200.
Nakajima, A., Tanaka, M., Kameshima, Y. and Okada, K., 2004. Sonophotocatalytic destruction of 1, 4-dioxane in aqueous systems by HF-treated TiO2 powder. Journal of Photochemistry and Photobiology A: Chemistry, 167(2-3): 75-79.
Nakatani, H. and Hiromi, K., 1984. Kinetic-Study of Beta-Cyclodextrin-Dye System by High-Pressure Temperature-Jump Method. Journal of Biochemistry, 96(1): 69-72.
Nelson, D.W. and Sommers, L.E., 1996. Chapter 34, Total Carbon, Organic Carbon and Organic Matter. In: D.L. Sparks (Editor), Methods of Soil Analysis Part 3 – Chemical Methods. Soil Science Society of America and American Society of Agronomy, 677 S Segoe Rd, Madison, WI 53771.
Nidheesh, P.V., 2017. Graphene-based materials supported advanced oxidation processes for water and wastewater treatment: a review. Environmental Science and Pollution Research, 24(35): 27047-27069.
Ondo, D. et al., 2011. Interaction of Ionic Liquids Ions with Natural Cyclodextrins. Journal of Physical Chemistry B, 115(34): 10285-10297.
Otto, M. and Nagaraja, S., 2007. Treatment technologies for 1, 4-Dioxane: Fundamentals and field applications. Remediation Journal, 17(3): 81-88.
Pennell, K.D., Abriola, L.M. and Loverde, L.E., 1996. The Use of Surfactants to Remediate NAPL-Contaminated Aquifers. In: L. Reddi (Editor), Non-aqueous phase liquids (NAPLs) in subsurface environment : assessment and remediation : proceedings of the specialty conference held in conjunction with the ASCE National Convention. ASCE, Washington, D.C.
Pennell, K.D., Adinolfi, A.M., Abriola, L.M. and Diallo, M.S., 1997. Solubilization of dodecane, tetrachloroethylene, and 1,2-dichlorobenzene in micellar solutions of ethoxylated nonionic surfactants. Environmental Science & Technology, 31(5): 1382-1389.
Pera-Titus, M., Garcia-Molina, V., Banos, M.A., Gimenez, J. and Esplugas, S., 2004. Degradation of chlorophenols by means of advanced oxidation processes: a general review. Applied Catalysis B-Environmental, 47(4): 219-256.
Raj, C.B.C., Ramkumar, N. and Chidambaram, S., 1997. Biodegradation of acetic, benzoic, isophthalic, toluic and terephthalic acids using a mixed culture: effluents of PTA production. Process safety and environmental protection, 75(4): 245-256.
Randazzo, S., Scialdone, O., Brillas, E. and Sirés, I., 2011. Comparative electrochemical

treatments of two chlorinated aliphatic hydrocarbons. Time course of the main reaction by-products. Journal of hazardous materials, 192(3): 1555-1564.
Riga, A., Soutsas, K., Ntampegliotis, K., Karayannis, V. and Papapolymerou, G., 2007. Effect of system parameters and of inorganic salts on the decolorization and degradation of Procion H-exl dyes. Comparison of H2O2/UV, Fenton, UV/Fenton, TiO2/UV and TiO2/UV/H2O2 processes. Desalination, 211(1-3): 72-86.
Rivas, F.J., 2006. Polycyclic aromatic hydrocarbons sorbed on soils: a short review of chemical oxidation based treatments. Journal of Hazardous Materials, 138(2): 234-251.
Ross, A.B., 1975. Selected Specific Rates of Reactions of Transients From Water in Aqueous-Solution - Hydrated Electron, Supplemental Data. Nbs Monograph(43): 1-43.
Rouse, J.D., Sabatini, D.A., Deeds, N.E., Brown, R.E. and Harwell, J.H., 1995. Micellar Solubilization of Unsaturated Hydrocarbon Concentrations As Evaluated By Semiequilibrium Dialysis. Environmental Science & Technology, 29(10): 2484-2489.
Saba, T., Illangasekare, T.H. and Ewing, J., 2001. Investigation of surfactant-enhanced dissolution of entrapped nonaqueous phase liquid chemicals in a two-dimensional groundwater flow field. Journal of Contaminant Hydrology, 51(1-2): 63-82.
Saenger, W., 1980. Cyclodextrin Inclusion-Compounds in Research and Industry. Angewandte Chemie-International Edition in English, 19(5): 344-362.
Salimi, M. et al., 2017. Contaminants of emerging concern: a review of new approach in AOP technologies. Environmental Monitoring and Assessment, 189(8).
Schaerlaekens, J. and Feyen, J., 2004. Effect of scale and dimensionality on the surfactant-enhanced solubilization of a residual DNAPL contamination. Journal of Contaminant Hydrology, 71(1-4): 283-306.
Scheffer, B. and van de Ven, E., 2010. Experiences of Perozone and C-Sparge at Two Former Dry Cleaner Sites in the Netherlands. Ozone-Science & Engineering, 32(2): 130-136.
Schroth, M.H., Ahearn, S.J., Selker, J.S. and Istok, J.D., 1996. Characterization of miller-similar silica sands for laboratory hydrologic studies. Soil Science Society of America Journal, 60(5): 1331-1339.
Schwarzenbach, R.P., Gschwend, P.M. and Imboden, D.M., 2003. Environmental organic chemistry. Wiley, Hoboken, N.J., xiii, 1313 p. pp.
Seol, Y., Zhang, H. and Schwartz, F.W., 2003. A review of in situ chemical oxidation and heterogeneity. Environmental & Engineering Geoscience, 9(1): 37-49.
SERDP, 2006. Final Report: SERDP/ESTCP Expert Panel Workshop on Reducing the Uncertainty of DNAPL Source Zone Remediation, Strategic Environmental Research and Development Program (SERDP)
Setschenow, J.Z., 1889. Uber die konstitution der salzosungenauf grunf auf ihres verhaltens zu kohlensure. Z. Phys. Chem. , 4: 117-125
Shen, W. et al., 2017. Kinetics and operational parameters for 1, 4-dioxane degradation by the photoelectro-peroxone process. Chemical engineering journal, 310: 249-258.
Shiau, B., Davi, A.S. and Harwell, J.H., 1994. Solubilization and Microemulsification of Chlorinated Solvents Using Direct Food Additive (Edible) Surfactants. Ground Water Journal, 32: 561-569.
Shin, J., Lee, Y.C., Ahn, Y. and Yang, J.W., 2012. 1,4-Dioxane degradation by oxidation and sonication in the presence of different-sized ZVI in open-air system. Desalination and Water Treatment, 50(1-3): 102-114.
Shirin, S., Buncel, E. and vanLoon, G.W., 2003. The use of beta-cyclodextrins to enhance the aqueous solubility of trichloroethylene and perchloroethylene and their removal from soil

organic matter: Effect of substituents. Canadian Journal of Chemistry-Revue Canadienne De Chimie, 81(1): 45-52.
Siegrist, R.L., 2001. Principles and practices of in situ chemical oxidation using permanganate. Battelle Press.
Sillanpaa, M., Ncibi, M.C. and Matilainen, A., 2018. Advanced oxidation processes for the removal of natural organic matter from drinking water sources: A comprehensive review. Journal of Environmental Management, 208: 56-76.
Simonich, S.M. et al., 2013. Probabilistic analysis of risks to us drinking water intakes from 1, 4-dioxane in domestic wastewater treatment plant effluents. Integrated environmental assessment and management, 9(4): 554-559.
Skold, M.E., Thyne, G.D., Drexler, J.W., Macalady, D.L. and McCray, J.E., 2008. Enhanced Solubilization of a Metal-Organic Contaminant Mixture (Pb, Sr, Zn, and Perchloroethylene) by Cyclodextrin. Environmental Science & Technology, 42(23): 8930-8934.
Son, H.-S., Choi, S.-B., Khan, E. and Zoh, K.-D., 2006. Removal of 1, 4-dioxane from water using sonication: Effect of adding oxidants on the degradation kinetics. Water research, 40(4): 692-698.
Son, H.-S., Im, J.-K. and Zoh, K.-D., 2009. A Fenton-like degradation mechanism for 1, 4-dioxane using zero-valent iron (Fe0) and UV light. water research, 43(5): 1457-1463.
Stepien, D.K., Diehl, P., Helm, J., Thoms, A. and Püttmann, W., 2014. Fate of 1, 4-dioxane in the aquatic environment: From sewage to drinking water. Water research, 48: 406-419.
Stickney, J.A. et al., 2003. An updated evaluation of the carcinogenic potential of 1, 4-dioxane. Regulatory Toxicology and Pharmacology, 38(2): 183-195.
Stiff, M.J., 1971. Copper/bicarbonate equilibria in solutions of bicarbonate ion at concentrations similar to those found in natural water. Water Research, 5(5): 171-176.
Suh, J.H. and Mohseni, M., 2004. A study on the relationship between biodegradability enhancement and oxidation of 1,4-dioxane using ozone and hydrogen peroxide. Water Research, 38(10): 2596-2604.
Sunder, M. and Hempel, D.C., 1997. Oxidation of tri- and perchloroethene in aqueous solution with ozone and hydrogen peroxide in a tube reactor. Water Research, 31(1): 33-40.
Sung, M.H., Teng, C.H. and Yang, T.H., 2017. Dissolution enhancement and mathematical modeling of removal of residual trichloroethene in sands by ozonation during flushing with micro-nano-bubble solution. Journal of Contaminant Hydrology, 202: 1-10.
Suthersan, S. et al., 2016. Making strides in the management of “emerging contaminants”. Groundwater Monitoring & Remediation, 36(1): 15-25
Suzuki, J., Hukushima, K. and Suzuki, S., 1978. Effect of Ozone Treatment Upon Biodegradability of Water-Soluble Polymers. Environmental Science & Technology, 12(10): 1180-1183.
Szejtli, J., 1998. Introduction and general overview of cyclodextrin chemistry. Chemical Reviews, 98(5): 1743-1753.
Taylor, T.P., Pennell, K.D., Abriola, L.M. and Dane, J.H., 2001. Surfactant enhanced recovery of tetrachloroethylene from a porous medium containing low permeability lenses - 1. Experimental studies. Journal of Contaminant Hydrology, 48(3-4): 325-350.
Tian, G.P., Wu, Q.Y., Li, A., Wang, W.L. and Hu, H.Y., 2014. Enhanced decomposition of 1,4-dioxane in water by ozonation under alkaline condition. Water Sci Technol, 70(12): 1934-40.
Tick, G.R., Lourenso, F., Wood, A.L. and Brusseau, M.L., 2003. Pilot-scale demonstration of

cyclodextrin as a solubility-enhancement agent for remediation of a tetrachloroethene-contaminated aquifer. Environmental Science & Technology, 37(24): 5829-5834.
Tomiyasu, H., Fukutomi, H. and Gordon, G., 1985. Kinetics and Mechanism of Ozone Decomposition in Basic Aqueous-Solution. Inorganic Chemistry, 24(19): 2962-2966.
Toride, N., Leij, F.J. and van Genuchten, M.T., 1999. The CXTFIT code for estimating transport parameters from laboratory or field tracer experiments. Version 2.1. Research Report No. 137, U.S. Salinity Laboratory, USDA, ARS, Riverside, CA. 121 p.
Tsitonaki, A. et al., 2010. In Situ Chemical Oxidation of Contaminated Soil and Groundwater Using Persulfate: A Review. Critical Reviews in Environmental Science and Technology, 40(1): 55-91.
Urynowicz, M.A., 2008. In situ chemical oxidation with permanganate: Assessing the competitive interactions between target and nontarget compounds. Soil & Sediment Contamination, 17(1): 53-62.
Valentine, R.L. and Wang, H.C.A., 1998. Iron oxide surface catalyzed oxidation of quinoline by hydrogen peroxide. Journal of environmental engineering, 124(1): 31-38.
Valocchi, A.J., 1985. Validity of the local equilibrium assumption for modeling sorbing solute transport through homogeneous soils. Water Resources Research, 21(6, June): 808-820.
Veignie, E., Rafin, C., Landy, D., Fourmentin, S. and Surpateanu, G., 2009. Fenton degradation assisted by cyclodextrins of a high molecular weight polycyclic aromatic hydrocarbon benzo[a]pyrene. Journal of Hazardous Materials, 168(2-3): 1296-1301.
Verschueren, K.X., 1985. Handbook of Environmental Data on Organic Chemicals. LWW.
Vescovi, T., Coleman, H.M. and Amal, R., 2010. The effect of pH on UV-based advanced oxidation technologies–1, 4-dioxane degradation. Journal of hazardous materials, 182(1-3): 75-79.
von Sonntag, C. and von Gunten, U., 2012. Chemistry of Ozone in Water and Wastewater Treatment. IWA Publishing, London, 302 pp.
Waldemer, R.H. and Tratnyek, P.G., 2006. Kinetics of contaminant degradation by permanganate. Environmental Science & Technology, 40(3): 1055-1061.
Waldemer, R.H., Tratnyek, P.G., Johnson, R.L. and Nurmi, J.T., 2007. Oxidation of chlorinated ethenes by heat-activated persulfate: Kinetics and products. Environmental Science & Technology, 41(3): 1010-1015.
Wang, A.S. and Matsui, Y., 1994. Solvent Isotope Effect on the Complexation of Cyclodextrins in Aqueous-Solutions. Bulletin of the Chemical Society of Japan, 67(11): 2917-2920.
Wang, H.J. et al., 2015. Kinetics and energy efficiency for the degradation of 1,4-dioxane by electro-peroxone process. Journal of Hazardous Materials, 294: 90-98.
Wang, J., Zhang, X. and Li, G.H., 2012. Effects of ozonation on soil organic matter of contaminated soil containing residual oil. Journal of Soils and Sediments, 12(2): 117-127.
Wang, J.M., Marlowe, E.M., Miller-Maier, R.M. and Brusseau, M.L., 1998. Cyclodextrin-enhanced biodegradation of phenanthrene. Environmental Science & Technology, 32(13): 1907-1912.
Wang, X.J. and Brusseau, M.L., 1993. Solubilization of Some Low-Polarity Organic-Compounds by Hydroxypropyl-Beta-Cyclodextrin. Environmental Science and Technology, 27(13): 2821-2825.
Wang, X.J. and Brusseau, M.L., 1995. Simultaneous Complexation of Organic-Compounds and Heavy-Metals by a Modified Cyclodextrin. Environmental Science & Technology, 29(10): 2632-2635.
Wang, X.J. and Brusseau, M.L., 1998. Effect of pyrophosphate on the dechlorination of

tetrachloroethene by the Fenton reaction. Environmental Toxicology and Chemistry, 17(9): 1689-1694.
Watts, R.J., Finn, D.D., Cutler, L.M., Schmidt, J.T. and Teel, A.L., 2007. Enhanced stability of hydrogen peroxide in the presence of subsurface solids. Journal of Contaminant Hydrology, 91(3-4): 312-326.
Wei, C.H., Zhang, F.Z., Hu, Y., Feng, C.H. and Wu, H.Z., 2017. Ozonation in water treatment: the generation, basic properties of ozone and its practical application. Reviews in Chemical Engineering, 33(1): 49-89.
West, C.C. and Harwell, J.H., 1992. Surfactants and Subsurface Remediation. Environmental Science & Technology, 26(12): 2324-2330.
Xu, M., Gu, X., Lu, S., Qiu, Z. and Sui, Q., 2014. Role of reactive oxygen species for 1, 1, 1-trichloroethane degradation in a thermally activated persulfate system. Industrial & Engineering Chemistry Research, 53(3): 1056-1063.
Xu, X. and Thomson, N.R., 2009. A long-term bench-scale investigation of permanganate consumption by aquifer materials. Journal of Contaminant Hydrology, 110: 73--86.
Xu, X.Y. and Thomson, N.R., 2010. Hydrogen Peroxide Persistence in the Presence of Aquifer Materials. Soil & Sediment Contamination, 19(5): 602-616.
Yan, N., Liu, F., Chen, Y.F. and Brusseau, M.L., 2016. Influence of Groundwater Constituents on 1,4-Dioxane Degradation by a Binary Oxidant System. Water Air and Soil Pollution, 227(12).
Yan, N., Liu, F. and Huang, W., 2013. Interaction of oxidants in siderite catalyzed hydrogen peroxide and persulfate system using trichloroethylene as a target contaminant. Chemical engineering journal, 219: 149-154.
Yan, N. et al., 2015. Degradation of trichloroethene by siderite-catalyzed hydrogen peroxide and persulfate: Investigation of reaction mechanisms and degradation products. Chemical Engineering Journal, 274: 61-68.
Yang, J.S., Baek, K., Kwon, T.S. and Yang, J.W., 2006. Competitive immobilization of multiple component chlorinated solvents by cyclodextrin derivatives. Journal of Hazardous Materials, 137(3): 1866-1869.
Yeom, I.T., Ghosh, M.M., Cox, C.D. and Robinson, K.G., 1995. Micellar Solubilization of Polynuclear Aromatic-Hydrocarbons in Coal Tar-Contaminated Soils. Environmental Science & Technology, 29(12): 3015-3021.
Zalibera, M., Rapta, P., Staško, A., Brindzová, L. and Brezová, V., 2009. Thermal generation of stable spin trap adducts with super-hyperfine structure in their EPR spectra: An alternative EPR spin trapping assay for radical scavenging capacity determination in dimethylsulphoxide. Free radical research, 43(5): 457-469.
Zeng, Q., Dong, H., Wang, X., Yu, T. and Cui, W., 2017. Degradation of 1, 4-dioxane by hydroxyl radicals produced from clay minerals. Journal of hazardous materials, 331: 88-98.
Zenker, M.J., Borden, R.C. and Barlaz, M.A., 2003. Occurrence and Treatment of 1,4-Dioxane in Aqueous Environments. Environmental Engineering Science, 20(5): 423--432.
Zhang, S., Gedalanga, P.B. and Mahendra, S., 2016. Biodegradation Kinetics of 1,4-Dioxane in Chlorinated Solvent Mixtures. Environmental Science & Technology, 50(17): 9599-9607.
Zhang, S., Gedalanga, P.B. and Mahendra, S., 2017. Advances in bioremediation of 1,4-dioxane-contaminated waters. Journal of Environmental Management, In Press.
Zhang, T. et al., 2014. Efficient Peroxydisulfate Activation Process Not Relying on Sulfate Radical Generation for Water Pollutant Degradation. Environmental Science & Technology, 48(10): 5868-5875.

Zhang, T., Zhu, H. and Croué, J.-P., 2013. Production of Sulfate Radical from Peroxymonosulfate Induced by a Magnetically Separable CuFe2O4 Spinel in Water: Efficiency, Stability, and Mechanism. Environmental Science & Technology, 47(6): 2784-2791.
Zhao, B.W., Chen, X.M., Zhu, K. and Zhu, L.Z., 2007. Micellar solubilization of TCE and PCE by mixed surfactant: Effects of surfactant partitioning and DNAPL mixing (Retracted article. See vol. 327, pg. 144, 2008). Colloids and Surfaces a-Physicochemical and Engineering Aspects, 296(1-3): 167-173.
Zhao, Q.X. et al., 2017. Metal-free carbon materials-catalyzed sulfate radical-based advanced oxidation processes: A review on heterogeneous catalysts and applications. Chemosphere, 189: 224-238.
Zhong, H. et al., 2015. In-situ activation of persulfate by iron filings and degradation of 1,4-dioxane. Water Research, 83: 104-111.
Zhou, L., Song, W., Chen, Z. and Yin, G., 2013. Degradation of Organic Pollutants in Wastewater by Bicarbonate-Activated Hydrogen Peroxide with a Supported Cobalt Catalyst. Environmental Science & Technology, 47(8): 3833-3839.

7. APPENDICES

7.1 Supplementary Data

Refined data collected during the research project are provided in the Results and Discussion section above in the form of tables and graphs. Additional supporting information is available in the journal publications listed below and the supplemental data included below.

1.1 Cyclodextrin Inclusion Complex Measurement Background (Ozone Stabilized by Cyclodextrin)

Khan, N.A., Johnson, M.D., Carroll, K.C. (2018) Spectroscopic Methods for Aqueous Cyclodextrin Inclusion Complex Binding Measurement for 1,4-dioxane, Chlorinated Co-Contaminants, and Ozone. Journal of Contaminant Hydrology.

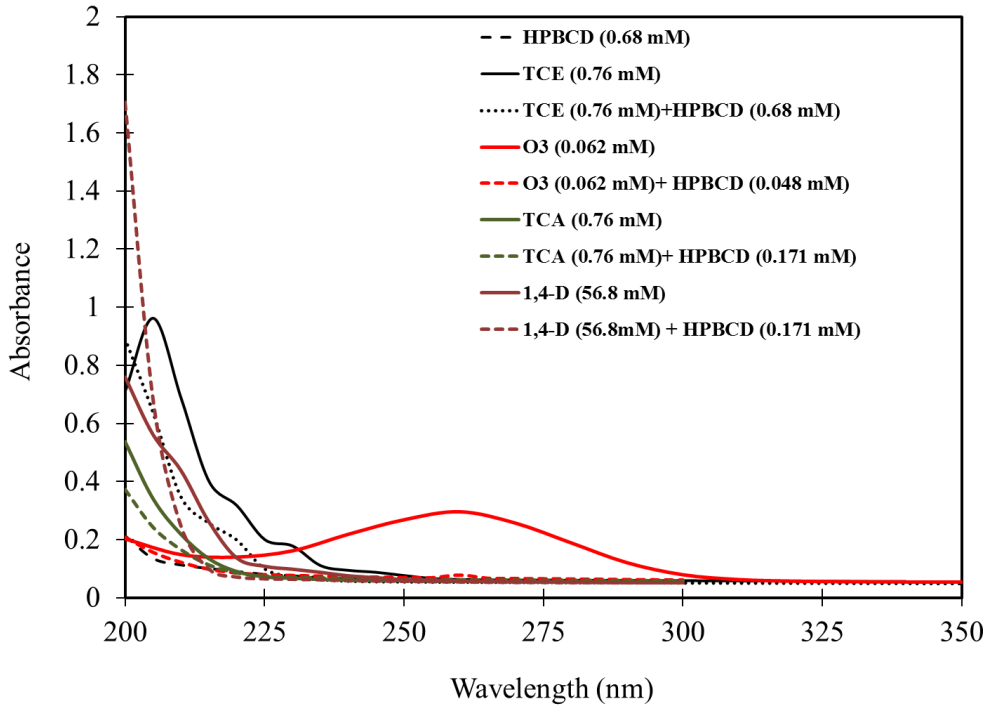

Fig. S1. UV-vis spectroscopy absorbance versus wavelength for 1,4-D, co-contaminants and O_3 with and without HPβCD. Shift of UV spectra for TCE and O_3 observed upon addition of HPβCD.

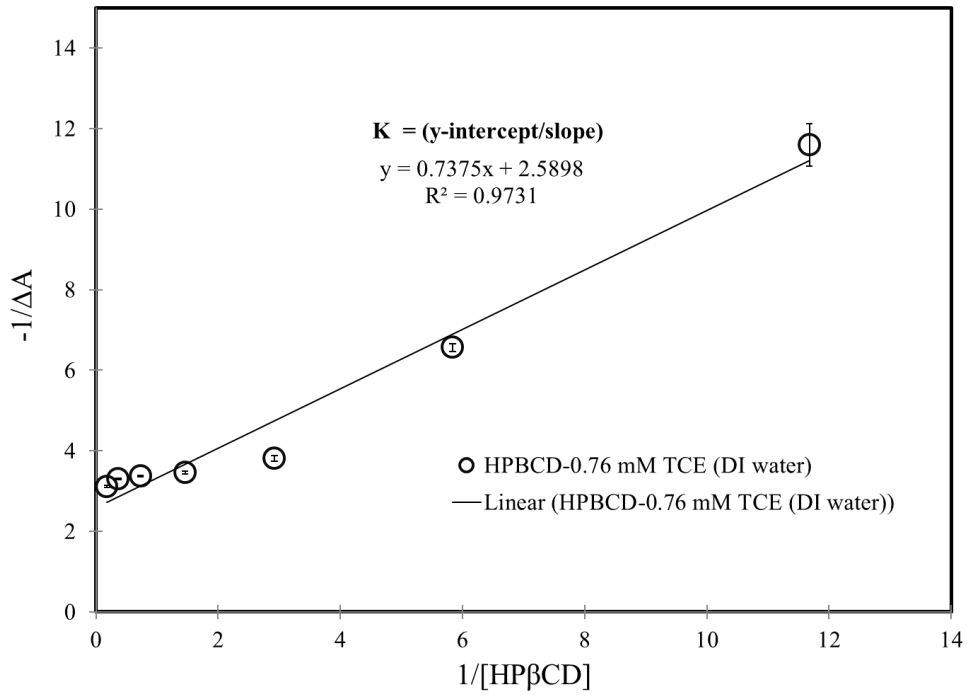

Fig. S2. Benesi-Heldibrand plot illustrating repeatability with mean values plotted with standard deviation error bars calculated from three repeat experiments.

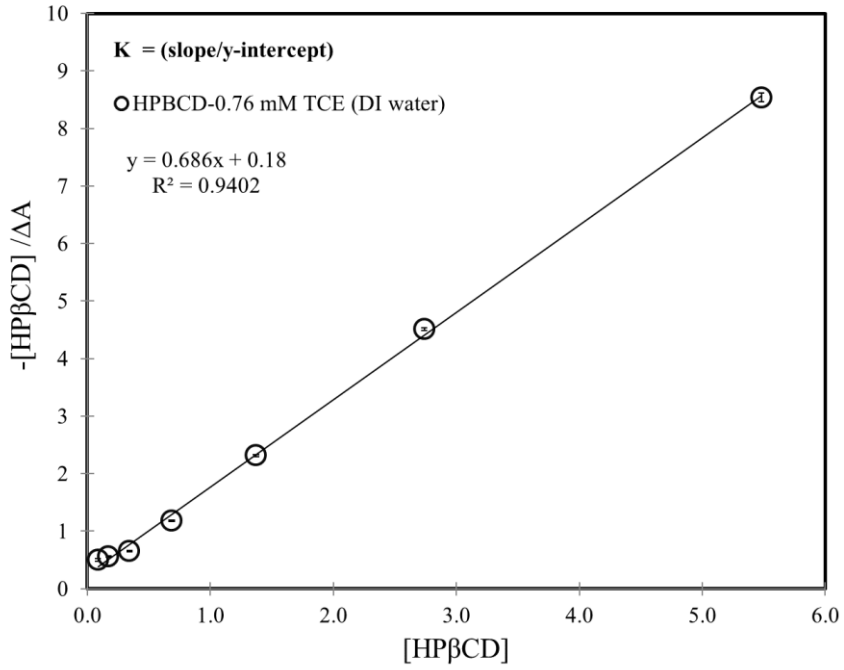

Fig. S3. Scott's plot illustrating repeatability with mean values plotted with standard deviation error bars calculated from three repeat experiments.

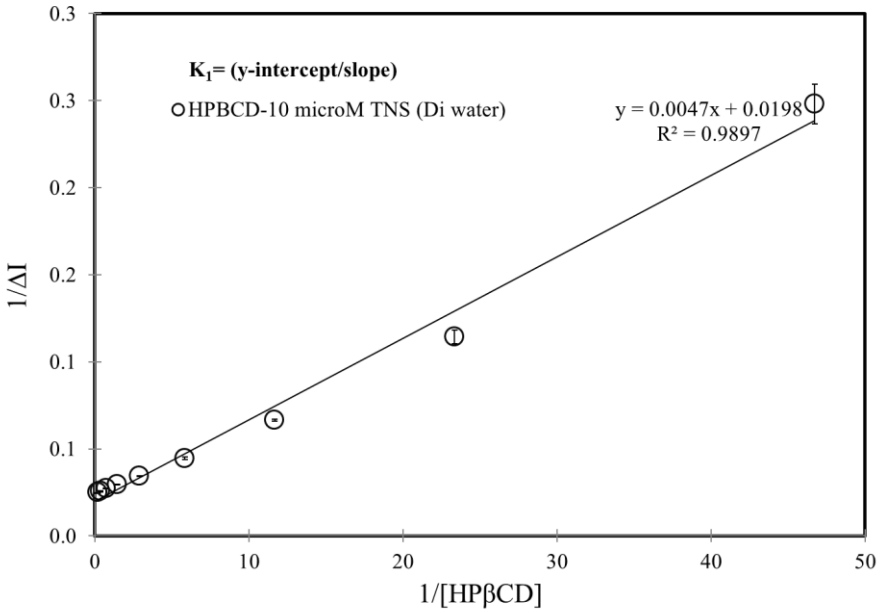

Fig. S4. Benesi-Heldibrand plot for TNS illustrating repeatability with mean values plotted with standard deviation error bars calculated from six repeat experiments.

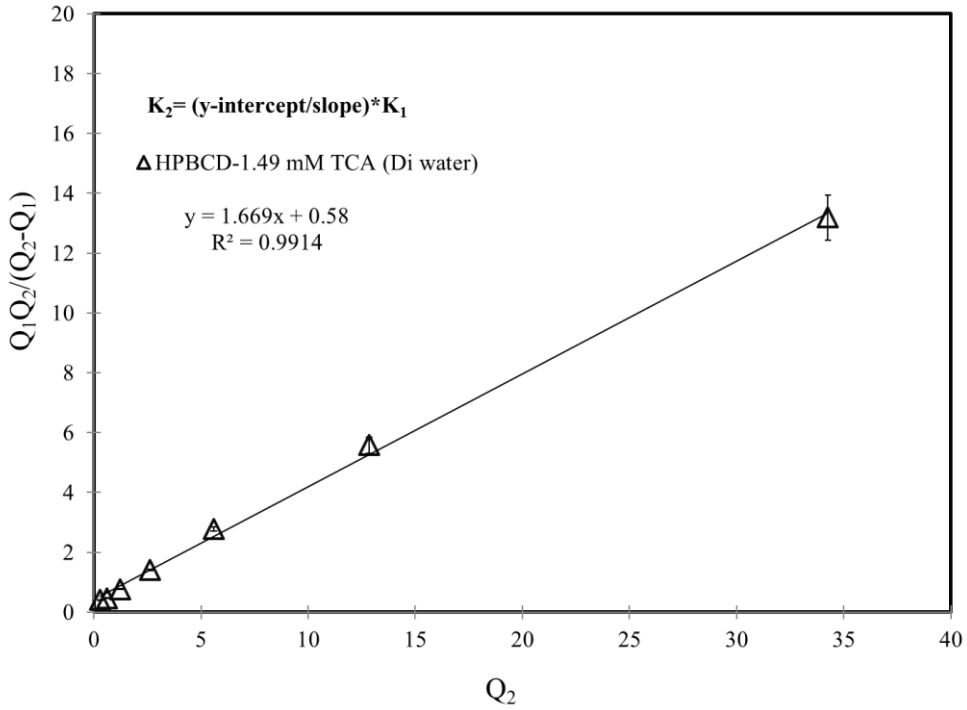

Fig. S4. Competitive complexation plot for TCA and TNS illustrating repeatability with mean values plotted with standard deviation error bars calculated from six repeat experiments.

1.2 Cyclodextrin Enhanced Ozonation of 1,4-Dioxane Background (Ozone Stabilized by Cyclodextrin)

Khan, N.A., Johnson, M.D., Holguin, F.O., Dungan, B., Carroll, K.C. (In Review) Cyclodextrin-Enhanced Treatment Kinetics for 1,4-dioxane and Chlorinated Co-Contaminants Using Stabilized Aqueous Ozone. Journal of Hazardous Materials.

Supplementary Results:

Experimental control results

Control experiments were conducted for each contaminant compound without oxidant addition, and control experiments were conducted with 1,4-D with and without HPβCD when no oxidant was added.

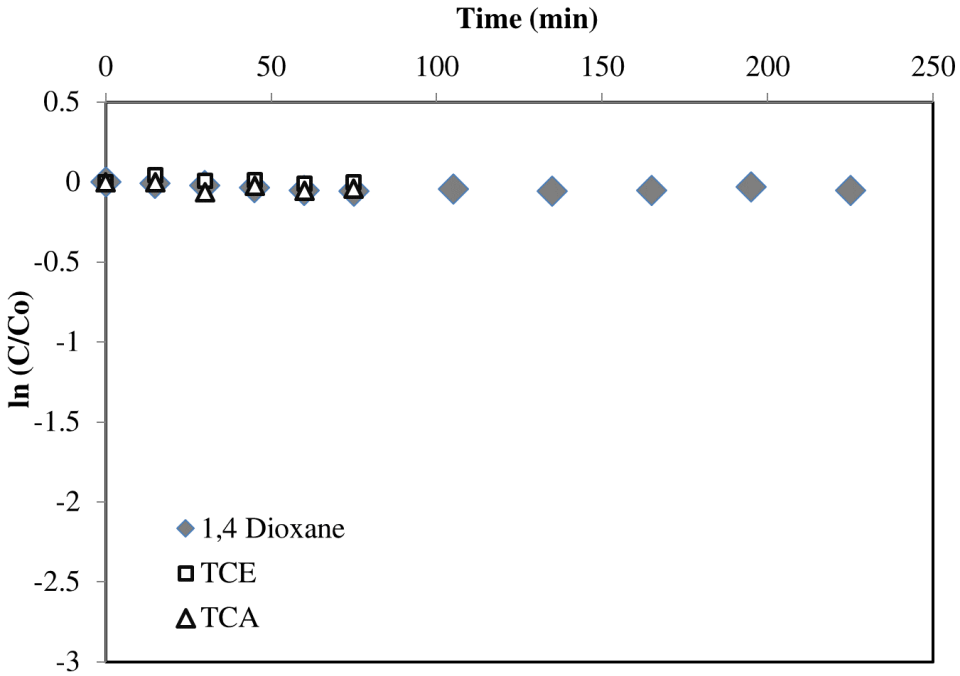

Fig. S1. Removal kinetics of 1,4-dioxane, TCE, and TCA in control experiments without O_3 as single contaminant systems.

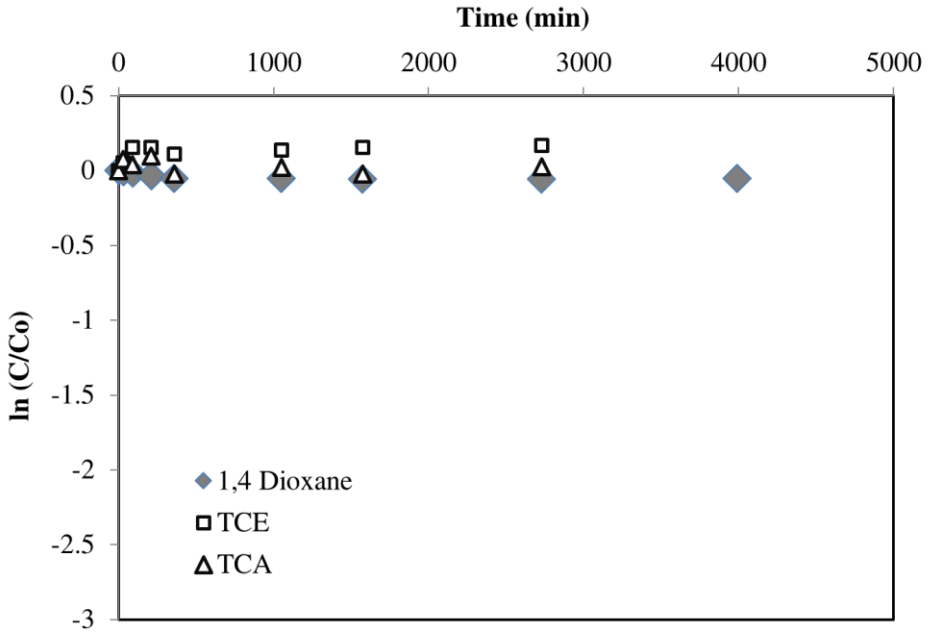

Fig. S2. Removal kinetics of 1,4-dioxane, TCE, and TCA in control experiments without O_3 as multiple contaminant systems.

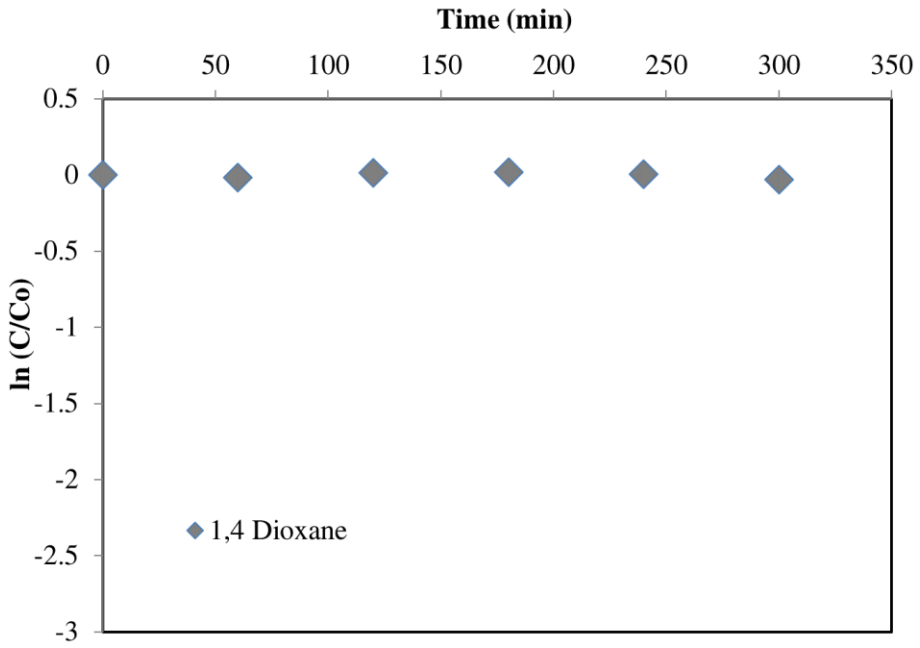

Fig. S3. Removal kinetics of 1,4-dioxane in control experiment without O_3 with and without HPβCD.

Transformation reaction products

Byproducts from 1,4-D and O_3 reactions produced during kinetic experiments and identified by gas chromatography mass spectrometry:

Organic acid	Aldehyde or organic aldehyde	Other compounds
Amino methane sulfonic acid	Acetamide, 2,2-dichloro-	1,3-Dioxolane, 4-ethyl-
Benzoic acid, 2-methoxy-, 2-oxo-2-phenylethyl ester		
Phthalic acid, cyclohexyl methyl 4-isopropylphenyl ester	4-Ethylbenzamide	Diethylene glycol, trimethylsilyl ether
4-Ethylbenzoic acid, 1-(cyclopentyl)ethyl ester	Acetaldehyde	Oxalic acid

Barndok et. al., (2014) observed ethylene glycol and oxalic acids as a byproduct of O_3 and 1,4-D reaction at high pH 9.

Klecka et. al., (1986), mentioned that organic acids and aldehydes with low molecular weight are usually form as a byproduct of 1,4-D and O_3 reaction.

Adams et. al., (1994) found 1,3-dioxolane as a byproduct during oxidation of 1,4-D by O_3 with H_2O_2.

Single component contaminant removal kinetics

The pseudo 1st order kinetic plots are presented below (Fig. S1 and S2) for TCE and TCA in single component experiments, and the slope of the regression lines presents the rate constant results.

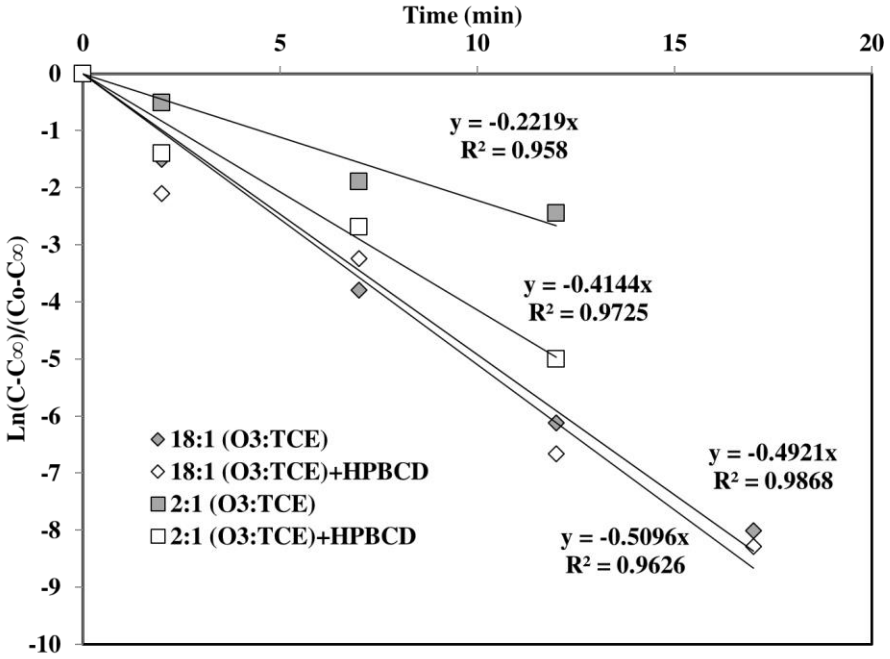

Fig. S4. Removal kinetics of TCE using O_3 with and without HPβCD in single contaminant systems at various oxidant to contaminant ratios. At the higher oxidant to contaminant ratio TCE was degraded too fast to measure the reaction rate. Symbols indicate mean values, and lines present regression results used for pseudo 1st order kinetic analysis.

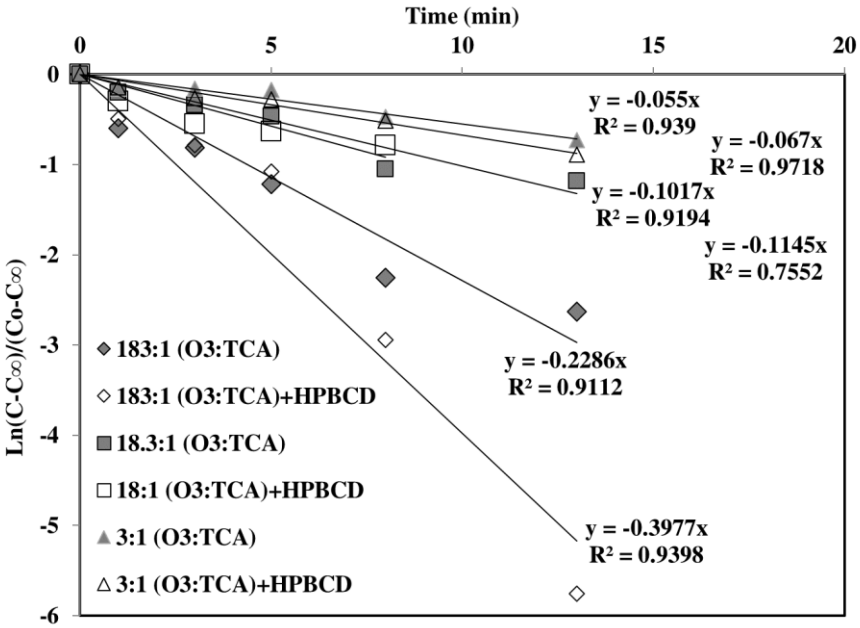

Fig. S5. Removal kinetics of TCA using O_3 with and without HPβCD in single contaminant systems at various oxidant to contaminant ratios.

Multiple component contaminant removal kinetics

Fig. S3 presents the multicomponent experiment data and psuedo 1st order rate analysis results for 1,4-D and TCA with and without HPβCD.

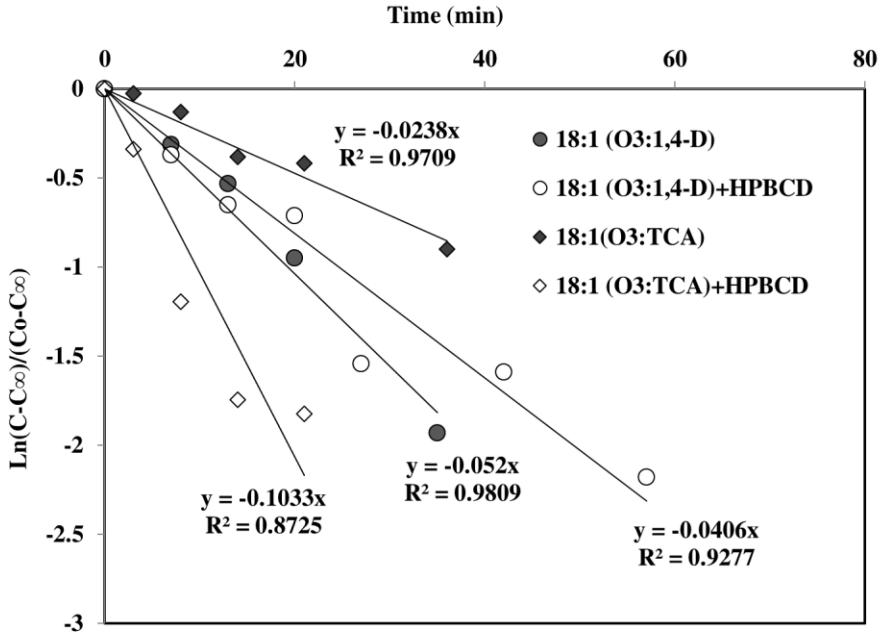

Fig. S6. Removal kinetics for 1,4-D using O_3 with and without HPβCD in multiple contaminant systems at 18:1 oxidant to contaminant ratios. TCE degraded too fast in multiple contaminant system using both O_3 with and without HPβCD to measure the removal rate constant.

Impact of initial pH value on contaminant removal kinetics

Fig. S4 and S5 present experiment data and psuedo 1st order rate analysis results for 1,4-D with and without HPβCD for 3 pH values. The 3 pH value results with and without HPβCD for TCE are all presented in Fig. S6, and Fig. S7 and S8 present experiment data and psuedo 1st order rate analysis results for TCA with and without HPβCD for 3 pH values.

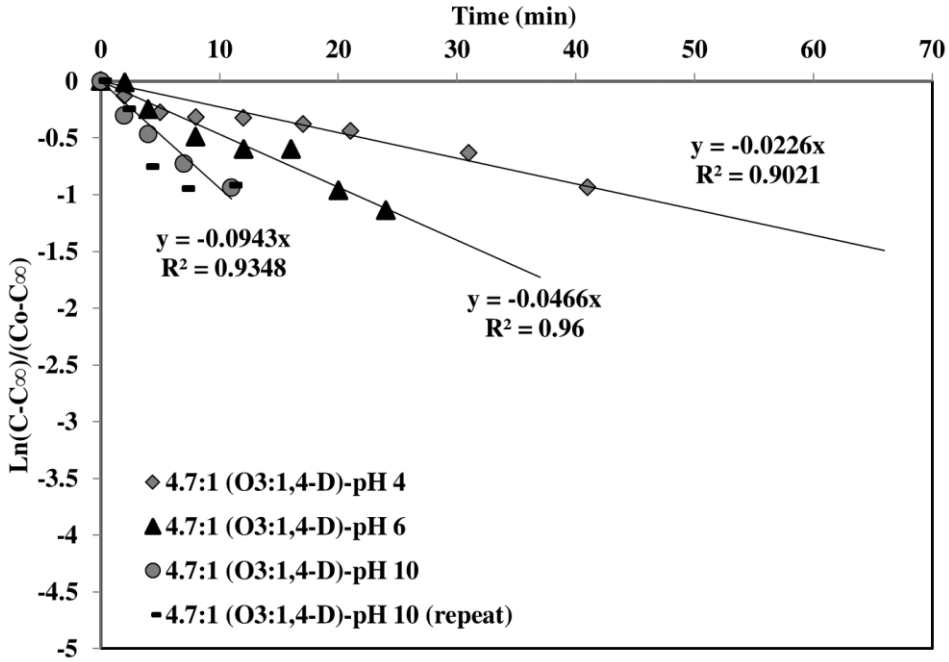

Fig. S7. Removal kinetics for 1,4-D using O_3 without HPβCD in multiple contaminant systems over a range of different initial pH values.

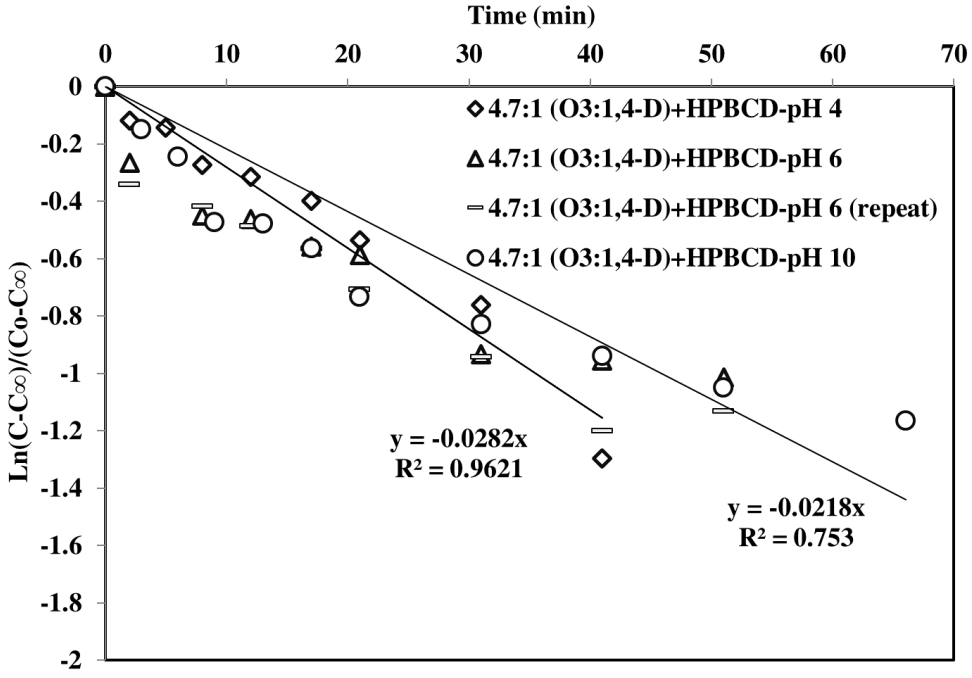

Fig. S8. Removal kinetics for 1,4-D using O_3 with HPβCD in multiple contaminant systems over a range of different initial pH values.

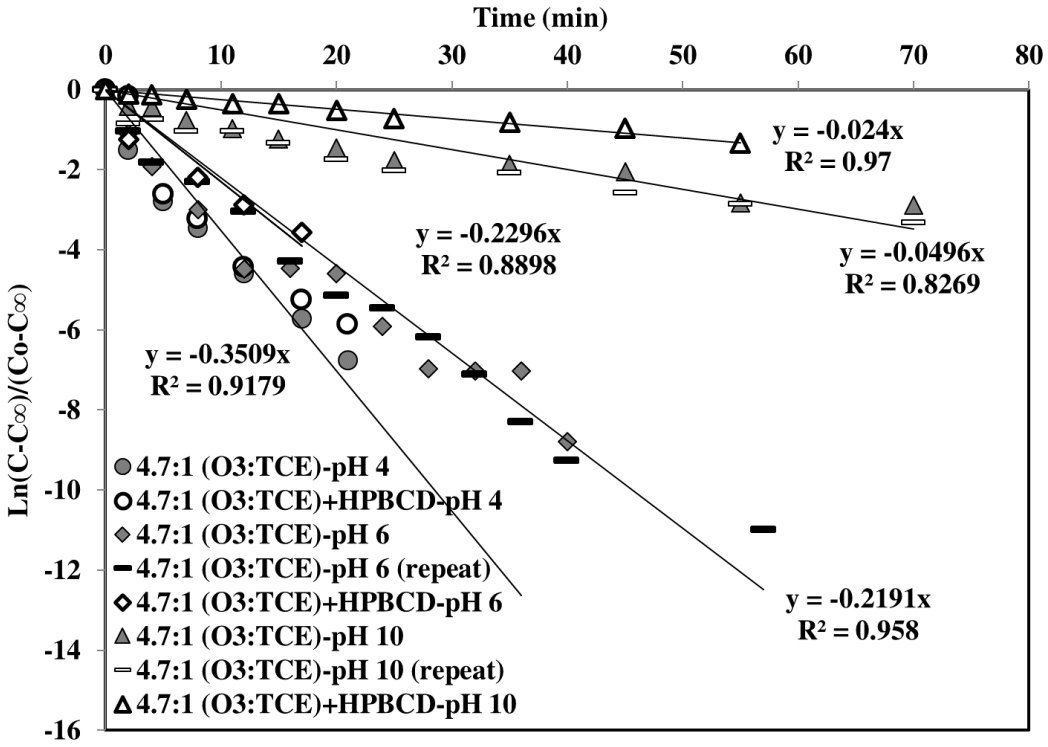

Fig. S9. Removal kinetics for TCE using O_3 with and without HPβCD over a range of different initial pH values

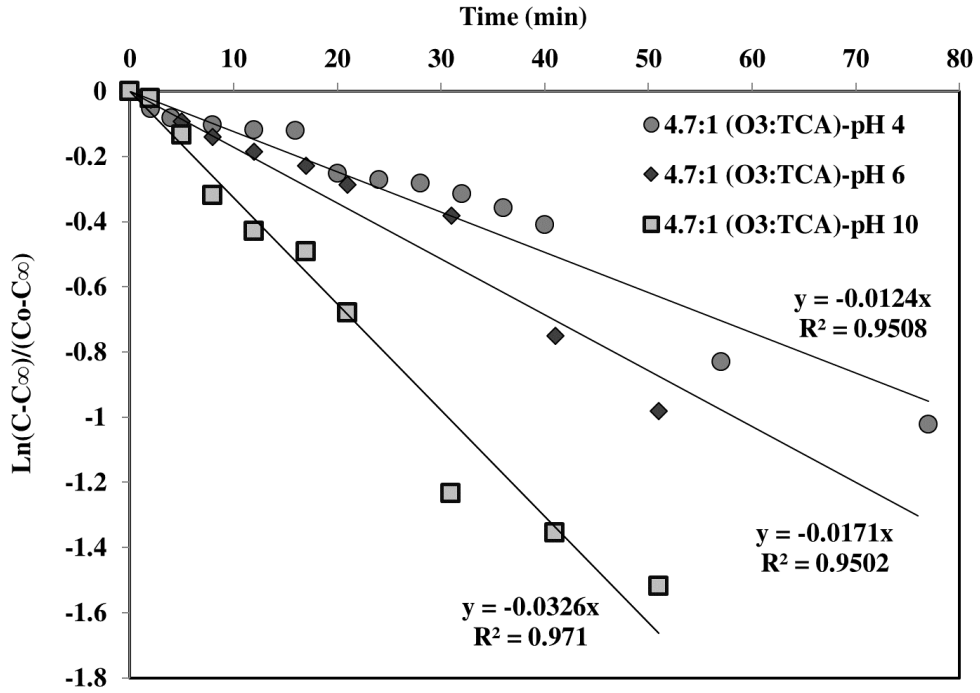

Fig. S10. (A) Removal kinetics for TCA using O_3 without HPβCD at three different pH in multiple contaminant systems for 4.7:1 oxidant to contaminant ratio.

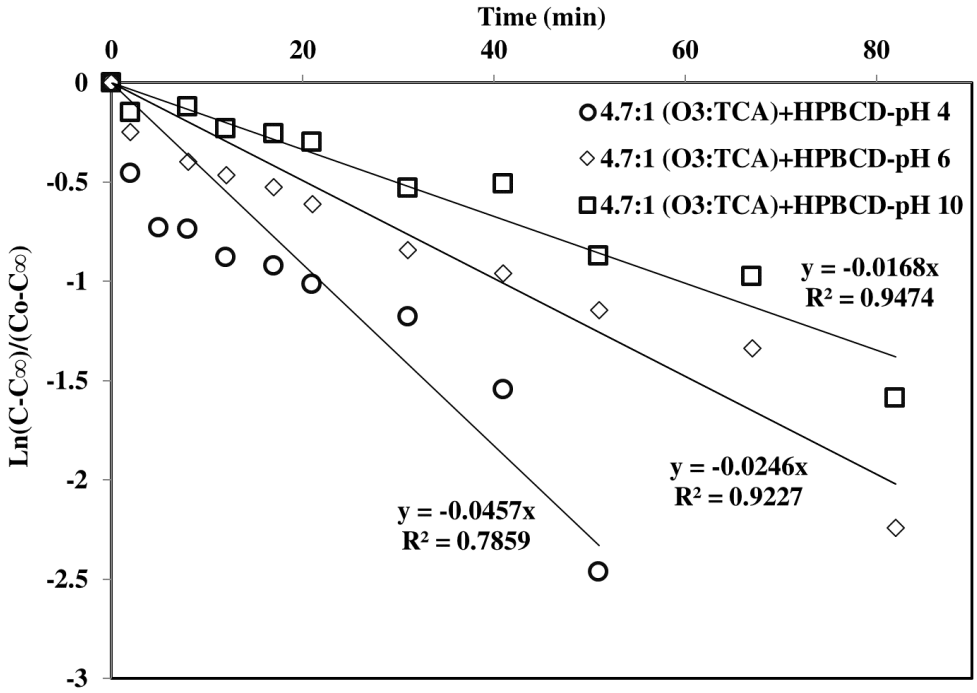

Fig. S11. Removal kinetics for TCA using O_3 with HPβCD at three different pH in multiple contaminant systems for 4.7:1 oxidant to contaminant ratio.

Impact of salt additions on contaminant removal kinetics

Fig. S9 shows UV absorbance spectrophotometry versus wavelength for solutions of HPβCD, 1,4-D, and 1,4-D with HPβCD for DI water and 100 mM NaCl solutions. Fig. S10 and S11 present single and multicomponent (respectively) experiment data and psuedo 1st order rate analysis results for 1,4-D with and without HPβCD with and without salt additions. The impact of two types of salt additions on TCE removal kinetics are all presented in Fig. S12, and Fig. S13 present experiment data and psuedo 1st order rate analysis results for TCA with and without HPβCD and with and without salt additions.

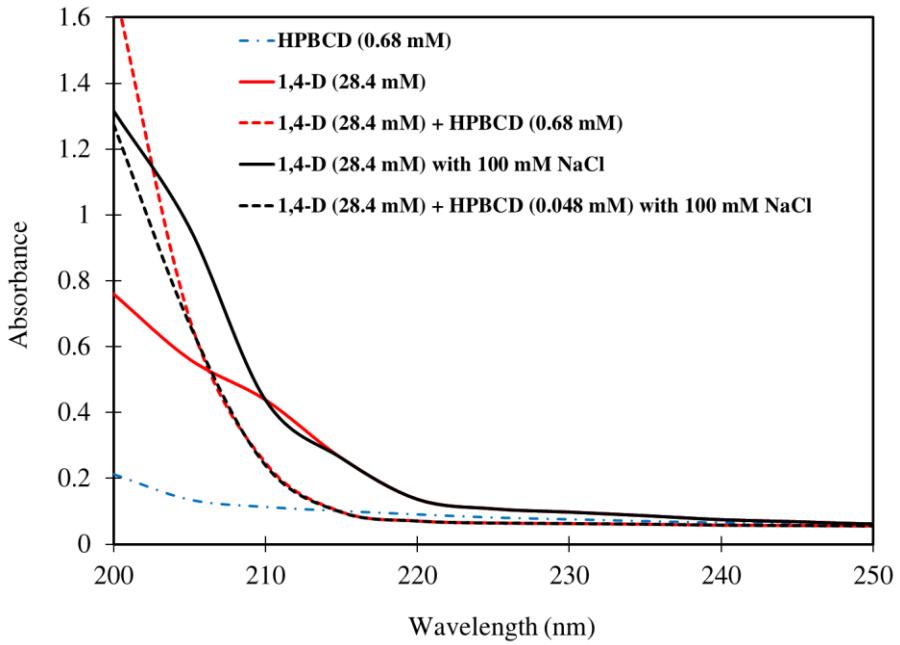

Fig. S12. UV absorbance versus wavelength for solutions of HPβCD, 1,4-D, and 1,4-D with HPβCD for DI water and 100 mM NaCl solutions. Changes in absorbance with HPβCD addition and the isosbestic cross over point both indicate that 1,4-D forms inclusion complex with HPβCD.

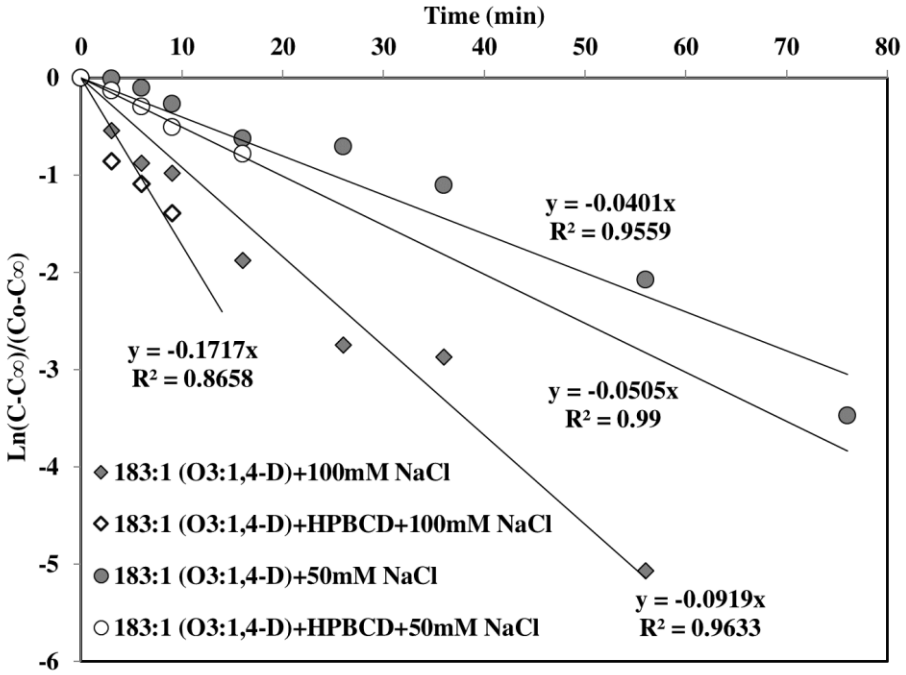

Fig. S13. Removal kinetics concentration removal for 1,4-D using O_3 (183:1 oxidant to contaminant ratio) with and without HPβCD in presence of two different NaCl concentrations in single contaminant systems.

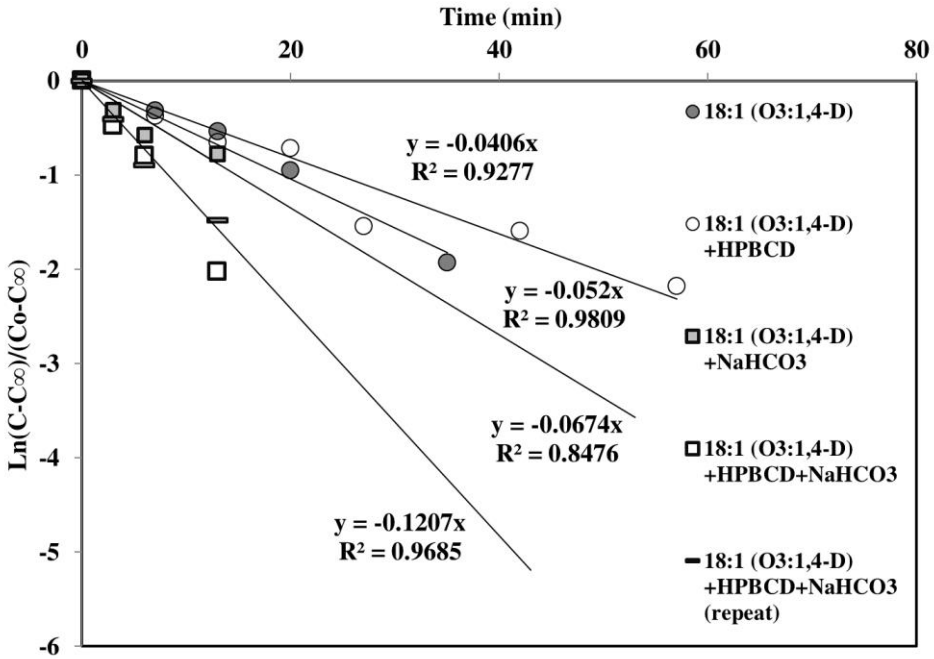

Fig. S14. Removal kinetics for 1,4-D using O_3 (18:1 oxidant to contaminant ratio) with and without HPβCD in presence of NaCl or $NaHCO_3$ in multiple contaminant systems.

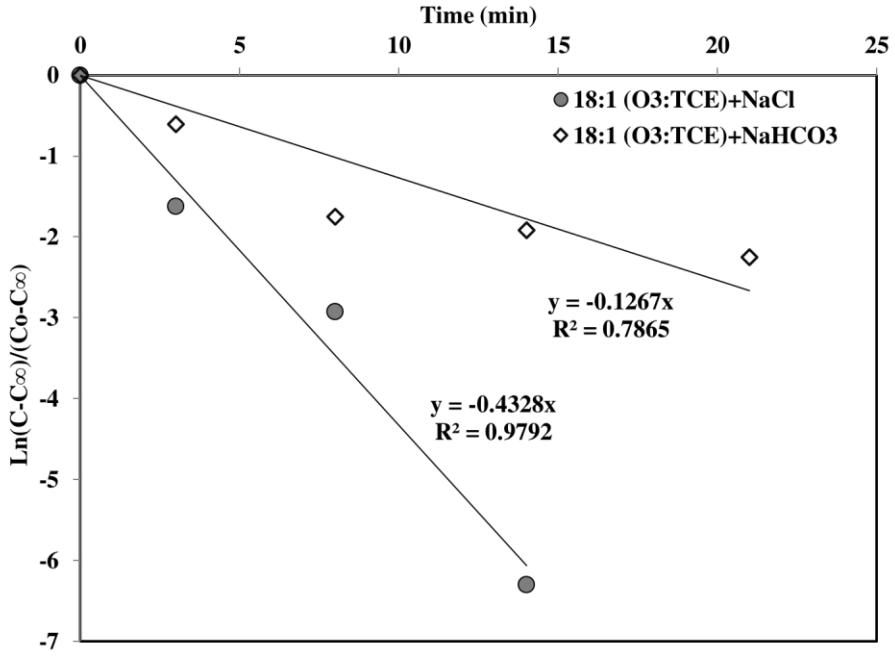

Fig. S15. Removal kinetics for TCE using O_3 (18:1 oxidant to contaminant ratio) without HPβCD in presence of NaCl or $NaHCO_3$ in multiple contaminant systems. All reactions with HPβCD reacted too quickly to determine rate constant values.

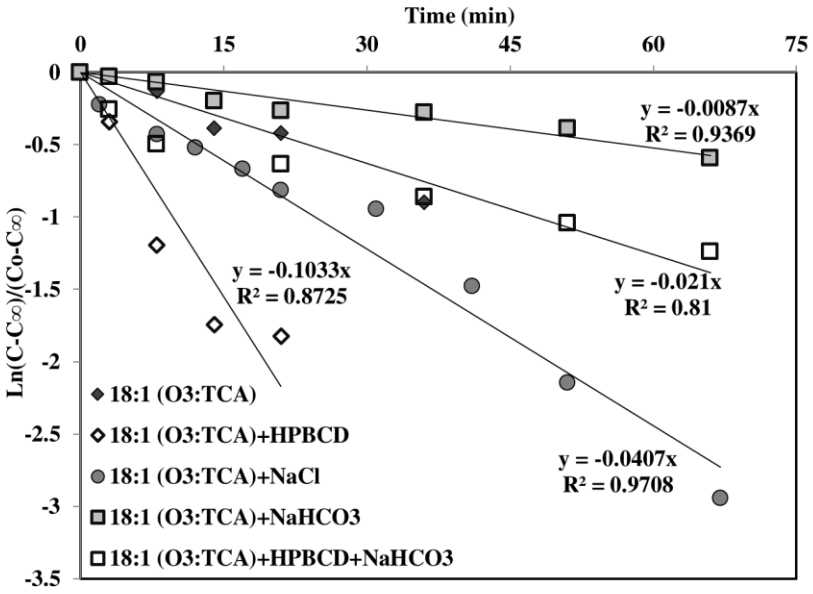

Fig. S16. Removal kinetics for TCA using O_3 (18:1 oxidant to contaminant ratio) with and without HPβCD in presence of NaCl or $NaHCO_3$ in multiple contaminant systems.

1.3 Peroxone Activated Persulfate Treatment of 1,4-Dioxane Background (Peroxone Activated Persulfate)

Eberle, D., Ball, R., Boving, T.B. (2016) Peroxone activated persulfate treatment of 1,4-dioxane in the presence of chlorinated solvent co-contaminants. Chemosphere 144:728-735.

Supplementary Material

The purge and trap method used for the analysis of 1,4-dioxane is based on methods developed by Draper et al. (2000), OI Analytical (2006), and Environmental Laboratory Services (2009).

Settings	Time/Temp
Trap:	
Trap Type:	#7 (Tenax)
Sample Temp:	
Sparge Mount:	40 C
Sample:	35 C
Purge Times & Temp:	
Purge Time:	11 min
Dry Purge Time:	1 min
Trap Temp:	40 C
Water Management Temps:	
Purge:	120 C
Desorb:	40 C
Bake:	240 C
Bake:	
Bake Time:	10 min
Trap Temp:	210 C
Desorb Time & Temp:	
Desorb Time:	0.5 min
Trap Temp:	190 C
Desorb Preheat:	
Trap Temp:	125 C
Heated Zones:	
Transfer Line:	120 C
Valve Oven:	120 C

Table S1: Purge and trap conditions for 1,4-dioxane analysis

Injector Temp:	240ºC
Interface Temp:	230ºC
Oven Temp:	45ºC (hold 4.5 min.) to 100ºC @ 12ºC/min. to 240ºC (hold 1.3 min) @ 25ºC/min.
Column Inlet Pressure:	31.3 kPa
Column Flow:	0.8 mL/min
Linear Velocity:	31.5 cm/sec
Split Ratio:	35
Total Flow:	28 mL/min
Detector:	SIM mode, m/z (88, 58, 96, 64, 46)

Table S2: GCMS conditions for 1,4-dioxane analysis

Settings	Time/Temp
Trap:	
Trap Type:	#7 (Tenax)
Sample Temp:	
Sparge Mount:	40 C
Sample:	30 C
Purge Times & Temp:	
Purge Time:	11 min
Dry Purge Time:	N/A
Trap Temp:	20 C
Water Management Temps:	
Purge:	100 C
Desorb:	Ambient
Bake:	240 C
Bake:	
Bake Time:	5 min
Trap Temp:	200 C
Desorb Time & Temp:	
Desorb Time:	0.5 min
Trap Temp:	180 C
Desorb Preheat:	
Trap Temp:	170 C
Heated Zones:	
Transfer Line:	120 C
Valve Oven:	120 C

Table S3: Purge and trap conditions for TCE and 1,1,1-TCA analysis

Injector Temp:	225ºC
Interface Temp:	230ºC
Oven Temp:	35ºC (hold 5 min.) to 60ºC @ 11ºC/min. to 220ºC (hold 2.0 min) @ 20ºC/min.
Column Inlet Pressure:	86.9 kPa
Column Flow:	1.6 mL/min
Linear Velocity:	45.6 cm/sec
Split Ratio:	15
Total Flow:	26.7 mL/min
Detector:	Scan mode, m/z (41-300)

Table S4: GCMS conditions for TCE and 1,1,1-TCA analysis

ORP and pH in 72 h 1,4-dioxane Single-Contaminant Oxidation Experiment:

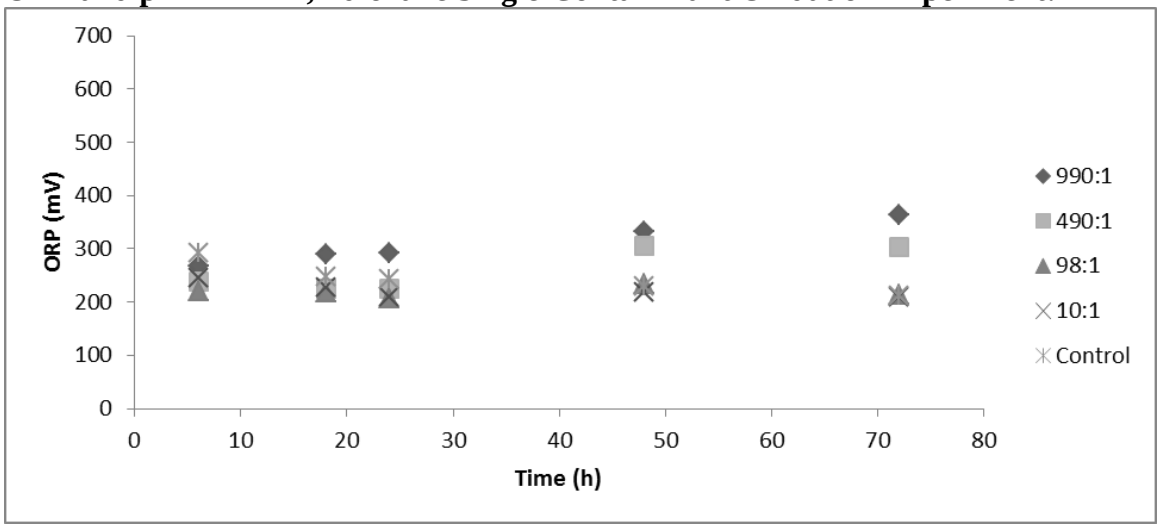

Figure S1: ORP in 72 hour 1,4-dioxane single-contaminant oxidation experiment

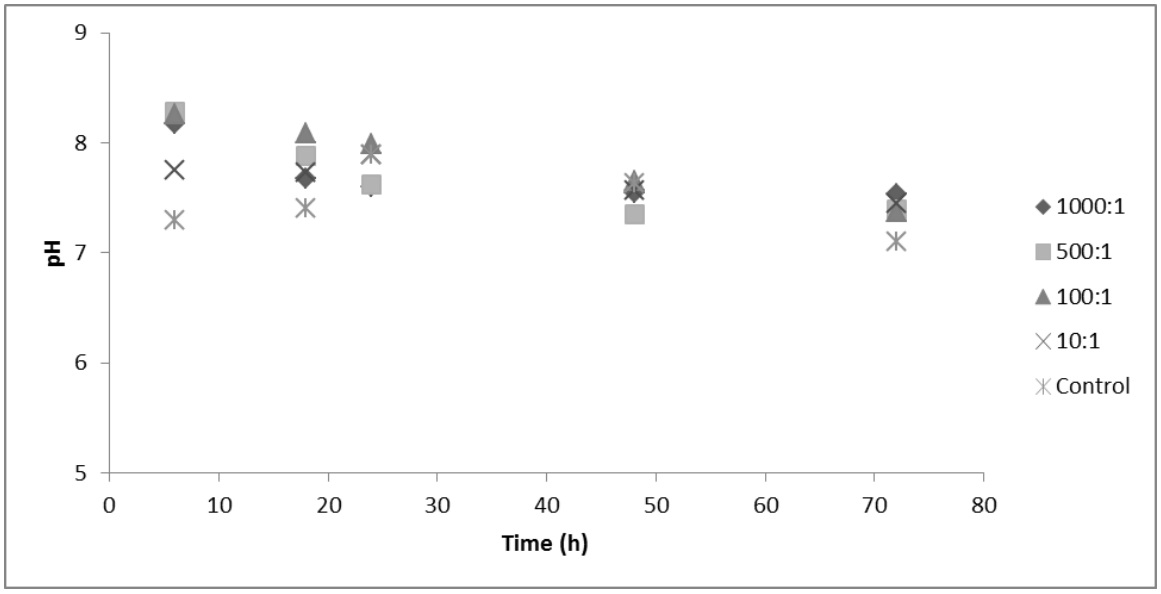

Figure S2: pH in 72 hour 1,4-dioxane single-contaminant oxidation experiment

ORP and pH in 312 h 1,4-Dioxane Single-Contaminant Oxidation Experiment:

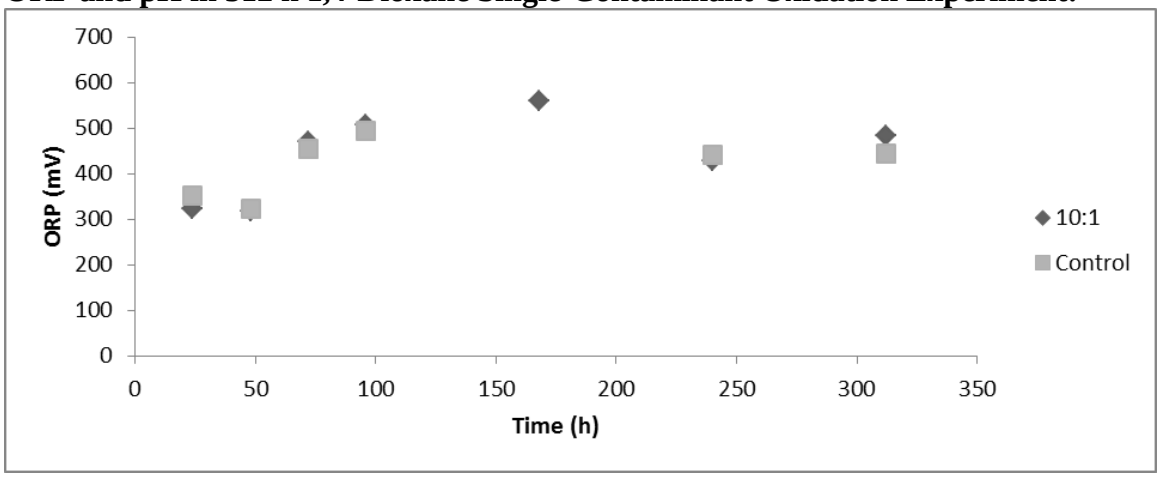

Figure S3: ORP in 312 h 1,4-dioxane single-contaminant oxidation experiment

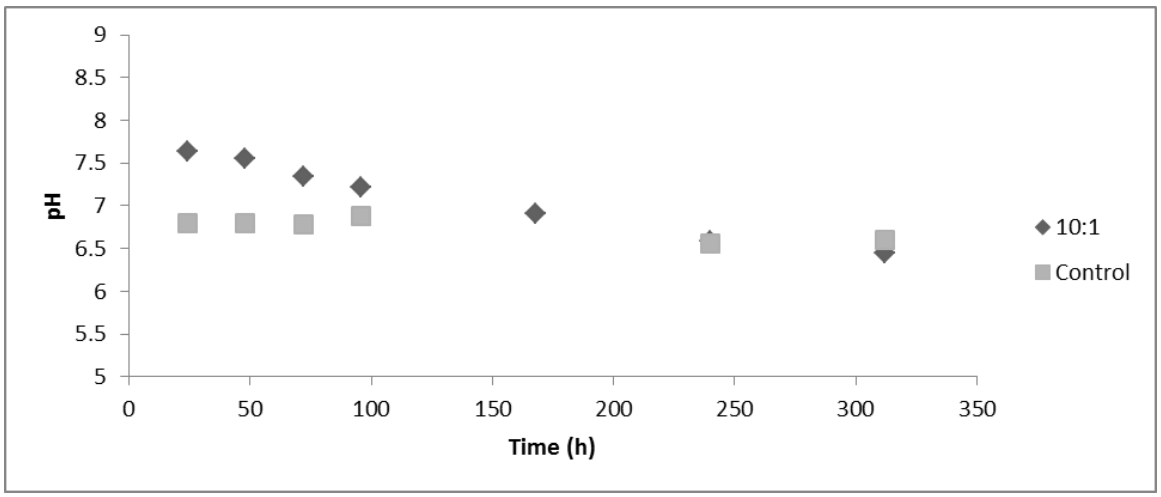

Figure S4: pH in 312 h 1,4-dioxane single-contaminant oxidation experiment

ORP and pH in 24 h 1,4-Dioxane Single-Contaminant Oxidation Experiment:

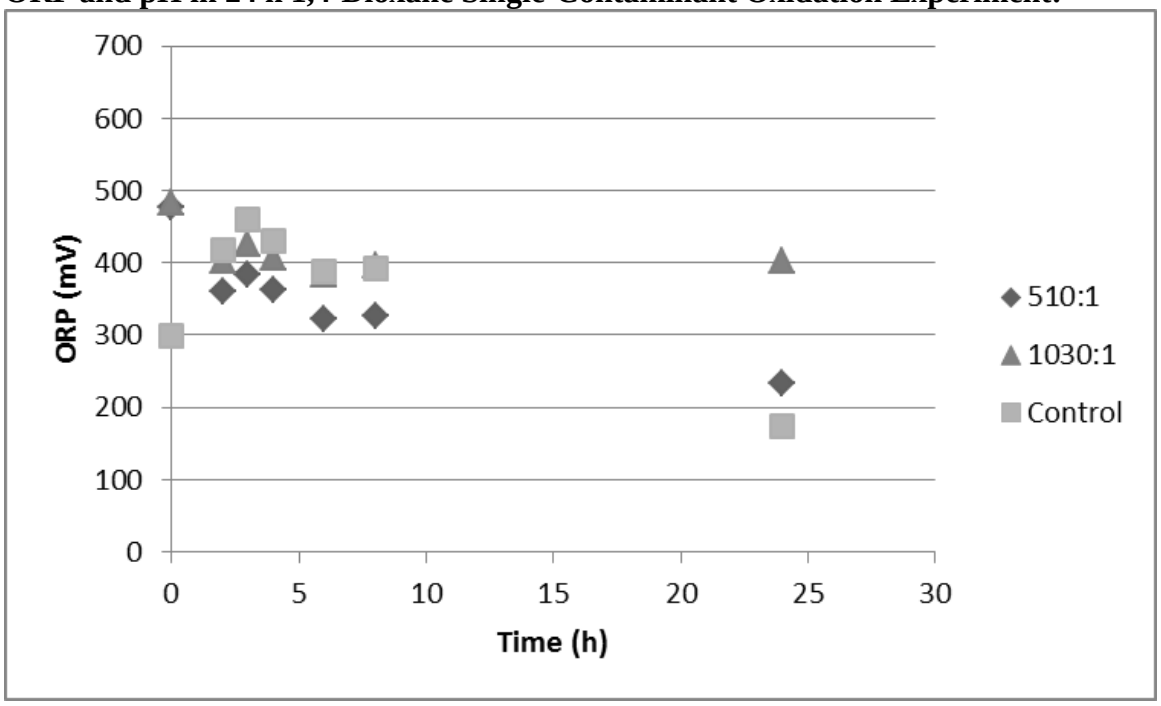

Figure S5: ORP in 24 h 1,4-dioxane single-contaminant oxidation experiment

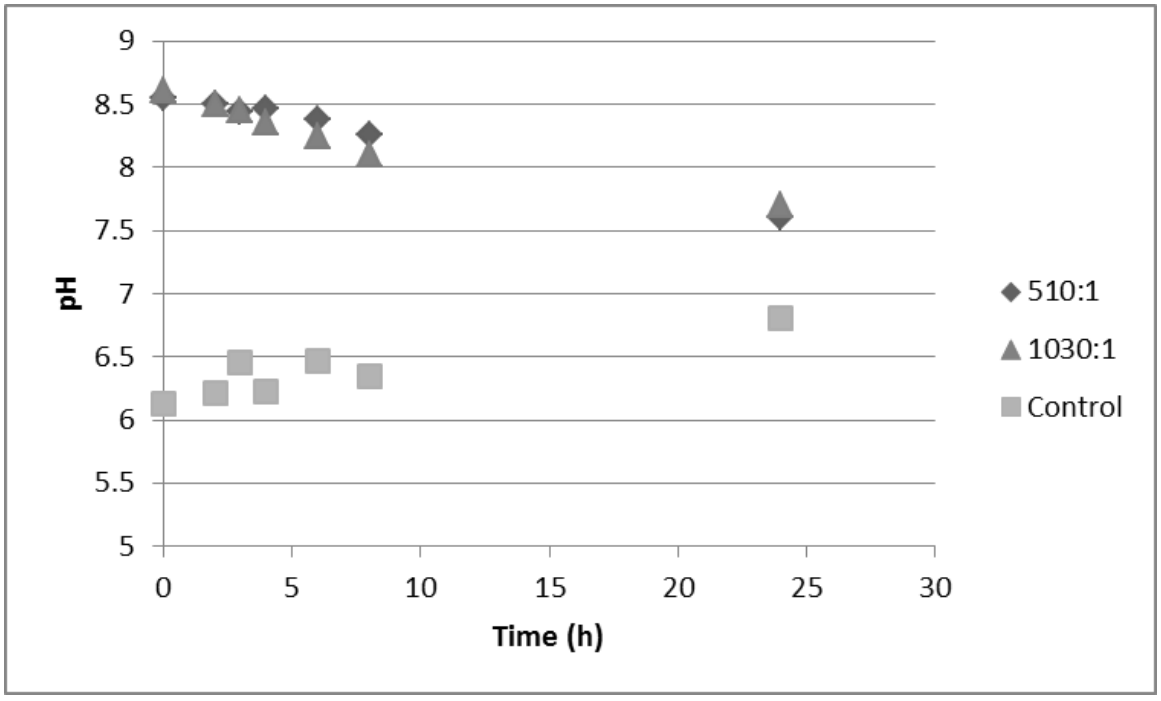

Figure S6: pH in 24 h 1,4-dioxane single-contaminant oxidation experiment

ORP and pH in 312 h 1,1,1-TCA Single-Contaminant Oxidation Experiments:

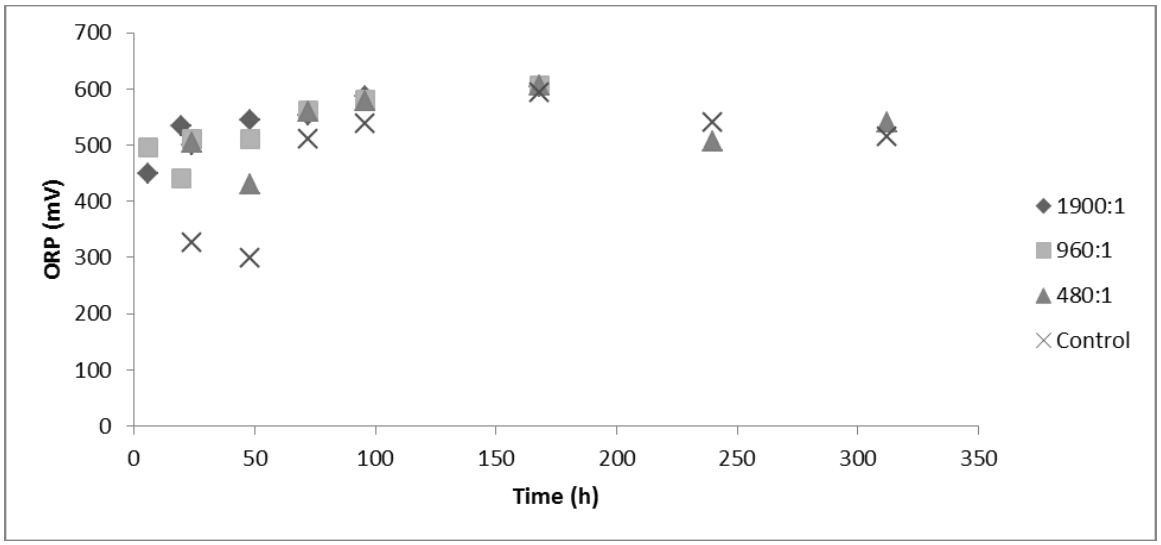

Figure S7: ORP in 312 h 1,1,1-TCA single-contaminant oxidation experiment

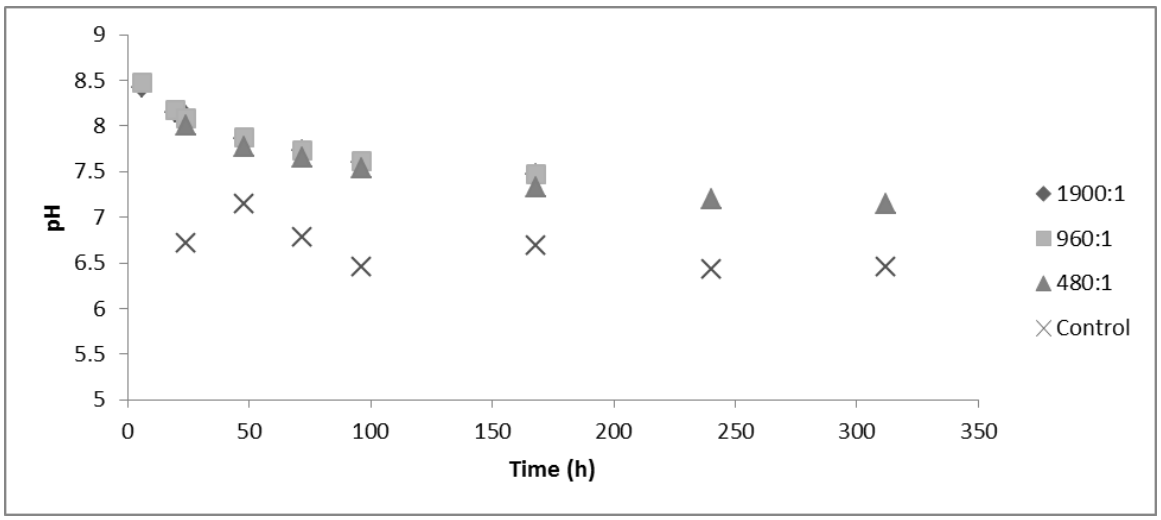

Figure S8: pH in 312 h 1,1,1-TCA single-contaminant oxidation experiment

ORP and pH in 72 h TCE Oxidation Experiments

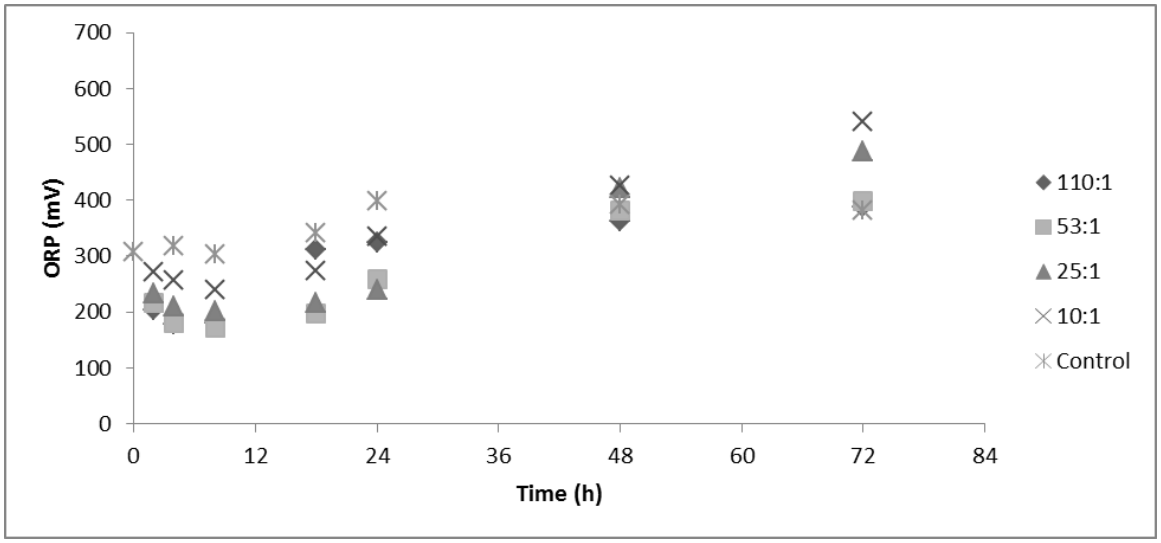

Figure S9: ORP in 72 h TCE single-contaminant oxidation experiment

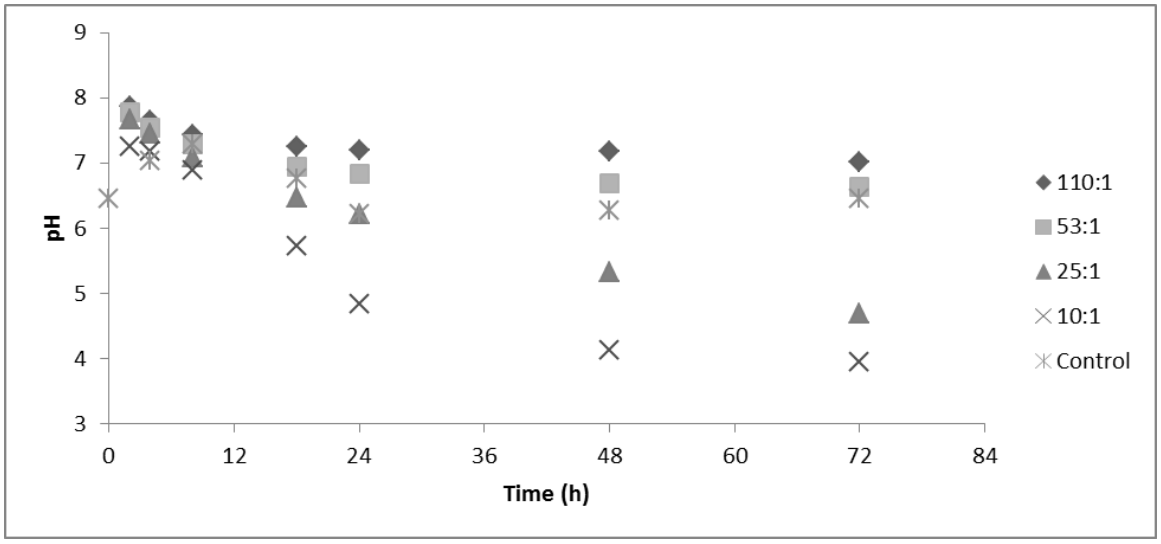

Figure S10: ORP in 72 h TCE single-contaminant oxidation experiment. Note: scale of y-axis differs from previous figures.

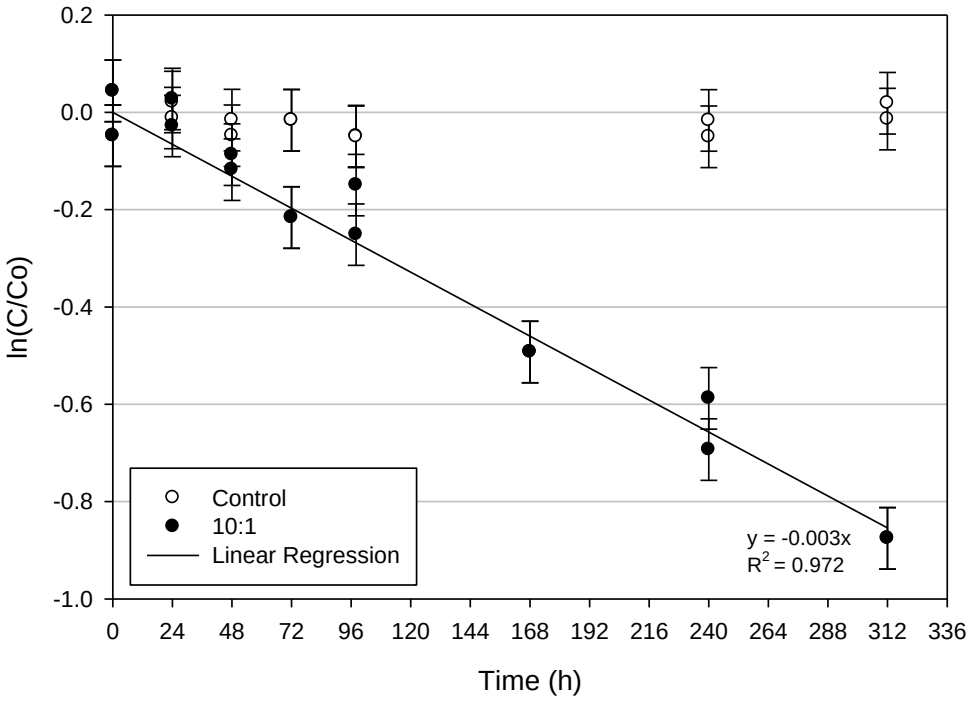

Figure S11: Results of 312 h 1,4-dioxane oxidation experiment at 10:1 oxidant:contaminant ratio. The results confirmed the findings observed in the 72 h duration 10:1 experiment and show that PAP oxidation of 1,4-dioxane may continue for up to 13 days. Error bars of some data points are obscured by the datum point symbol.

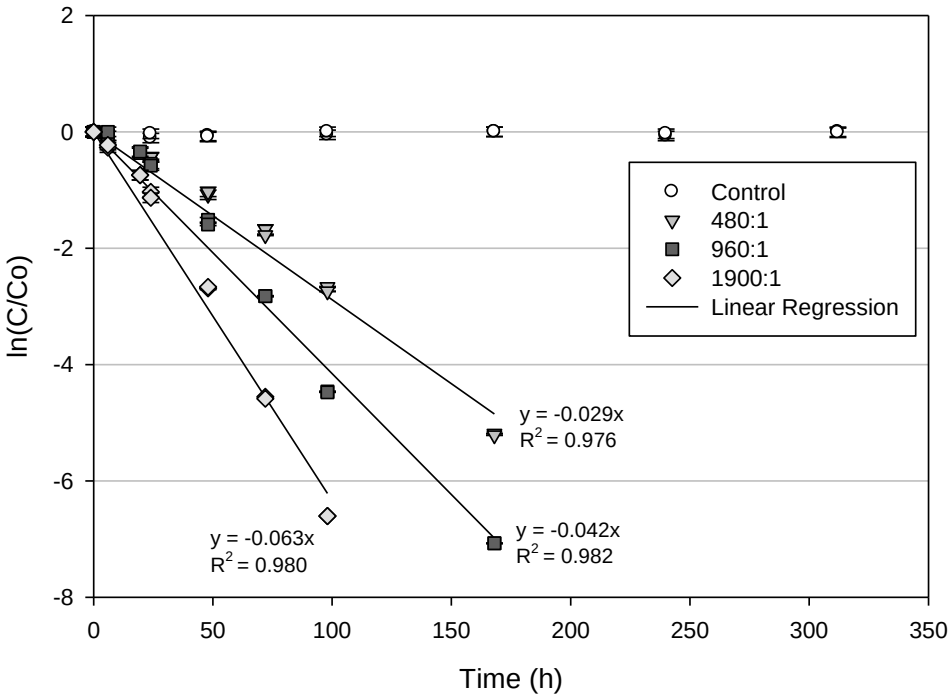

Figure S12: Oxidation of 1,1,1-TCA by PAP. Three oxidant:contaminant ratios were investigated. Due to the more recalcitrant nature of 1,1,1-TCA elevated oxidant:contaminant ratios and a longer experimental duration (312 h) was used. Error bars of some data points are obscured by the datum point symbol.

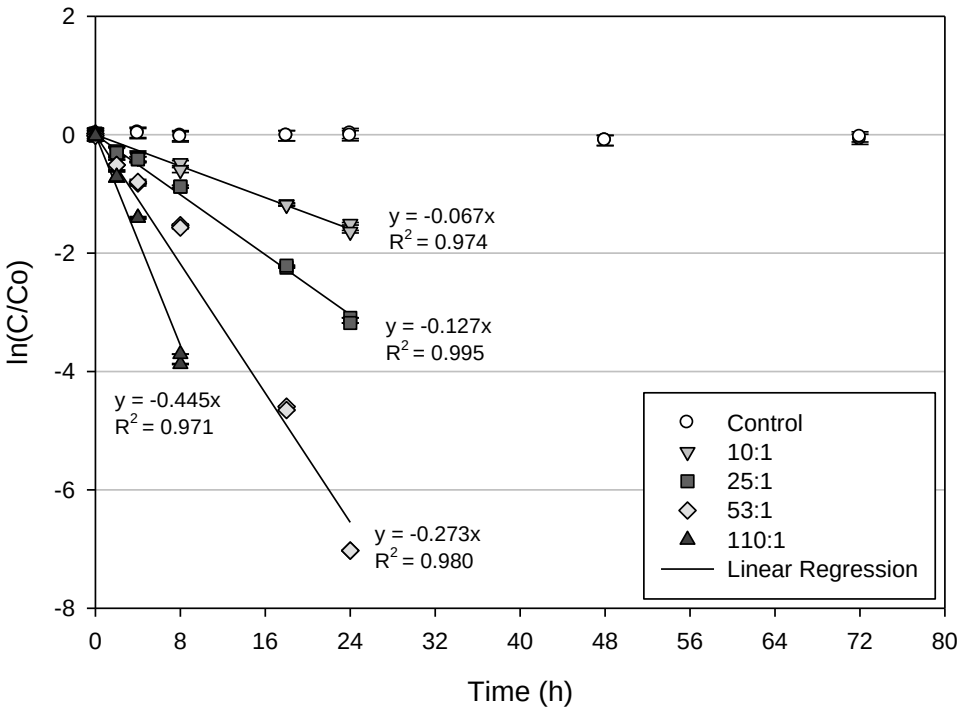

Figure S13: Oxidation of TCE by PAP. Four oxidant:contaminant ratios were investigated. Since TCE is more easily oxidized than 1,4-dioxane, lower oxidant:contaminant ratios were used. Error bars of some data points are obscured by the datum point symbol.

ORP and pH in 96 h Multi-Contaminant Oxidation Experiment

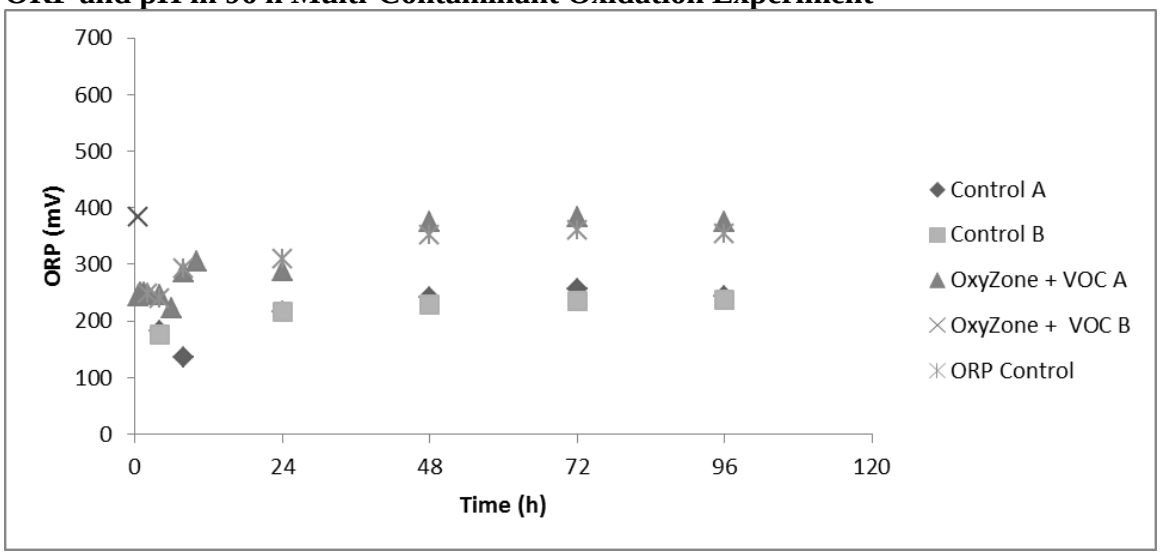

Figure S14: ORP in 96 h multi-contaminant oxidation experiment

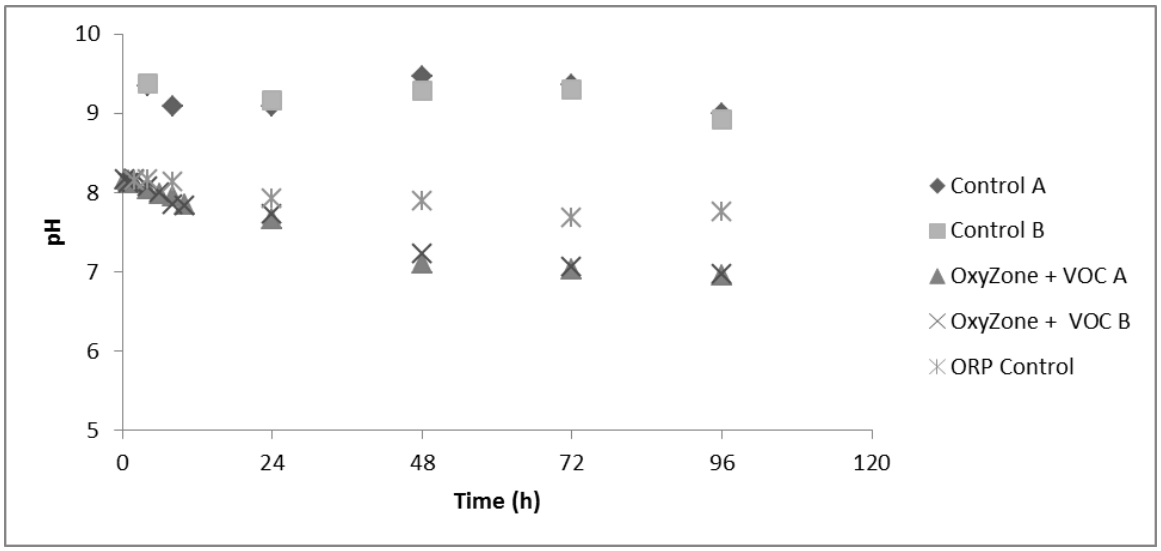

Figure S15: pH in 96 h multi-contaminant oxidation experiment. Note: scale of y-axis differs from previous figures.

Persulfate Concentration in 96 h Multi-Contaminant Oxidation Experiment

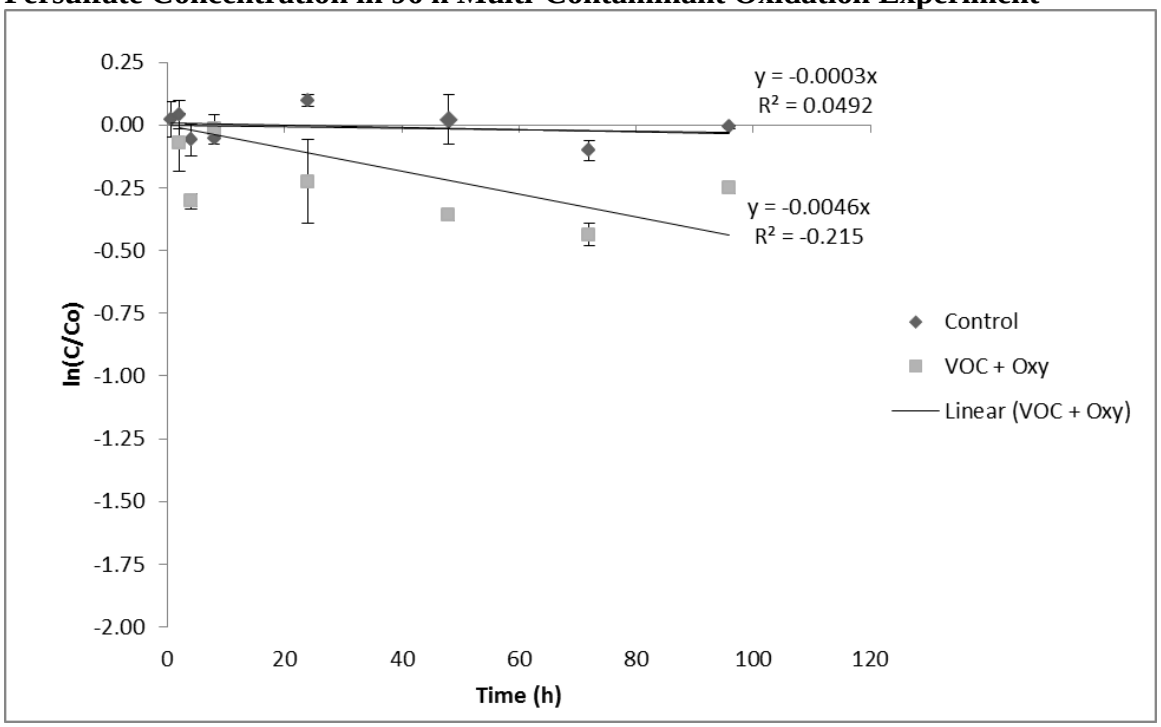

Figure S16: Persulfate Concentration in 96 h multi-contaminant oxidation experiment. Data points represent the average of two measurements and error bars denote the range**.**

Works Referenced in Supplementary Materials

Draper, W.M. et al., 2000. Trace-level determination of 1,4-dioxane in water by isotopic dilution GC and GC-MS. The Analyst, 125(8), pp.1403–1408.

Environmental Laboratory Services, 2009. 1,4-Dioxane Determination Rev D, ELS-105.

OI Analytical, 2006. Low-level Detection of Ethanol, 1.4-Dioxane, and Other Oxygenates Using the Eclipse Purge-and-Trap Sample Concentrator. In Conference on Analytical Chemistry and Applied Spectroscopy. O.I. Analytical, p. 12.

1.4 Transport and Peroxone Activated Persulfate Treatment of 1,4-Dioxane (Peroxone Activated Persulfate)

Cashman, M.A., Boving, T.B. (In Preparation 2018) 1,4-Dioxane treatment with peroxone activated persulfate: Large scale column experiments. Manuscript prepared for submission.

Methods and Instrumentation

Sodium Chloride Concentration (mg/L)	2000	1000	500	200	20	2	0
Electric Conductivity (µS/cm)	3510	1904	959	414	40.09	3.46	1.06

Table B1: Sodium chloride calibration curve.

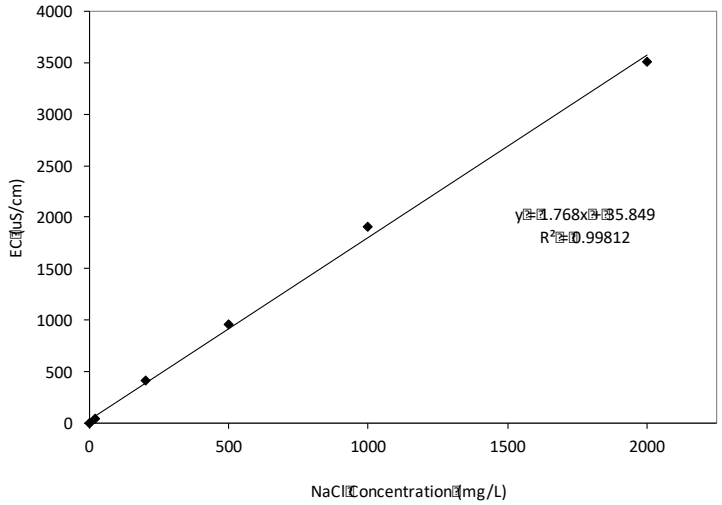

Fig. B1: Linear relationship between electric conductivity and concentration of sodium chloride in solution.

Settings	Time (min) / Temp °C
Trap	
Trap Type	#7 Tennax
Sparge Mount	40 C
Sample	35 C
Purge Times & Temperature Parameters	
Purge Time	11 min
Dry Purge Time	1 min
Trap Temp	40 C
Water Management Temperature Parameters	
Purge Temp °C	120
Desorb Temp °C	40
Bake Temp °C	240
Bake Parameters	
Bake Time	10 min
Trap Temp °C	210
Desorb Time & Temperature Parameters	
Desorb Time min	0.5
Trap Temperature °C	190
Desorb Preheat °C	125
Trap Temperature Parameters	
Heated Zones	
Transfer Line °C	120
Valve Oven °C	120

Table B2: Purge and trap method settings.

Injector Temperature °C	240
Interface Temperature °C	230 C
Oven Temperature °C	45 (hold 4.5 min) to 100 (at rate of 12 C/min) to 240 (hold 1.3 min; at rate of 25 C/ min)
Column Inlet Pressure kPa	31.3
Column Flow	0.8 mL/min
Linear Velocity	31.5 cm/sec
Split ratio	35
Total Flow	28 mL/min
Detector	SIM mode m/z (88,58, 96, 64, 46)

Table B3: GC-MS method settings.

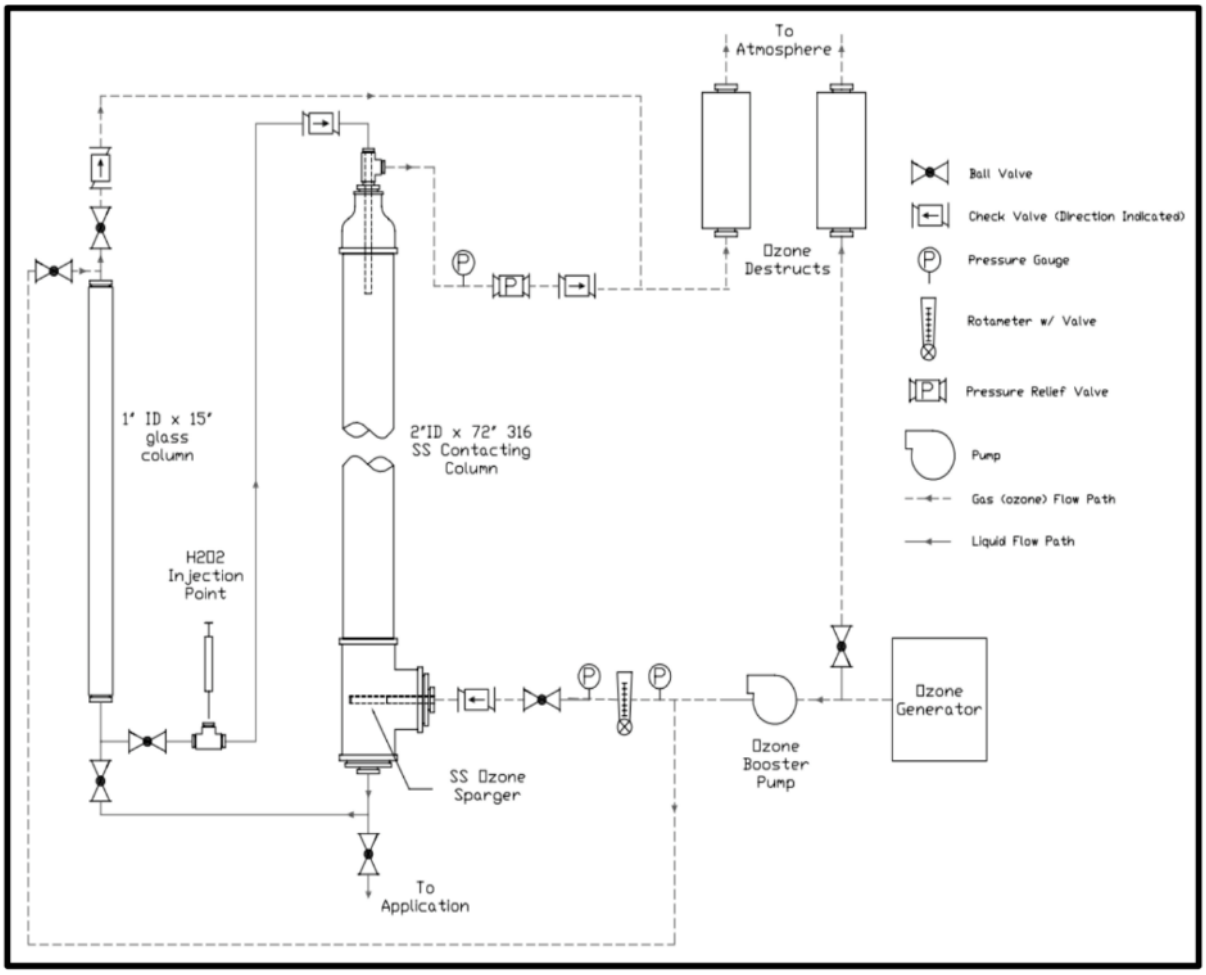

Fig. B2: Diagram of bench-scale ozone generator.

Laboratory Experiments

	Control	**100:1**	**250:1**	**500:1**	**1000:1**
k_1 h^{-1}	0	0.0025	0.009	0.0348	0.0946
$T_{1/2}$ (h)	n/a	277	77	20	7

Table C1: Oxidation of 1,4-Dioxane over 24 hours at varying oxidant: contaminant molar ratios (0:1 [Control], 100:1, 250:1, 500:1, 1000:1).

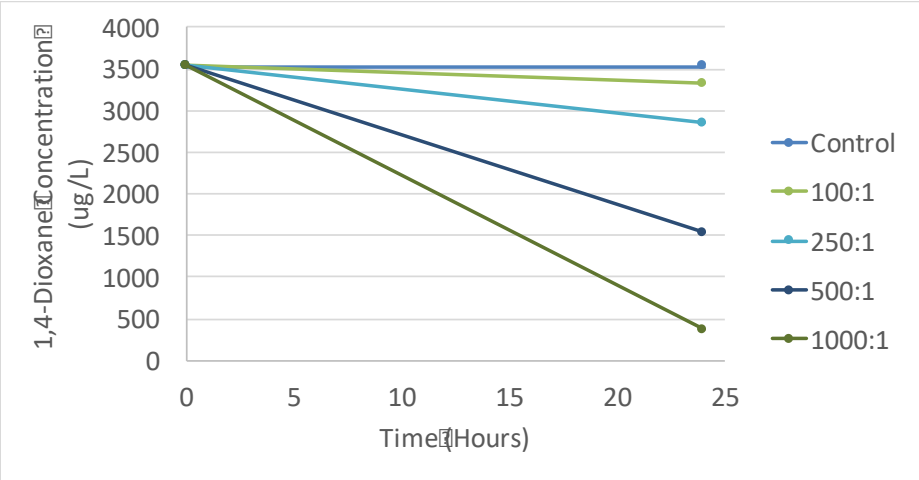

Fig. C1: Concentration of 1,4-Dioxane in initial 24-hour pilot study.

	Control		**250:1**	
	pH	ORP (mv)	pH	ORP (mv)
T=0 hour	202.9	8,853	226.6	8.448
T=2 hours	183.1	8.301	187.6	8.187
T= 8 hours	212.2	8.241	167.5	8.171
T=1 day	243.9	6.535	226	8.201
T=2 days	165.5	8.055	183.7	6.717
T=4 days	143.5	7.469	166.9	7.793
T= 8 days	155.6	8.652	150.8	7.714
T= 16 days	137.2	7.996	166.9	6.865

Table C2: pH and ORP for 250:1 16-day batch scale pilot study.

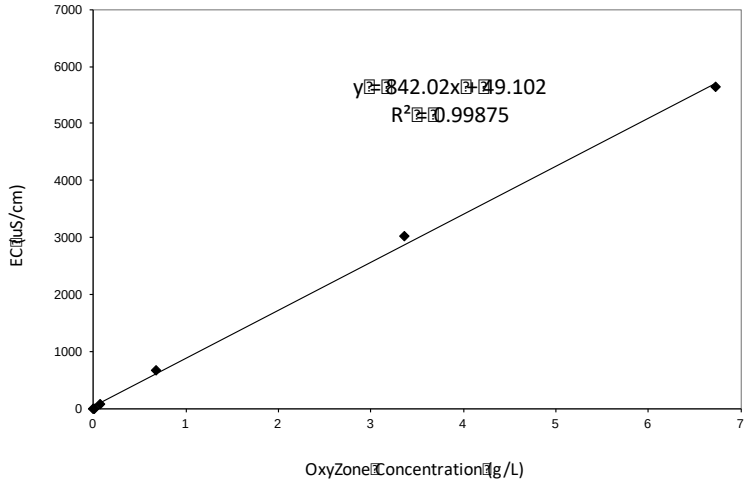

Fig. C3: OxyZone electric conductivity calibration curve.

	M_O (%)	M_1 (PV)	M_2 (D_L)	M_3 (PV)

Scenario I, Test I	50.81	0.76	143	130
Scenario I, Test II	76.25	1.10	178	58
Scenario II	76.67	1.5	135	102

Table C3: Moment analysis data.

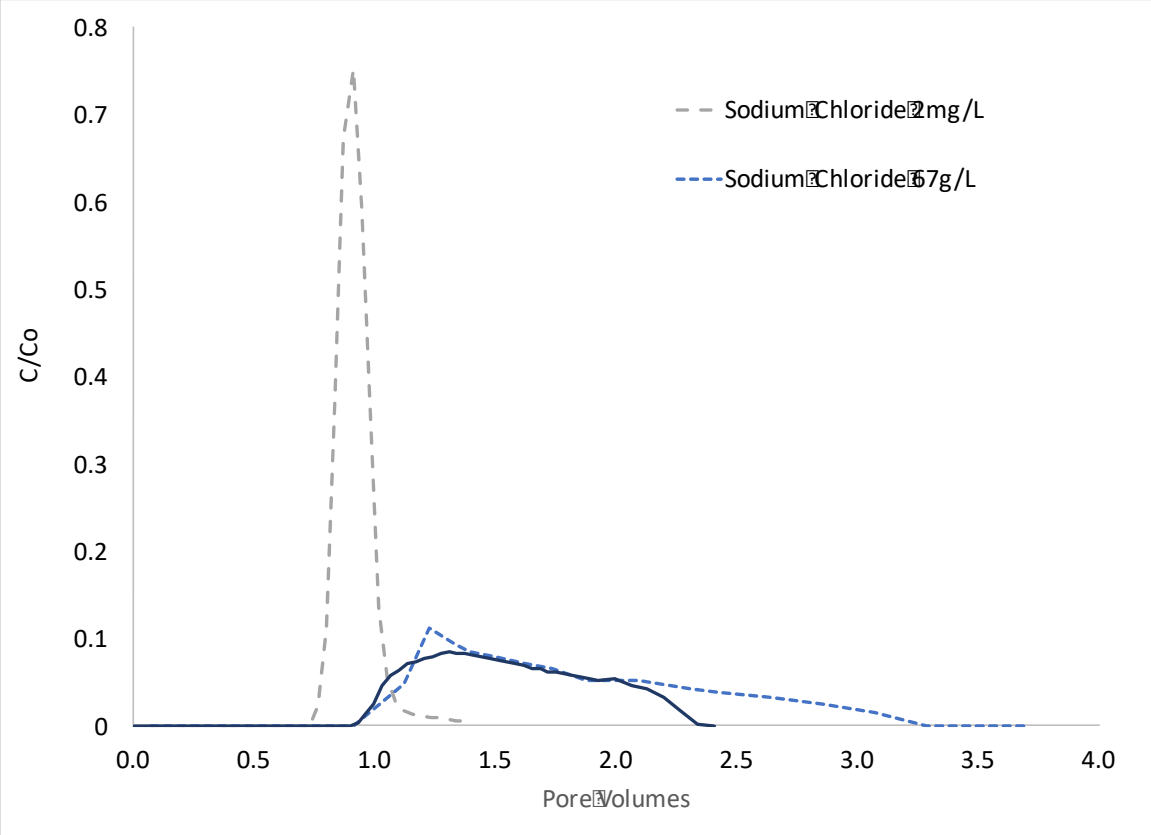

Fig. C4: Sodium Chloride breakthrough curves as a function of concentration and density. The density of the dilute solution was approximately the same as water. That of the concentrated tracer solution was 1.05 g/cm^3.

1.5 1,4-Dioxane Treatment Using Persulfate Activated By Iron Filings (Oxidant Mixture with Iron Activation)

Zhong, H., Brusseau, M.L., Wang, Y., Yan, N., Quig, L., Johnson, G.R. (2015) In situ activation of persulfate by iron filings and degradation of 1,4-dioxane. Water Research, 83, 104-111.

Table 1S. ICP-MS-based Metal concentrations in bulk solution after contact of 5 mM persulfate solution or pure water with iron filings at a liquid/solid ratio of 10:1 (v/w). The flask reactor was shaken at 200 rpm, 30±1°C. The metals with concentration lower than 0.01 mg/L are not included.

Analyte	1 h contact	24 h contact	24 h contact with water
Metals measured by ICP-MS method (mg/L)			
Na	195.84	186.56	1.52
Fe	168.26	115.97	0.14
Mn	5.96	9.53	0.01
Ca	0.61	0.69	0.05
Ni	0.51	0.05	0.00
K	0.50	0.65	0.29
Mg	0.30	0.44	0.03
Ba	0.03	0.02	0.00
Co	0.02	0.01	0.00
Zn	0.01	0.01	0.00
Mo	0.00	0.03	0.00
Cu	0.00	0.01	0.00
Sulfur and iron species measured by spectrophotometric method (mg/L)			
Fe^{2+}	111.74	82.77	0.12
Fe^{3+}	102.45	55.38	-0.04
Total Fe	214.19	138.15	0.08
pH	4.70	5.28	6.42

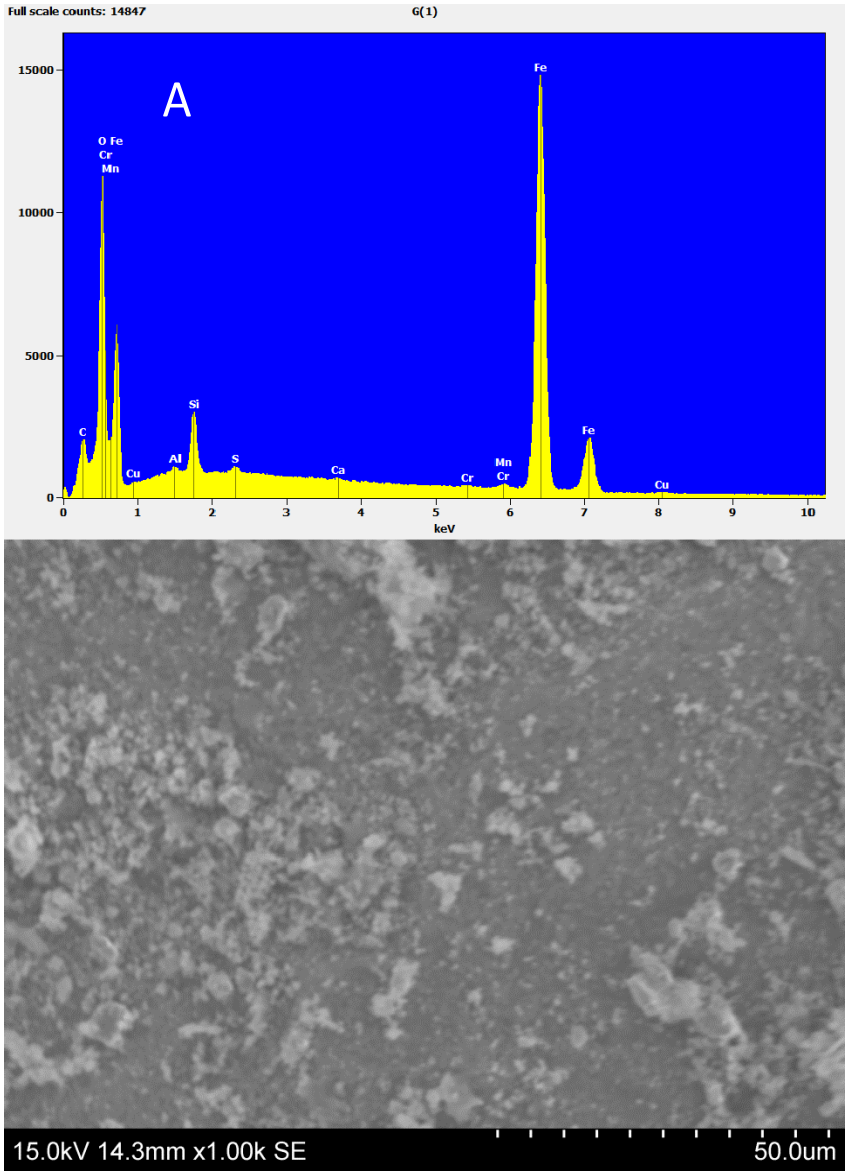

Figure S1. (A) SEM-EDS spectroscopy and the image of scanned area for iron filing sample.

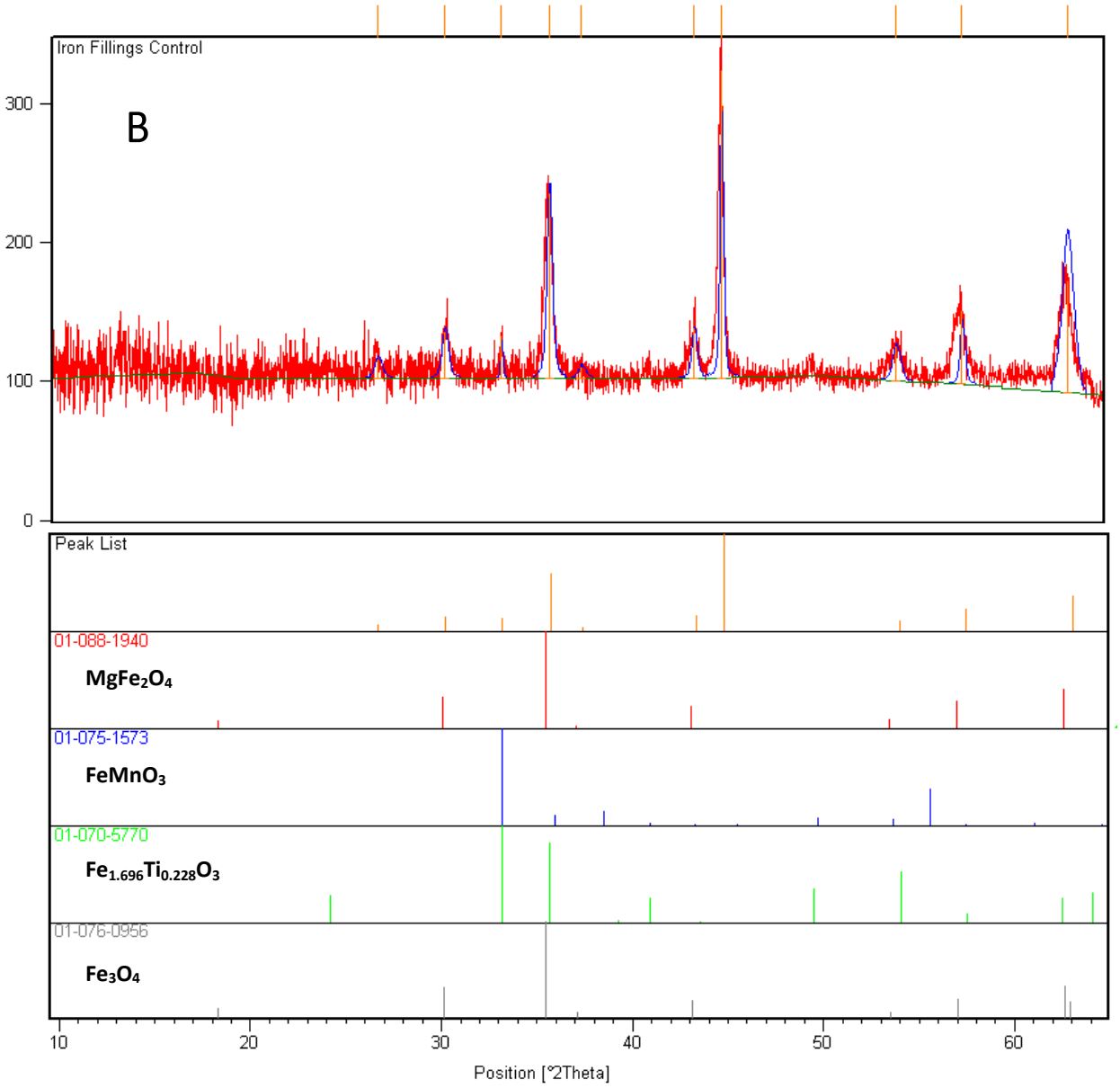

Figure S2. (B) XRD spectroscopy and identified minerals for iron filing sample.

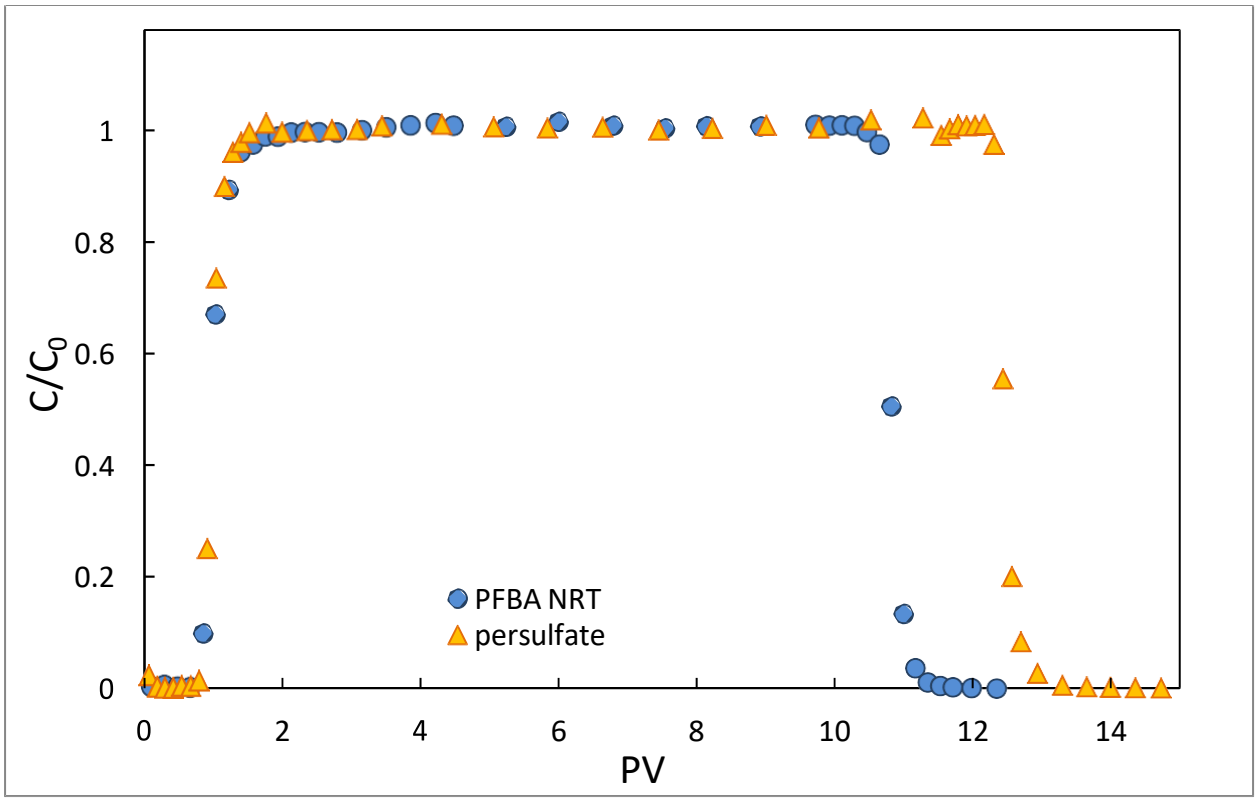

Figure S3. Breakthrough curves of non-reactive tracer pentafluorobenzoate (PFBA NRT) and persulfate in sand-packed column.

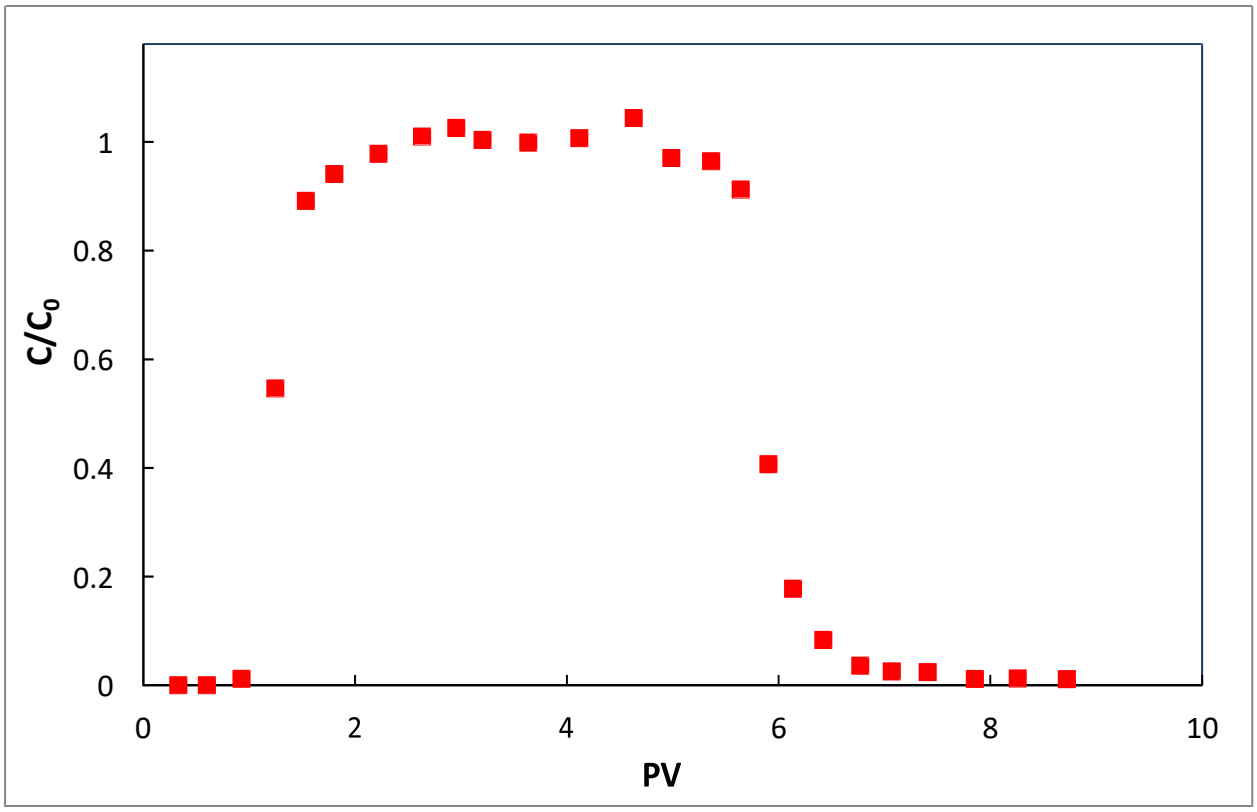

Figure S4. Breakthrough curve of dioxane in the iron-filing-packed column in the absence of oxidants. Influent dioxane concentration is approximately 0.5 mM. Pore-water velocity is 3.0 cm/h.

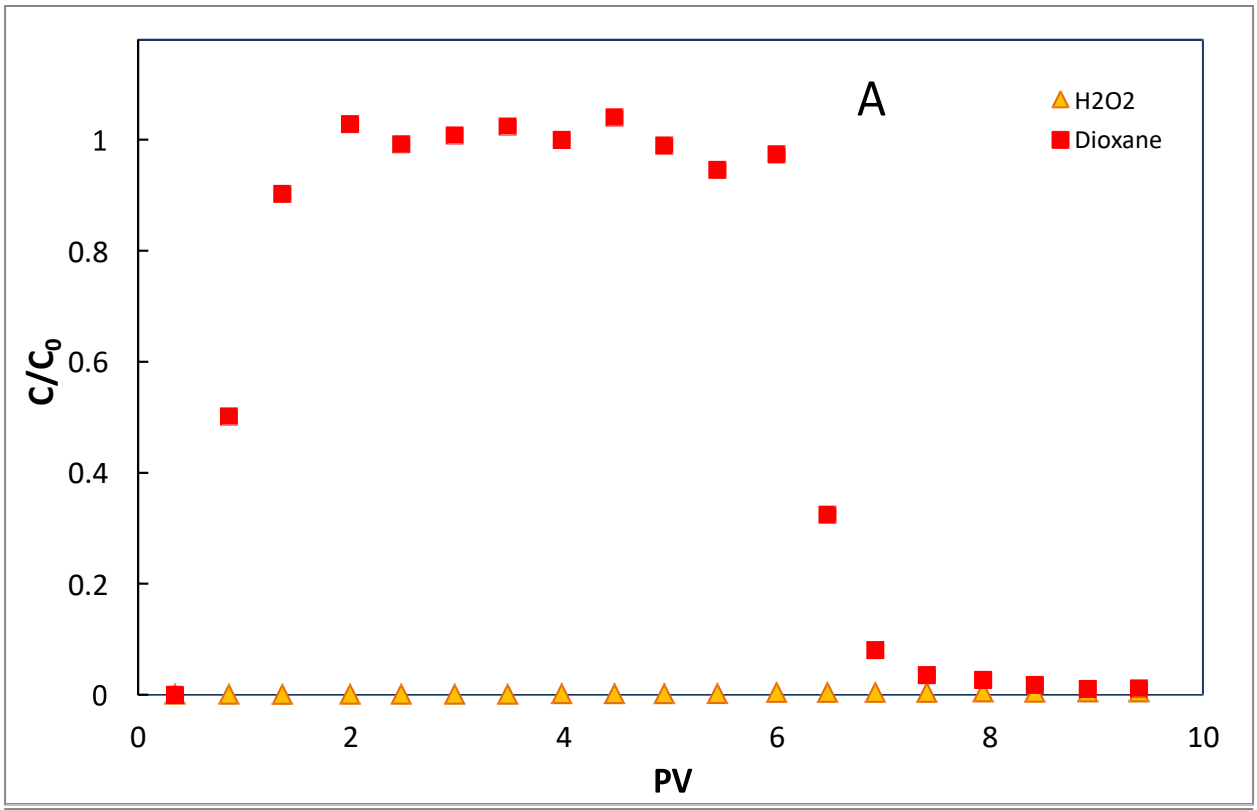
A
H2O2
Dioxane
C/C0
PV
0
0.2
0.4
0.6
0.8
1
0
2
4
6
8
10

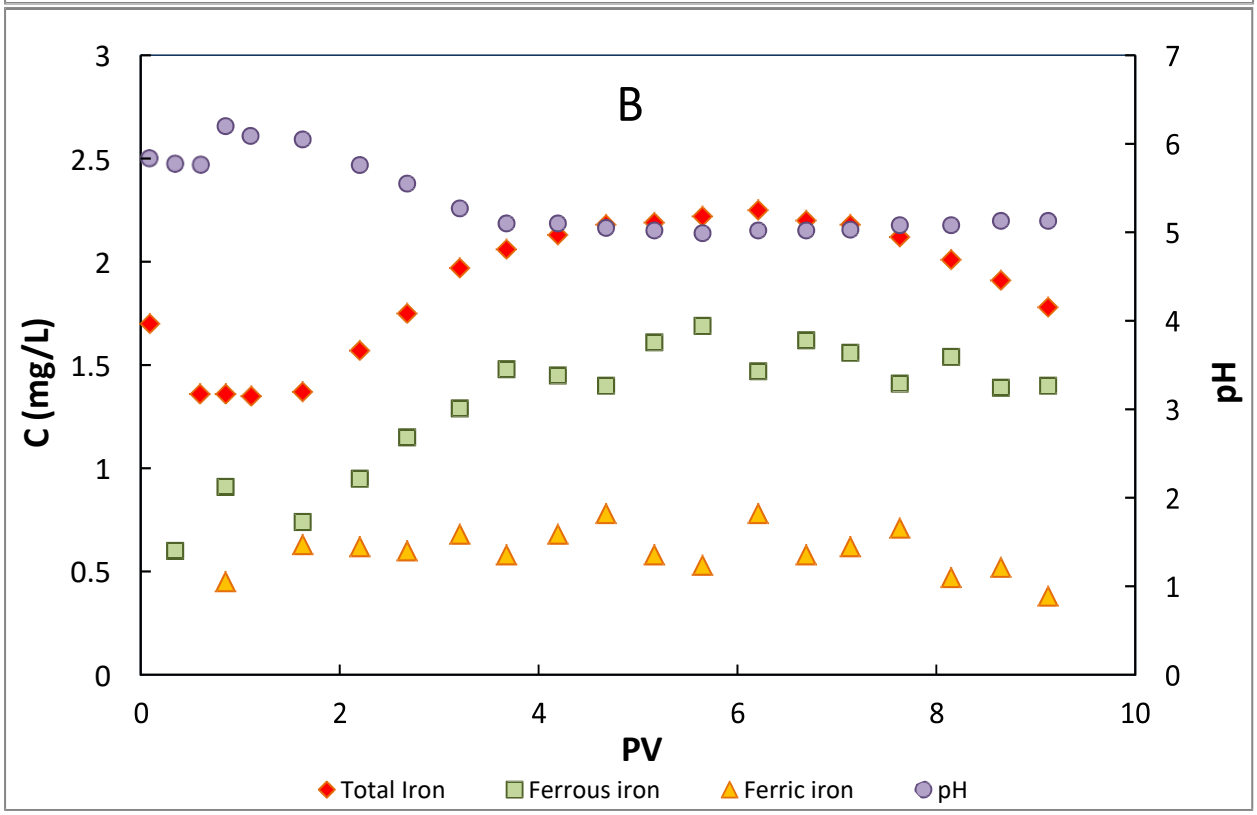
B
C (mg/L)
pH
PV
Total Iron
Ferrous iron
Ferric iron
pH
0
0.5
1
1.5
2
2.5
3
0
1
2
3
4
5
6
7
0
2
4
6
8
10

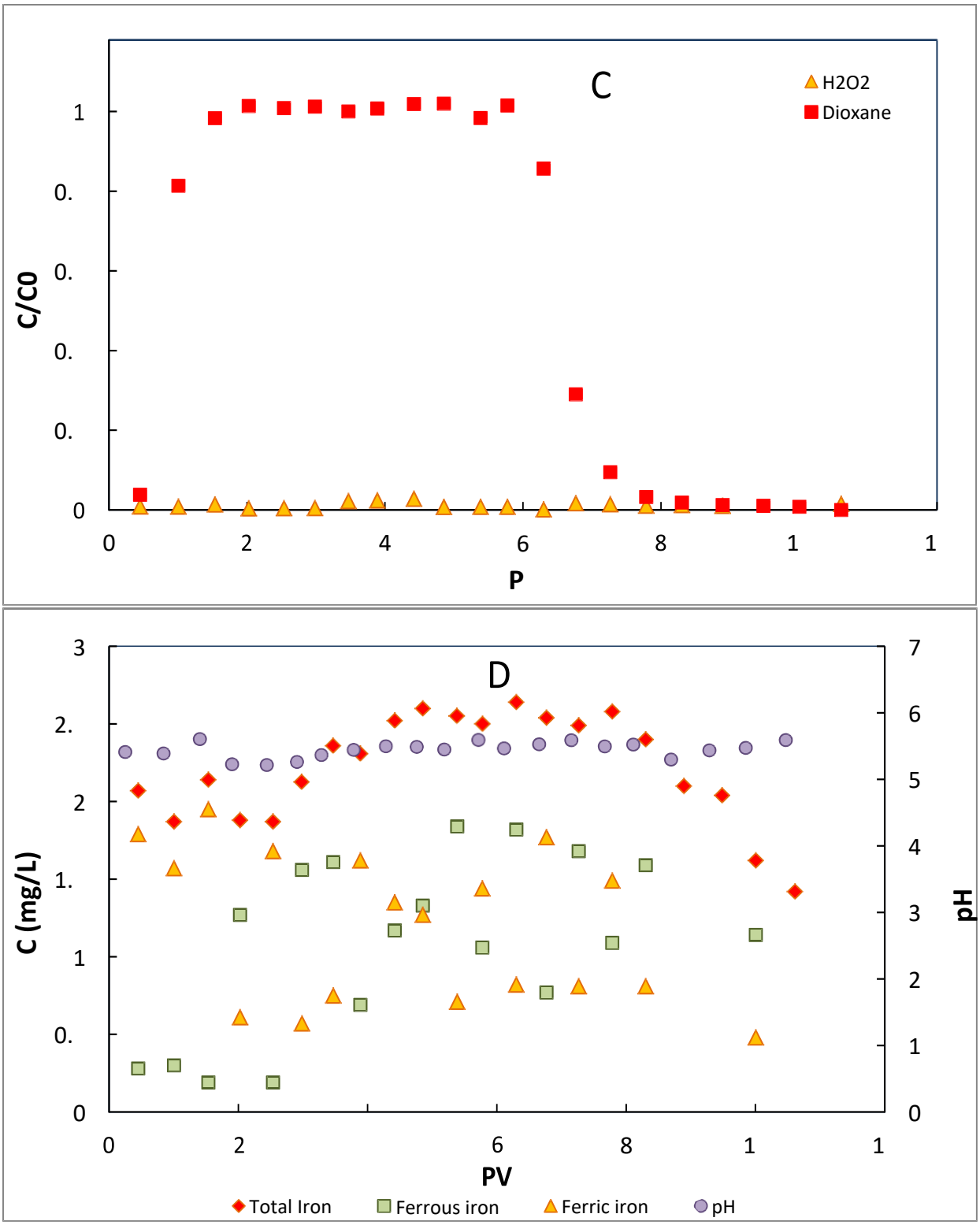

Figure S5. Degradation of dioxane by H_2O_2 in iron-filing-packed column and the related solution chemistry. Influent H_2O_2 and dioxane concentrations are 5 mM and 0.5 mM, respectively. (A) Breakthrough curves of H_2O_2 and dioxane at the pore-water velocity of 31 cm/h. (B) Concentration of

iron species and pH in the effluent at the pore-water velocity of 31 cm/h. (C) Breakthrough curves of H_2O_2 and dioxane at the pore-water velocity of 3.0 cm/h. (D) Concentration of iron species and pH in the effluent at the pore-water velocity of 3.0 cm/h.

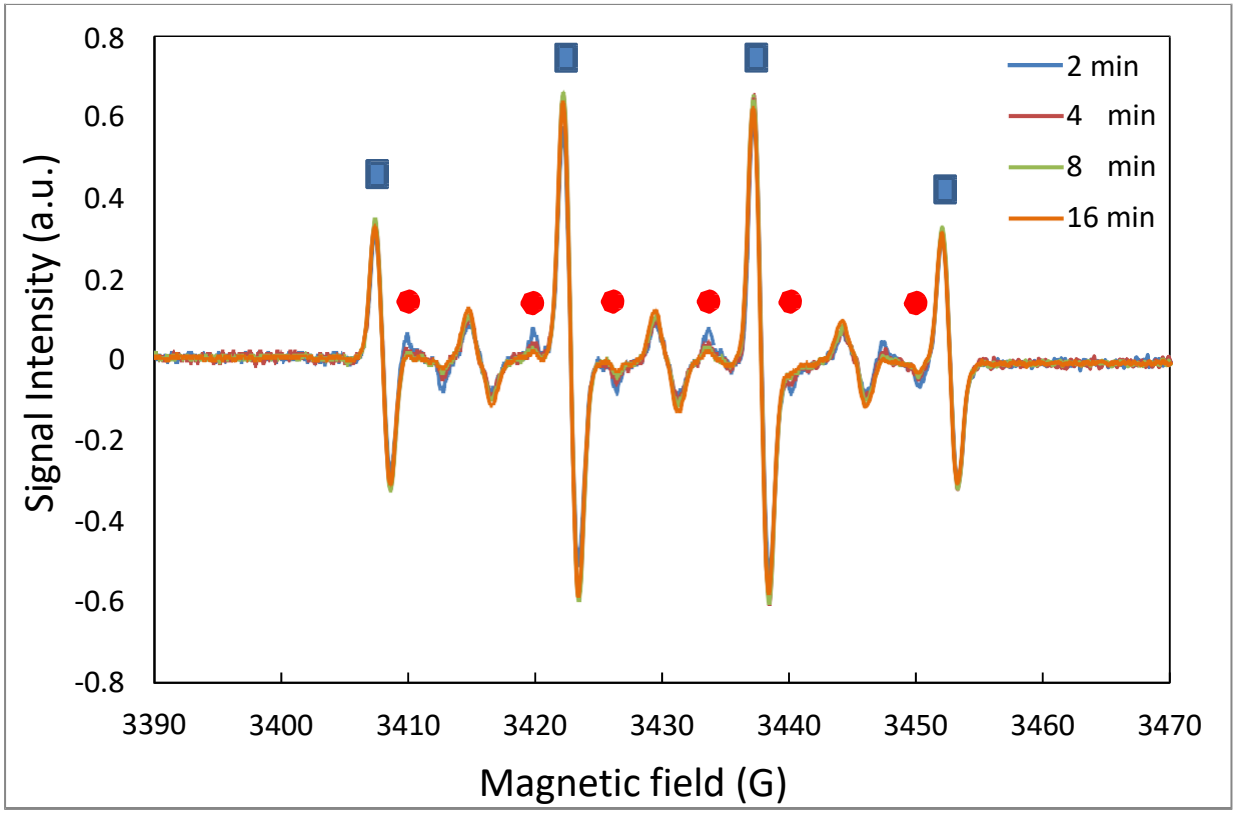

Figure S6. EPR spectra of persulfate solution over time. ▮ DMPO-OH; ● DMPO-SO_4.

7.2 List of Scientific/Technical Publications

7.2.1 Journal Articles (in order published)

1. Zhong, H., Brusseau, M.L., Wang, Y., Yan, N., Quig, L., Johnson, G.R. (2015) In-situ activation of persulfate by iron filings and degradation of 1,4-dioxane. Water Research, 83, 104-111.

2. Eberle, D., Ball, R., Boving, T.B. (2016) Peroxone activated persulfate treatment of 1,4-dioxane in the presence of chlorinated solvent co-contaminants. Chemosphere 144:728-735.

3. Chen, H., Carroll, K.C. (2016) Metal-Free Catalysis of Persulfate by Nitrogen-Doped Graphene and Aminated Graphene. Environmental Pollution, 215: 96–102. doi:10.1016/j.envpol.2016.04.088.

4. Yan, N., Liu, F., Chen, Y., Brusseau, M.L. (2016) Influence of groundwater constituents on 1,4-dioxane degradation by a binary oxidant system. Water Air Soil Pollution, 227: article 436.

5. Dettmer, A., Ball, R., Boving, T.B., Khan N.A., Schaub, T., Sudasinghe, N., Fernandez, C.A., Carroll, K.C. (2017) Stabilization and Prolonged Reactivity of Aqueous-Phase Ozone with Cyclodextrin. Journal of Contaminant Hydrology, 196:1–9.

6. Yan, N., Li, M., Liu, Y., Liu, F., Brusseau, M.L. (2017) Kinetic and Thermodynamic Studies of Chlorinated Organic Compound Degradation by Siderite-Activated Peroxide and Persulfate. Water Air Soil Pollution, 228, article 453.

7. Farooq, U., Danish, M., Lu, S., Brusseau, M.L., Naqvi, M., Fu, X., Zhang, X., Sui, Q., Qiu, Z. (2017) Efficient Transformation in Characteristics of Cations Supported-Reduced Graphene Oxide Nanocomposites for Destruction of Trichloroethane. Applied Catalysis A, General, 544, 10–20.

8. Khan, N.A., Johnson, M.D., and Carroll, K.C. (2018) Spectroscopic methods for aqueous cyclodextrin inclusion complex binding measurement for 1, 4-dioxane, chlorinated co-contaminants, and ozone. Journal of Contaminant Hydrology, 210(March): 31-41.

9. Khan, N.A., Johnson, M.D., Kubicki, J.D., Holguin, F.O., Dungan, B., Carroll, K.C. (In Review) Cyclodextrin-Enhanced 1,4-Dioxane Treatment Kinetics with TCE and 1,1,1-TCA Using Aqueous Ozone. In review.

10. Yan, N., Liu, F., Brusseau, M.L. (In Review) Treatment of 1,4-dioxane and trichloroethene co-contamination by an activated binary oxidation process. In review.

11. Yan, N., Brusseau, M.L., Zhong, H., Li, M.. (In Review) The natural activation ability of subsurface media to promote in-situ chemical oxidation of 1,4-dioxane. In review.

12. Bridges, L., Brusseau, M.L., Mohamed, R., Papelis, C., Carroll, K.C. (In Review) Persulfate Activation and Enhanced Degradation of 1,4-Dioxane in Water Using Manganese Amendment for In Situ Chemical Oxidation. In Review.

13. Khan, N.A., Carroll, K.C. (In Review) Transport of Aqueous Ozone in Saturated Porous Media with Oxidant Attenuation and Demand Assessment for In Situ Contaminant Oxidation. In Review.

14. Milavec, J., Tick, G.R., Carroll, K.C. (In Preparation 2018) 1,4-Dioxane Co-Contaminant Mixture Cosolvency Impacts on Trichloroethene Dissolution in Groundwater and Sorption to Aquifer Materials. Manuscript prepared for submission.

15. Cashman, M.A., Boving, T.B. (In Preparation 2018) 1,4-Dioxane treatment with peroxone activated persulfate: Large scale column experiments. Manuscript prepared for submission.

16. Cashman, M.A., Boving, T.B. (In Preparation 2018) Investigation of oxidant radicals involved in treatment of 1,4-Dioxane with peroxone activated persulfate. Manuscript prepared for submission.

7.2.2 Presentations

1. Carroll, K.C. (2013) Mass-Flux Source Attribution and Application to Subsurface Contaminant Remediation Evaluation. Invited Presentation: the School of Mathematical and Natural Sciences at Arizona State University, Phoenix, AZ, Aug. 29.

2. Carroll, K.C. (2013) Mass-Flux Source Attribution and Application to Subsurface Contaminant Remediation Evaluation. Invited Presentation: the Earth and Environmental Science Department Seminar, New Mexico Tech, March 3.

3. Carroll, K.C. (2013) Mass-Flux Source Attribution and Application to Subsurface Contaminant Remediation Evaluation. Invited Presentation: the Earth & Planetary Sciences Department Seminar, University of New Mexico, Jan. 31.

4. Mateas, D.J., G.R. Tick, and K.C. Carroll (2014) Novel, In-situ NAPL Modification Technique for Persistent Source Zone Control and Remediation. American Geophysical Union Fall Meeting, Fall Meet. Suppl., Abstract H51A-0566.

5. Padgett, M., G.R. Tick, and K.C. Carroll (2014) Rate Limited Diffusion and Dissolution of Multicomponent Nonaqueous Phase Liquids (NAPLs) and Effects on Mass Discharge in Groundwater. American Geophysical Union Fall Meeting, Fall Meet. Suppl., Abstract H51A-0565.

6. Carroll, K.C. (2014) Restoring and Preserving Our Water Resources for Future Generations. Invited Presentation: the Science Cafe, Las Cruces Museum of Nature and Science,

Dec. 4.

7. Dettmer, A., S. Cruz, B. Dungan, F.O. Holguin, A.L. Ulery, B. Hunter, and K.C. Carroll (2014) Natural Oxidant Demand Variability, Potential Controls, and Implications for in Situ, Oxidation-Based Remediation of Contaminated Groundwater. American Geophysical Union Fall Meeting, Fall Meet. Suppl., Abstract H51A-0569.

8. Carroll, K.C. (2014) Subsurface Contaminant Source Attribution and Remediation Evaluation. Invited Presentation: Geological Sciences Department Seminar, Univ. of Texas El Paso, Nov. 20.

9. Dettmer, A., S. Cruz, B. Dungan, F.O. Holguin, A.L. Ulery, B. Hunter, and K.C. Carroll (2014) Natural Oxidant Demand Variability, Potential Controls, and Implications for in Situ, Oxidation-Based Remediation of Contaminated Groundwater. NM WRRI's 59th Annual New Mexico Water Conference, New Mexico's Water Future: Connecting Stakeholder Needs to Water Information, Nov. 18-19, Santa Fe, NM.

10. Wang, Y., H. Zhong, N. Yan, and M.L. Brusseau (2014) In situ Activation of Persulfate by Iron Filings and Oxidation of 1,4-Dioxane. Presentation at the American Geophysical Union Fall Meeting, Fall Meet. Suppl., Abstract.

11. Boving, T.B., D.E. Eberle, and R. Ball, (2014) Activated Persulfate Treatment of 1,4-Dioxane in the Presence of Chlorinated Solvent Co-contaminants. American Geophysical Union Fall Meeting, Fall Meet. Suppl., Abstract #H44C-03.

12. Carroll, K.C. (2015) What is in your water? Environmental Science and Engineering Grand Challenges. Invited Presentation: The New Mexico Alliance for Minority Participation (NM AMP) 2015 Student Research Conference, Las Cruces Convention Center, October 2.

13. Chen, H. and K.C. Carroll (2015) Sulfamethoxazole Treatment by Advanced Oxidation Process with Graphene Oxide. The Association of Environmental Engineering & Science Professors (AEESP) 2015 Conference, Yale University, June 13-16.

14. Carroll, K.C. (2015) Flexible Subsurface Science: Pore-Scale Imaging of Two & Three-Phase Immiscible-Fluid Transitions and Switchable Fluids for Hydraulic Fracturing in Geothermal Systems. Invited Presentation: the EES/IGPP Frontiers of Geoscience Colloquium at Los Alamos National Laboratory, May 18.

15. Yan, N., M.L. Brusseau, H. Zhong, and M. Li. (2015) The natural activation ability of subsurface media during in-situ chemical oxidation of 1,4-dioxane. Presentation at the American Geophysical Union Annual Meeting, San Francisco, CA, Dec 2015.

16. Ball, R., T.B. Boving, and D. Eberle (2015) Peroxone activated persulfate treatment of 1,4-dioxane in the presence of chlorinated solvent co-contaminants. Annual conference of the Association for Environmental Health and Sciences Foundation (AEHS) “Assessment, Remediation, Regulation, and the Energy Environmental Interface”. University of Massachusetts - Amherst, October 19-22, 2015.

17. Boving, T.B. (2015) Remediation Technologies. Universitas Islam Indonesia/URI International Short Course on Water Resources and Management Jogjakarta, Indonesia. May 2015.

18. Boving, T.B. (2015) Innovative groundwater remediation technologies. Presentation to Universitas Islam Indonesia. Yogyakarta, Indonesia. Jan. 2015 (Invited).

19. Boving, T.B. (2015) Remediation Technologies - An Introduction. TERI University, Delhi, India. Feb. 2015.

20. Mateas, D.J., G.R. Tick, and K.C. Carroll (2016) In Situ NAPL Modification for Contaminant Source-Zone Passivation, Mass Flux Reduction, and Remediation. American Geophysical Union Fall Meeting, Fall Meet. Suppl., Abstract H33A-1504.

21. Khan, N., A. Dettmer, M. Johnson, and K.C. Carroll (2016) Complexation of Contaminants and Aqueous-Phase Ozone with Cyclodextrin for Emerging Contaminant Oxidative Degradation. American Geophysical Union Fall Meeting, Fall Meet. Suppl., Abstract H33A-1506.

22. Carroll, K.C., and H. Chen (2016) Functionalized Graphene Metal-Free Carbocatalysis of Persulfate and Emerging Contaminant Oxidative Degradation. American Geophysical Union Fall Meeting, Fall Meet. Suppl., Abstract H33A-1507.

23. Khan, N., A. Dettmer, R. Ball, T.B. Boving, and K.C. Carroll (2016) Stabilization and Prolonged Reactivity of Aqueous-Phase Ozone with Cyclodextrin. ASA-CSSA-SSSA Meeting, Phoenix, AZ, Nov. 6-9.

24. Carroll, K.C., and H. Chen (2016) Metal-Free Catalysis of Persulfate Activation and Organic-Pollutant Degradation by Nitrogen-Doped Graphene and Aminated Graphene. ASA-CSSA-SSSA Meeting, Phoenix, AZ, Nov. 6-9.

25. Wang, Y., and M.L. Brusseau (2016) Retention and Transport of Graphene in Porous Media. Presented at American Society of Agronomy, Crop Science Society of America, and Soil Science Society of America Annual Meeting, Phoenix, AZ, November 6-9.

26. Zhong, H., Brusseau, M. L., Yan, N., Zhang, L., and Cui, P. (2016) Innovative In-situ Oxidation Technologies for Treating Groundwater Contaminated by Chlorinated Solvents and 1,4-Dioxane. Presented at the International Conference on Environmental Science and Technology sponsored by the American Academy of Sciences, Houston, TX, June 6-10.

27. Cashman, M.A. and T.B. Boving (2016) Radical Detection During Chemical Oxidation of 1,4-Dioxane. Poster presented at the New England Graduate Student Water Symposium, Amherst, MA., Sept. 10-12, 2016.

28. Eberle, D., R. Ball, and T.B. Boving (2016) Impact of Advanced Oxidation Treatment on

Recalcitrant Contaminants. Submission ID# 131415. 2016 World Environmental & Water Resources Congress. May 2016, W. Palm Beach, FL.

29. Abbott, J.B., G.R. Tick, G.R. Greenberg, and K.C. Carroll (2017) Quantifying Mass Transfer Processes in Groundwater as a Function of Molecular Structure Variation for Multicomponent NAPL Sources. American Geophysical Union Fall Meeting, Fall Meet. Suppl., Abstract.

30. Chen, W., N. Yan, X. Fu, K.C. Carroll, F.O. Holguin, and M.L. Brusseau (2017) Adsorption and Retardation of PFASs in Soil. American Geophysical Union Fall Meeting, Fall Meet. Suppl., Abstract.

31. Carroll, K.C., and H. Chen (2017) Metal-Free Catalysis of Persulfate Activation and Organic-Pollutant Degradation by Nitrogen-Doped Graphene and Aminated Graphene. SERDP and ESTCP Symposium 2017, Nov. 28-30, Washington, DC.

32. Khan, N.A., M.D. Johnson, F.O. Holguin, B. Dungan, and K.C. Carroll (2017) Advanced oxidation of 1,4-dioxane and co-contaminants by aqueous ozone with and without a stabilization agent. SERDP and ESTCP Symposium 2017, Nov. 28-30, Washington, DC.

33. Carroll, K.C. (2017) Reactors in the Rocks: A Couple of Chemical Engineering Applications in the Subsurface. Invited Presentation: New Mexico State University Chemical Engineering Department Seminar, September 1.

34. Carroll, K.C., and H. Chen (2017) Nitrogen-Doped Graphene and Aminated Graphene Catalysis of Persulfate Activation and Emerging Contaminant Degradation in Wastewater. NM WRRI's 62nd Annual New Mexico Water Conference, Hidden Realities of New Water Opportunities, Aug. 15-16, Socorro, NM.

35. Hennessey, J.R., and K.C. Carroll (2017) Using Contaminant Mass Discharge and Attenuation Rate Analysis to Develop Pump-and-Treat Remediation System Closure Criteria for Transition to Monitored Natural Attenuation. NM WRRI's 62nd Annual New Mexico Water Conference, Hidden Realities of New Water Opportunities, Aug. 15-16, Socorro, NM.

36. Milavec, J., G.R. Tick, and K.C. Carroll (2017) Nonaqueous Phase Liquid Solubilization and Soil Adsorption Behavior of 1,4-Dioxane and Trichloroethylene Mixtures. NM WRRI's 62nd Annual New Mexico Water Conference, Hidden Realities of New Water Opportunities, Aug. 15-16, Socorro, NM.

37. Bridges, L., M.L. Brusseau, and K.C. Carroll (2017) Manganese Dioxide Activation of Sodium Persulfate for Contaminant Oxidation. NM WRRI's 62nd Annual New Mexico Water Conference, Hidden Realities of New Water Opportunities, Aug. 15-16, Socorro, NM.

38. Khan, N.A., M.D. Johnson, F.O. Holguin, B. Dungan, and K.C. Carroll (2017) Cyclodextrin Stabilization of Advanced Oxidation of 1,4-Dioxane and Co-Contaminants Using Aqueous Ozone for Contaminated Groundwater Treatment. NM WRRI's 62nd Annual New

Mexico Water Conference, Hidden Realities of New Water Opportunities, Aug. 15-16, Socorro, NM.

39. Carroll, K.C. (2017) Water & Energy at the Nexus of Hydrology & Environmental Engineering. Invited Presentation: Arizona State University Environmental Engineering Department Seminar, March 1.

40. Carroll, K.C. (2017) Subsurface Contaminant In-Situ Chemical Oxidation: Coupling of Hydrogeology and Geochemistry. Invited Presentation: San Diego State University Geology Department Seminar, Jan. 19.

41. Yan, N., M.L. Brusseau, and F. Liu. (2017) Influence of subsurface environment on oxidant activation and 1,4-dioxane degradation by in-situ chemical oxidation. Presentation at the American Geophysical Union Annual Meeting, New Orleans, LA, Dec.

42. Boving, T.B., and M.A. Cashman (2017) 1,4-Dioxane treatment with peroxone activated persulfate: Large scale column experiments. SERDP/ESTCP Symposium 2017, Washington D.C., November 28-30, 2017.

43. Cashman, M.A., and T.B. Boving (2017). 1,4-Dioxane Oxidation with Peroxone Activated Persulfate. Platform presented at the New England Graduate Student Water Symposium, Amherst, MA., Sept. 9, 2017.

44. Boving, T.B. (2017) Remediation of Soil and Groundwater Contamination: One Generation Later. International workshop on “Sustainable Soil and Groundwater Protection and Remediation”, August 21, 2017 at National Cheng Kung University (NCKU), Tainan City, Taiwan (Invited).

45. Boving, T.B. (2017) Remediation of Soil and Groundwater Contamination: One Generation Later. International workshop on “Sustainable Soil and Groundwater Protection and Remediation”, August 24, 2017 at National Taiwan University (NTU), Taipei, Taiwan (Invited).

46. Mateas, D.J., G.R. Tick, and K.C. Carroll (2018) In Situ Stabilization of NAPL Contaminant Source-Zones as a Remediation Technique to Reduce Mass Flux to Groundwater. Battelle Conference, Eleventh International Conference on Remediation of Chlorinated and Recalcitrant Compounds; Palm Springs, California.

7.2.3 Other Supporting Material

1. MS Thesis Adam Dettmer (2015): In Situ Complexation and Facilitated Transport of Oxidants. M.S. in the WSM Program, NMSU.

2. PhD Thesis Mr. Eberle (2015): ISCO of volatile organic contaminants using peroxone activated persulfate. Geosciences / Civil and Environmental Engineering URI.

3. Senior Thesis Sativa Cruz (2016): Soil Natural Oxidant Demand Variability and

Controlling Processes. Undergraduate Env. Science Research, NMSU.

4. MS Thesis Justin Milavec (2017): NAPL Source Release and Sorption of 1,4-Dioxane. M.S. in the WSM Program, NMSU.

5. MS Thesis Logan Bridges (2017): Persulfate Activation and Oxidation of 1,4-Dioxane. M.S. in the WSM Program, NMSU.

6. MS Thesis Mrs. Cashman (2017): In-situ treatment of 1,4-dixoane under column scale condition. Geosciences / Civil and Environmental Engineering URI.

7. PhD Thesis Ni Yan (2018): In Situ Oxidation of 1,4-Dioxane with Persulfate-Based Oxidation Activated by Iron Minerals. Ph.D. in the Hydrology Program, University of Arizona.

8. PhD Thesis Naima Khan (2018): Cyclodextrin Stabilization of Advanced Oxidation of 1,4-Dioxane and Co-Contaminants Using Aqueous Ozone for Contaminated Groundwater Treatment. Ph.D. in the WSM Program, NMSU.